Issue No.
01

Interpolytechnic Congress on Research and Posgraduate Studies (ICRGS-2024)

HORIZONTES

de Investigación y Desarrollo

Diciembre 2025 • Vol. 01 • ISSN In process

DIRECTORIO

INSTITUTO POLITÉCNICO NACIONAL

Arturo Reyes Sandoval
DIRECTOR GENERAL

Ismael Jaidar Monter
SECRETARIO GENERAL

María Isabel Rojas Ruiz
SECRETARIO ACADÉMICO

Martha Leticia Vázquez González
SECRETARIA DE INVESTIGACIÓN Y POSGRADO

Yessica Gasca Castillo
SECRETARIA DE INNOVACIÓN E INTEGRACIÓN SOCIAL

Marco Antonio Sosa Palacios
SECRETARIO DE SERVICIOS EDUCATIVOS

Noel Miranda Mendoza
SECRETARIO EJECUTIVO DE LA COMISIÓN DE OPERACIÓN Y FOMENTO DE ACTIVIDADES ACADÉMICAS

José Alejandro Camacho Sánchez
SECRETARIO EJECUTIVO DEL PATRONATO DE OBRAS E INSTALACIONES

Marx Yazalde Ortiz Correa
ABOGADO GENERAL

Modesto Cárdenas García
PRESIDENTE DEL DECANATO

Orlando David Parada Vicente
COORDINADOR GENERAL DE PLANEACIÓN E INFORMACIÓN INSTITUCIONAL

Andrés Falcón García
COORDINADOR GENERAL DEL CENTRO NACIONAL DE CÁLCULO

Marco Antonio Ramírez Urbina
COORDINADOR DE IMAGEN INSTITUCIONAL

HORIZONTES DE INVESTIGACIÓN Y DESARROLLO

Dr. Francisco Gutiérrez Galicia
Dr. Miguel Antonio Domínguez Crespo
Dr. Jorge Roberto Vargas
Dr. Luis Gerardo Zepeda Vallejo
Dr. Humberto Ríos Bolívar
Dra. Aidé Minerva Torres Huerta
Mtra. Mónica Edhali Flores Suárez
Lic. Sonia Estefani Guel Zamora
EDITORS

Mtra. Mónica Edhali Flores Suárez
Lic. Sonia Estefani Guel Zamora
Dr. Miguel Antonio Domínguez Crespo
Dra. Karen Ailed Neri Espinoza
TECHNICAL AND LOGISTICAL TEAM

Mtra. Itzel Eugenia Sánchez Flores
Lic. Víctor Hugo Rivera de Anda
EDITORIAL DESIGN & LAYOUT

Mtra. Itzel Eugenia Sánchez Flores
Lic. Víctor Hugo Rivera de Anda
SIP PORTAL WEB

www.ipn.mx
www.ipn.mx/sip/

HORIZONTES DE INVESTIGACIÓN Y DESARROLLO, No. 01, diciembre 2025. Es una publicación semestral editada por el IPN a través de la Secretaría de Investigación y Posgrado, Unidad Profesional "Adolfo López Mateos", av. Luis Enrique Erro s/n, col. Zacatenco, C.P. 07738, Ciudad de México. Conmutador: 55 5729-6000 ext. 50563. Las opiniones expresadas por los autores no necesariamente reflejan la postura del editor de la publicación.

PROLOGUE

With great pleasure, I introduce the inaugural issue of Horizons of Research and Development, a scientific journal published by the Secretariat for Research and Postgraduate Studies at the Instituto Politécnico Nacional (IPN). The purpose of this journal is to emphasize and strengthen the impact of research conducted by our postgraduate students.

This inaugural issue compiles full-length papers from the First Interpolytechnic Congress on Research and Postgraduate Studies 2024. In addition to national and international institutions, the event brought together more than 39 IPN academic units and research centers. The congress showed our dedication to academic excellence and applied science while reaffirming IPN's leadership in research and postgraduate education.

During the Congress, we received proposals from all four main areas of knowledge at our institution: Engineering and Physical-Mathematical Sciences, Medical and Biological Sciences, Social and Administrative Sciences, and Interdisciplinary Studies. Over 10% of these contributions included international collaboration, showing our community's openness to new ideas and the global impact of research at the IPN.

The submitted works underwent a rigorous selection process. Each submission was thoroughly reviewed by a scientific committee of more than 50 academics to ensure that every study had a real social impact and made a significant contribution to the advancement of knowledge. The authors of the best contributions were asked to submit full papers based on their presentations; 44 of these were ultimately accepted for publication in this issue, serving as the finest representations of our graduate students' research efforts.

We highlight the importance of spaces where students can share research and receive constructive feedback. In these forums, they contribute to the scientific and technological progress of our country. We also honor the caliber and diversity of work in this inaugural issue of Horizons of Research and Development. This journal gives our young researchers a platform to share ideas, voices, and projects with an academic community that values diligence, creativity, and quality.

The Secretariat for Research and Postgraduate Studies reaffirms its dedication to advancing research and developing highly skilled personnel at the IPN with this publication. This program is an additional step in establishing the Instituto Politécnico Nacional as a world leader in the creation of frontier knowledge while giving our students the skills they need to succeed in their chosen fields.

I encourage everyone reading this first issue to reflect on its contents and to continue collaborating to enhance science and technology for the betterment of society.

Martha Leticia Vázquez González
Secretary of Research and Postgraduate Studies

HORIZONTES DE INVESTIGACIÓN Y DESARROLLO, No. 01, diciembre 2025. Es una publicación semestral editada por el IPN a través de la Secretaría de Investigación y Posgrado, Unidad Profesional "Adolfo López Mateos", av. Luis Enrique Erro s/n, col. Zacatenco, C.P. 07738, Ciudad de México. Conmutador: 55 5729-6000 ext. 50563. Las opiniones expresadas por los autores no necesariamente reflejan la postura del editor de la publicación.

SCIENTIFIC REVIEW COMMITTEE

INDEX ID

ID		PAGES
	I. PHYSICAL-MATHEMATICAL SCIENCES AND ENGINEERING	1
4-I-PO	ANALYSIS AND CHARACTERIZATION OF S-BAND FERRITE MATERIALS: TWO HIGH POWER APPLICATIONS	2
49-I-PO	EVALUATION OF Ag0.1/Cu2O-ZnO FOR THE ELECTROCHEMICAL CO2 REDUCTION REACTION	7
94-I-PO	BALANCING METHODS FOR DEVELOPING MEDIUM POWER LIPO CELL BATTERY BANKS	13
95-I-PO	DEVELOPMENT OF A HYBRID BALANCING METHOD FOR POSSIBLE APPLICATION IN AN 11.2 KWH LIPO BATTERY BANK	20
114-I-PO	A COMPREHENSIVE CHARACTERIZATION PROTOCOL FOR PEM ELECTROLYZERS USING ELECTROCHEMICAL IMPEDANCE SPECTROSCOPY AND POLARIZATION CURVES	27
134-I-PO	EVALUATION OF THERMAL COMFORT IN A STANDARD MEXICAN HOUSE UTILIZING PHASE CHANGE MATERIALS	32
139-I-PO	EVALUATING THERMAL STORAGE SOLUTIONS IN SOLAR DISK COLLECTORS: TRADITIONAL METHODS VS. PHASE CHANGE MATERIAL	39
201-I-PO	THEORETICAL ANALYSIS OF FLAT PLATE SOLAR COLLECTORS USING COPPER OXIDE (CUO) AND MULTI-WALLED CARBON NANOTUBE (MWCNT) NANOFLUIDS	44
212-I-PO	EVALUATION OF FLUID BEHAVIOR IN A CITRUS GREENHOUSE IN THE VERACRUZ AREA USING CFD ANALYSIS	50
217-I-PO	MODELING AND SIMULATION OF ABSORPTION COOLING SYSTEM WITH EVAPORATION TEMPERATURE BELOW ZERO CELSIUS	55
253-I-PO	ELECTROCHEMICAL REDUCTION OF CO2 OVER Ag@Bi AND Ag@Sn ELECTROCATALYSTS TOWARDS THE GENERATION OF FORMIC ACID AND FORMALDEHYDE	61
301-I-PP	IMPACT OF ALTERNATIVE GRAVITY THEORIES ON THE LARGE-SCALE STRUCTURE OF THE UNIVERSE	67
312-I-PO	EVALUATION OF FLAT PLATE SOLAR COLLECTORS USING SIMPLE NANOFLUIDS (COPPER OXIDE (CuO) AND FULLERENE (C60)	73
366-I-PO	EVALUATION OF THE INFLUENCE OF MICROSTRUCTURAL CHARACTERISTICS ON SUSCEPTIBILITY TO STRESS CORROSION CRACKING IN API 5L STEELS IN NEAR-NEUTRAL PH ENVIRONMENTS	79
395-I-PO	INFLUENCE OF COMPUTATIONAL PARAMETERS ON RANS-BASED PREDICTIONS OF AXIAL-FLOW COMPRESSOR PERFORMANCE	87

II. MEDICAL-BIOLOGICAL SCIENCES		**94**
7-II-PO	CHARACTERIZATION OF MACROPHAGE POLARIZATION IN EARLY STAGES OF SYSTEMIC LUPUS ERYTHEMATOSUS: ANALYSIS IN A MOUSE MODEL INDUCED WITH LIPID PARTICLES	95
59-II-PP	COMPARISON OF THE CHANGE OF MICROBIOTA IN BILE FLUID IN PATIENTS WITH CHOLELITHIASIS AND CHOLANGITIS	102
84-II-PP	VALIDATION OF THE TWO BEST SURROGATE INSULIN RESISTANCE AND OBESITY MARKERS TO IDENTIFY METABOLIC SYNDROME IN MEXICAN ADULTS	107
115-II-PP	EVALUATION OF 2-AMINOBENZOTHIAZOLE DERIVATIVES AS ALDOSE REDUCTASE INHIBITORS IN DIABETES TREATMENT AND THEIR MICRO- AND MACROVASCULAR COMPLICATIONS	112
160-II-PP	IN SILICO EVALUATION OF BASIC AMINO ACID BOROXAZOLIDONES AS INHIBITORS OF BACTERIAL ENZYMES	117
162-II-PP	LIGAND-RECEPTOR ANALYSIS BY DOCKING OF ANTHRANILIC ACID-DERIVATED DIELS-ALDER ADDUCTS ON COX-1 AND 2	122
166-II-PP	IN SILICO DESIGN AND EVALUATION OF NEW LACTONES WITH DUAL ANTIMICROBIAL ACTIVITY	128
171-II-PO	HUMAN PAPILLOMAVIRUS AS A RISK FACTOR IN THE DEVELOPMENT OF PROSTATE CANCER	135
172-II-PP	DIFFERENTIAL EXPRESSION OF NRF2 TARGET GENES AFTER EXPOSURE TO INORGANIC ARSENIC IN HEPATOCELLULAR CARCINOMA CELLS (HEPG2)	139
259-II-PP	EVALUATION OF GABA AMINOTRANSFERASE INHIBITOR DIELS-ALDER ADDUCTS WITH POTENTIAL ANTICONVULSANT ACTIVITY	145
302-II-PP	EVALUATION OF THE DIETARY PATTERN IN MORBIDLY OBESE ADULTS	151
402-II-PO	CYTOTOXICITY OF IMMUNOSTIMULANT MOLECULES WITH POTENTIAL ADJUVANT ACTIVITY	155
III. SOCIAL AND ADMINISTRATIVE SCIENCES		**159**
17-III-PP	HUMAN CAPITAL MANAGEMENT FOR THE MANAGEMENT OF PSYCHOSOCIAL RISKS IN MEXICAN SMES	160
21-III-PP	GREEN BONDS TO IMPROVE THE GROWTH OF THE BIOENERGY MARKET IN MEXICO	166
44-III-PO	COMPETITIVE AND INNOVATIVE STRATEGIES IMPLEMENTED BY MSMES IN SOUTHERN MEXICO CITY TO SURVIVE THE COVID-19 CRISIS	172
61-III-PO	ACCESSIBILITY IN TOURIST SITES FOR THE CARE OF VISITORS WITH CHRONIC-DEGENERATIVE DISEASES IN THE MUNICIPALITY OF CULIACAN, SINALOA	175
90-III-PP	MANAGEMENT STRATEGIES FOR IMPROVING FINANCIAL EDUCATION IN FEMALE HIGH SCHOOL STUDENTS	180

109-III-PO MANAGEMENT PRACTICES FOR THE ACCREDITATION OF ENGINEERING PROGRAMS IN MEXICO 187

118-III-PP INTEGRATION OF RENEWABLE ENERGY FOR A SUSTAINABLE SMART CITY. THE CASE OF: ICELAND, NORWAY, AND DENMARK 193

157-III-PO DESIGN OF A VIRTUAL REALITY ENVIRONMENT AS DIGITAL TOURISM MARKETING TOOL IN PAHUATLÁN 199

325-III-PP IN SEARCH OF A VIABLE WATER MANAGEMENT SYSTEM MODEL IN BOUTIQUE HOTELS IN TULUM 203

371-III-PP TOWARDS A DECISION SUPPORT SYSTEM FOR HUMAN RESOURCES MANAGEMENT IN 4-STAR HOTEL SMEs IN MEXICO CITY 210

IV. INTERDISCIPLINARY **216**

39-IV-PO EXTRACTION AND CHARACTERIZATION OF NANOCELLULOSE FROM AGROINDUSTRIAL WASTE TO OBTAIN HYDROGELS 217

145-IV–PO CHARACTERIZATION OF COOPERATIVISM FROM THE CREATIVE ECONOMY APPROACH 224

203-IV-PO INSECTS AS AN ALTERNATIVE TO HUMAN AND ANIMAL NUTRITION 231

250-IV-PO SYNTHESIS AND CHARACTERIZATION OF SiO_2 MESOPOROUS NANOPARTICLES AS NANOCARRIERS OF IRON 238

281-IV-PO BAKERY WITH COFFEE PULP AS A CIRCULAR ECONOMY STRATEGY IN OAXACA 243

321-IV-PP ULTRASOUND ASSISTED SYNTHESIS OF ZnO-GO CORE-SHELL WITH ENHANCED OPTICAL PROPERTIES OF NITROGEN AND SULFUR FUNCTIONALIZED 247

AUTHOR INDEX 252

HORIZONTES

de Investigación y Desarrollo

I

Physical-Mathematical Sciences and Engineering

4-I-PO ANALYSIS AND CHARACTERIZATION OF S-BAND FERRITE MATERIALS: TWO HIGH POWER APPLICATIONS

A. Trejo León[1], F. Martínez Zúñiga[1], J. R. Sosa Pedroza[1]*

[1]Instituto Politécnico Nacional, Escuela Superior de Ingeniería Mecánica y Eléctrica, Unidad Zacatenco, Sección de Estudios de Posgrado e Investigación, Av. Luis Enrique Erro S/N, Unidad Profesional Adolfo López Mateos, Zacatenco, C.P. 07738 CDMX, México.

*Correspondence: atrejol1201@alumno.ipn.mx

Abstract: This paper presents the analysis and characterization of ferrite materials in the S-band, with a focus on two high-power applications, circulators and attenuators. The magnetic and dielectric properties of some ferrite materials are investigated, evaluating their performance under high-power conditions at S-band. Through modeling and optimization, the characteristics that affect the efficiency and stability of these two devices are highlighted, such as the geometry and location of the ferrite materials within WR-284 waveguides. Implications for efficiency improvement in communications and, primarily, in radar systems will be discussed.

Keywords: Bandwidth; Ferrite Circulator; Magnetic Field; Rectangular waveguide; Y-junction

1. INTRODUCTION

The analysis and characterization of ferrite materials are crucial to the advancement of high-power microwave applications [1], especially in circulators and attenuators. Ferrites exhibit magnetic properties that allow effective electromagnetic field steering. In addition, ferrite materials allow high powers to be handled in circulators and attenuators, with the operating frequency being a key operator in determining some properties of ferrite materials to be implemented. A key aspect of this characterization is the analysis of the permeability tensor, which quantifies the anisotropic response of ferrites under external magnetic fields, which significantly influences their operating efficiency. Microwave ferrite circulators are passive three-port devices that are used in radio frequency (RF) applications whenever it is necessary to direct power to a specific point and isolate it from another. The circulating condition of circulators, in which the RF signal is directed circularly from one port and attenuated in the reverse direction, arises due to the non-reciprocal properties of the ferrite material. The basic operation of a circulator is based on magnetized microwave ferrite material [2], a ceramic material with non-reciprocal behavior, meaning that its behavior in one direction is very different from that in the other direction [3]. Also, ferrite-based attenuators are designed to precisely control signal amplitude, minimizing interference and ensuring stable performance in high-power scenarios. A thorough characterization involves evaluating critical properties such as permeability, loss tangent, and saturation magnetization, along with a detailed analysis of the impact of the permeability tensor on device behavior. This paper aims to provide an in-depth exploration of ferrite materials in an S-band application, with magnetic behavior in ferrite materials as the primary focus. By integrating this knowledge, we contribute significantly in RF applications, improving the performance of critical communication and radar systems.

2. ANALYSIS OF PERMEABILITY TENSOR

To complete our two tasks (high-power applications) an analysis of materials with magnetic anisotropy (tensor permeability) must be performed. Some of the most practical anisotropic materials for RF applications are ferrimagnetic compounds, also known as ferrite materials, such as yttrium iron garnet (YIG) or calcium vanadium doped materials (TVG). Ferrimagnetic material has significant resistivity and anisotropic permeability at RF frequencies when subjected to a strong direct current (DC) magnetic field. The strength of the bias field

aligns the magnetic dipoles in the ferrite material causing them to process at a given frequency. This produces a non-zero overall magnetic dipole moment [4]. A microwave signal circularly polarized in the same direction as this precession frequency interacts strongly with the dipole moments, while the oppositely polarized signal interacts less strongly and is significantly attenuated. The main component of the microwave circulator that causes the circulating action are magnetically polarized ferrite disks. Another useful feature of ferrimagnetic materials is that the interaction with an applied microwave signal can be controlled by adjusting the strength of the polarization field. This effect gives rise to a wide variety of control devices, such as phase shifters, switches, resonators, tunable filters and attenuators [5] [6].

The anisotropic permeability tensor of an arbitrarily shaped ferrite material magnetically polarized in the $\hat{z}$ direction is given in Eq. (1) [7].

$$[\mu] = \begin{bmatrix} \mu & jk & 0 \\ -jk & \mu & 0 \\ 0 & 0 & \mu_0 \end{bmatrix} H_0\, \hat{z} \qquad \textit{Eq. (1)}$$

Where $\mu = \mu_0(1+\chi_{xx}) = \mu_0(1+\chi_{yy})$ and $k = -j\mu_0\chi_{xy}$, the variable χ is the magnetic susceptibility and according to the direction of interaction (x and y axes) of the magnetic susceptibility the direction indices will change [8]. For our applications it is important to know the geometry of ferrite material because it defines the surface demagnetization factors. The first application will have a ferrite disk with the following factors $N_x = N_y = 0.5$ and $N_z = 0$ [9], while the second application will have a ferrite plate with the following factors $N_x = N_y = 0$ and $N_z = 1$. Considering the resonant losses, the magnetic susceptibilities of the ferrite material are complex, given by Eq. (2) for the $\hat{x}$ and $\hat{y}$ directions.

$$\chi_{(xx|yy)} = \chi'_{(xx|yy)} - j\chi''_{(xx|yy)} \qquad \textit{Eq. (2)}$$

Where

$$\chi'_{(xx|yy)} = \frac{\omega_m[\omega_r^2 - \omega^2(1+\phi^2)]\left(\omega_0 + N_{y|x}\omega_m\right) + 2\omega_r\phi^2\omega^2}{(\omega_r^2 - \omega^2 - \phi^2\omega^2)^2 + 4\phi^2\omega^2\omega_r^2}$$

$$\chi''_{(xx|yy)} = \frac{2\omega_m\omega_r\phi\omega\left(\omega_0 + N_{y|x}\omega_m - \phi\omega\right)}{(\omega_r^2 - \omega^2 - \phi^2\omega^2)^2 + 4\phi^2\omega^2\omega_r^2}$$

And in Eq. (3) for the $\widehat{xy}$ direction [8].

$$\chi_{(xy)} = -\chi''_{(xy)} - j\chi'_{(xy)} \qquad \textit{Eq. (3)}$$

Where

$$\chi'_{(xy)} = \frac{\omega\omega_m[\omega_r^2 - \omega^2(1+\phi^2)]}{(\omega_r^2 - \omega^2 - \phi^2\omega^2)^2 + 4\phi^2\omega^2\omega_r^2}$$

$$\chi''_{(xy)} = \frac{2\omega_m\omega_r\phi\omega^2}{(\omega_r^2 - \omega^2 - \phi^2\omega^2)^2 + 4\phi^2\omega^2\omega_r^2}$$

For Eqs. (2) and (3) $\phi = (2.8\times10^6[Hz/Oe])\Delta H/2\omega$ this is the Gilbert damping factor. Similarly, ω_m is the electron spin frequency at magnetic saturation, ω_0 is the Larmor frequency due to the bias field, ω is the frequency of the applied RF signal and ΔH is the linewidth of the ferrite material [10]. With the analysis of the permeability tensor and the geometries of the ferrite materials, it will be able to quantify the relationship between the magnetic field strength and the magnetic flux density in the material, considering its propagation direction, so the next step is to define the working frequencies. For this point, a working range of the WR-284 rectangular waveguide was taken, which goes from 2.6 GHz to 3.95 GHz [9], these intervals are defined by the dimensions of the waveguide and the propagation modes of the electromagnetic field. It is here that the second point requires the propagation mode, for this case it is an electric transverse propagation mode ($TE_{1,0}$), because the polarization direction of the ferrite material for the circulator will be in the z axis, and from this we can know the operating range of the circulator.

The size of the ferrite disk is calculated assuming it as a dielectric resonator in unbiased state, keeping $\mu_r = 1$, using Eq. (4).

$$\omega_{111} = \frac{1.841}{\sqrt{\mu\varepsilon}\mathrm{R}}\sqrt{\left(1 + 2.912\left(\frac{\mathrm{R}^2}{\mathrm{d}^2}\right)\right)} \qquad \textit{Eq. (4)}$$

Where ω is the resonance frequency, R is the disk radius, d is the disk height and the value 1.841 corresponds to the lowest value for the propagation mode $TE_{1,0}$ and is the result of the root of the first derivative of the Bessel

function (J_n) with respect to its argument because $m = n = p = 1$ [11].

3. TWO-APPLICATION DESIGN WITH FERRITE MATERIAL

Next, the design and simulation of a circulator and an attenuator using the properties of a TTVG-1600 ferrite will be addressed, with the objective of applying and validating the theoretical analysis of the magnetic field. In this way, the performance of ferrites in RF applications is guaranteed.

3.1 Circulator

As previously mentioned, we will use the WR-284 waveguide and the 3.1 GHz frequency is taken as the resonance frequency because this frequency is contained in the resonance frequency range of Eq. (4). TTVG-1600 material is selected as the ferrimagnetic material for the ferrite disks of the circulator and the ferrite plates of the attenuator. The electrical and mechanical properties of TTVG-1600 are shown in Table 1. The bias strength was set to 1600 G (equivalent to the magnetic saturation of ferrite), and the initial dimensions of the ferrite disk were calculated as $r = 28$ mm and $h = 4.3$ mm.

Table 1. Properties of the ferrimagnetic material TTVG-1600.

Property	Value	Property	Value
Magnetization $4\pi M_s$	1600 [G]	Line Width	≤10 [Oe]
Dielectric Constant	14.6	Loss Tangent	≤0.0002
Curie Temperature	220 °C	Electric Conductivity	0.01 [S/m]

After making the corresponding analysis of the ferrite material we proceed to simulate our first application which is the circulator, for this purpose we use a commercial electromagnetics element design software considering all the design parameters of the ferrite material. Figure 1 (a) shows the external structure of the proposed circulator, while Figure 1 (b) shows the internal structure of the circulator. In the external structure it can be observed three poles that help in the stabilization of the external bias magnetic field for the ferrite disks that are located at the circulator node, the dimensions of the waveguide ports take as reference the dimensions of the WR-284 rectangular guide. While for the internal structure, a PTFE disk can be observed surrounding the ferrite disks, this is to change the electromagnetic field interaction velocity at the interaction point of the ferrite disks. These ferrite disks have a separation of 31.5 mm from the top faces. The electric field signal flow is mainly from port 1 to port 2, while port 3 is isolated, which makes it a circulator with right-hand bias direction and is reciprocal to all ports, this is because there is no difference in the ports.

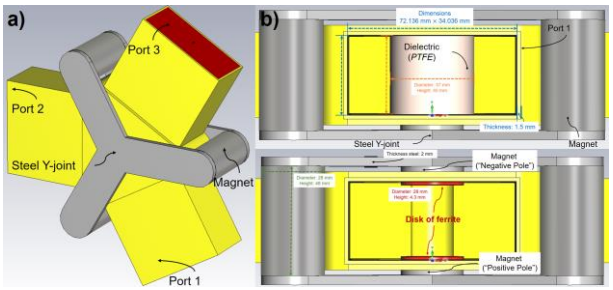

Figure 1. Circulator. (a) External structure; (b) Internal structure.

Figure 2 shows the S parameters of the circulator, for this case it is only considered that port 1 is the power port so we will only have three curves: The first S parameter is the coupling ($S_{1.1}$) with a bandwidth of 800 MHz and resonance frequency of 3.1 GHz; the second parameter S is the transmission parameter ($S_{1,2}$) which is the loss that will exist between the signal flow between port 1 and port 2 which is kept at 1 dB as average for the highest coupling frequency; the last parameter S is the isolation parameter ($S_{1,3}$) having −17 dB of isolation at the resonance frequency. These parameters are suitable for high-power circulators with ferrite. The simulation is performed with a power supply of 500 W and with a propagation mode $TE_{1,0}$, thus ensuring all our design parameters.

3.2 Attenuator

The ferrite attenuator will use the same ferrite material as the circulator, only, in this application, the ferrite geometry will be in the shape of a pyramid, which is very similar to having ferrite plates stacked to form the ferrite. Therefore, the demagnetization factor will be

different and will only be applicable to the z-axis, as mentioned in Eq. 2.

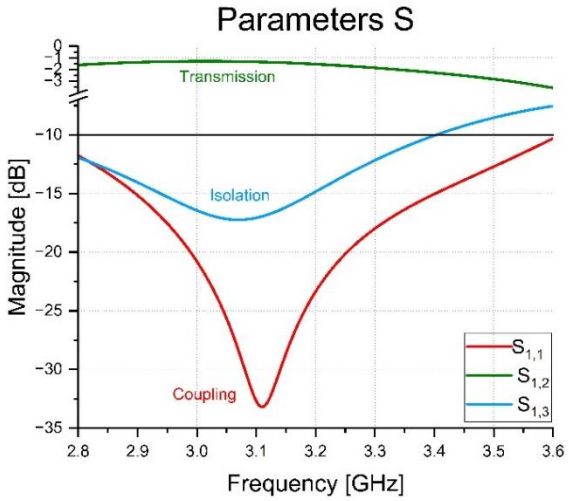

Figure 2. Circulator S-parameters.

The ferrite attenuator will be the second application, and its design will be easier to construct, since only a 100 mm long WR-284 waveguide is needed in which two ferrite pyramids will be placed, as shown in Figure 3. This geometry is because the propagation of the electric field will be in the z-direction and the angle of incidence of the electric field components will cause a direct penetration into the ferrite material, which will cause a large attenuation of the field along the material. However, the interaction of the field with the material causes a small amount of reflection, so a geometry that considers reflection is required. For this leakage, a pyramid with distinct faces was used (see Figure 3). The faces of pyramid 1 have a width of half the length of side an of the rectangular waveguide, while the faces of pyramid 2 have different widths, so there is an area without ferrite material that allows the electromagnetic field to escape and attenuate along the rectangular waveguide. For its design, a two-port waveguide configuration was used to determine the ratio of the S_{21} parameter.

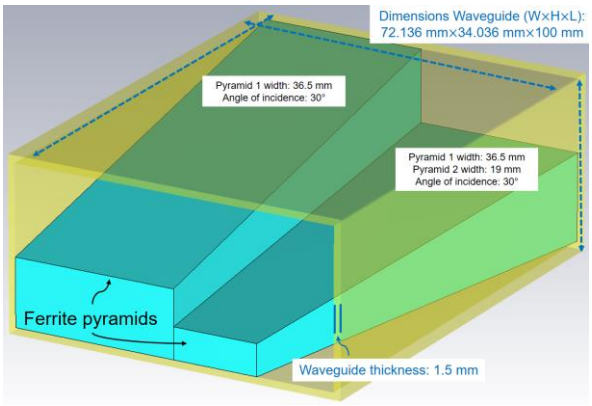

Figure 3. Attenuator structure.

This relationship is necessary to know the isolation magnitude of the attenuator, which for this application will be an attenuation magnitude. Figure 4 shows a coupling of −35 dB for the range of interest and an attenuation of −90 dB at best. At a design frequency of 3.1 GHz, the attenuation is −78 dB.

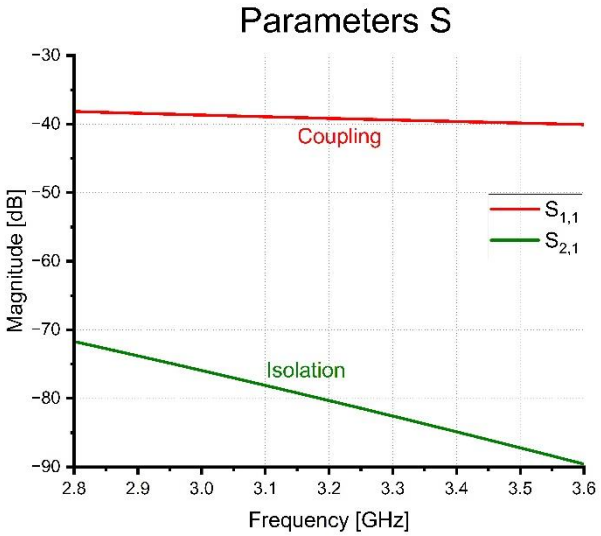

Figure 4. Attenuator S-parameters.

4. CONCLUSIONS

In this work, an analysis of the magnetic field in ferrite materials for S-band applications is used, where a circulator with ferrite disks and high-power dielectric core and a ferrite material attenuator has been designed. Standard design equations were used, and permeability tensor analysis was performed. Both applications were designed and simulated in commercial electromagnetic component software with 500 W input power. Both results are quite promising, so the next

step is the construction and characterization of both devices.

Conflicts of Interest

The authors declare no conflict of interest.

REFERENCES

[1] Baden Fuller AJ. Ferrites at Microwave Frequencies London, United Kingdom: Peter Perogrinus Ltd; 1987.

[2] Jiles D. Introduction to Magnetism and Magnetic Materials. Third Edition ed.: CRC Press; 2016.

[3] Auld BA. The Synthesis of Symmetrical Waveguide Circulators. IRE Transactions on Microwave Theory and Techniques. 1959; 7(2): p. 238-246.

[4] Collin RE. Foundations for Microwave Engineering New York: McGraw Hill; 1992.

[5] Soohoo R. Microwave ferrite materials and devices. IEEE Transactions on Magnetics. 1968; 4(2): p. 118-133.

[6] Adam JD, Davis LE, Dionne GF, Schloemann EF, Stitzer SN. Ferrite devices and materials. IEEE Transactions on Microwave Theory and Techniques. 2002; 50(3): p. 721-737.

[7] Polder D. VIII. On the theory of ferromagnetic resonance. The London, Edinburgh, and Dublin Philosophical Magazine and Journal of Science. 1948;: p. 99-115.

[8] Özgür Ü, Alivov Y, Morkoc H. Microwave ferrites, part 1: fundamental properties. J Mater Sci: Mater Electron. 2009; 20: p. 789-834.

[9] Pozar DM. Microwave Engineering. Fourth Edition ed.: JohnWiley & Sons, Inc.; 2012.

[10] Freeman R, King J, Lafyatis G. Electromagnetic Radiation: Oxford University Press; 2019.

[11] Jackson JD. Classical Electrodynamics John Wiley & Sons, inc.; 1999.

49-I–PO EVALUATION OF $Ag_{0.1}/Cu_2O$-ZnO FOR THE ELECTROCHEMICAL CO_2 REDUCTION REACTION

M. Á. Soto-Mendoza[1], C. X. Tirado-López[1], A. Manzo-Robledo[2], R. G. Sánchez-Alvarado[1], A. Ezeta-Mejía[1]*

[1]Instituto Politécnico Nacional, Escuela Superior de Ingeniería Química e Indústrias Extractivas. Departamento de Metalurgia y Materiales. UPALM. Edif. 7, C.P. 07830, CDMX, México.

[2]Instituto Politécnico Nacional, Escuela Superior de Ingeniería Química e Indústrias Extractivas. Laboratorio de Electroquímica y Corrosión. UPALM. Edif. Z5, C.P. 07830, CDMX, México.

*Correspondence: aezetam@ipn.mx

Abstract: In this work, a Cu_2O-ZnO catalytic matrix was synthesized though the hydrothermal method then Ag ($10\%_{wt}$) nanoparticles were deposited via conventional impregnation on the matrix surface. The morphology, composition, particle size, and identification of crystal phases were analyzed through SEM-EDX and XRD techniques. The electrocatalytic activity, and stability of the electrocatalysts in the reaction of CO_2 reduction (CO_2RR) were evaluated by the electrochemical techniques of cyclic voltammetry (CV) and chronoamperometry (CA) in a 0.1 M $KHCO_3$ supporting electrolyte, showing favorable results in stability and cathodic current of -2.0 and -1.9 mA, respectively. The products obtained from CO_2RR were identified *in situ* by DEMS, demonstrating high selectivity between hydrogen, methane, and its fragments.

Keywords: Electrochemistry, Electrocatalyst, Conversion, CO_2 utilization.

1. INTRODUCTION

The intensified greenhouse effect is a world-wide problematic due to the additional warming of Earth's atmosphere as a result of the increased concentrations of greenhouse gases (GHG's) released from human activities such as energy production, fossil fuel burning, deforestation, and industrial processes. This natural phenomenon occurs when solar radiation reaches Earth, part of the energy is absorbed by the surface and is re-emitted as infrared radiation. Greenhouse gases, including carbon dioxide (CO_2), methane (CH_4), nitrous oxide (N_2O), and fluorinated gases, trap this infrared radiation in the atmosphere [1-2]. This trapping effect has become magnified as GHG's concentrations rises, causing more heat to remain in the atmosphere. Furthermore, CO_2 levels have risen since pre-industrial times, reaching 422 parts per million (ppm) in September 2024, which is unprecedented in the recent geological record. The intensified greenhouse effect has extensive consequences on global systems, impacting all ecosystems, weather patterns, and sea levels [3-4].

Utilizing CO_2 is a promising strategy for mitigating climate change while generating valuable chemical products and renewable fuels. The utilization strategies focus on transforming CO_2 into useful chemicals through various processes, with the electrochemical methods emerging as the most effective due to their efficiency, scalability, and potential for low-carbon footprint production, as these methods leverage on renewable electricity to promote the CO_2 reduction reactions [5-7].

Electrochemical CO_2 reduction (CO_2RR) has gained attention for its versatility and high potential for coupling with renewable energy

sources. This approach involves using an electrochemical cell, where CO_2 is reduced on the cathode to form various valuable products, and oxygen which is produced at the anode. The advantages of the electrochemical pathways highlight the *High Selectivity and Energy Efficiency*, enabling selective conversion of CO_2 into specific products like carbon monoxide (CO), methane (CH_4), ethylene (C_2H_4), or formic acid (HCOOH). *Integration with Renewable Energy*, for highly selective CO_2RR systems to produce formates ($COOH^-$) with minimal carbon footprint. *Catalyst Innovation,* focused on the research and development of new electrocatalysts made from earth-abundant metals like copper, zinc and silicon for the production of hydrocarbons and alcohols. And *Scalability and Modularity* oriented for the capture and conversion systems, where small-scale reactors are deployed into industrial facilities and power plants, mitigating CO_2 emissions at the source [8-11].

Therefore, the structure, conversion, selectivity, and electrochemical performance at room temperature of $Ag_{0.1}/Cu_2O$-ZnO electrocatalyst synthesized by a two-step hydrothermal method is explored in this work, and aims to enhance the synergistic effect and electrochemical performance of Cu_2O, ZnO, and Ag, through a highly stable and homogeneous oxide matrix. Furthermore, DEMS offered *in-situ* analysis during polarization allowing precise identification of CO_2 reduced species generated by $Ag_{0.1}/Cu_2O$-ZnO.

2. MATERIALS AND METHODS

2.1 Synthesis of Cu_2O-ZnO electro-catalyst

Cu_2O-ZnO electrocatalyst was synthesized using the hydrothermal method. A solution 0.02 M of sodium hydroxide and 1 mM of sodium citrate in 400 mL of deionized water (DI water) was prepared. Then, stoichiometry amounts of copper chloride and zinc chloride in a molar ratio of 1:1 (Cu:Zn) was added and dissolved in the solution under magnetic stirring until a homogeneous solution was attained. The resulting mixture was transferred to a Teflon vessel and sealed inside a hydrothermal reactor which was heated to 140 °C for 5 hours. Afterwards, the solution was filtered, and the resulting powder was washed with ethanol and DI water and let dry overnight.

2.2. Synthesis of $Ag_{0.1}/Cu_2O$-ZnO electrocatalyst

$Ag_{0.1}/Cu_2O$-ZnO electrocatalyst was synthesized by adding 0.25 g of Cu_2O-ZnO, and 10 wt% of silver nitrate, and 1 mM of sodium citrate in 50 mL of DI water and ethanol in a ratio of (1:1). The solution was under continuous stirring and heating at a 50 °C for 3 hours. The resulting powder was filtered and washed with ethanol and acetone, the electrocatalyst was dried at room temperature.

2.3 Preparation of catalytic ink

To perform the electrochemical analysis, a catalytic ink (10% wt.) was prepared using the electrocatalyst powder $Ag_{0.1}/Cu_2O$-ZnO, Vulcan carbon, Nafion®, and acetone. The resulting mixture was sonicated for 30 minutes to ensure a homogeneous suspension. Finally, it was deposited on a glassy carbon electrode and dried at room temperature.

2.4 Characterization methods and conditions

X-Ray Diffraction (XRD) measurements were performed on a Panalytical X'pert PRO at 20 kV and 10 mA with CuKα radiation (λ=1.54 Å) from 20° to 100° in 2 theta. Scanning Electron Microscopy (SEM) images were obtained with a JEOL JSM 7800F at 10 kV and 5 mA. The electrochemical evaluation was carried out in a potentiostat/galvanostat VersaSTAT 4 from Princeton Applied Research, and performed in a standard three-electrode electrochemical cell at room conditions, in a 0.1 M $KHCO_3$ electrolyte. A glassy carbon electrode 3 mm in diameter was used as working electrode, the counter electrode was a platinum wire, and a standard hydrogen electrode (SHE) was used as a reference electrode. DEMS was used to monitor *in-situ* the ionic current (mass signal) for selected mass to charge ratios (m/z) with a

simultaneous faradaic current using the cyclic voltammetry technique.

3. RESULTS AND DISCUSSION

Figure 1 shows the diffraction pattern and crystal planes of $Ag_{0.1}/Cu_2O$-ZnO. The diffraction peaks match with Cu_2O (ICDD 00-005-0667), CuO (ICDD 01-078-0428), and ZnO (ICDD 03-065-0523) phases and planes (111), (200), (220), (311), (222), and (400) corresponding to angles at 2θ = 36.4°, 42.29°, 61.35°, 73.49°, 77.35°, 92.36°, and 92.36°, respectively. In addition, a CuO phase was also identified at 36.4°, 40.1°, and 42.6° corresponding to (111), (200), and (220) planes, respectively. The diffraction peaks also show the Ag metallic nanoparticles spectra according to JCPDS 04-0783 [12].

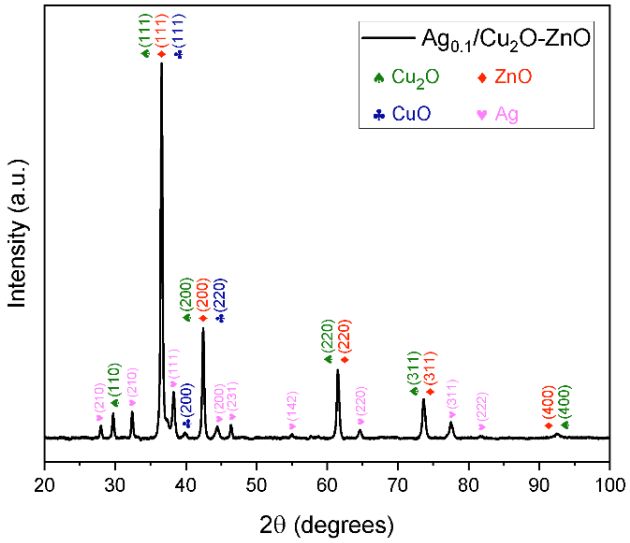

Figure 1. XRD analysis of $Ag_{0.1}/Cu_2O$-ZnO.

Crystallite size was calculated from modified Scherrer Eq. (1), where, *D* is the crystallite size in nm, *K* is the Scherrer constant (0.94 for cubic symmetry), λ is the wavelength from CuKα (1.5417 Å), β is the FWHM of XRD peak, and θ is the peak position.

$$ln(\beta) = ln\frac{1}{\text{Cos }\theta} + ln\frac{K\lambda}{D} \qquad \text{Eq. (1)}$$

The average crystallite size for $Ag_{0.1}/Cu_2O$-ZnO electrocatalyst was calculated at 23±0.1 nm.

SEM images show the morphology of $Ag_{0.1}/Cu_2O$-ZnO electrocatalyst. For ZnO, a nanosheet morphology can be seen in Figure 2 (a-b) and Cu_2O shows irregular polyhedral morphology with no specific size distribution.

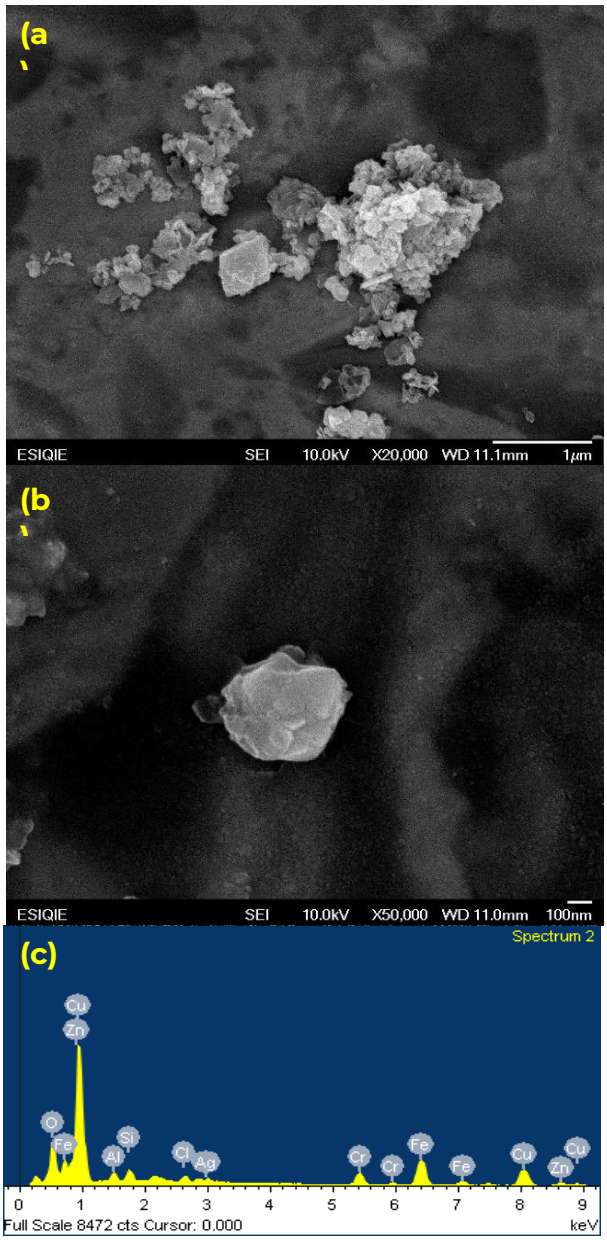

Figure 2. SEM micrographs (a-b) of $Ag_{0.1}/Cu_2O$-ZnO and EDS analysis (c).

EDS analysis of $Ag_{0.1}/Cu_2O$-ZnO in Figure 1 (c) demonstrated the presence of Ag, Cu, Zn and O spectra, elements from the metallic probe used for the analysis were also identified.

Figure 3 (a) shows the characteristic electrochemical profile of $Ag_{0.1}/Cu_2O$-ZnO/C in absence and presence (red) of CO_2. On the

cathodic sweep (black) is observed a peak (C_1) at -0.93 V/SHE corresponding to $Cu^{1+} \rightarrow Cu^0$, a second peak (C_2) at -1.25 V/SHE corresponding to $Zn^{2+} \rightarrow Zn^0$ in CO_2 free conditions. On the anodic sweep, an anodic peak (A_1) is observed at -0.44 V/SHE (red) and -0.46 V/SHE (black) at free and saturated CO_2 conditions, respectively, corresponding to $Cu^0 \rightarrow Cu^{1+}$ which is visible in the recorded potential window as reported by Zhang [13] regarding Cu_2O electrochemical profile. When the solution is saturated with CO_2 (red), a decrease in the overpotential can be observed, the shift of peak C_1 (at a measured value of -0.88 V/SHE), the absence of peak C_2, and the shift of peak A_1 occur due to variations in the pH of the supporting electrolyte (from 8 to 7) and changes in the adsorption/desorption mechanisms involving H^+ and CO_2^*. Additionally, a decrease in the cathodic current was also observed from -2.08 mA to -1.91 mA. However, this reduction in the current does not infer a lower electrochemical performance towards the electroreduction of CO_2.

To determinate the long-term stability and performance of the electrocatalyst during HER (hydrogen evolution reaction) and CO_2RR, chronoamperometry analysis was performed at -1.05 V/SHE, -1.2 V/SHE for 500 s and -1.6 V/SHE for 3600 s, respectively, as shown in Figure 3 (b) in absence and presence of CO_2. In CO_2 free conditions (black), a cathodic current starting at ca. -2.1 mA decreased to maintain a stabilized current at ca. -1.9 mA until end of polarization time. In presence of CO_2 (red), shows a cathodic initial current at ca. -2.0 mA and decreased towards ca. -1.8 mA, the current varied at values between -1.9 and -1.75 mA due to the constant adsorption, generation, and desorption of hydrogen and CO_2 reduction products from the surface of $Ag_{0.1}/Cu_2O$-ZnO.

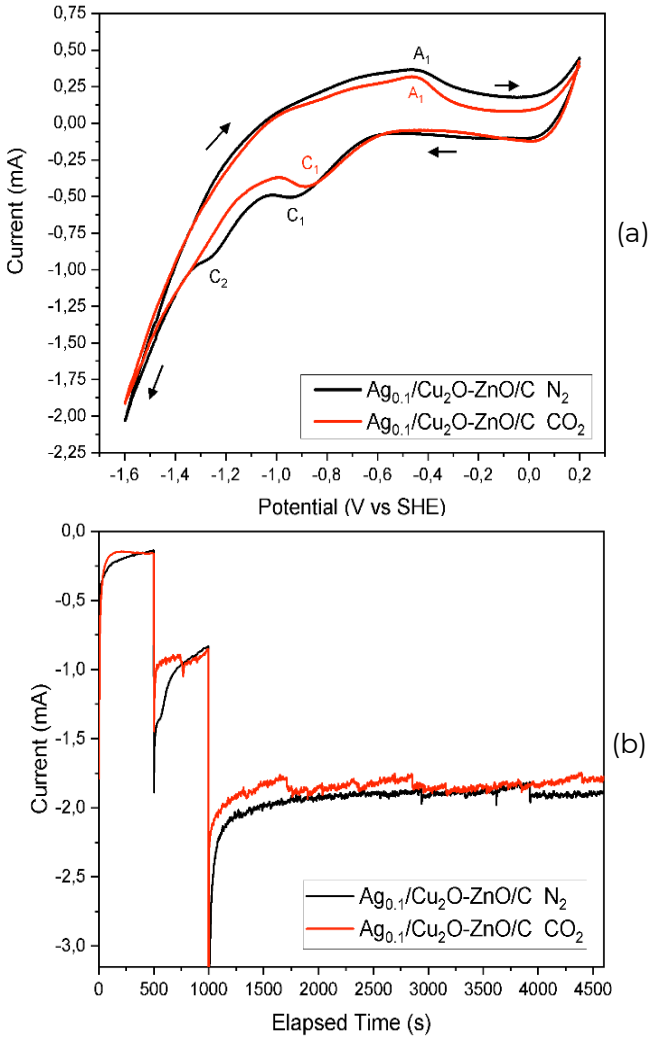

Figure 3. CV (a) and CA (b) evaluation of $Ag_{0.1}/Cu_2O$-ZnO.

Through DEMS, it was possible to monitor the mass signals *in situ* of the products generated in the interface of the electrocatalyst as shown in Figure 4. In absence of CO_2 as seen in Figure 4 (a), when performing the cathodic polarization only the production of m/z=2 related to H_2 can be observed (equation 2), which started at ca. -0.92 V for $Ag_{0.1}/Cu_2O$-ZnO/C.

$$2H^+ + 2e^- \rightarrow H_2 \qquad \text{Eq. (2)}$$

Since there is no slope in another ionic signals (m/z= 1, 16, 17 and 18), it is proven that there is no production of those species during polarization. In Figure 4 (b) it was possible to identify the signals m/z= 1, 16, 17 and 18 corresponding to protons (1), methane (16) and

methane fragments (17 and 18), respectively when CO_2 was saturated in the solution. The electrochemical reaction necessary for the generation of methane is indicated in the equation 3.

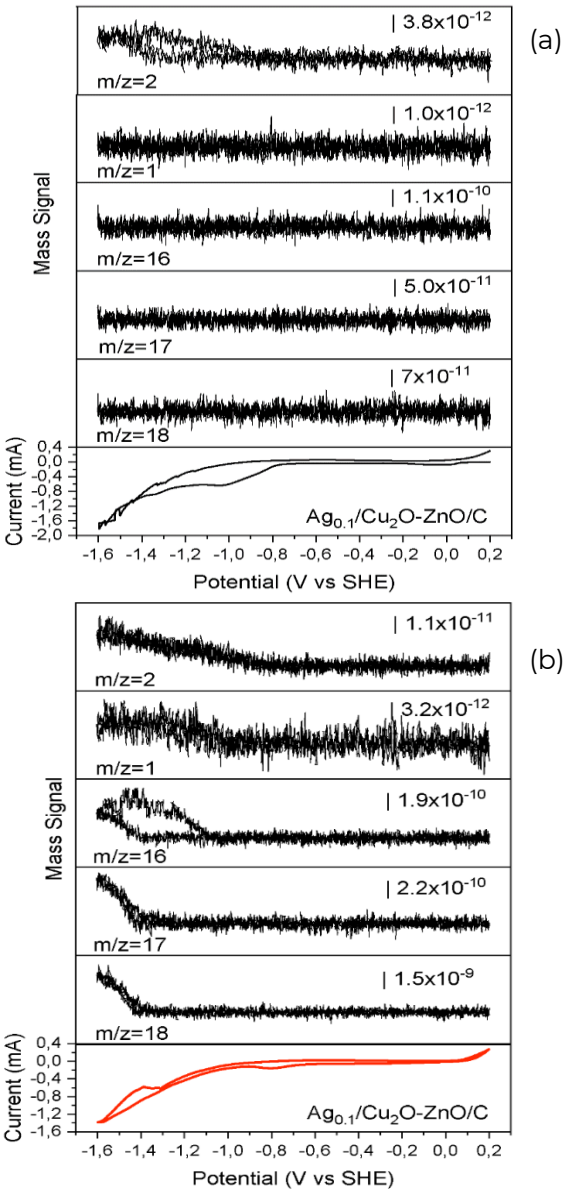

Figure 4. Current-potential characteristics of $Ag_{0.1}/Cu_2O$-ZnO/C in absence (a) and presence (b) of CO_2.

$$CO_2 + 8H^+ + 8e^- \leftrightarrow CH_4 + 2H_2O \qquad \text{Eq. (3)}$$

Therefore, it is demonstrated that the electrocatalyst is highly selective towards hydrogen and methane during CO_2RR.

4. CONCLUSIONS

In conclusion, XRD analysis confirmed the correct synthesis of $Ag_{0.1}/Cu_2O$-ZnO by indexing the crystalline planes of metallic Ag, Cu_2O and ZnO, while determining the crystallite size at 23±0.1 nm. SEM analysis revealed the polyhedral and nanoflake morphology of Cu_2O and ZnO, respectively, and EDS analysis confirmed the presence of Ag, Cu, Zn and O elements in the sample. Cyclic voltammetry technique showed cathodic currents of -2.08 mA and -1.91 mA in absence and presence of CO_2, respectively. The chronoamperometry technique showed long-term stability of the electrocatalysts during HER and CO_2RR. Finally, DEMS analysis allowed the identification *in situ* of products generated during CO_2RR, identifying H^+, H_2 and CH_4, which demonstrates that $Ag_{0.1}/Cu_2O$-ZnO/C is highly selective towards the generation of hydrogen and methane.

Acknowledgements

The authors acknowledge the Instituto Politécnico Nacional (Mexico) for the financial support received through project SIP-20240528. The authors gratefully acknowledge Gerardo González Arenas and the CNMN-IPN for the characterization of materials facilities. The authors, M.Á. Soto-Mendoza and C.X. Tirado-Lopez, acknowledge CONAHCYT for a doctorate study fellowship.

Conflicts of Interest

The authors declare no conflict of interest.

REFERENCES

[1]. Intergovernmental Panel on Climate Change (IPCC, 2021). Climate Change 2021: The Physical Science Basis. Contribution of Working Group I to the Sixth Assessment Report. https://www.ipcc.ch/report/ar6/wg1/ Accessed 2 September 2024

[2]. Doney, S. C., Busch, D. S., Cooley, S. R., & Kroeker, K. J. (2020). https://doi.org/10.1146/annurev-environ-012320-083019

[3]. National Aeronautics and Space Administration (NASA, 2024). Retrieved from https://climate.nasa.gov/vital-signs/carbon-dioxide. Accessed 2 September 2024

[4]. National Oceanic and Atmospheric Administration (NOAA, 2023). Recent monthly average Mauna Loa CO_2. https://gml.noaa.gov. Accessed 2 September 2024

[5]. Aresta, M., Dibenedetto, A., Angelini, A. (2020). https://doi.org/10.1021/acs.chemrev.9b00846

[6]. Li, F., Zhang, X., Wang, H. (2021). https://doi.org/10.1021/acs.accounts.1c00264

[7]. Ren, L., Xie, H., He, S., Li, X. (2021). https://doi.org/10.1021/acssuschemeng.0c07343

[8]. Jouny, M., Luc, W., Jiao, F. (2019). https://doi.org/10.1021/acs.iecr.8b05083

[9]. Wang, X., Ji, Y., Zhang, Y., Zhang, Y. (2022). https://doi.org/10.1016/j.jcat.2022.03.028

[10]. Zhao, S., Ye, L., Li, Y. (2022). https://doi.org/10.1016/j.jechem.2021.06.010

[11]. Zhou, Y., Zhang, B., Lin, S. (2023). https://doi.org/10.1039/D3EE00507A

[12]. Lanje, A. S., Sharma, S. J., Pode, R. B. (2010). ISSN No: 0975-7384.

[13]. Zhang, B., Yang, G., Li, C., Huang, K., Wu, J., Hao, S., Huang, Y. (2018). https://doi.org/10.1007/s12274-018-2010-3

94-I-PO BALANCING METHODS FOR DEVELOPING MEDIUM POWER LIPO CELL BATTERY BANKS

C. D. Téllez-Uribe[1]*, R. K. Salgado-Cristobal[1], N. Mondragón-Escamilla[1], I. Araujo-Vargas[1], J. F. Villegas-Alcaraz[2]

[1]Instituto Politécnico Nacional, Escuela Superior de Ingeniería Mecánica y Eléctrica, Unidad Culhuacán, Av. Santa Ana 1000, Col. San Francisco Culhuacán, C.P. 04430 CDMX, México.
[2]Instituto Politécnico Nacional, Unidad Profesional Interdisciplinaria de Ingeniería Campus Guanajuato, Av. Mineral de Valenciana 200, Fraccionamiento Industrial Puerto Interior, C.P. 36275 Silao de la Victoria, Guanajuato, México.

*Correspondence: ctellezu1400@alumno.ipn.mx

Abstract: This work presents the comparison between two balancing methods to validate their implementation in medium power banks, to extend the life of the batteries and their correct operation. Two balancers were developed and tested using two Lithium Polymer (LiPo) cells with a nominal voltage of 7.2 V and 16 Ah connected in series, the active balancer was performed using a DC-DC converter, which works through a peak current control (PCC), this allows to follow the inductor current to reduce or increase the voltage to be shared between a pair of cells. Whereas the passive balancer works with a switching resistor that allows the excess voltage of each battery to be transformed into heat, the resistor being controlled by a microcontroller while balancing the pair of cells. The purpose of comparing the active and passive balancing methods is to obtain the most suitable method for designing, manufacturing and scaling a prototype battery balancer with an electrical power of 5.6 kWh for an 83 kW two-wheeled electric vehicle.

Keywords: Battery Balancer; Active Balancer, DC-DC Converter, Passive Balancer, LiPo cells.

1. INTRODUCTION

At the present the reduction of the carbon footprint is a global issue, and researchers around the world are working to propose solutions to this problem. A clear example of this is the new EURO 5[1] standard, which consists of a series of regulations that set limits for pollutant emissions for internal combustion vehicles and marks a transition period to a more sustainable vehicle fleet. Although it is not a priority in Mexico now, but it is important to reduce carbon emissions, it is evident that we are suffering from important climate changes such as high temperatures and droughts. One solution is to support and develop the path to electromobility, this can be an Electric Vehicle or a hybrid Vehicle.

The Laboratory for Research in Electrical Energy Quality and Conversion (LINC^{2}E^2 in Spanish) [2], in its electromobility research line, developed an 83kW electric motorbike prototype, with certain specifications based on international competitions [3]. The prototype uses a battery bank, built with a series connection of lithium polymer (LiPo) cells, whose electrical characteristics are good in relation to their gravimetric energy density [4]. In addition, the laboratory is developing the ecosystem necessary for the use of an electric vehicle (EV), including the use of a battery charger, which requires a balancing network for each of its cells.

In Figure 1, a block diagram of the battery system developed by the laboratory is shown, as a central element, we have the battery bank, this element lacks a balancer to balance the voltage between all the cells and start charging or discharging from the same point [5], this will allow us to add a protection system that prevents dangerous conditions, such as short circuits, overloads and overheating, as well as maximizing its correct operation, extending its useful life and making correct use of energy [6,7].

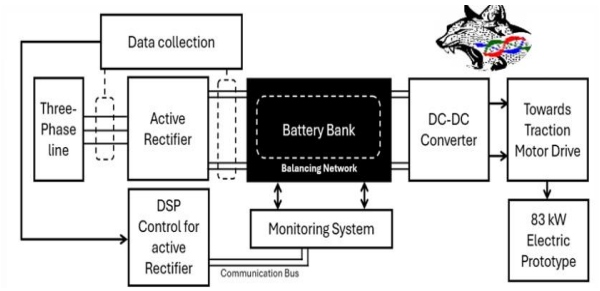

Figure 1. Block diagram of the battery system under development in the LINC²E² laboratory.

The main objective of performing a comparative evaluation on physical systems of LiPo cell battery banks is to select the most suitable balancing method for medium power operation and to support researchers who are considering the use of these balancing strategies. The technical specifications of the LiPo cells used in the development and construction of both balancers are shown in Table 1.

Table 1. Technical Specifications of a LiPo Cell.

Characteristics	**Specifications**
Nominal Voltage	3.7 V
Minimum Operating Voltage	2.75 V
Maximum Operating Voltage	4.23 V
Storage Voltage	3.8 V
Nominal Capacity	16 Ah 0.2C discharge
Internal Impedance	≤ 30mΩ
Cell Weight	200 g
Dimensions	Overall dimensions (W x H x D) 70mm x 162mm x 11mm
Charge	Standard Charge 4.8 h Rapid Charge 2.5 h

The importance of developing this type of technology that is complementary to the main branch of electromobility is paramount as batteries need to be protected and maintained in optimal condition, if they are damaged and disposed of quickly, one would have to wonder whether we would really have a sustainable method for the environment. In addition, it helps with alternatives to traditional fuels and is able to create and manufacture such devices.

2. MATERIALS AND METHODS

A battery balancer, in simple terms, is an electronic device that equalizes the voltage of all cells present in a battery bank (regardless of the number of cells) to start charging or discharging the batteries. It does this by two methods, passive and active.

Figure 2 shows the natural tendency of batteries to have different voltages, this may be due to manufacturing problems, accuracy of the charging equipment, etc. The first method is Passive Balancing, this consists of a resistor that transforms excess electrical energy into heat, the disadvantage is that, if there is a big voltage difference, a lot of energy will be wasted and a lot of heat will be produced as shown in the figure. The second method is Active Balancing, which consists of moving the excess energy between the cells by averaging them, the main problem is that having a larger number of cells makes the process more complex and time consuming.

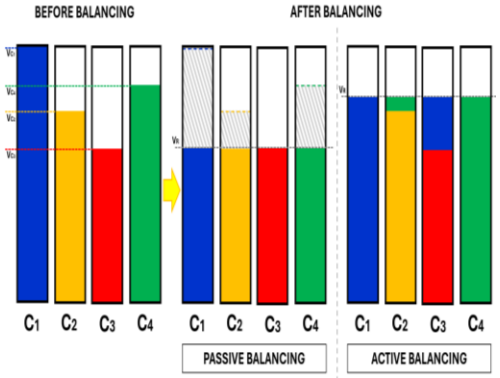

Figure 2. Balancing Methods.

2.1 ACTIVE BALANCER PROPOSAL

An active balancer is an electronic device that allows to move the excess energy from one cell to another with lower voltage, achieving an average balance between them. The active proposal consists of assembling a Buck-Boost Direct (B-B-D) converter, to carry out the balancing [8], which shall be controlled by a peak-current control (PCC) circuit, as shown below.

2.1.1. Buck-Boost Converter Proposed Circuit

Figure 3 shows the proposed circuit diagram, showing two LiPo batteries mounted at the ends of the Direct Buck-Boost converter, with two switching branches and an inductor mounted between the switchover branches and the batteries, removing the charging resistor and capacitor from the B-B-D conventional converter. Furthermore, the PCC control circuit is shown and from where it obtains the inductor current signal.

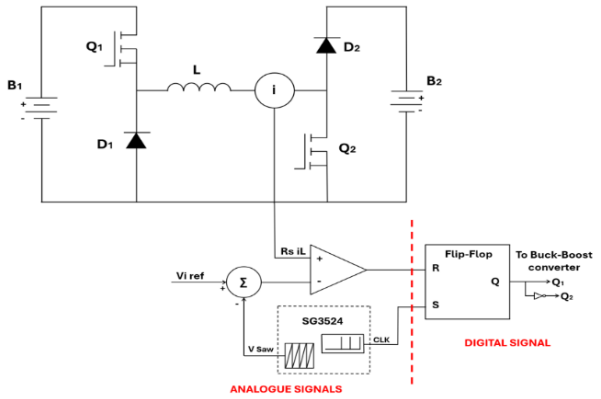

Figure 3. Direct Buck-Boost circuit with PCC.

The circuit works in two sections, the part of the digital signals and the analogue signals, starting with the analogue signals, it is important to mention a fundamental element, this is the integrated circuit SG3524, which is in charge of setting the switching frequency with which the converter will work, the Vsaw ramp and the clock, which will be the Set of the control circuit. In addition, it is used TL084 as an amplifier and conditioner for certain signals.

As it is a current control, it is very important to define which current is the most convenient for the control, this signal is called RS IL, as it is the current waveform in terms of voltage using a current shunt to obtain the signal. Using that waveform and the subtraction of Viref-Vsaw by means of a comparison with the circuit LM311, to obtain the current follower. From this comparator the Reset of the circuit is also obtained, this is the point between the digital signals with the analogue ones. Finally, a flip-flop Set-Reset was constructed using a logic gate NOR (74LS02) where the previous signals enter their respective pin to finally have an output Q, this being a 100% digital signal that will control the converter, this will vary according to the other signals of the analogue process based on the voltage of the pair of cells connected.

2.1.2. Buck-Boost Converter Prototype

The prototype was made by means of two GaN E-HEMT system boards and its daughter board GS66508T, this is a board that allows us to evaluate and validate various types of circuits, such as various types of converters, as it has a switching branch attached to it. To form a B-B-D converter it's necessary to have two transistors and two diodes, with each GaN board it's possible to configure a transistor and a diode so that's the reason to use two boards. The inductor, according to the diagram, should be between the batteries and the switching branches, as it is a board used to validate several circuits, it is not possible to see this arrangement graphically, but according to the GAN SYSTEMS datasheet [9], it should be mounted on the "Con 1" pin of both boards. At the output of the inductor, the 0.1Ω resistor was placed as a current shunt, which will be used to obtain the current signal in terms of

voltage to be used for control as shown in Figure 4.

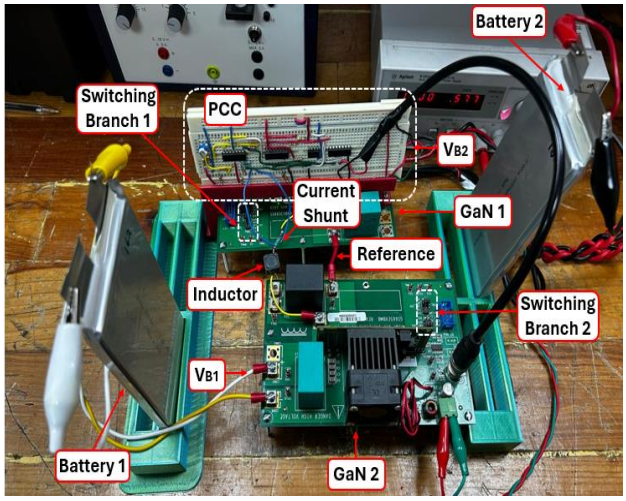

Figure 4. Buck Boost converter prototype rig.

2.2. PASSIVE BALANCER PROPOSAL.

A passive balancer is an electronic device that allows the excess energy to be removed from each cell with respect to the lower voltage cell, transforming into heat, achieving a voltage balance in each cell.

The proposal of this balancer is based on the switching resistance method, it is less complex than an active balancer because the elements that make it up are simpler and easier to use, and it also represents lower manufacturing costs compared to the elaboration of a CD-DC converter.

In Figure 5, a block diagram of the elements present in the passive balancer is shown. A pair of cells were used, to which were connected in parallel voltage sensors, the program takes these analogue voltage signals and transforms them into a digital signal, which will serve to activate or turn off the relay. The circuit that contains the discharge resistor is coupled to the relay module, opening or closing the passage according to the voltage signal of each battery, which by means of a cycle while it will allow transforming the excess voltage into heat until it reaches the balance between cells, ending up in the Passive Balancer Plate.

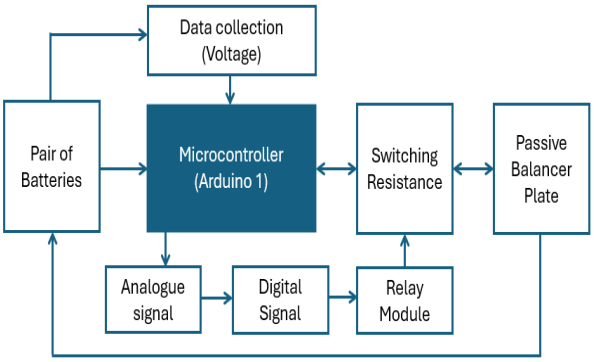

Figure 5. Block Diagram of the Passive Balancer.

The voltage Sensor is the FZ0430, and is intended to work with the Arduino ecosystem, that works with voltages lower than 5 V, the sensor uses a voltage divider to measure voltages up to 25 V, this can be calculated with Eq. (1).

$$V_{cc} = (V_S)(\frac{R_1 + R_2}{R_2}) \qquad \text{Eq. (1)}$$

The balancer code provides Eq. (1) to be able to measure the battery voltage and use this value to process the analogue to digital signal and perform the resistor switching.

The passive balancer connection diagram shows in Figure 6, the Arduino controller, a 3D model of a base that contains the pair of cells, two voltage sensors that are connected to the analogue pins and two digital pin outputs that go to the 4-relay module, they are interconnected to the passive balancer plate. Additionally, an OLED display was added to show the voltage in real time of the balancing process.

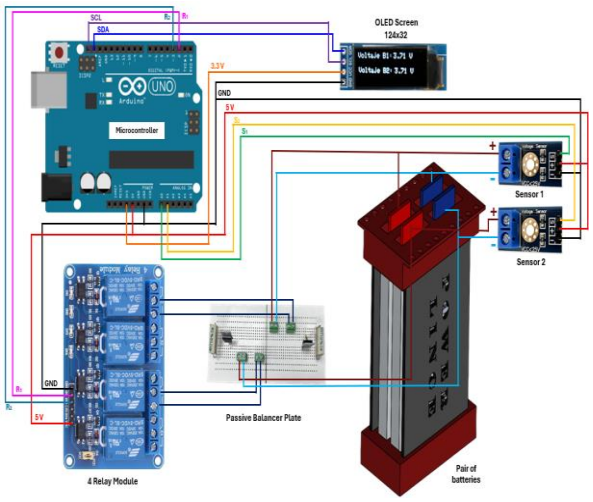

Figure 6. Connection Diagram of the passive balancer.

2.2.1. Proposed Circuit

Figure 7 shows the prototype of the passive balancer for two cells connected in series. This was made with an Arduino UNO, a Relay module, and a PCB board was manufactured with the switching resistor circuit, the selected resistor was 4.7Ω 5 W, to discharge the battery to just under 1 A. Finally, the OLED display is shown with the real time voltages of each cell.

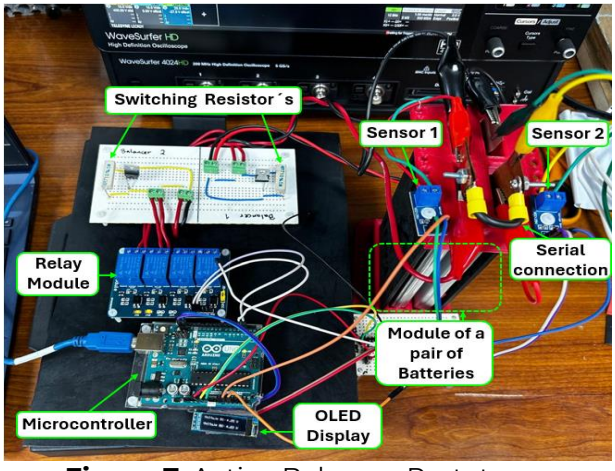

Figure 7. Active Balancer Prototype.

3. RESULTS AND DISCUSSION

3.1 Active Balancer Results

For the waveforms shown in Figure 8 a roll type data acquisition was set up on the oscilloscope, with a 2000 seconds per division scale and a voltage scale of 200 mV per division with a central approach at 4 V. The initial conditions for battery one was 4.101 V (blue signal) and for battery two were 3.902 V (red signal) as shown in the figure below. It is important to note that the VB1 signal has an increasing trend, that is battery one was charged, while the VB2 signal has a downward trend, battery two was discharged, so that both could come to balance with a final voltage of 4.0 V.

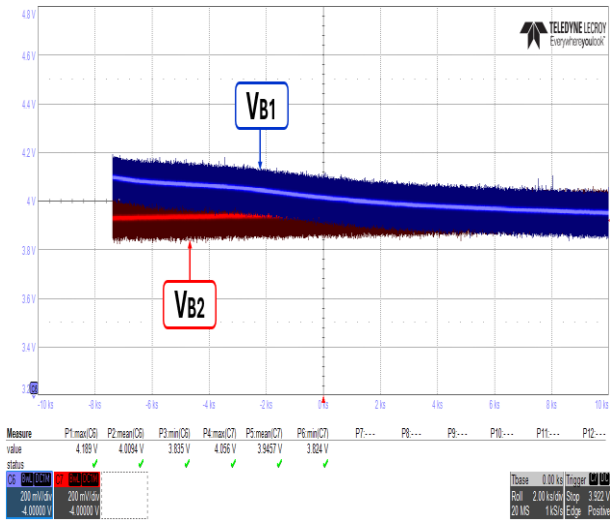

Figure 8. Active Balancing Experimental Waveforms**.**

The results of the active balancer, was achieved in a balancing time of 8 divisions plus one half and one quarter of the next division, giving a time in seconds of 17 250 seconds, this time in hours is equal to 4.8 with an approximate current of 0.36 A.

3.2 Passive Balancer Results

For the passive balancer waveforms, Figure 9 shows the downward trend of both signals, this means that both batteries were discharged, the initial conditions of battery one was 4.20 V (yellow signal) and battery two 4.18 V (green signal), achieving the balancing

of both cells with a final voltage of 3.8 V, trying to recreate the storage condition for these cells.

A roll type data acquisition was configured in the Lecroy, with a scale of 1000 seconds per division and a voltage scale of 200 mV. The results of the Passive balancing of this pair of cells were achieved in 9 divisions plus four-fifths of the last division, giving a time in seconds of 9 800 seconds, this time in hours is equal to 2.7 with an approximate current of 0.9 A.

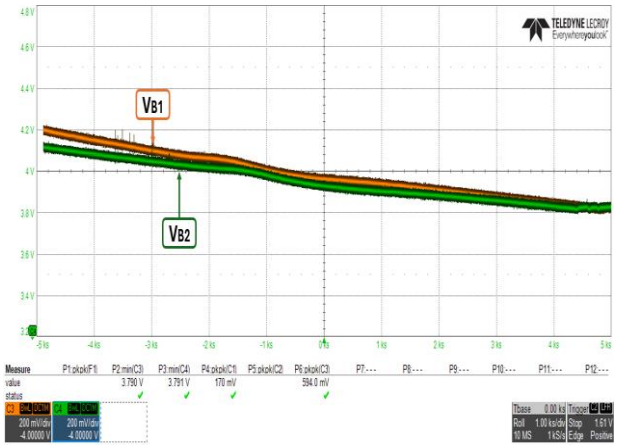

Figure 9. Passive Balancing Experimental Waveforms**.**

3.3 Comparatives Results

For the comparison process between the balancers, the final passive balancing voltage was set at 3.8 V (to emulate the storage mode of the battery) while for the active balancer a final voltage of 4 V was set as the average of two batteries. It should be noted that it was decided to balance a higher voltage difference in the passive, as it is faster to realise, because it does not move energy, but only transforms it into heat based on the Joule effect.

Table 2 shows the operating conditions of both prototypes. In the first section of the table the shared parameters are presented, showing the voltage difference of both batteries in each balancing process. The second part of the table shows the specific parameters for each balancing method and is marked with N/A for the non-balancing counterpart. The last part of the table shows three main things: the balancing current used in each test, the time it took to equalise the voltages in each battery and, finally, the cost of manufacturing the prototype.

Table 2. Operating Conditions of Each Balancer and Comparatives Results.

Shared parameter	**Active balancer**	**Passive balancer**
Initial Voltage Conditions of Each Battery	Battery 1= 4.101 V Battery 2= 3.902 V	Battery 1= 4.20 V Battery 2= 4.18 V
Final Voltage of Both Batteries After Balancing Process	4 V	3.8 V
Power supply	12 V for the converter +12 V and -12V for the PCC	5 V and 3.3 V for the microcontroller
Independent Parameter	Active Balancer	Passive Balancer
Switching frequency (F)	50 kHz	N/A
Duty Cycle	Established by PCC	N/A
Switching Resistance	N/A	4.7 Ω
RESULTS	Active Balancer	Passive Balancer
Balancing Current	0.36 A	0.9 A
Balancing time	4.8 hours	2.7 Hrs.
Manufacturing Costs	$ 230 USD	$ 110 USD

4. CONCLUSIONS

As a conclusion, after the fabrication and comparison of these two balancers, there is .6a winning tendency towards the passive balancer as it was easier and cheaper to build, it also obtained a shorter balancing time, making a difference of 2.1hrs, with a higher voltage difference and a saving of $120 USD compared to his active opponent. It is therefore concluded that the most appropriate method to scale to the medium power ratings required by the LINC²E² laboratory (5. 6 kWh) is the passive strategy,

emphasizing that for this balancer to work better, a thermal study of the heat dissipation for the resistors must be carried out for a greater number of cells. Also, to extrapolate the model it is proposed to use a microcontroller with a larger processor, make an HMI interface on a touch display and take the operation of the passive balancer to increase the number of cells and achieve working with medium power battery banks.

Conflicts of Interest

The authors declare no conflict of interest.

REFERENCES

[1] G. Fontaras, V. Franco, P. Dilara, G. Martini, & U. Manfredi; (2014). https://doi.org/10.1016/j.scitotenv.2013.09.043

[2] Laboratorio de Investigación en Calidad y Conversión de la Energía Eléctrica, "LINC²E²" (2024), https://linc2e2.wordpress.com/

[3] MotoStudent Organization: "VIII MotoStudent Competition: Administrative and Technical Regulations", Rev. 1, February 2024.

[4] Torrejón Pérez, C.: "Diseño de un pack de baterías para motocicletas eléctricas", Master's tesis, Universidad Carlos III Madrid Escuela Politécnica superior, 2010.

[5] J. Cao, N. Schofield & A. Emadi: "Battery balancing methods: A comprehensive review," IEEE Vehicle Power and Propulsion Conference, pp. 1-6, September 2008. https://doi.org/10.1109/VPPC.2008.4677669

[6] F. Baronti, G. Fantechi, E. Leonardi, R. Roncella, & R. Saletti, IEEE Vehicle Power and Propulsion Conference, pp. 1-6, 2011. https://doi.org/10.1109/VPPC.2011.6043074

[7] A. Ziegler, D. Oeser, B. Arndt & A. Ackva, (CANDO-EPE), pp. 000015-000020, 2018. https://doi.org/10.1109/CANDO-EPE.2018.8601165

[8] A. Kelkar, Y. Dasari, & S. S. Williamson, IEEE (PESGRE2020), pp. 1-6 January 2020. https://doi.org/10.1109/PESGRE45664.2020.9070666

[9] GaN Systems Inc: "650V GaN-HEMT Evaluation Board User's Guide" 2018, www.gansystems.com

95-I-PO DEVELOPMENT OF A HYBRID BALANCING METHOD FOR POSSIBLE APPLICATION IN AN 11.2 KWH LIPO BATTERY BANK

R. K. Salgado-Cristobal[1]*, C. D. Téllez-Uribe[1], N. Mondragón-Escamilla[1], I. Araujo-Vargas[1], S. Pérez-Rodríguez[2]

[1]Instituto Politécnico Nacional, Escuela Superior de Ingeniería Mecánica y Eléctrica, Unidad Culhuacán, Av. Santa Ana 1000, Col. San Francisco Culhuacán, C.P. 04430 CDMX, México.
[2]Instituto Politécnico Nacional, Centro Interdisciplinario de Investigaciones y Estudios sobre Medio Ambiente y Desarrollo, Av. Luis Enrique Erro S/N, Unidad Profesional Adolfo López Mateos, Zacatenco, C.P. 07738 CDMX, México.

*Correspondence: salgado.karina25@gmail.com

Abstract: This paper describes the development of a hybrid balancing method to improve energy storage for possible application an 11.2 kWh lithium polymer battery bank using a DC-DC buck-boost converter. In recent decades, the growth of the electric vehicle industry and storage systems has increased the demand for these batteries, appreciated for their high energy density, long lifetime and low self-discharge. However, the charge imbalance between individual cells represents a significant challenge that can affect their performance and longevity. The proposed method employs peak current control (PCC) to achieve efficient balancing. Waveforms of a balancing of two 16 Ah LiPo cells and nominal voltage of 3.7 V per cell were analysed to demonstrate its effectiveness. Experimental results validate this hybrid approach, highlighting its ability to improve battery bank performance and lifetime

Keywords: DC-CD Buck-boost converter, LiPo Cells, Peak current control, Battery balancer.

1. INTRODUCTION

Electrochemical energy storage systems, such as rechargeable batteries, are popular for their cost and effectiveness, noted for their high energy density, efficiency, long life cycles and fast responsiveness. Lithium batteries are preferred in applications such as portable electronics and electric vehicles because of their high energy density [1]. There are different types of lithium batteries, differentiated by the type of electrolyte: liquid and polymeric. Liquid electrolyte batteries are more prone to problems such as short circuits and fires due to the formation of dendrites [2]. In contrast, polymer electrolyte batteries are safer, with higher thermal stability and better ability to suppress dendrite growth. This research focuses on batteries with polymer electrolyte [3]. Battery banks, consisting of cells connected in series or parallel, face challenges, mainly state-of-charge (SOC) imbalance of the cells, which can reduce the performance and lifetime of the system [4]. To solve this problem, battery balancing techniques are used (Figure

1), such as passive balancing, which uses discharge resistors and is easy to implement, but has low energy efficiency and is time consuming. Active balancing, which uses electronic circuits to redistribute the load more efficiently, is faster but is expensive and requires complex algorithms [5-8].

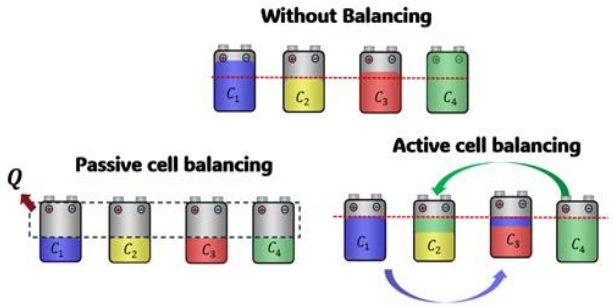

Figure 1. Cell balancing techniques.

The hybrid battery balancer model combines the best of both techniques, using a buck-boost DC-DC converter to achieve efficient cell balancing, improve performance and extend the lifetime of lithium batteries in energy storage systems and electric vehicles, overcoming the limitations of traditional methods and adapting to different applications.

2. INTENDED ELECTRIC VEHICLE

An 83 kW Electric Vehicle (EV) has been developed at the Research Laboratory of Quality and Power Conversion (LINC^{2}E^2 in Spanish), [9] This EV (Figure 2-(a)) integrates a 11.2 kWh lithium Polymer (LiPo) battery bank, as depicted in Figure 2-(b). A block diagram of the electric power train is shown in Figure 3, where the balancing network is highlighted on the left-hand side of the battery block. The research at LINC^{2}E^2 explores various balancing strategies, focusing on a novel hybrid methodology to optimize performance.

Figure 2. Photograph of (a) 83 kW Electric Sport Motorbike (b) Battery Bank at LINC^{2}E^2.

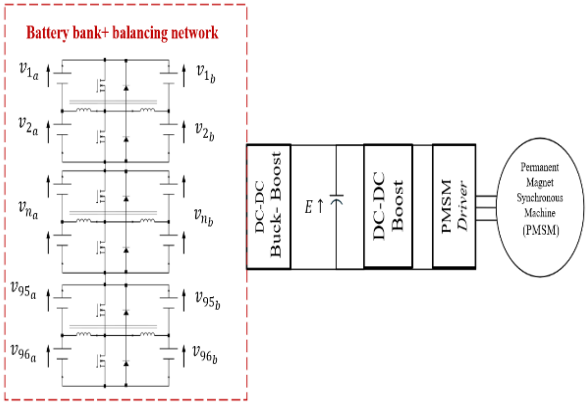

Figure 3. Block Diagram of the Drive Train.

3. BATTERY HYBRID BALANCING SYSTEM

3.1. Cell Balancing Circuit

Figure 4 shows the proposed design for a Buck-Boost DC-DC converter. The power stage has two switching branches, each with four cells that have a nominal voltage of 3.5 V to 3.7 V. The cells are arranged in a series-parallel configuration: each branch contains two LiPo cells connected in series, and the two branches are connected in parallel. Specifically, branch 'a' includes cells V_{1a} and V_{2a} connected in series, while branch 'b' includes cells V_{1b} and V_{2b}.

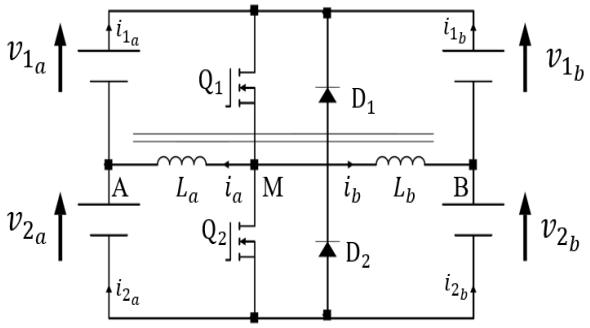

Figure 4. Electric diagram of the hybrid balancing circuit.

Alternatively, the system can also be analysed using just the series connection, that is, branch 'a'. The control of these switching branches is managed by the transistors, which operate in a complementary way: when Q_1 is on, Q_2 is off. This configuration is considered the active part of the balancer.

3.2. Passive topology

The purpose of passive topology in the balancers is to remove excess energy in the cells through heat, the use of a coupled inductor was chosen to avoid the waste of this energy by storing it through this. This inductor is shown in Figure 4 at the AMB nodes. Using Faraday's law, we have that the current flowing through an inductor is:

$$\boldsymbol{i = \frac{1}{L}\int V_L dt} \qquad \text{Eq. (1)}$$

Therefore, the inductor current at node AM is:

$$\boldsymbol{i_a = \frac{1}{L_a}\int V_{L_a} dt} \qquad \text{Eq. (2)}$$

And the inductor current MB is:

$$\boldsymbol{i_b = \frac{1}{L_b}\int V_{L_b} dt} \qquad \text{Eq. (3)}$$

However, being a coupled inductor, the individual control of these inductors is simplified instead of having to control four transistors, the control of two transistors is used and finally the current that charges or discharges the batteries is given by:

$$\boldsymbol{i_{dif} = i_a - i_b} \qquad \text{Eq. (4)}$$

The direction of loading or unloading is a function of the duty cycle (D).

$$\boldsymbol{D = \frac{v_{a_2}}{v_{a_1} + v_{a_2}}} \qquad \text{Eq. (4)}$$

Defined $D = f(v_{a1}, v_{a2})$

Finally, in Figure 5 we can observe two transistors Q_1 and Q_2 respectively which work in two modes of operation; for mode 1 we have that Q_1= ON directs i_{dif} to the top and charges $cell_{1a}$ and $Cell_{2a}$ as show in Figure 5-(a) and for mode 2 we have the complementary behaviour when Q_2= ON (Figure 5-(b)).

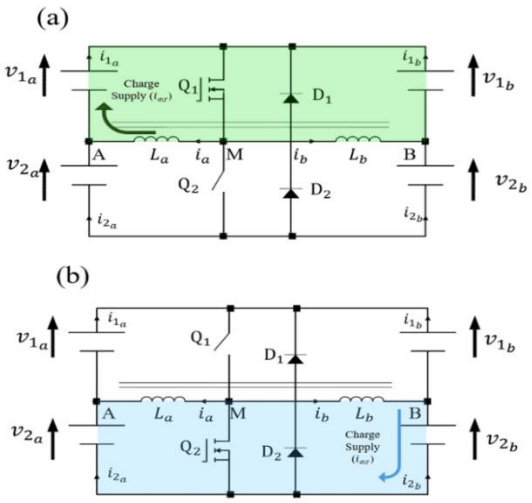

Figure 5. Differential currents.

4. Peak current control (Active topology)

During the development of this research, one of the challenges was the adjustment of the duty cycle, since the DC-DC converters are governed by the input and output voltages: $D = f(v_{1a}, v_{2a})$.When incorporating batteries with a factory-established nominal voltage, a control mechanism is needed to regulate the duty cycle. To achieve this adjustment, as observed in Section 3, the differential current plays a key role in the charging and discharging processes. Consequently, peak current control (PCC) was selected as the method for managing these processes. Research indicates that PCC is crucial for controlling the pulse width of the PWM modulator through the inductor. This method focuses on monitoring the current flowing through the inductor during each switching cycle. When the current reaches a predetermined maximum level, the PWM controller automatically adjusts the duty cycle, which helps optimize the energy efficiency of the converter.

Figure 6. Shows the hybrid balancer circuit, where the PCC was adapted, this circuit starts with the measurement of current passing in the inductor which this signal one passing through an amplifier, the other signal passing in the amplifier is the result of the comparator of an adjustable reference V_{iref}, with V_{saw} which is a reference signal. The output of this amplifier is the RESET input of a flip-flop (FF). For the SET signal required by FF, a Clock signal is used for the synchronization and precise coordination of the operations in the FF digital system to finally obtain the required Q_1 output.

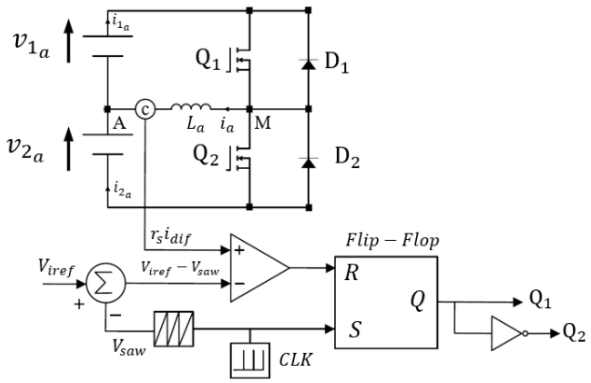

Figure 6. Electric diagram of the hybrid balancing circuit and implementation of PCC.

The ideal waveforms of the PCC are shown in Figure 7. During the DT period, the instant when the SET and RESET are activated is observed. This is a comparison process based on the position of V_{iref}, which moves according to the measured current i_{dif}. Finally, this process results in the pulse width modulation (PWM) signal Q_1.

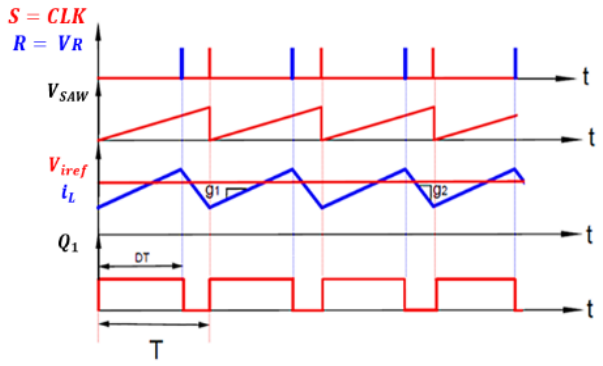

Figure 7. Ideal waveforms of PCC.

4.1. Prototype

The PCC circuit was coupled with the hybrid buck-boost configuration of two cells [10] connected in series, that is, the 'a' branch. This configuration was specifically chosen to verify the proposed waveforms, given the availability of such cells in the laboratory for this study. The Buck-boost circuit was performed on a GaN E-HEMT system DC-DC converter test board and daughter board GS66508T because they have a built-in switching branch on the board as shown in Figure 8. The inductor L_a is connected between the switching branch (Node M) and the cells connected in series (Node A). In this case, i_{dif} is equal to i_a. This inductor was selected based on the need to have a current ripple (ΔI_l) of 5% of the standard charge [11], based on the following equation:

$$\Delta I_L = g_1 = \frac{V_{1a} DT}{L} \qquad \text{Eq. (5)}$$

The inductor is connected in series to a resistor r_s=0.1 Ω, as a current shunt was designed to measure the inductor current in terms of voltage. The PCC circuit was initially built on a protoboard to test its functionality before moving on to a printed circuit board. To obtain the Flip-Flop RESET signal, a TL084 amplifier was used. The comparison of V_{iref} and the V_{saw} was performed using an LM311. The Clock and V_{saw} signals were generated with an SG3524, which also set the switching frequency to 50 kHz according to the manufacturer's specifications. Finally, the flip-flop was implemented using an SN74LS02N gate.

Additionally, the development of a second control loop for the V_{iref} signal is still in progress, aimed at enabling automatic adjustment to respond to transient variations.

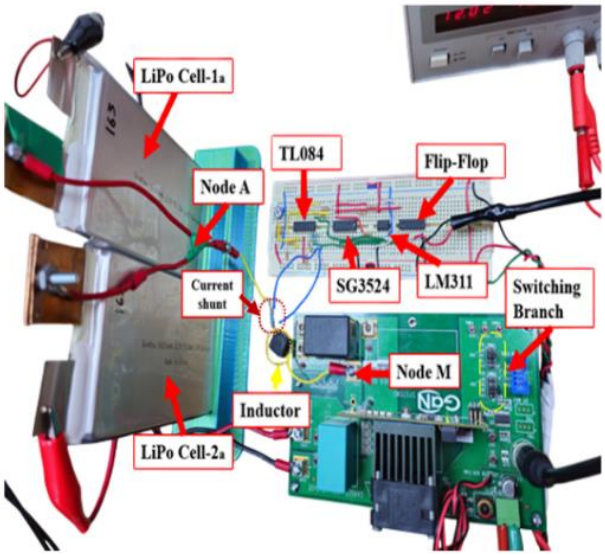

Figure 8. Hybrid balancing prototype.

5. EXPERIMENTAL RESULTS

The results shown in Figure 9 correspond to the balancing process of the two cells connected in series configuration described in section 4.1. These measurements include a roller data capture of 16 ks (1.00ks/div) and two cells where at the beginning Cell1a (yellow signal, 200 mV/div, -4 V offset) starts with a load of 3.958 V and Cell2a (Pink signal 200 mV/div, -4 V offset) with 3.824 V, After some time, the hybrid circuit equalizes the voltages of both cells to 3.922 V.

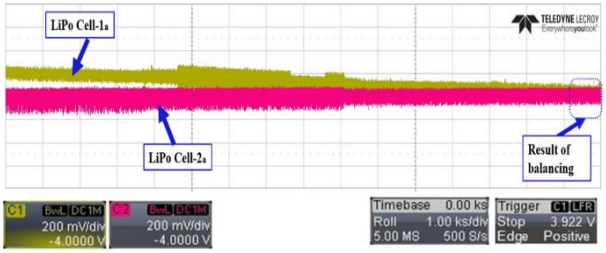

Figure 9. Balancing of two LiPo Cells using the hybrid configuration connection.

Figure 10 shows the experimental results obtained from the oscilloscope which are the corresponding results of the PCC. These are divided into two plots for better visualization. The upper part shows: (a)V_{saw} (Pink signal, with a scale of 2 V/div and an offset of 2.85V); the results of (b)V_{iref}-V_{saw} correspond to the cyan signal (200 mV/div and offset -365 mV); the most important result of this upper plot is the (c) $r_s i_{dif}$ which is the measurement of the current shunt corresponding to the Navy blue signal (50 mV/div and offset 136 mV); and finally to corroborate the result of the shunt, the current measurement was made by using the (d) oscilloscope probe current signal (Orange signal 100 mA/div, offset 241.5 mA).

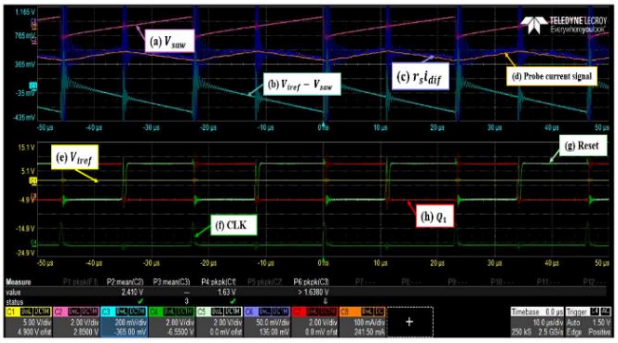

Figure 10. Experimental waveforms result of PCC.

Analysing the signals of the lower plot we have as the first signal (e) Viref (yellow signal, scale of 5 V/div and an offset of 4.9 V); (f) The CLK signal corresponds to green colour (2 V/div and an offset of -6.55 V); (g) The RESET signal corresponds to turquoise colour (2 V/div, 0. mV offset); Finally the most important signal of this plot is the output is (h) Q1 red signal (2 V/div and 0 mV offset).

Figure 11 illustrates the operation of the transistors, where it is verified that they operate complementarily without causing any short circuits. Q1 is the pink signal, 2 V/div, 0 offset and Q2 is the yellow signal 5 V/div, 0 offset.

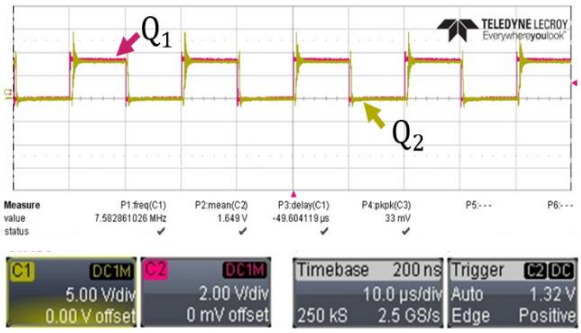

Figure 11. Results of switching transistors.

6. CONCLUSIONS

The experimental results validate the objective of the hybrid balancing circuit as it does manage to equalise the energy in the cells. However, to obtain a shorter balancing time, the current flowing through the inductor needs to be increased, for which a new numerical study is proposed where the inductor reaches the maximum load current of the cells established by the manufacturer. The experimental results for the PCC are presented, validating the ideal waveforms proposed in Section 4. Future work will involve designing a printed circuit board (PCB) to filter the signals by reducing the distances between connections.

Conflicts of Interest

The authors declare no conflict of interest.

REFERENCES

[1] Landi BJ, Ganter MJ, Cress CD, DiLeo RA, Raffaelle RP. Carbon nanotubes for lithium-ion batteries. Energy Environ Sci. 2009;2(6):621–628. https://doi.org/10.1039/b906623f

[2] Sanjinés Zeballos R. El oro blanco de los Andes: Paradigmas de la minería e industrialización de litio en Bolivia. 1st ed. 2022.

[3] Li J, et al. Polymers in lithium-ion and lithium metal batteries. Adv Energy Mater. 2021;11 (15): 2003239. https://doi.org/10.1002/aenm.202003239

[4] Altaf F, Johannesson L, Egardt B. Simultaneous thermal and state-of-charge balancing of batteries: A review. In: Proceedings of the 2014 IEEE Vehicle Power and Propulsion Conference; Oct 2014; pp. 1-7.

[5] Kim, J., & Kowal, J.: 'Development of a Matlab/Simulink Model forMonitoring Cell State-of-Health and State-of-Charge via Impedance ofLithium-Ion Battery Cells. Batteries', 2022,8(2), 8. https://doi.org/10.3390/batteries8020008

[6] Vulligaddala, V. B., Vernekar, S., Singamla, S., et al.: 'A 7-cell, stackable,li-ion monitoring and active/passive balancing IC with in-built cell balancing switches for electric and hybrid vehicles', IEEE Transactions on Industrial Informatics, 2019, 16(5), 3335-3344. https://doi.org/10.1109/TII.2019.2916469

[7] Hemavathi, S: 'Overview of cell balancing methods for Li-ion battery technology', Energy storage, 2021, 3(2), e203., pp. 2-9. https://doi.org/10.1002/est2.203

[8] Lee, Y., Jeon, S., & Bae, S.: 'Comparison on cell balancing methods for energy storage applications', Indian Journal of Science and Technology, 2016, pp. 2-6

[9] Laboratorio de Investigación en Calidad y Conversión de la Energía Eléctrica, "LINC²E²", https://linc2e2.wordpress.com/, Accessed February 15, 2024.

[10] Shenzen Grepow Battery CO., LTD, 'Grepow's Testing Criterion for Lithium Polymer Battery', 2020

[11] A. S. Aziz and R. N. Ali, Design of a Non-Ideal Buck Converter, 2016.

114-I-PO A COMPREHENSIVE CHARACTERIZATION PROTOCOL FOR PEM ELECTROLYZERS USING ELECTROCHEMICAL IMPEDANCE SPECTROSCOPY AND POLARIZATION CURVES

R. Montoya González[1,2]*, R. G. González Huerta[2], M. L. Hernández Pichardo[1], J. M. Sandoval Pineda[3], J. L. Reyes Rodríguez[2].

[1]Instituto Politécnico Nacional, Escuela Superior de Ingeniería Química e Industrias Extractivas, Laboratorio de Nanomateriales Sustentables, UPALM, Av. Luis Enrique Erro S/N, Unidad Profesional Adolfo López Mateos, Zacatenco, C.P. 07738 CDMX, México.
[2]Instituto Politécnico Nacional, Escuela Superior de Ingeniería Química e Industrias Extractivas, Laboratorio de Electroquímica y Corrosión, UPALM, Zacatenco, Av. Luis Enrique Erro S/N, Unidad Profesional Adolfo López Mateos, Zacatenco, C.P. 07738 CDMX, México.
[3]Instituto Politécnico Nacional, Escuela Superior de Ingeniería Mecánica y Eléctrica, Unidad Azcapotzalco, Sección de Estudios de Posgrado e Investigación, Av. de las Granjas 682, Col. Santa Catarina, CP 02250 CDMX, México.

*Correspondence: richy.mg95@gmail.com

Abstract: The transition to clean energy sources is a critical global challenge. Hydrogen, a versatile energy carrier, offers a promising solution. Proton exchange membrane (PEM) electrolyzers are a key technology for producing hydrogen efficiently. However, the high cost and limited availability of noble metal catalysts, such as Ir/Ru for the anode and Pt for the cathode, hinder widespread adoption. To address this challenge, it is imperative to explore and validate alternative materials under real-world operating conditions.

This work presents a comprehensive characterization protocol for PEM electrolyzers, encompassing operational parameters, data acquisition, and analysis techniques. Polarization curves and electrochemical impedance spectroscopy are employed as diagnostic tools to assess performance and identify potential limitations.

Keywords: PEM, Hydrogen, electrochemistry.

1. INTRODUCTION

There is a growing global energy demand, which is estimated to increase between 20 and 50% by 2050 [1]. This increase will also be drastically reflected in greenhouse gas (GHG) emissions, since in 2016 73.2% of GHG emissions were due to the energy sector [2]. Given the above, the environmental impact of power generation and the projected increase in its demand, it is essential to achieve a viable energy transition to mitigate the environmental effects that this may cause. Hydrogen has been a source of attention in recent decades as an attractive solution for energy generation and storage, however, only 4% of the hydrogen generated in the world comes from renewable energy (green hydrogen) [3], this is mainly due to the low competitiveness of renewable energy costs and investment in generation equipment. One of the most studied and striking technologies to produce green hydrogen is proton exchange membrane electrolysis (PEM), whose main advantage is its rapid response (3-5 s) to power changes, something typical in generation systems. of renewable energies, which makes them optimal for their coupling to these. On the other hand, PEM electrolysers have as their main drawback the high costs of their components, 38% of the cost of the membrane electrode assembly (MEA) is due to

the noble metals used as catalysts [1,4]. MEA is typically conformed of a protonic exchange membrane with noble metals as electrocatalysts. On the anode it has a mixture of IrO_2 and RuO_2, where the oxygen evolution reaction takes place. On the cathode Pt is used to catalyze the hydrogen evolution reaction. This has led to the search for new alternatives to replace noble metals without sacrificing the performance and useful life of the system, while reducing costs and environmental impact. Some of the most promising materials to replace Pt as catalysts for HER are transition metal dicalcogenides such as MoS_2 [5], $NiOS_x$ [6] or VS_2 [7].

To study the effect of using non noble electrocatalysts in real life conditions, a 5 cm^2 PEM electrolyzers, which design and manufactured in ESIME Azcapotzalco by our work group [8], was used to develop an electrocatalysts full-cell characterization protocol. Polarization curves and electrochemical impedance spectroscopy are employed as diagnostic tools to assess performance and identify potential limitations. This will help future material characterization in both, anodic and cathodic reactions, in real life operation conditions.

2. MATERIALS AND METHODS

2.1 Membrane electrode assembly (MEA) preparation.

Nafion® 115 was selected for the membranes. Membranes were previously adequate with a series of rinses made with H_2SO_4, H_2O_2 and deionized (DI) water at 80 °C and then they were stored in DI water for its prior use. On one side, a mixture of 25% of IrO_2 and 75 % of RuO_2 (Ir/Ru) was selected for the anodic reaction (AR) provided by Sigma Aldrich. On the other side, 40 % weight Pt/C mesh was used for the cathodic reaction (CR) bought from Fuel Cell Store.

Catalytic ink was prepared with 10 mg of Ir/Ru, 1.2 mL of DI water, 1.2 mL of isopropanol and 67 uL of Nafion. This was applied to the membrane using air spraying on one side of membrane. At the other side, the Pt/C mesh was sintered at 120 °C and 100 bar for 3 minutes with a hydraulic press. In Figure 1 the final membrane with both catalysts is shown.

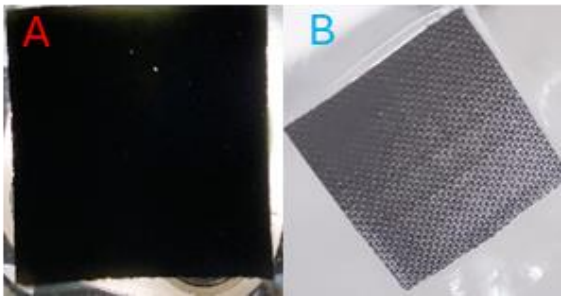

Figure 1. MEA with a 5 cm^2 active area **A.** Membrane on the anode side. **B**. Membrane on the cathode side.

2.2 Membrane characterization.

Figure 2 shows the set-up use for MEA characterization. The electrochemical workstation (Autolab PGSTAT302N) and a B&K Precision 1694 DC Power Supply was used for the membrane characterization. The previously adequate membrane is integrated to PEM electrolyzer. Then DI water at 80 °C flows into the electrolyzer at 1.7 L min^{-1}. Once the MEA reached the thermal equilibrium a set of currents were applied from 10 mA to 8 A and the potential was recorded in every point in order to construct a polarization curve. Then electrochemical impedance spectroscopy was used (EIS) was carried out at a constant current at 1.5 in a frequency range of 0.1 Hz to 100 kHz with a potential amplitude of 1x10^{-5} V.

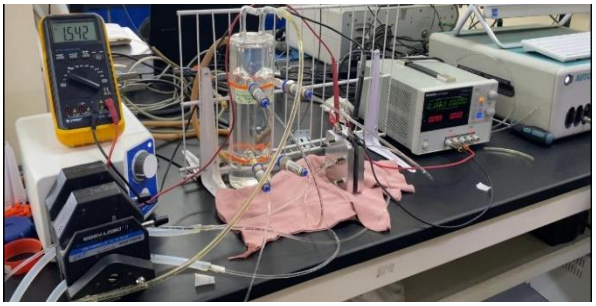

Figure 2. Set up for PEM characterization.

3. RESULTS AND DISCUSSION

Provide Polarization curve of PEM electrolyzers recorded at 80 °C is shown in Figure 3. The

polarization curve of PEM electrolysis is used to evaluate the electrochemical performance of MEAs. An increase of cell potential at a certain current means a decrease of voltage efficiency since the same amount of hydrogen is produced using more energy. At low current densities, between 0 and 0.2 A cm^2, the ohmic resistances can be neglected, hence charge transfer kinetics is the domain process. Then, a linear behavior appears, this is a domain potential where charge transfer resistance is low a cell resistance becomes the predominant process. Finally, at high current densities gas screening effect along mass transport limitation. The hydrogen production is related to current density according to Faradays law. Furthermore, at high current densities more hydrogen is produced per unit of time, nevertheless, these operation conditions increase the degradation rate and reduce the voltage efficiency. To avoid membrane degradation, the maximum applied potential must be 2.2 V [9,10].

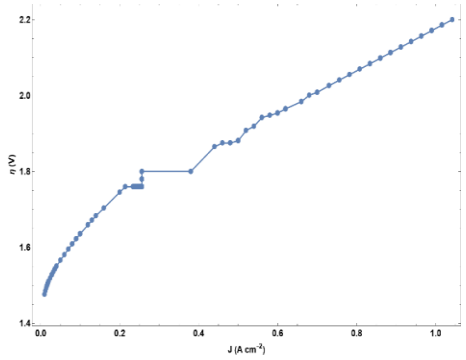

Figure 3. Polarization curve of PEM electrolyzer recorded at 80°C with a flow rate of 1.7 L min^{-1}.

EIS is an excellent diagnostic tool for electrochemical processes, since it allows us to differentiate between different phenomena in the basis of different relaxation times of a process. Also, the relationship between components and an equivalent circuit allows to change parameters and identify its impact e.g. potential, current density or electrocatalysts. Furthermore, a detail EIS analysis of MEAs performance under operation conditions, such as: temperature, flow rate, and commercial materials is required to understand the impact of any modification made during the characterization protocol [11].

Figure 4 shows the selected equivalent circuit which is widely use to fit experimental EIS data of these systems [11–13]. This includes an ohmic resistance (R_s) connected in series with two parallel components, these consists essentially in a resistance, which is associated with faradaic process and a constant phase element. The first resistance is associated with the CR and the second one with the AR.

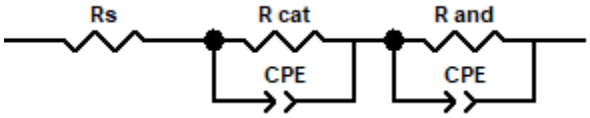

Figure 4. Equivalent circuit used to fit EIS experimental data.

Figure 5 shows Nyquist diagram recorded at a fix potential of 1.5 V; this region was selected since catalytic effect should be relevant. On one hand, the interception of the semicircle with x axis at high frequencies shows the ohmic resistance (R_s), which are a series of resistance from PEM electrolyzers interfaces. On the other hand, the interception with the same axes at low frequencies is assumed as the polarization resistance (R_p). The sum of these resistance is known as the differential resistance of polarization curves. R_s had a value of 0.6 Ω cm^2 and R_p of 1.165 Ω cm^2 which indicates that electrochemical processes had a 2 times higher impact on the total system resistance.

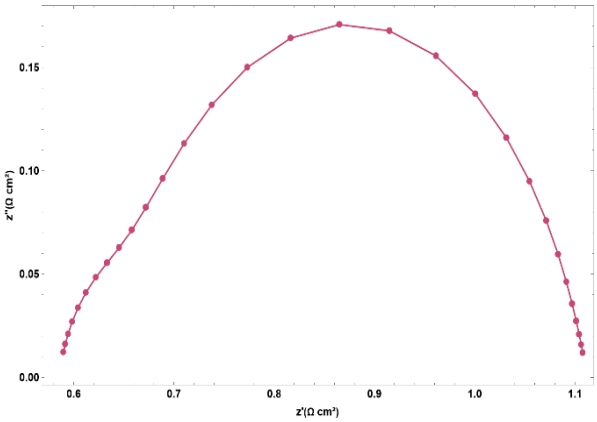

Figure 5. Nyquist diagram recorded at a fixed potential of 1.5 V.

Figure 6 presents Bode diagram recorded at a fix potential of 1.5 V. Nyquist diagram shows two overlapping semicircles. The one at high frequencies is associated with CR, which had a ultra-low resistance due to the high amount of Pt. The arc at low frequencies is attributed to the anode. This is also reflected in two relaxation times on the Bode diagram. Subsequently, AR is the slowest reaction. Which in good agreement with literature [11].

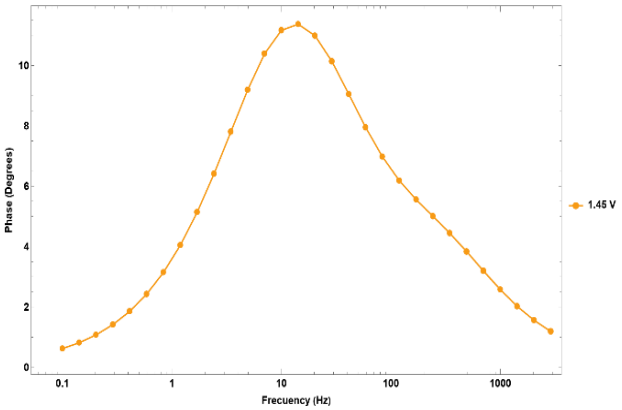

Figure 6. Bode diagram recorded at a fixed potential of 1.5 V.

4. CONCLUSIONS

This work highlights the importance of establishing a robust characterization protocol, encompassing operational conditions, data analysis, and a thorough understanding of physical and electrochemical processes. Polarization curves and EIS were employed to achieve this, enabling the evaluation of system modifications such as varying electrocatalysts, temperatures, or flow rates.

Acknowledgements

We acknowledge the National Polytechnic Institute for financing, spaces and equipment provided that are fundamental for the development of the project. IPN-SIP multidisciplinary project 2181 and the innovation project SIP-20241096. We acknowledge CONAHCyT for the recognition of the “Laboratorio Nacional CONAHCyT en Tecnologías del Hidrógeno”, proposal 53.

Conflicts of Interest

The authors declare no conflict of interest.

REFERENCES

[1] Taibi E, Blanco H, Miranda R. Green hydrogen cost reduction: Scaling up electrolysers to meet the 1.5C climate goal. Abu Dhabi: International Renewable Energy Agency; 2020.

[2] Ritchie H, Roser M, Rosado P. CO_2 and Greenhouse Gas Emissions. Our World in Data 2020.

[3] Kayfeci M, Keçebaş A, Bayat M. Hydrogen production. Solar Hydrogen Production, Elsevier; 2019, p. 45–83. https://doi.org/10.1016/B978-0-12-814853-2.00003-5

[4] Eikeng E, Makhsoos A, Pollet BG. Critical and strategic raw materials for electrolysers, fuel cells, metal hydrides and hydrogen separation technologies. International Journal of Hydrogen Energy 2024;71:433–64. https://doi.org/10.1016/j.ijhydene.2024.05.096

[5] Kim JH, Kim H, Kim J, Lee HJ, Jang JH, Ahn SH. Electrodeposited molybdenum sulfide as a cathode for proton exchange membrane water electrolyzer. Journal of Power Sources 2018;392:69–78. https://doi.org/10.1016/j.jpowsour.2018.04.087

[6] Kim H, Kim J, Kim S-K, Ahn SH. A transition metal oxysulfide cathode for the proton exchange membrane water electrolyzer. Applied Catalysis B: Environmental 2018;232:93–100. https://doi.org/10.1016/j.apcatb.2018.03.023

[7] Qu Y, Shao M, Shao Y, Yang M, Xu J, Kwok CT, et al. Ultra-high electrocatalytic activity of VS_2 nanoflowers for efficient hydrogen evolution reaction. J Mater Chem A 2017;5:15080–6. https://doi.org/10.1039/C7TA03172F

[8] Cruz Flores JA. Diseño y manufactura de un electrolizador de Membrana de Intercambio Protónico (PEM) de prueba, con un área activa de 5 cm2. T E S I S PARA OBTENER EL GRADO DE: MAESTRO EN INGENIERIA DE MANUFACTURA. Instituto Politécnico Nacioinal, Escuela Superior de Ingeniería Mecánica y Leéctrica Unidad Azcapotzalco, 2024.

[9] Lettenmeier P, Kolb S, Sata N, Fallisch A, Zielke L, Thiele S, et al. Comprehensive investigation of novel pore-graded gas diffusion layers for high-performance and cost-effective proton exchange membrane electrolyzers. Energy Environ Sci 2017;10:2521–33. https://doi.org/10.1039/C7EE01240C

[10] Chatenet M, Pollet BG, Dekel DR, Dionigi F, Deseure J, Millet P, et al. Water electrolysis: from textbook knowledge to the latest scientific strategies and industrial developments. Chem Soc Rev 2022;51:4583–762. https://doi.org/10.1039/D0CS01079K

[11] Siracusano S, Trocino S, Briguglio N, Baglio V, Aricò AS. Electrochemical Impedance Spectroscopy as a Diagnostic Tool in Polymer Electrolyte Membrane Electrolysis. Materials 2018;11:1368. https://doi.org/10.3390/ma11081368

[12] Elsøe K, Grahl-Madsen L, Scherer GG, Hjelm J, Mogensen MB. Electrochemical Characterization of a PEMEC Using Impedance Spectroscopy. J Electrochem Soc 2017;164:F1419. https://doi.org/10.1149/2.0651713jes

[13] Lickert T, Fischer S, Young JL, Klose S, Franzetti I, Hahn D, et al. Advances in benchmarking and round robin testing for PEM water electrolysis: Reference protocol and hardware. Applied Energy 2023;352:121898. https://doi.org/10.1016/j.apenergy.2023.121898

134-I-PO EVALUATION OF THERMAL COMFORT IN A STANDARD MEXICAN HOUSE UTILIZING PHASE CHANGE MATERIALS

B. Gamboa Loya[1], R. Jäckel[2, 3], G. Gutiérrez Urueta[1], C. Monreal Jiménez[1]*, M. Romero[1], O. Guarneros[1], H. Méndez[1]

[1]Autonomous University of San Luis Potosí, Faculty of Engineering, San Luis Potosí, México
[2]University of Rio de Janeiro, Mechanical Engineering Program (PEM/COPPE/UFRJ).
[3]Rio de Janeiro State University (UERJ), Department of Mechanical Engineering, Rua São Francisco Xavier 524, Rio de Janeiro, 20550-011, Brazil.

*Correspondence: cintia.monreal@uaslp.mx

Abstract: This study analyzes the effectiveness of Phase Change Materials (PCM) in reducing thermal discomfort across various climates in Mexican cities. To cover diverse climatic conditions, eight cities across different Köppen climate zones in Mexico were selected, each represented by a standard Mexican home with typical dimensions, materials, and occupancy patterns. A simulation was developed to analyze indoor temperature fluctuations and relative humidity for both summer and winter seasons, used to quantify thermal discomfort experienced by occupants. Results indicate that PCM reduces thermal discomfort, especially in winter, as high daytime temperatures in summer prevent the PCM from solidifying, limiting its cooling effect at night. The most notable improvements were observed in Monterrey during summer and in Xalapa during winter, situated in a dry steppe (BS) zone and a temperate (Cf) zone, respectively. By contrasting scenarios with and without PCM, this study demonstrates PCM's value in improving residential thermal comfort and energy sustainability across varied climates.

Keywords: Thermal comfort, EnergyPlus, PCM, TDC.

1. INTRODUCTION

Temperature variations in Mexico impact quality of life and drive higher energy use, with residential and commercial sectors consuming 17% of total energy. [1,2]. Enhancing building energy efficiency can be achieved by incorporating thermal energy storage within building envelopes. Phase change materials (PCMs) play a crucial role in this process, moderating temperature fluctuations by storing and releasing latent heat as temperatures vary throughout the day. PCMs may be integrated into construction materials through methods such as direct incorporation, immersion, encapsulation, shape stabilization, and form-stable composites [3]. Numerous studies highlight the potential of PCMs in diverse fields like aeronautic [4] or improving thermal comfort, thus reducing energy consumption in buildings. Research has focused on PCM integration with ventilation strategies to lower operative temperatures and discomfort levels, particularly in challenging climates. Investigations include analyses of PCM and natural ventilation to enhance comfort in lightweight structures in regions like Kazakhstan, evaluations of PCM combined with nighttime ventilation for tropical residential settings, and simulations on PCM's impact on energy use in Mediterranean-style homes. Additionally, factors influencing thermal comfort—such as personal, environmental, and climate-related variables—have been well-documented, offering a foundation for PCM applications across diverse climates [5–8]. A parameter known as Discomfort Index (DI) was recommended by [9], introducing the Total

Discomfort Change (TDC) to aid PCM selection for comfort improvements.

This study seeks to evaluate the influence of phase change materials (PCMs) on thermal comfort within a range of representative climates in Mexico. Eight cities, each representing unique climatic conditions, were selected to investigate the potential of PCMs to improve thermal comfort and reduce reliance on air conditioning in residential settings throughout the country.

2. MATERIALS AND METHODS

The construction geometry was based on plans obtained from INFONAVIT (National Workers' Housing Fund Institute of Mexico) to create a housing model representative of a standard low-cost Mexican home, as shown in Fig. 1 The detailed housing model construction and materials used are offered in [10].

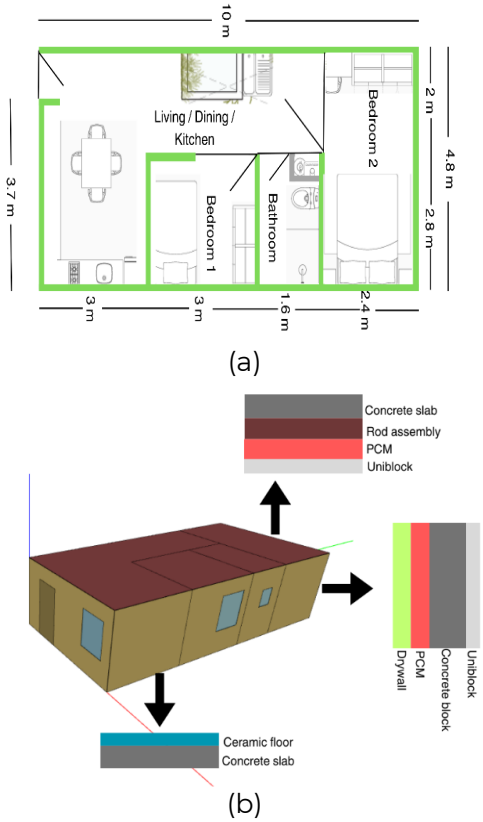

Figure 1. (a) Blueprint of the INFONAVIT sample house plan. (b) Example of a low-cost standard Mexican home and materials used for the housing model.

The simulation period covered one winter month, from January 10 to February 10, and one summer month, from July 15 to August 15, both in 2020. The housing model, which comprises several rooms designated as "thermal zones" in the EnergyPlus software, incorporates factors such as occupancy schedules, lighting usage, electrical equipment, and gas usage. This study used the Köppen-Geiger climate classification, which defines nine climate regions in Mexico, listed in Table 1 with the selected cities.

Table 1. Selected cities for the study.

Climatic group	Climatic region	City
Tropical	**Af,** tropical with year-round rainfall	Tuxtla Gutiérrez
	Am, tropical with monsoon rains	Villahermosa
	Aw, tropical with summer rains	Mérida
Dry	**BS**, dry steppe	Monterrey
	BW, dry desert	Hermosillo
Temperate	**Cf**, temperate with year-round rainfall	Xalapa
	Cw, temperate with summer rains	Guadalajara
	Cs, temperate with winter rains	Toluca
Polar	**EB**, high mountain polar	Omitted

Regarding the PCM used for simulations, the primary criterion for selecting a PCM is its melting point, as PCMs store and release energy during phase changes near this temperature. Ideally, the environmental temperature should vary around this melting point, so a PCM with a melting temperature of 21°C was selected.

The PCM chosen for the simulations is a commercial product named RT 21 HC [11], with a melting point of 21°C and was applied as a 2 cm-thick layer in each wall and the ceiling of the housing model. Its thermophysical properties are latent heat capacity of 190 kJ/kg, density (ρ) of 800 kg/m³, and specific heat capacity (Cp) of 2 kJ/kg-K.

2.1. Thermal comfort indicators

The Discomfort Index (DI) [9] is a metric used to assess thermal comfort, calculated using Eq. 1 [12]:

$$\boldsymbol{DI = T_{db} - 0.55(1 - 0.01RH)(T_{db} - 14.5)} \quad \text{Eq. 1}$$

where T_{db} is the dry bulb temperature, and RH is the relative humidity in percentage, both measured indoors and determined through simulations in EnergyPlus.

A classification representing comfort criteria for both summer and winter days, based on the DI value and assuming standard clothing was used [10]. This proposed Discomfort Index range is adapted from the literature [12], with finer resolution to better capture classification shifts when using PCM.

Total Discomfort Change (TDC) is a concept used to assess the thermal impact of PCM in housing. It is determined for each hour of the simulation [5] using Eq. (2).

$$\boldsymbol{TDC = \sum_1^k n(Discomfort\ Reduction) - \sum_1^k n(Discomfort\ Increase)} \quad \text{Eq. (2)}$$

Where k represents the total number of hours in the simulation period and n is a natural integer number.

TDC values are calculated by comparing hourly Discomfort Index values in the PCM-enhanced housing model to those from the same period without PCM. The TDC is the total of each hourly discomfort reduction (counted positively for comfort improvement) and increase (counted negatively for comfort decline), as shown in Eq. 2.

3. RESULTS AND DISCUSSION

Figures 2 and 3 illustrate a comparison of interior temperatures when PCM is used or not, along with exterior temperature, to assess the impact of PCM on indoor temperature. As an example, the city of Monterrey was selected, due to the temperature fluctuations during the day that this city experiences.

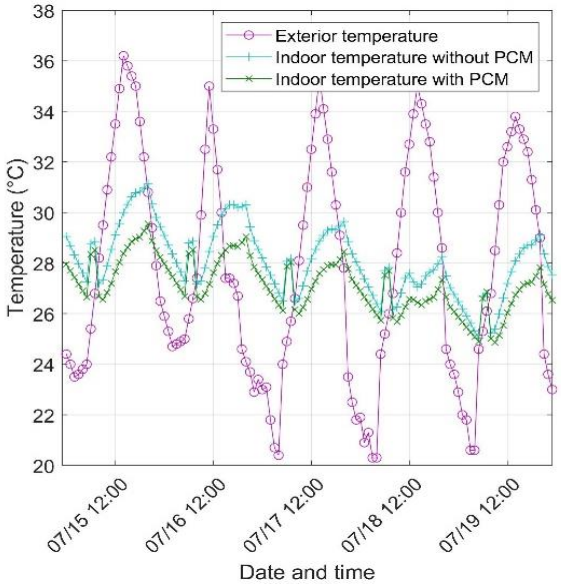

Figure 2. Comparison between interior temperatures in Monterrey (BS) during winter with and without PCM.

In Fig. 2, the comparison encompasses five winter days in Monterrey (BS) and demonstrates that the interior temperature with PCM is lower than the interior temperature without PCM during high exterior temperature peaks, which coincide with low relative humidity peaks. Furthermore, the interior temperature with PCM rises when the exterior temperature has low peaks, aligning with high relative humidity peaks.

This behavior illustrates the attenuating effect of the PCM, as it absorbs or releases latent heat during exterior temperatures near the PCM's melting point. This process helps maintain a stable interior temperature with PCM, keeping it closer to a comfortable level. This effect is amplified because the exterior temperature fluctuates around the PCM's melting point (21 °C). However, during the summer months in

Monterrey (BS) (see Fig. 3), when the exterior temperature consistently exceeds the PCM's melting point, this behavior changes significantly. In instances of very high exterior temperatures, the interior temperature with PCM decreases compared to the scenario without PCM.

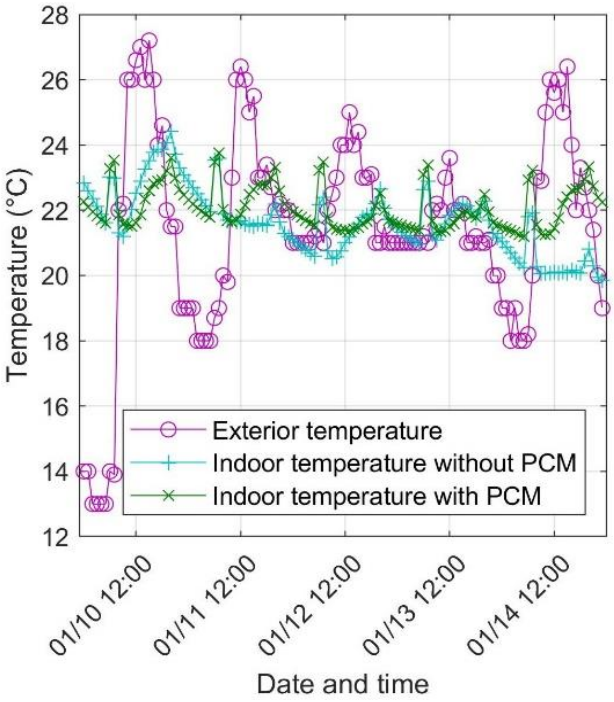

Figure 3. Comparison between interior temperatures in Monterrey (BS) during summer with and without PCM.

Figure 4 illustrates the hourly variation of the internal temperature of the simulated housing model in Monterrey (BS) over 8 days (192 hours) of summer simulation. The temperature curves for scenarios with and without the incorporation of PCM in the walls and roof are compared, with a particular emphasis on the first 36 hours.

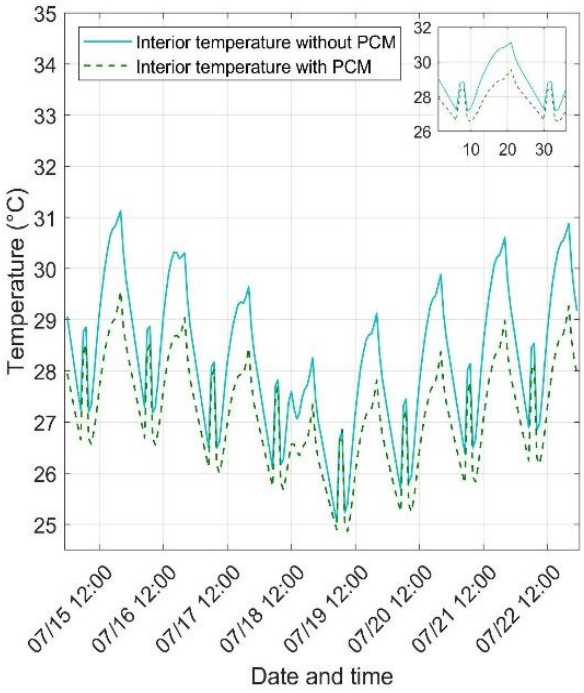

Figure 4. Variation of indoor temperature in Monterrey (BS) during the summer, hourly, with and without PCM.

When comparing both curves, it is evident that the temperature fluctuations of the interior with incorporated PCM are smoother than in the scenario without PCM. This effect is apparent in the simulation model as a reduction in high temperatures. Consequently, it can be concluded that PCM provides a damping effect within the housing during high temperature extremes in Monterrey's (BS) summer.

Figure 5 depicts a scenario in which the use of PCM leads to an overall increase in indoor temperature, comparing indoors temperatures of the housing model in Tuxtla Gutiérrez (Af) during the summer. It is evident that the internal temperature rises at temperature peaks when PCM is used. Therefore, it can be concluded that incorporating PCM in Tuxtla Gutiérrez (Af) during the summer results in higher internal temperatures.

The examples presented in Figs. 4 and 5 are the best- and worst-case scenarios for the use of PCM in summer, due to the decreasing and

increasing, respectively, in the discomfort hours inside the house model.

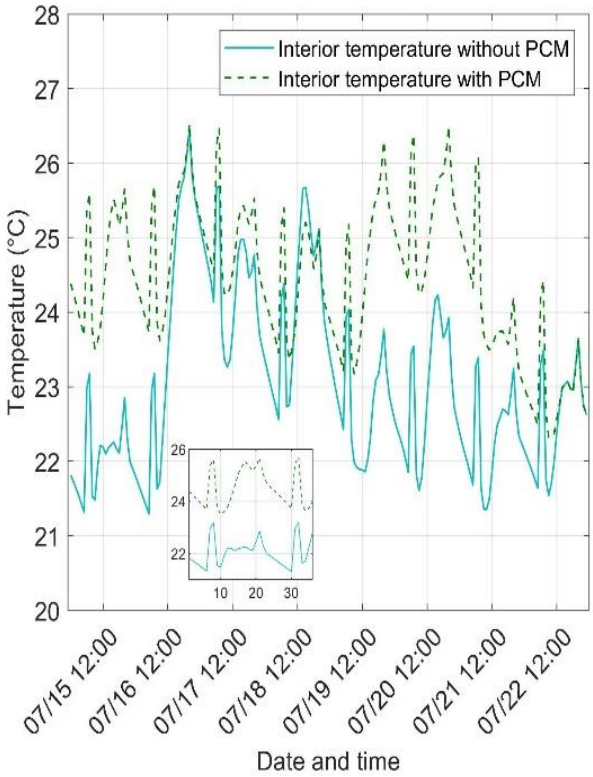

Figure 5. Variation of indoor temperature per hour in Tuxtla Gutiérrez (Af) during the summer, with and without PCM.

Figure 6 shows the Total Discomfort Change (TDC) of PCM for each city and season in the simulation period. Monterrey (BS) has the highest summer TDC, while Xalapa (Cf) has the highest for winter. Tuxtla Gutiérrez (Af) recorded the lowest summer TDC, and Mérida (Aw) had the lowest for winter. Villahermosa (Am), Monterrey (BS), Guadalajara (Cw), and Toluca (Cs) all had positive TDCs in both seasons, whereas Mérida (Aw) showed a negative TDC in both. Overall, Monterrey (BS) achieved the best thermal comfort improvement with the highest combined TDC, while Mérida (Aw) had the poorest performance with a negative TDC in both seasons.

Within the same climatic group (see Table 1), noticeable differences in the obtained TDC results for each city suggest that PCM behavior cannot be universally generalized within the same climatic group. Each city within a specific climatic group shows distinct PCM performance, even though they share certain environmental characteristics.

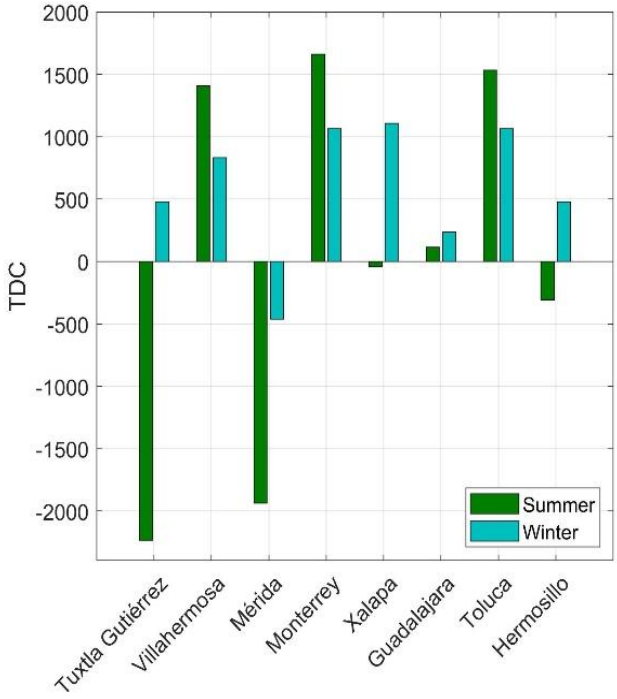

Figure 6. TDC of the PCM in each city and season of the simulation period.

Table 2. TDC values per city in summer and the increase or decrease in discomfort hours due to PCM.

City	TDC	Decrease/increase in discomfort hours
Monterrey	1660	-184
Toluca	1533	-169
Villahermosa	1410	-157
Guadalajara	115	-13
Xalapa	-43	4
Hermosillo	-308	32
Mérida	-1938	213
Tuxtla Gutiérrez	-2235	246

Table 3. TDC values per city in winter and the increase or decrease in discomfort hours due to PCM.

City	TDC	Decrease/increase in discomfort hours
Xalapa	1106	-121
Monterrey	1065	-117
Toluca	1064	-117
Villahermosa	832	-92
Hermosillo	478	-53
Tuxtla Gutiérrez	478	-53
Guadalajara	236	-26
Mérida	-463	51

Tables 2 and 3 provide the numeric TDC value per city and season, with the increasing and decreasing discomfort hours for the house model. Through the tables, it is noted that the decrease in thermal discomfort hours using PCM is higher during winter than in summer, and the cities of Villahermosa, Monterrey, Guadalajara and Toluca having positive TDC for both seasons; meanwhile, Mérida is the only city with negative TDC for both seasons.

4. CONCLUSIONS

The use of Phase Change Materials (PCM) demonstrates considerable potential for improving thermal comfort, particularly in winter, where lower temperatures allowing effective heat absorption and release. In summer, however, PCM performance is more limited. In warmer climates, such as those in Tuxtla Gutiérrez (Af) and Hermosillo (BW), high daytime temperatures often keep PCM in a liquid state, thus preventing the material from solidifying and recharging effectively. This not only limits its cooling benefit at night but can also exacerbate thermal discomfort as heat is released when temperatures dip. In contrast, cities like Villahermosa (Am) and Monterrey (BS) show better summer performance due to nighttime temperatures that frequently approach the PCM's melting point, allowing for efficient heat release and cooling.

Among the cities studied, Monterrey (BS) displayed the best individual performance in reducing thermal discomfort, while temperate climates overall achieved the most significant improvements. These findings suggest that PCM is particularly advantageous in winter and in temperate regions, where it can contribute to energy savings and effective indoor climate regulation, supporting sustainable design in diverse climates.

Conflicts of Interest

The authors declare no conflict of interest.

REFERENCES

[1] M. Rollos, Indoor Environment (1993) https://doi.org/10.1159/000463257

[2] SENER, Balance Nacional De Energía, 2022. https://www.gob.mx/sener/es/articulos/balance-nacional-de-energia-296106 Accessed 02/11/2024

[3] S.A. Memon, Renewable and Sustainable Energy Reviews (2014) https://doi.org/10.1016/j.rser.2013.12.042

[4] R. Jäckel, F. Tapia, G. Gutiérrez, C. Monreal, Flow Measurement and Instrumentation (2020) https://doi.org/10.1016/j.flowmeasinst.2020.101817

[5] I. Adilkhanova, S.A. Memon, J. Kim, A. Sheriyev, Energy (2021) https://doi.org/10.1016/j.energy.2020.119390

[6] A. Sheriyev, S.A. Memon, I. Adilkhanova, J. Kim, Energies (2021) https://doi.org/10.3390/en14092699

[7] M. Zhussupbekov, S.A. Memon, S.A. Khawaja, K. Nazir, J. Kim, Journal of Building Engineering (2023) https://doi.org/10.1016/j.jobe.2023.106335

[8] Auliciems Andris, Szokolay Steven, THERMAL COMFORT, 2nd ed. (The University of Queensland, 2007).

[9] Y. Epstein, D.S. Moran, Industrial Health. (2006) https://doi.org/10.2486/indhealth.44.388

[10] B.G. Gamboa-Loya, R. Jäckel, G. Gutiérrez, C. Monreal-, J. Rojas, R. Peña, Revista Mexicana de Ingeniería Química. (2024). https://doi.org/10.24275/rmiq/IE24351

[11] Rubitherm, (2024) https://www.rubitherm.eu/en/productcategory/organische-pcm-rt, Accessed 20-oct-2024.

[12] L. Siami, A. Ramadhani, KnE Social Sciences (2019) https://doi.org/10.18502/kss.v3i21.4987

139-I-PO EVALUATING THERMAL STORAGE SOLUTIONS IN SOLAR DISK COLLECTORS: TRADITIONAL METHODS VS. PHASE CHANGE MATERIAL

J. Rojas-Rica[1], R. Jäckel[2], G. Gutiérrez-Urueta[1]*, C. Monreal[1], F. Pérez[1], F. Oviedo[1], D. de Lange[1]

[1]Autonomous University of San Luis Potosí, Faculty of Engineering, San Luis Potosí, México.
[2]Rio de Janeiro State University (UERJ), Department of Mechanical Engineering, Rua São Francisco Xavier 524, Rio de Janeiro, 20550-011, Brazil.

*Correspondence: geydy.gutierrez@uaslp.mx

Abstract: This research proposes a solar collection system design that integrates latent heat storage using Phase Change Materials (PCMs). These materials can absorb or release latent heat as they transition between solid and liquid states, providing a more consistent energy source during periods without sunlight. Using average climatic data from Mexico, a methodology was developed to determine the design parameters for a solar collector-receiver system that incorporates PCMs for thermal storage, aimed at meeting the energy needs of a typical Mexican household. A salt hydrate-based PCM solution was selected as the most suitable option for this design. In addition to outlining the key design parameters of this prototype, this study compares the thermal performance of the PCM-equipped receiver unit with that of a steel-based system, evaluating the improvement in thermal stability over a continuous 24-hour period. The results indicate that the integration of PCMs significantly enhances temperature stability, maintaining heat storage temperatures above 100°C throughout the night. Furthermore, after daylight hours, the PCM solution stored almost 60 % more than the energy stored in the conventional system, highlighting the ability of PCMs to increase the hours of operation of solar collection systems in Mexico.

Keywords: renewable energy, sensible heat storage, latent heat storage.

1. INTRODUCTION

Solar energy holds significant promise as a renewable resource, but its intermittent nature presents major challenges for continuous energy supply. To mitigate this, heat-accumulating materials can be utilized to store surplus energy during the day for use at night, enhancing the efficiency of power plants and industrial processes. These materials are classified into three types: organic, inorganic, and eutectic [1]. Phase Change Materials (PCMs) and sensible heat storage materials are particularly noteworthy for their ability to store or release latent heat during the phase transition between solid and liquid states.

Recent advancements have improved the thermal performance of PCMs. For example, the incorporation of nanoparticles into salts has enhanced heat transfer efficiency without sacrificing storage capacity [2]. Additionally, research has demonstrated a linear relationship between the duration of energy storage and the length of the thermal storage unit. It has been recommended to maintain temperature stability during charging and discharging cycles to optimize performance [3]. One study highlighted the advantages of using LiOH/KOH in thermal energy storage systems, which exhibited high energy density, low volumetric expansion, minimal supercooling, and no material segregation, improving overall efficiency [4]. For concentrated solar power plants, encapsulated PCMs were suggested for storing energy at a certain temperatures range, depending on the climatic

conditions [5]. Additionally, potential materials for thermal storage at temperatures between 120°C and 1000°C were reviewed, emphasizing the need to assess their thermal stability and chemical compatibility [6].

This article focuses on comparing the effectiveness of PCMs and sensible heat storage materials for thermal energy storage in the 100-250°C range. It aims to determine how well PCMs reduce heat loss compared to conventional materials, particularly for maintaining high temperatures overnight to meet the energy demands of an average household in Mexico.

2. MATERIALS AND METHODS

The model is based on average environmental conditions in Mexico and solar irradiation, comparing the performance of two materials in two scenarios: one with constant storage volume and the other with equal mass. Finite element simulations of the thermal energy storage system using PCM and steel will assess efficiency improvements, nighttime energy retention, and alignment with household energy needs.

2.1. Climatic conditions and material selection

To analyze a solar capture and storage system, factors like solar irradiation, wind speed, atmospheric pressure, and ambient temperature were evaluated across Mexico's climatic zones (Köppen classification). An annual average day was determined for selected cities, using NASA's 2021 data. The household energy consumption was modeled using Energy Plus, with an average daily usage of 5.1 kWh for four people [7].

This study compares a sensible heat storage material capable of thermal energy storage without phase change, selecting steel due to its ability to withstand high temperatures. Initial tests showed an average temperature of 140°C, so PCM 31.7$LiNO_3$-68KNO_3, with a melting point of 135°C, was tested, resulting in an average temperature of 170°C. Therefore, PCMs with melting points close to the test average were prioritized.

A review of commercial materials focused on compounds suitable for energy storage during nighttime hours, with an emphasis on hydroxide and nitrate blends. The rule of mixtures was applied to estimate properties, like specific heat and thermal conductivity, for different PCMs. A list of materials closest to the melting point of 170°C was compiled, evaluating properties such as latent heat, density, and conductivity, as shown in Table 1.

Table 1 Properties of the materials.

Material	Melt. point (°C)	Latent heat (kJ/kg)	Cp (kJ/kg·K)	K (W/m K)	□ (kg/m³)
58.1LiNO-41.9KCl	166	272	1.43	0.65	1918
Steel	1398	N/A	0.5	16.3	7860

To objectively select materials, the Analytic Hierarchy Process (AHP) was used, assigning weights to criteria like proximity to the target temperature, latent he at capacity, sensible heat capacity, thermal conductivity, and density. The AHP matrix achieved a consistency ratio of 9.6%, deemed acceptable [8]. Among the top materials selected, the compound 58.1$LiNO_3$-41.9KCl ranked first, offering the best balance of properties for effective thermal energy storage in the studied conditions.

2.2. Modeling

A parabolic solar dish with a cylindrical receiver is modeled to analyze solar energy concentration on the receiver, the system's entry point (Fig. 1).

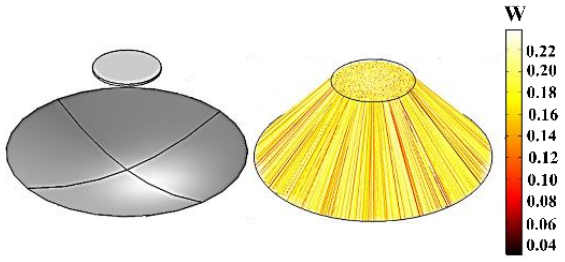

Figure 1. Ray tracing simulation to determine the source of energy input to the store.

The boundary conditions for the solar collector model include solar radiation as the input energy flux, with an approximate solar irradiance of 5.5 kW/m². The receiver is defined with an absorption boundary condition to simulate the energy capture process. The dish has a 1.08 m focal length, 2.52 m² reflective area, and a 0.3 m receiver diameter. Parameters include a maximum solar disk angle of 4.65°, a surface slope error of 1.75, and a reflectivity of 0.9. Using Monte Carlo ray tracing and finite element analysis, simulations employed 1 million rays per unit area, A rectangular mesh is applied to the model, with a progressive refinement ranging from 10,000 elements to 500 elements to analyze the effects of mesh density, achieving less than 5% error across over 1000 rectangular mesh elements. Energy input distribution shows maximum concentration at the center, decreasing uniformly outward.

The governing equation of the system is

$$C_p \frac{\partial T}{\partial t} + \nabla \cdot q = Q \qquad \text{Eq. (1)}$$

The model utilized to simulate the phase change relies on the apparent heat capacity method [8]. This approach uses a smooth step function, known as the Heaviside function ϴ(T), which represents the phase change fraction as temperature varies. The function is defined within a range determined by the melting temperature of the PCM, T_f , and the temperature difference between the phases $\left(T_f - \frac{\Delta T}{2} \text{ y } T_f + \frac{\Delta T}{2}\right)$. Using this step function, thermal properties such as thermal conductivity k, density ρ, specific heat C_{eq}, and mass fraction (α_m) are defined and a pulse function (Dirac) is utilized to describe the distribution of latent heat C_L (T), which is dependent on the material's latent heat property L. The equations involved in this methodology are given below [9]:

$$\rho\theta_1 = \Theta(T) \; and \; \theta_2 = 1 - \Theta(T) \qquad \text{Eq. (2)}$$

$$k = \theta_1 k_1 + \theta_2 k_2 \qquad \text{Eq. (3)}$$

$$\rho = \theta_1 \rho_1 + \theta_2 \rho_2 \qquad \text{Eq. (4)}$$

$$C_{eq} = \frac{1}{\rho}(\theta_1 \rho_1 Cp_1 + \theta_2 \rho_2 Cp_2) \qquad \text{Eq. (5)}$$

$$\alpha_m = \frac{1}{2}\frac{\theta_1\rho_2 - \theta_2\rho_1}{\theta_1\rho_1 + \theta_2\rho 2} \qquad \text{Eq. (6)}$$

$$C_L(T) = L\frac{d\alpha}{dT} \qquad \text{Eq. (7)}$$

$$C_p = \frac{1}{\rho}(\theta_1 \rho_1 Cp_1 + \theta_2 \rho_2 Cp_2) + C_L \qquad \text{Eq. (8)}$$

A cylindrical storage model, with a volume of 0.04 m³ and a mesh consisting of 17,806 elements, was analyzed, A convergence study showed deviations below 5% for both the chosen spatial and temporal discretization. Several cycles of charging during daylight and discharging at night due to temperature drops were simulated, evaluating the performance of steel and PCM within anticipated temperature ranges. The analysis details the boundary conditions, and the type of mesh applied. Additionally, the temperatures recorded at 12:00 hours on the second day of simulation are presented to assess the system's thermal behavior under these conditions.

3. RESULTS AND DISCUSSION

A simulation was conducted to assess steel's stability as a sensible heat storage material over daily cycles, examining its energy retention and temperature fluctuations. As depicted in Fig. 2, steel's stored energy declines as temperatures drop, showing expected behavior for steel with significant reductions in accumulated energy during the night.

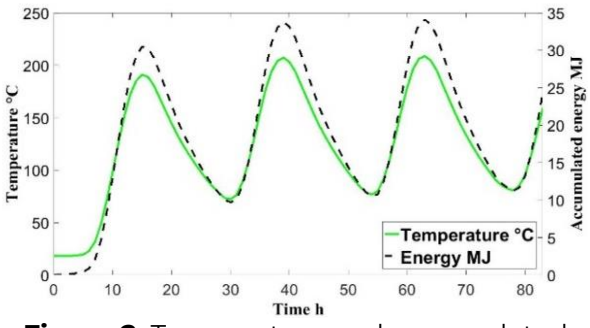

Figure 2. Temperature and accumulated energy of steel vs time.

The performance of the PCM 58.1LiNO₃-41.9KCl was evaluated as it maintains temperatures

above 100°C after the first 24 hours, even with temperature drops, due to its melting temperature of 166°C. This PCM's ability to stabilize temperatures without falling below critical limits demonstrated that melting point, rather than merely latent heat capacity, is pivotal for this application. The PCM, selected for its 166°C melting temperature and 272 kJ/kg latent heat, showed superior performance over other options tested, aligning closely with the target temperature of 170°C for optimal operation.

For an effective comparison of PCM versus conventional material, a simulation was performed in a setup with constant volume (0.042 m^3). This setup included two storage units of the same size but different weights: the steel had a density of 7860.3 kg/m^3, resulting in a 333 kg mass, while the PCM unit with a density of 1918 kg/m^3 had a mass of 81 kg. Fig. 3 shows a simulation at constant volume. The steel storage unit, with a significantly higher mass, accumulated more energy during peak hours, reaching 34 MJ, while the PCM only reached 19 MJ. However, during nighttime, steel's stored energy dropped to 11 MJ, whereas the PCM maintained 12 MJ, demonstrating its superior thermal stability.

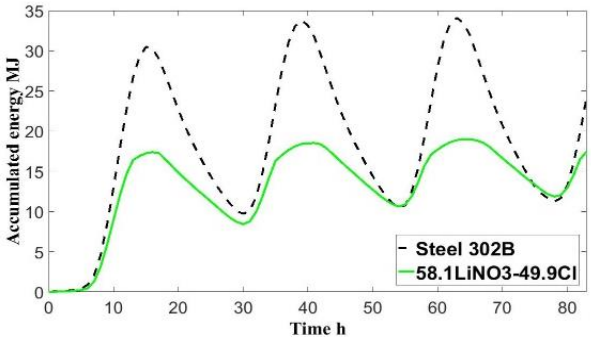

Figure 3. Comparison of energy accumulated for steel and PCM with the same volume vs time.

Given steel's substantial mass, it becomes impractical for rooftop thermal energy storage systems due to structural limitations. Thus, a further simulation was conducted adjusting the steel's thickness to reduce its mass to match the PCM's (81 kg), resulting in a smaller steel storage volume of 0.0103 m^3. Fig. 4 illustrates that while steel experiences significant energy losses overnight, PCM better mitigates these fluctuations, retaining the energy better. Although PCM's peak accumulation is lower than steel's, it loses far less energy overnight; steel falls to just 2 MJ while PCM retains 12 MJ. This makes PCM better suited to meet nighttime energy demands, offering 233.75 kJ/kg, or 58% more energy storage than the sensible heat storage material on a per-mass basis under environmental conditions alone.

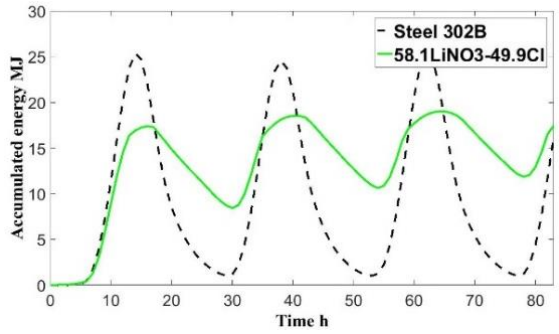

Figure 4. Comparison of energy accumulated for steel vs PCM with the same mass vs time.

To optimize storage performance, the reflective area was increased to 3.36 m^2 from an initial 2.52 m^2 to meet the continuous energy flow demands of the system. By the third day of simulation, as seen in Fig. 5, steel could not sustain the energy needed during nighttime, exhibiting a 7.42% overnight energy loss. PCM, on the other hand, remained more stable, preserving adequate energy despite minor drops.

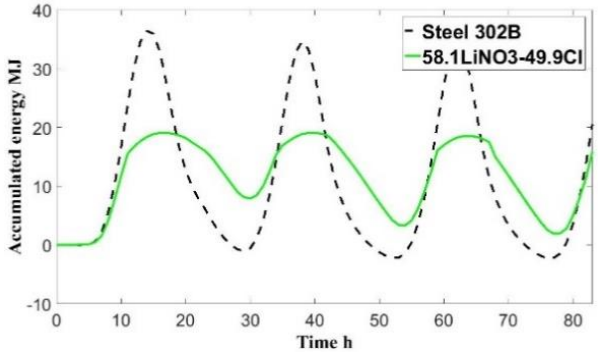

Figure 5. Comparison of energy accumulated for steel vs PCM with discharge of consumption.

These findings highlight PCM's advantage in retaining stored energy under fluctuating environmental conditions, achieving consistent energy availability with lower mass and improved retention over steel. This makes PCM, especially 58.1$LiNO_3$-41.9KCl, a more efficient choice for thermal energy storage in solar energy applications, balancing storage stability and meeting energy demands over extended cycles.

4. CONCLUSIONS

This study examines Mexico's climatic conditions and average energy consumption to simulate the environmental parameters for a thermal energy storage system using finite element analysis. The performance of a TES system with phase change materials versus steel was compared, analyzing both scenarios with and without household energy consumption, focusing on PCM 58.1$LiNO_3$-41.9KCl. Steel, as a sensible heat storage material, stores a maximum of 25 MJ but drops to 2 MJ at night. PCM 58.1$LiNO_3$-41.9KCl proved more effective, outperforming steel. At night, PCM maintained 12 MJ of energy, compared to steel's 2 MJ. PCM stored 58% more energy than steel under the same conditions and retained energy more effectively during discharge, with steel losing 7.4% overnight.

Acknowledgements

Acknowledgments to CONAHCYT for the support given through a fellowship granted to Jonathan Eli Rojas Ricca.

Conflicts of Interest

Authors declare no conflict of interest.

REFERENCES

[1] S. Barbi, F. Barbieri, S. Marinelli, B. Rimini, S. Merchiori, M. Bottarelli, M. Montorsi, Polymers 14, 620 (2022). https://doi.org/10.3390/POLYM14030620

[2] A. Miliozzi, R. Liberatore, T. Crescenzi, E. Veca, Energy Procedia 82, 754–759 (2015) https://doi.org/10.1016/j.egypro.2015.11.799

[3] A.K. Ababneh, A.S. Hijazin, A.M. Jawarneh, Solar Energy 162, 1–10 (2018). https://doi.org/10.1016/j.solener.2018.01.060

[4] C. Prieto, L.F. Cabeza, M.C. Pavón-Moreno, E. Palomo, J. Energy Storage 74, 110618 (2024). https://doi.org/10.1016/j.est.2024.110618

[5] S. Baghaei Oskouei, M. ... [completar autores], Energy Convers. Manag. 290, 118117 (2024). https://doi.org/10.1016/j.enconman.2024.118117

[6] M.M. Kenisarin, Renew. Sustain. Energy Rev. 14, 955–970 (2010). https://doi.org/10.1016/j.rser.2009.11.011

[7] M. Contreras, M. Serrano-Medrano, O. Masera, Cuaderno Temático 1: Energía, CONAHCyT, https://conahcyt.mx/cuaderno-tematico-1/ Accessed 20 Oct. 2024.

[8] A. Ishizaka, P. Nemery, Multi-Criteria Decision Analysis (John Wiley & Sons, 2013). https://doi.org/10.1002/9781118644898

[9] R. Jäckel, F. Tapia, G. Gutiérrez, C. Monreal, Flow Meas. Instrum. 75, 101817 (2020) https://doi.org/10.1016/j.flowmeasinst.2020.101817

201-I-PO THEORETICAL ANALYSIS OF FLAT PLATE SOLAR COLLECTORS USING COPPER OXIDE (CUO) AND MULTI-WALLED CARBON NANOTUBE (MWCNT) NANOFLUIDS

J. Michael Cruz[1,2], G. Gutiérrez Urueta[3]*, A. Zacarías[1], G. Romage[1], J. G. Sánchez[4], E. E. Barrera[4], C. Jiménez[1]

[1]Instituto Politécnico Nacional, Escuela Superior de Ingeniería Mecánica y Eléctrica, Unidad Azcapotzalco, Av. de las Granjas 682, Col. Santa Catarina, C.P. 02250 CDMX, México.
[2]Universidad Autónoma de Tlaxcala, Facultad de Ciencias Básicas, Ingeniería y Tecnología, San Luis Apizaquito, C.P. 90401, México.
[3]Universidad Autónoma de San Luis Potosí, Facultad de Ingeniería, C.P. 78290, San Luis Potosí, México.
[4]Instituto Politécnico Nacional, Centro de Investigación en Ciencia Aplicada y Tecnología Avanzada, Unidad Querétaro, Cerro Blanco 141, Colinas del Cimatario, C.P. 76090 Querétaro, México.

*Correspondence: geydy.gutierrez@uaslp.mx

Abstract: This study evaluates the thermal performance of flat plate solar collectors using nanofluids based on copper oxide (CuO) and multi-walled carbon nanotubes (MWCNT). Simulations were conducted with a 0.1 volume fraction of each nanofluid using Engineering Equation Solver (EES). Results show that the addition of nanoparticles increases the removal factor, thermal diffusivity, and Nusselt number, enhancing the useful heat and thermal efficiency of the collectors. MWCNT nanofluids exhibit slightly higher performance than CuO, achieving an efficiency of 0.6876 compared to 0.6856 for CuO, due to superior thermal diffusivity that offsets lower specific heat and high viscosity. This study confirms that nanofluids can improve solar collector efficiency, offering promising advancements for energy applications at low to moderate temperatures.

Keywords: Nanofluids; Thermal efficiency; Flat plate solar collectors.

1. INTRODUCTION

Flat plate solar collectors have been extensively used for water heating and space heating applications requiring low or moderate temperatures, up to approximately 90 °C, as observed in the works of Belessiotis et al. [1] and Duffie [2]. Although these devices have been studied for many years, they continue to exhibit relatively low efficiency. Venegas et al. [3] and Dincer et al. [4] indicated that efficiency losses in conventional flat plate collectors can be categorized as optical losses, which are associated with the incidence angles of solar radiation, and thermal losses, which increase considerably with working temperature intensities. Despite their limited efficiency, flat plate collectors (FPCs) have the advantage of capturing both direct and diffuse radiation, which enhances their efficiency at lower temperatures, as demonstrated by Bhowmik et al. (2017) [5]. Studies on these collectors suggest that improving their efficiency requires maximizing the energy absorbed while minimizing losses to the environment. Additionally, Javadi et al. [6] concluded that efficiency can be further increased by improving the rate of heat transfer from the absorbing plate to the heat transfer fluid and subsequently from the fluid to the end user.

Previous research [7, 8,9,10] identifies various methods for enhancing the thermal performance of flat plate collectors. Among these methods is the addition of high thermal conductivity nanoparticles, such as carbon,

metals, or metal oxides, to the heat transfer fluid to increase the overall conductivity of the working fluid. The low thermal conductivity of water highlights the need for alternatives to optimize collector performance. With advances in nanotechnology, a new category of fluids, known as nanofluids, has emerged, consisting of nanoscale particles suspended in a base fluid. Consequently, to improve the efficiency of solar collectors, conventional fluids have been replaced with nanofluids. This study presents an evaluation of flat plate solar collectors using simple nanofluids of CuO and MWCNT.

2. MATERIALS AND METHODS

Based on Figure 1 mathematical modeling is raised, whose detail and validation is shown in [11] and based on several works [12-18]:

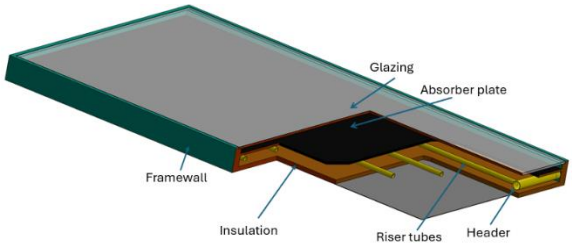

Figure 1. Sectional view of the flat plate solar collector.

2.1. Solar collector

According to [11], the useful heat is determined by the following expression:

$$Q_u = A_C F_R[I\tau\alpha - U_L(T_i - T_a)], \quad \text{Eq. (1)}$$

where Ac, I, $\tau\alpha$, represent the collector area, irradiance, and the product of transmittance and absorptance, respectively. T_i and T_a denote the inlet temperature and the ambient temperature, respectively. The heat removal factor, also known as the heat dissipation factor F_R, is determined as:

$$F_R = \frac{\dot{m}Cp}{A_C U_L}\left[1 - \exp\left(\frac{U_L F' A_C}{\dot{m}Cp}\right)\right], \quad \text{Eq. (2)}$$

The efficiency factor of the flat-plate solar collector, F', is calculated using the eq. (3) presented in [12]

$$F' = \frac{1/U_L}{W\left[\frac{1}{U_L[D_o + (W - D_o)F]} + \frac{1}{C_b} + \frac{1}{\pi D_{in} h_{fi}}\right]} \quad \text{Eq. (3)}$$

where W, D_{in}, and D_o represent the distance between fins and the internal and external diameters of the pipes, respectively. The conductance at the joints is denoted as C_b.

The standard fin efficiency, F, is determined by Eq. (4):

$$F = \frac{\tanh[m(W-D_o)/2]}{m(W-D_o)/2}, \quad \text{Eq. (4)}$$

The convective heat transfer coefficient, h_{fi} is calculated as:

$$h_{fi} = \frac{Nuk}{D_i} \quad \text{Eq. (5)}$$

where the Nusselt number is determined as suggested in [14]:

Laminar Flow: $Nu = 0.4328(1 + 11.285\phi^{0.754}Pe^{0.218})Re^{0.333}Pr^{0.4}$ Eq. (6)

Turbulent Flow: $Nu = 0.0059(1 + 7.6286\phi^{0.6886}Pe^{0.001})Re^{0.9238}Pr^{0.4}$ Eq. (7)

This relationship is valid for Re ≤ 2300 in laminar flow and Re > 2300 in turbulent flow.

The overall heat loss coefficient, U_L is calculated by:

$$U_L = U_t + U_b + U_\theta \quad \text{Eq. (8)}$$

where U_t, U_b and U_θ and are the top, bottom, and side loss coefficients, respectively. These loss coefficients are determined as:

$$U_t = \left\{ \frac{\frac{1}{N}}{\frac{C}{T_P\left[\frac{T_P - T_a}{N+f}\right]^{0.33} + \frac{1}{h_a}}} \right\} + \left\{ \frac{\sigma(T_P + T_a)(T_P^2 + T_a^2)}{\varepsilon_p + 0.5N(1-\varepsilon_p) + \frac{2N+f-1}{\varepsilon_g}} \right\} \quad \text{Eq. (9)}$$

$$U_b = k_b / x_b \quad \text{Eq. (10)}$$

$$U_e = A_e / A_C \quad \text{Eq. (11)}$$

The collector efficiency, η is calculated by

$$\eta = F_R\left[\tau\alpha - \frac{U_L(T_i - T_a)}{I}\right], \quad (12)$$

2.2. Simple nanofluids

The specific heat capacity of the nanofluid is determined as suggested in [15], using the eq. (13):

$$Cp_{nf} = \frac{Cp_{bf}\rho_{bf}(1-\emptyset) + Cp_{np}\rho_{np}\emptyset}{\rho_{nf}} \quad \text{Eq. (13)}$$

where Cp, ρ, ⌀ represent the specific heat capacity, density, and volume fraction, respectively. The subscripts n_f, n_p, b_f refer to nanofluid, nanoparticle, and base fluid, respectively.

The nanofluid density is determined as proposed in [16]:

$$\rho_{nf} = (1-\emptyset)\rho_{bf} + \emptyset\rho_{np} \quad \text{Eq. (14)}$$

The Brownian motion of the nanoparticles was considered in the study by [11] and in this work to estimate the thermal conductivity of the nanofluid, k_{nf}, with spherical nanoparticle:

$$k_{nf} = \left[\frac{k_{np} + 2k_{bf} - 2\emptyset(k_{bf} - k_{np})}{k_{np} + 2k_{bf} + \emptyset(k_{bf} - k_{np})} + \frac{\rho_{np}\phi Cp_{np}}{2k_{nf}}\sqrt{\frac{k_B T_m}{3\pi r_c \mu_{nf}}}\right] k_{bf} \quad \text{Eq. (15)}$$

For cylindrical nanoparticles, the thermal conductivity of the nanofluid, k_{nf}, was estimated with n=6:

$$k_{nf} = \left[\frac{k_{np} + 2k_{bf} - 2\emptyset(k_{bf} - k_{np})}{k_{np} + 2k_{bf} + \emptyset(k_{bf} - k_{np})}\right] k_{bf} \quad \text{Eq. (16)}$$

The model presented was programmed using the specialized software Engineering Equation Solver (EES) [19]. The simulation was conducted with a volume fraction of 0.1 for the CuO and MWCNT nanofluids. The properties of the base fluid were obtained from the data provided in [20], while the properties of the nanoparticles were assigned as shown in Table 1. The various parameters used in the simulation are listed in Table 2.

Table 1. Thermophysical properties of nanoparticles at 20 ° C

Nano-particles	□□ (kg/m³)	Cp (J/kg K)	K (W/mK)	Ref.
CuO	6000	551	33	[16]
MWCNT	1350	650	1500	[24]

Table 2. Parameters used in the simulation

Parameters	Value
FPSC inclination, β [°] [17]	20
Inlet temperature, Ti [°C]	30
Mass flow rate, $\dot{m}$, [kg⁄s]	0.08

3. RESULTS AND DISCUSSION

Figure 2 illustrates that the removal factor (FR) increases as the volume fraction rises for both nanofluids (CuO and MWCNT). The figure also shows that, for a volume fraction of 0.1, the MWCNT nanofluid achieves an FR of 0.8899,

slightly higher than that of the CuO nanofluid, which has an FR of 0.8873. Given that FR integrates the thermophysical properties of the fluid and represents the ratio of the actual useful energy gain of a collector to the useful gain if the entire collector surface were at the fluid's inlet temperature, an increase in FR would also enhance the useful heat and thermal efficiency of the solar collector.

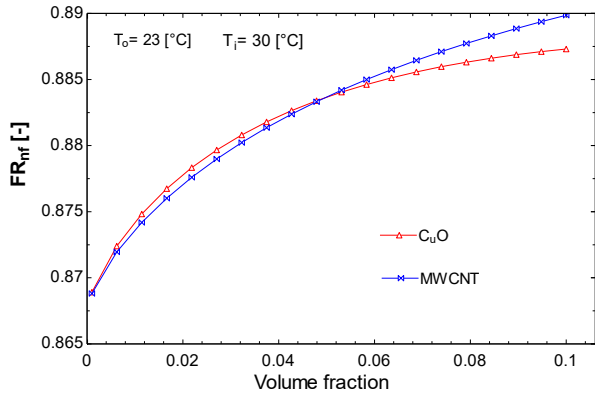

Figure 2. Heat removal factor (FR) depending on the volume fraction for copper oxide nanofluids and multiple wall carbon nanotubes (MWCNT).

Figure 3 displays useful heat in relation to the volume fraction of the nanofluids. The figure shows that useful heat increases with the addition of nanoparticles for the nanofluids studied (CuO and MWCNT). Multi-walled carbon nanotubes (MWCNT) demonstrate moderately higher values of useful heat output compared to copper oxide (CuO), achieving 582.7 kW for MWCNT and 581 kW for copper oxide at a volume fraction of 0.1.

Figure 4 presents the thermal efficiency of the flat plate solar collector as a function of the nanofluids' volume fraction (ratio of the volume of nanoparticles to the total volume of the mixture). It shows that thermal efficiency increases with the volume fraction in the studied nanofluids (CuO and MWCNT). Using multi-walled carbon nanotubes (MWCNT) results in slightly higher thermal efficiency compared to copper oxide (CuO), reaching a value of 0.6876 for MWCNT and 0.6856 for CuO at a 0.1 volume fraction.

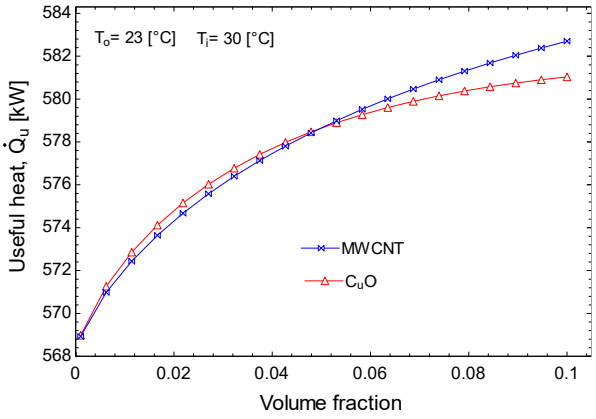

Figure 3. Useful heat vs. volume fraction for nanofluids of copper oxide (CUO) and multiple wall carbon nanotubes (MWCNT).

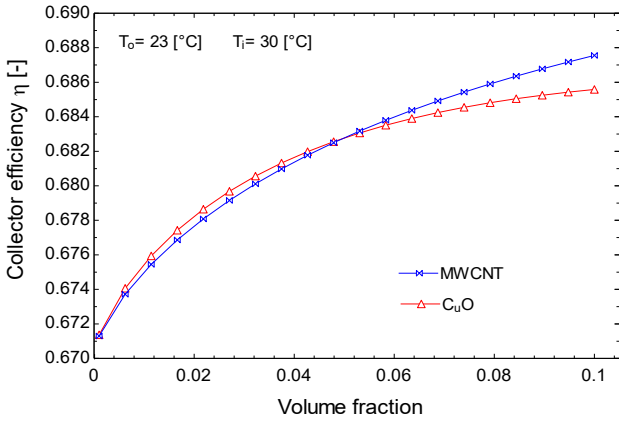

Figure 4. Collector efficiency vs. volume fraction for nanofluids of copper oxide (CUO) and multiple wall carbon nanotubes (MWCNT).

Results of Q_u and □□depend on the thermophysical properties of the aforementioned nanofluids. Additionally, the nanofluids studied can be compared to the base fluid (water), where the efficiency value corresponds to the case when the volume fraction is zero (see Figure 4). Based on the performance results of the FSC, it can be concluded that multi-walled carbon nanotube (MWCNT) and copper oxide (CuO) nanoparticles enhance the FSC efficiency by 2.41% and 2.12%, respectively, compared to the base fluid.

Figure 5 illustrates the change in thermal diffusivity and the Nusselt number with increasing volume fraction. The use of metallic oxide and carbon nanofluids results in an

increase in the removal factor, which subsequently enhances useful heat and thermal efficiency. This effect is beneficial and can be attributed primarily to the thermal diffusivity of the nanoparticles ($\alpha=k/\rho Cp$), in addition to their diameter. This property offsets the thermal storage effect and compensates for relatively low specific heat values, high density, and viscosity.

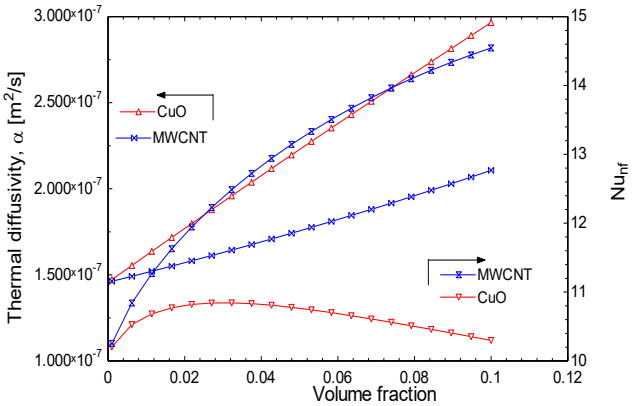

Figure 5. Thermal diffusivity, Nusselt number with respect to the volume fraction for copper oxide nanofluids and multiple wall carbon nanotubes (MWCNT).

4. CONCLUSIONS

It can be concluded that incorporating metallic oxide and carbon-based nanofluids (CuO and MWCNT) enhances slightly the performance of flat plate solar collectors. Specifically, the addition of nanoparticles increases thermal diffusivity, Nusselt number, and removal factor, all of which can contribute to improve of useful heat and thermal efficiency. MWCNT nanofluids exhibit in small amount higher efficiency values than CuO, attributed to their superior thermal diffusivity, which compensates for challenges such as low specific heat and high density. Therefore, the application of nanofluids in solar collectors offers potential for improved energy conversion efficiency in low- to moderate-temperature solar applications.

Acknowledgements

The financial support of this study by the SIP20240435 scientific research scholarship, of the National Polytechnic Institute, IPN, is greatly appreciated. The authors also appreciate the financial support granted to postgraduate students by CONAHCYT, Mexico.

Conflicts of Interest

The authors declare no conflict of interest.

REFERENCES

[1] Belessiotis, V., Kalogirou, S., & Delyannis, E. Thermal Solar Desalination. Methods and Systems (AP, 2016), https://doi.org/10.1016/C2015-0-05735-5

[2] Duffie JA, Beckman WA. Solar engineering of thermal processes (Wiley, New York, 1991), https://doi.org/10.1002/9781118671603

[3] Venegas, M.; García-Hernando, N.; Zacarías, A.; De Vega, M., Applied Sciences (2020). https://doi.org/10.3390/app10082761

[4] Dincer, Y. Bicer, PV-Based energy conversion systems, iCompr. Energy Syst. (2018), https://doi.org/10.1016/B978-0-12-809597-3.00430-2

[5] H. Bhowmik, R. Amin, Energy Reports (2017) https://doi.org/10.1016/j.egyr.2017.08.002

[6] F.S. Javadi, R. Saidur, M. Kamalisarvestani, Renewable and Sustainable Energy Reviews (2013), https://doi.org/10.1016/j.rser.2013.06.053

[7] X.Q. Wang, A.S. Mujumdar, International Journal of Thermal Sciences (2007) http://dx.doi.org/10.1016/j.ijthermalsci.2006.06.010

[8] L. Godson, B. Raja, D.M. Lal, S. Wongwises, Renewable and Sustainable Energy Reviews (2010) https://doi.org/10.1016/j.rser.2009.10.004

[9] Pandey KM, Chaurasiya R. A, Renewable and Sustainable Energy Reviews (2017). https://doi.org/10.1016/j.rser.2016.09.078

[10] I. Wole-osho, E.C. Okonkwo, S. Abbasoglu, D. Kavaz, International

Journal of Thermophysics (2020). https://doi.org/10.1007/s10765-020-02737-1

[11] Cruz J.M. et al. Applied Sciences (2024) https://doi.org/10.3390/app14198732

[12] Goswami D.Y, Principles of Solar Engineering, 4th edn. (CRC Press, 2022). https://doi.org/10.1201/9781003244387.

[13] Kalogirou S.A., Solar Energy Engineering. Processes and Systems (AP, 2023). https://doi.org/10.1016/C2021-0-02041-1

[14] Sint, N.K.C. et al. Solar Energy (2017) https://doi.org/10.1016/j.solener.2017.06.055

[15] Alawi, O.A.; et al. Journal of Cleaner Production (2021). https://doi.org/10.1016/j.jclepro.2020.125725

[16] Pak, B.C.; Cho, Y.I. Experimental Heat Transfer (1998), https://doi.org/10.1080/08916159808946559

[17] Hawwash, A.A.; et al. in IEEE (2021) https://doi.org/10.1109/ACCESS.2021.3060004

[18] Xuan, Y.; Li, Q.; Hu, W. AIChE Journal (2023). https://doi.org/10.1002/aic.690490420

[19] Klein, S.A. (2018). Engineering Equation Solver, 1992-2015, f-Chart Software, https://fchartsoftware.com/ees/

[20] Said, Z.; Saidur, R.; Rahim, N.A. International Communications in Heat and Mass Transfer (2014), https://doi.org/10.1016/j.icheatmasstransfer.2014.10.010

212-I-PO EVALUATION OF FLUID BEHAVIOR IN A CITRUS GREENHOUSE IN THE VERACRUZ AREA USING CFD ANALYSIS

A. Adauto-Arriola[1]*, A. Reyes-Salas[1], Y. López-Grijalba[1], J. Cruz-Castro[1], J. Mares-Carreño[1], G. S. Abarca-Jiménez[1]

[1]Instituto Politécnico Nacional, Unidad Profesional Interdisciplinaria de Ingeniería Campus Hidalgo, carretera Pachuca-Actopan km 1+500, Distrito de Educación, Salud, Ciencia, Tecnología e Innovación, C.P. 42162, San Agustín Tlaxiaca, Hidalgo.

*Correspondence: aadautoa1601@alumno.ipn.mx

Abstract. Different forms of cultivation exist within the agricultural production of the country. Greenhouses have been implemented in the production of citrus plants in order to be able to control the environmental conditions that favor their development and as a protective barrier against the spread of diseases and pests. However, this greenhouse system can have its drawbacks due to the microclimate that is generated depending on the environmental conditions of the place, leading to an increase in humidity in the crop and therefore the possible spread of diseases. Due to this, a study of the internal conditions is presented through a 2D computational fluid analysis of a Cenital greenhouse with anti-aphid mesh for citrus located in the municipality of Martínez de la Torre, Veracruz where several problems have been registered. The anti-aphid mesh was characterized through an optical microscope to obtain the pore dimensions of the mesh and through experimental tests the porosity and pressure drop were obtained. These data and considering the most representative environmental conditions of the region such as temperature, humidity and wind speed, were used for the study with ANSYS® Fluent. From the results obtained, it is observed that, under certain environmental conditions, especially low wind speed, a stagnation effect is generated inside the greenhouse which results in low ventilation and increased humidity. However, it was observed in different scenarios that internal environmental conditions such as speed can vary around up to 49.76% when any of the climatic variables is affected. These conditions can lead to drastic changes in the greenhouse microclimate and, therefore, conditions that affect the crop in its growth stages or the generation of pests. For the above reasons, the results obtained can be used to propose solutions that optimize environmental conditions for citrus plant growth.

Keywords: Permeability, porous medium, CFD, microclimate.

1. INTRODUCTION

The production of citrus, specifically Persian lemons citrus in a large-scale greenhouse is vulnerable to the microclimate that is generated due to high humidity and temperature values that favor the generation of pests. It is important to mention that the process of citrus production in greenhouses must comply with Mexican Official Standard NOM-079-FITO_2002, whose objective is to establish phytosanitary regulations for the production and movement of propagating material free of viruses and other pathogens associated with citrus.

The use of meshing in greenhouses is recommended to prevent important crop damage. Their main function is to generate a physical barrier that prevents the passage of insects (pests) into the greenhouse and, therefore, to have a low incidence of diseases

caused by insects, thus reducing phytosanitary treatments.

The use of meshes is widely spread, but it has a disadvantage: the decrease of natural ventilation, which causes an increase of temperature and/or humidity in some areas of the greenhouse that could propitiate conditions for the propagation of pests and diseases in the crop, therefore, losses in production. The efficiency of these meshes depends mainly on the mesh size (it must be smaller than the thoracic diameter of the smallest insect to be excluded), its cross section and optical properties (such as color). The porosity of the mesh is the ratio of the pore area to the total area; it depends on the diameter of the thread and the number of threads per unit area. This determines the reduction in the natural ventilation rate. Due to this resistance, air velocity, temperature and humidity inside greenhouses are modified [1]. Similarly, light transmission may be reduced [2], seriously affecting crop growth and development. The screens normally used in greenhouses decrease the ventilation rate by approximately 40% in anti-insect screens, and 70-80% in anti-trip screens [3], although this decrease can be higher if the wind speed is very low [4]. To analyze the characteristics of the air flow through the screen in the greenhouse, it is important to determine its permeability (K, m^2) and its inertial factor (Y, nondimensional). These are two fundamental parameters for modeling the passage of air through a porous medium.

The objective of this study is to establish the methodology for the simulation of the microclimate in a greenhouse through Computational Fluid Dynamics (CFD) in order to generate proposals for effective solutions to be implemented and adapted in greenhouses for citrus production. Therefore, this work shows from the characterization of the anti-aphid mesh by experimental means to the numerical simulation using the conditions obtained in the experimentation to validate the computational solution models. By means of microscopic measurements and the use of a physical configuration for experimental purposes, the porosity of the mesh is calculated based on pressure drop and is used to determine its effect on the ventilation rate, permeability and its inertial factor.

2. MATERIALS AND METHODS

The efficiency of anti-aphid meshes as a physical barrier implemented in greenhouses depends on the pore dimensions between the mesh threads and the permeability.

a) Materials

For the development of the present work, the division between the experimental and the numerical part is made. The following components were used for the experimental section:

- *UNI-T*® brand anemometer, model UT363S
- *PerfectPrime*® model AR1890P1 digital manometer
- A sample of the anti-aphid mesh used
- *Mitutoyo*® brand optical microscope model PJ-R300
- *Makita*® UB-1103 wind generator

3. METHODS

According to different works focused on the analysis of the ventilation rate and the microclimate inside a greenhouse, studies have been carried out on the behavior of the wind currents used in the ventilation surface [5,6]. The variation of these currents is due to the use of different types of meshes, considering the geometry of their pores. The efficiency of the anti-avoidance mesh as a physical barrier depends on the dimensions of the pores between the threads of the mesh, so the diameter of the fibers must be known in order to calculate the average length of the pores in the two main directions of the mesh. For the development of this work, a theoretical-experimental methodology was proposed to validate the numerical models that can be proposed for the solution of the problem to be addressed. The preparation of

the sample of the type of anti-aphid mesh consisted of the selection of a portion of this, obtained from the greenhouse where this study was carried out. It was placed in a Mitutoyo® optical microscope model PJ-R300, being adjusted to a plane to obtain dimensions of the thread, such as constant diameter of the thread, number of threads in 1 cm^2 in the x and y direction, to calculate the dimension of the pore defined by four threads that intertwine to form the mesh. Subsequently, the porosity of the mesh is determined with equations (1) and (2) from [4].

$$L_x = \frac{10}{N_x} - D \qquad \text{Eq. (1)}$$

$$L_y = \frac{10}{N_y} - D \qquad \text{Eq. (2)}$$

Where: L_x is the average pore size in the x-direction and the L_y is the average pore size in the y direction. [7] established that in the analysis of meshes it is possible to have a different yarn diameter depending on the weft and warp directions by proposing number of yarns per unit length (yarns cm^{-1}). The weft *(Px)* and warp *(Py)* directions of the mesh were calculated using equations (3) and (4).

$$Px = \frac{1}{Lpy + dhx} \qquad \text{Eq. (3)}$$

$$Py = \frac{1}{Lpx + dhy} \qquad \text{Eq. (4)}$$

Where *Lpy* and *Lpx* are the characteristic dimensions of the mesh pores, *dhx* and *dhy* are the thickness of the warp and weft yarns, respectively. From the above, the following characteristics of the selected mesh have been obtained.

Table 1. Characteristic dimensions of the anti-aphid mesh

Dimension	(mm)
Lx	0.7300
Ly	0.2300
Px	1.0050
Py	1.5552

With the data obtained from the anti-aphid mesh, the porosity α was calculated, which is defined as the surface area occupied by the holes with respect to the total surface area of the mesh considering a constant wire diameter, calculated with equation (5).

$$\alpha = \frac{Lx\,Ly}{(Lx + D)(Ly + D)} \qquad \text{Eq. (5)}$$

Where *D* is the average diameter of the yarns. The anti-aphid mesh was experimentally characterized by performing tests in an experimental arrangement with a circular section, where the velocity was modified with the anti-aphid mesh, in order to obtain the pressure drop generated. The experimental arrangement consisted of a structure generated by cylindrical elements (CPVC pipe) and a Makita® UB-1103 wind generator. Figure 1 shows the generator, the structure, the location of the manometer and anemometer at the measurement points such as static pressure before and after the porous medium, inlet and outlet velocity.

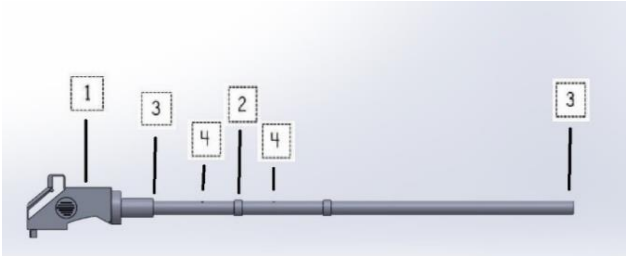

Figure 1. Diagram of the experimental structure.

Where 1 is a wind generator, 2 is the porous medium (anti-aphid mesh), 3 is an anemometer and 4 is a digital manometer. From the characterization, the parameters of the porous medium were determined, such as: inlet and outlet velocities, inlet and outlet static pressure with different operating conditions of the experimental arrangement that contributed to the CFD analysis. Subsequently, the data were plotted, and the characteristic equation was obtained to calculate the permeability coefficients (K), and pressure drop coefficient with the Forchheimer equation [8].

$$\Delta p = AV2 + BV + C \qquad \text{Eq. (6)}$$

The 2D model of the greenhouse shown in Figure 2 was made considering only one tunnel, with the purpose of analyzing the wind flow and the pressure drop through it.

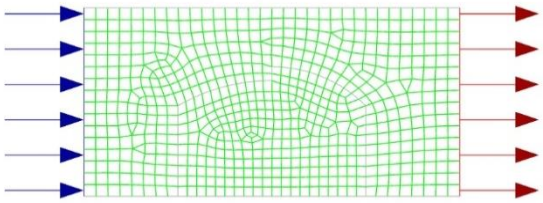

Figure 2. Discretization and boundary conditions.

The geometry was worked out in an ANSYS® Fluent module with different conditions at the inlet boundary. It was applied to the inlet a velocity inlet of 3.61 m/s, 8.33 m/s, 10.55 m/s, and 13.88 m/s. These cases were proposed based on the meteorological conditions registered through the year in Martínez de la Torre, Veracruz [9]. The purpose of these conditions is to compare the pressure drop and speed inside the greenhouse. Besides, the ambient temperature registered in these months was considered to calculate the physics properties of the air. The detailed boundary conditions are presented in Table 2.

Table 2. Fluid conditions (air).

Case	***Temperature [K]***	***Velocity [m/s]***	***Density [kg/m^3]***	***Viscosity [Pa.s] x10^{-6}***
1	*315.150*	*3.610*	*1.451*	*18.720*
2	*306.150*	*8.330*	*1.115*	*19.180*
3	*309.150*	*10.550*	*1.136*	*18.950*
4	*299.150*	*13.880*	*1.170*	*18.940*

4. RESULTS AND DISCUSSION

Four cases were analyzed based on the conditions mentioned in section 3. Figure 3 shows the velocity contours for case 4, with a velocity inlet of 13.88 m/s. A non-uniform distribution of velocity inside the greenhouse tunnel is noticed although the outside velocity of wind is high. In this sense, it is expected that the natural process of ventilation will not develop adequately. Above all in the middle zone of the tunnel.

Figure 4 shows the pressure contours. It is noticed that there is a loss of around 61%, comparing the inlet conditions versus the conditions inside the tunnel of the greenhouse. For this section it is only display the graphic conditions for the case with the major velocity wind applied in the cases of study. The results for the other cases are shown in Table 3.

Table 3. Internal greenhouse conditions obtained form the simulation.

Case	**Velocity (m/s)**	**Pressure (Pa)**
1	0.940	31.30
2	3.130	123.50
3	3.870	238.00
4	6.640	358.00

These analyses are limited to certain meteorological conditions of the site applied to the physical conditions in the air. However, the radiation condition was not considered in this case of study. Also, it was assumed that there were no plants inside the greenhouse and the humidity conditions expected. The incidence of the wind was considered normal to the inlet condition, so no different directions of the wind were considered in this study.

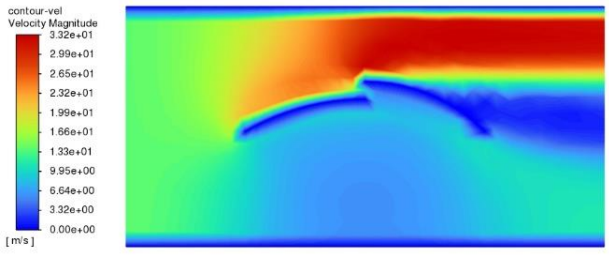

Figure 3. Velocity contours obtained in case 4.

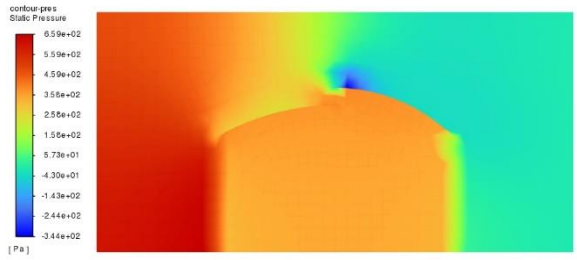

Figure 4. Pressure contours obtained in case 4.

Based on the results obtained from the permeability and pressure drop coefficient, the idea is to integrate these values into a 3D model of the tunnel. This model will include internal elements that simulate the crop inside the greenhouse, in order to analyze the behavior of internal ventilation.

5. CONCLUSIONS

Based on the results obtained from the CFD simulations, which are based on the permeability calculations and pressure drop coefficient of the anti-aphid mesh used, the pressure contours showed a significant drop within the greenhouse geometry, and the velocity contours reveal relatively low wind speeds. It is concluded that the combination of these factors indicates an air flow stagnation inside the greenhouse. This phenomenon negatively impacts the internal climatic conditions of the greenhouse.

The methodology applied to the characterization of the anti-aphid mesh replied from previous works mentioned in section 3 was validated by using an experimental and numerical evaluation. The characteristics obtained were applied as a porous boundary in a 2D CFD analysis to observe the pressure and velocity contour inside a tunnel of a greenhouse. However, in this study the meteorological conditions of the site were considered in comparison with other studies. It is important to make notice that these conditions modify the clime inside the greenhouse. The anti-aphid mesh applied in the studies can conduct different results. It is necessary to establish the external boundary conditions for each condition of the greenhouse.

A better understanding of the inside clime conditions of the greenhouse can be obtained based on the methodology shown in this paper. This can provide information to establish located solutions to diminish the high percentages of humidity and temperature registered in these types of greenhouses that promote the development of diseases and pests.

Conflicts of Interest

The authors declare no conflict of interest.

REFERENCES

[1] H. Fatnassi, T. Boulard, and L. Bouirden, (2003) https://doi.org/10.1016/S0168-1923(03)00071-6

[2] Von Zabeltitz, C., & von Zabeltitz, C. 1st edn. (Springer, Berlin Heidelberg. 2011). pp. 285-311

[3] J. I. Montero and A. Antón, (2000) https://doi.org/10.17660/ActaHortic.2000.534.3

[4] E. Ziemba, Information Technology for Management: New Ideas and Real Solutions. 1st edn. (Springer, AITM, 2016) pp. 222-241.

[5] Romero-Gómez, P., Choi, C. Y., & Lopez-Cruz, I. L. Agrociencia. 1 (1), (2010).

[6] D. L. Valera, A. J. Álvarez, and F. D. Molina, (2006) https://doi.org/10.5424/sjar/2006044-204

[7] A. J. Álvarez, R. M. Oliva, and D. L. Valera, (2012) https://doi.org/10.1016/j.compag.2012.01.001

[8] A. F. Miguel, N. J. Van De Braak, and G. P. A. Bot, (1997) https://doi.org/10.1006/jaer.1997.0157

[9] Meteoblue, Weather archive Martínez de la Torre, México, (2023). https://www.meteoblue.com. Accesed 10 August 2024

217-I-PO MODELING AND SIMULATION OF ABSORPTION COOLING SYSTEM WITH EVAPORATION TEMPERATURE BELOW ZERO CELSIUS

J. Castillo Cuauhtémoc[1]*, V. García Rodríguez[1], A. Zacarías Santiago[1], G. Romage[1], E. E. Barrera García[2]*

[1]Instituto Politécnico Nacional, Escuela Superior de Ingeniería Mecánica y Eléctrica, Unidad Azcapotzalco, Academia de Térmicas, Sección de Estudios de Posgrado e Investigación, Av. de las Granjas 682, Col. Santa Catarina, C.P. 02550 CDMX, México.
[2]Instituto Politécnico Nacional, Centro de Investigación en Ciencia Aplicada y Tecnología Avanzada, Unidad Querétaro, Cerro Blanco 141, Colinas del Cimatario, C.P. 76090 Querétaro, México.

*Correspondence: cjimenezc@ipn.mx, ebarrerag2300@alumno.ipn.mx

Abstract: This work presents the simulation of an absorption cooling system that operates with an Ammonia Lithium Nitrate solution, which is powered by solar energy at low temperature. It is proposed to use a flat solar collector which provides temperatures in the generator in a range of 75 to 80°C, using renewable energy as a thermal power source and thus facilitating the use of the solution. The thermodynamic behavior of the system with mass and energy balance of each component of the single-effect absorption system was analyzed. It has a cooling capacity of 0.1 to 2 kW, with evaporation temperatures of -10, -5 and 0 °C and the ambient temperature of 20, 25 and 30 °C, based on this the thermal capacities were determined. The results of the thermodynamic analysis show COP values of 0.6 to 0.7, to date there are few works with the Ammonia – Lithium Nitrate solution using solar energy at low temperatures as a supply. The model developed will be the point of comparison of the results of the start-up of the experimental absorption machine.

Keywords: Cooling, ammonia, lithium nitrate, solar energy.

1. INTRODUCTION

Absorption cooling (SRA) can replace electricity consumption through the use of thermal energy (e.g. heat from industrial waste, solar energy, etc.). Currently, non-adiabatic SRA operate with absorbers that transfer heat by releasing the absorbed heat into the environment, making them more expensive and durable because they use mechanisms to remove the resulting heat. In an SRA adiabatic absorber there is no heat transfer, only mass transfer, they use spray absorbers because they are simpler and more compact. These systems can be used to design machines with lower cooling capacity. The focus of SRA on achieving cooling using low-cost power sources for a variety of applications or needs, such as refrigeration and freezing, makes adiabatic SRA a viable source of heat generated by flat-panel solar collectors at low temperatures. The SRA has generated particular interest in this area of research over the past two decades.

For the record, SRA has been studied for decades [1], [2] and [3] and the literature investigates water vapor absorption using an aqueous solution of lithium bromide in an adiabatic aerosol, and three years later an absorption device was developed to use an adiabatic aerosol. The authors [4] also contributed, who analyzed the behavior of spray absorbers using ammonia and lithium nitrate solutions.

The research conducted by the authors [5], [6] and [7] was based on the use of

alternative energy sources (gas flame and electric resistance) for circulation in the absorption machine, however, these authors did not use flat solar collectors.

Some authors have developed experimental devices that use energy sources other than electricity and with different working solutions [8], [9] and [10]. However, these experimental machines were not yet mass-produced on the world market and largely replaced vapor compression systems. This work presents an adiabatic SRA together with computational and analytical methods to interpret the values obtained during system start-up.

2. DESCRIPTION OF THE SYSTEM

In order to explain the mathematical model of the adiabatic SRA, Fig. 1 is used to analyze the elements that compose it as follows: The system consists of a condenser, an expansion valve, an evaporator and a thermochemical compressor. The latter consists of a generator, a heat recovery unit, a subcooler, an adiabatic absorber and a feedwater pump. Likewise, the system is divided into two circuits or cycles that include the refrigerant and the solution. The refrigeration circuit starts from the condenser (1), where heat is exchanged with the external environment from the generator, after condensation, the refrigerant enters the expansion valve (2), resulting in a decrease in pressure and temperature without heat exchange, and continues. On its way to the evaporator (3), the evaporator (3) absorbs heat energy corresponding to the latent heat of vaporization and discharges it in the form of refrigerant vapor, thus creating a cooling effect.

For the solution circuit, the refrigerant vapour exits the evaporator and enters the adiabatic spray absorber (4), mass transfer only occurs in this system component and the absorption chamber disperses the incoming concentrated solution into the absorption chamber. The contact area between the solution and the refrigerant vapor is increased to obtain a dilute solution that is transported to the generator through the feed pump (5) and heat recovery (6). After reaching the generator (7), the remaining solution passes through the heat recovery device (8) and liquid expansion valve (9) before returning to the absorber. Finally, the heat generated in the absorption process is transferred to the subcooler (10). In this way, these two schemes complement each other and give rise to the 5.

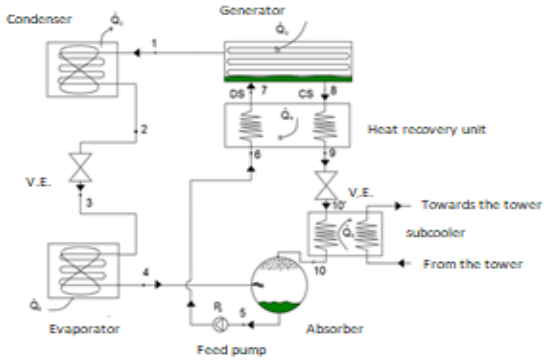

Figure 1. Diagram of an adiabatic absorption cooling system.

3. MATHEMATICAL MODEL

The purpose of developing a mathematical model of adiabatic SRA is to provide a method for its evaluation. This analysis is based on the mass and energy balance of each component of the system, as shown in Fig. 1. According to the simulation, the process that is carried out on each component or unit of the equipment in constant flow is considered ideal, without considering the losses of energy to the environment, and all processes are carried out in pairs. The points, entrances and exits of each element are evaluated in relation to aspects. Using the mass and energy balance, equations can be derived that describe the behavior of the solution as it passes through each part of the system. As we develop the model, we will discuss dilute and concentrated solutions with reference to the concentration of the absorbent. According to the order shown in the image. As shown in Figure 1, the refrigerant circuit and the solution circuit can be visualized as above in points 1-2-3-4 and 5-6-7-8-9-10 respectively. Likewise, diluted solutions include 5-6-7 points, and concentrated solutions

include 8-9-10 points. With these factors in mind, high and low pressures are determined using evaporator and condenser temperatures to begin mathematical modeling.

Once the pressure is established, the enthalpy of each refrigerant remains between points 1 to 4.

Proposing:

$$X_5 = X_6 = X_7$$

$$X_8 = X_9 = X_{10}$$

$$\dot{m}_r = \dot{m}_1 = \dot{m}_2 = \dot{m}_3 = \dot{m}_4$$

Where $X_5 = X_6 = X_7$ and $X_8 = X_9 = X_{10}$ are the solution concentrations at each of the points dimensionless, $\dot{m}_r = \dot{m}_1 = \dot{m}_2 = \dot{m}_3 = \dot{m}_4$ it is the mass flow of refrigerant at each of the points in kg/s.

The refrigerant flow for a cooling capacity of 2 kW is determined as follows:

$$\dot{m}_r = \frac{\dot{Q}_e}{h_{fg}} \qquad \text{Eq. (1)}$$

Where $\dot{Q}_e$ it is the heat that the evaporator can absorb in kW, h_{fg} is the latent heat of fusion of the refrigerant in kJ7kg.

Using the low pressure Pb and condenser temperature Tc, determine the concentration of the Xds solution at the outlet of the absorber. As a result, the concentration increases by 7% and the Xcs of the concentrated solution is calculated. Therefore we have:

$$\Delta X = X_{cs} - X_{ds}$$

$$X_{cs} = X_8 = X_9 = X_{10} = \Delta X + X_{ds} \qquad \text{Eq. (2)}$$

Where ΔX is the change in concentration, dimensionless, X_{cs} it is the quality of the concentrated, dimensionless, X_{ds} It is the quality of the diluted, dimensionless.

To determine the mass flow of a dilute solution, calculate as follows:

$$\dot{m}_{ds} = \dot{m}_R \left[\frac{(1-X_{cs})}{(X_{ds}-X_{cs})}\right] \qquad \text{Eq. (3)}$$

Where $\dot{m}_{ds}$ is the mass flow of the diluted solution in kg/s.

The flow of a concentrated solution is determined by the mass balance in the absorbent:

$$m_{cs} = \dot{m}_{ds} - \dot{m}_r \qquad \text{Eq. (4)}$$

Where m_{cs} is the mass flow of the concentrated solution in kg/s.

If the enthalpy at the outlet of the absorbent is equal to the enthalpy at the outlet of the pump, and if the efficiency of the heat exchanger is considered to be 70%, the temperature T9 can be determined by:

$$\varepsilon = \frac{T_8 - T_9}{T_8 - T_6} \qquad \text{Eq. (5)}$$

Where T_8, T_9, T_8, T_6 are the temperatures at each of the points shown °C.

The heat flow of each component is determined by the SRA energy balance as follows:

$$\dot{Q}_c = \dot{m}_r(h_1 - h_2) \qquad \text{Eq. (6)}$$

$$\dot{Q}_r = \dot{m}_{ds}(h_7 - h_6) \qquad \text{Eq. (7)}$$

$$\dot{Q}_r = \dot{m}_{cs}(h_8 - h_9) \qquad \text{Eq. (8)}$$

$$\dot{Q}_g = \dot{m}_r h_1 + \dot{m}_{cs} h_8 - \dot{m}_{ds} h_7 \qquad \text{Eq. (9)}$$

$$\dot{Q}_{SE} = \dot{m}_{cs}(T_{10'} - T_{10}) \qquad \text{Eq. (10)}$$

$$\dot{Q}_{SE} = \dot{m}_{agua} C_{p\,agua}(T_{12} - T_{11}) \qquad \text{Eq. (11)}$$

Where $\dot{Q}_c, \dot{Q}_r, \dot{Q}_g, \dot{Q}_{SE}$ are the heat in the condenser, heat in the recuperator, heat in the generator, heat in the heat exchanger respectively in kW, h_1, h_2, h_6, h_7, h_8, h_9 are the enthalpies at each of the points shown in kJ/kg, $T_{10'}, T_{10}, T_{12}, T_{11}$ are the temperatures at each of the points shown in °C, $C_{p\,agua}$ specific heat of cooling water in kJ/kg-K, $\dot{m}_{agua}$ cooling water mass flow kg/s.

In the case of mass flows, we have:

$$\dot{m}_{ds} = m_{cs} - \dot{m}_r \qquad \text{Eq. (12)}$$

$$\dot{m}_{ds} X_5 = m_{cs} X_{10} - \dot{m}_r X_4 \qquad \text{Eq. (13)}$$

$$\dot{m}_{ds}h_5 = m_{cs}h_{10} - \dot{m}_r h_4 \qquad \text{Eq. (14)}$$

We can obtain the mass and energy balance of the absorber. The coefficient of performance or COP is determined by the following formula:

$$COP = \frac{\dot{Q}_e}{\dot{Q}_g + \dot{W}_B} \qquad \text{Eq. (15)}$$

Where COP is the coefficient of performance dimensionless, $\dot{W}_B$ is the work of the solution pump in kW.

Developing a global energy balance, we have:

$$\Delta\dot{Q} = (\dot{Q}e + \dot{Q}_g) - (\dot{Q}_{SE} + \dot{Q}_r + \dot{Q}_c) \qquad \text{Eq. (16)}$$

Where $\Delta\dot{Q}$ is the overall energy balance in kW.

This ensures that the sum of all heat inputs and outputs results in zero. The mathematical model presented in this work proposes the cooling temperature, the evaporator temperature and the condensation temperature as independent variables to determine the properties of the fluid used and recommendations for its experimental configuration.

4. RESULTS AND DISCUSSION

To obtain the results, the Engineering Equation Solver software (EES) program was used to simulate the behavior of the SRA, as mentioned above, an energy and mass balance was performed for each component, as a result three representative figures were obtained, corresponding to the generation temperature versus the circulation ratio, the heat that can be obtained in the generator and the system performance coefficient, these three graphs with an evaporation temperature from 0 ° C to -10 ° C, as well as a condensation temperature of 25, 30, 35 and 40 ° C, the analysis is described below.

In Fig. 2 it can be seen that low power is required in the generator in particular conditions of T_g=60°C, Tc=30°C and Te=0°C compared when the conditions of T_g=85°C, Tc=35°C and Te=-10°C are met, it can be seen that the heat capacity of the generator increases four times more. It is noted that if the temperature of the condenser increases, the generation power will also increase having fixed values T_g and Te, on the contrary, if Te increases by setting T_g and Tc, it is lower. On the other hand, having Tg=85°C, Tc=35°C and Te=-10°C, a very high power in the generator of approximately 11kW is needed.

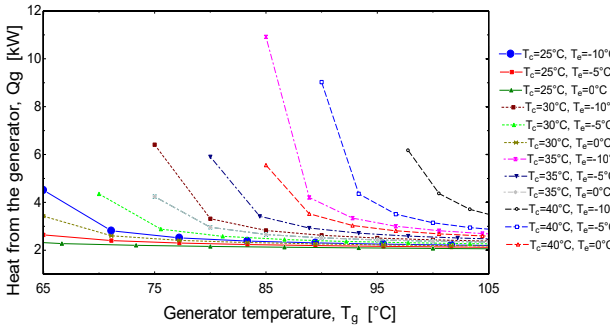

Figure 2. Generation power against generation temperature for different condensation and evaporation temperatures, working system with lithium ammonia nitrate solution.

In Fig. 3 there is the graph of the circulation relationship with respect to the generation temperature, it can be seen that when the temperature of the generator increases, the circulation ratio can decrease, having the highest point when there is a generation temperature of approximately 85°C, with -5°C in the evaporator there is a circulation ratio of 50, however, at the generator temperature of 100°C and 0°C in the evaporator the ratio factor is approximately 2.5.

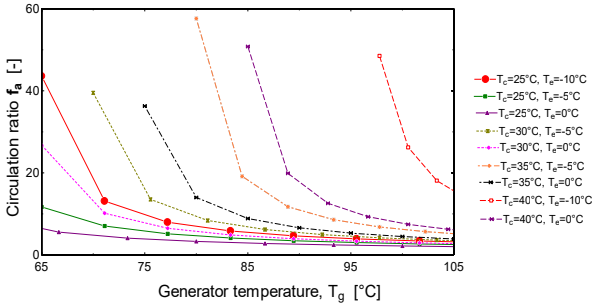

Figure 3. Circulation ratio against generation temperature for different condensation and evaporation temperatures, working system with lithium ammonia nitrate solution.

In fig. 4 you can see the SRAA simulation, in which the generation temperature (**Tg**) is presented against the operating coefficient (COP) with an evaporation capacity of 2kW. For the ammonia-lithium nitrate solution, as can be seen, the highest COP has a value of 1 with the conditions of Tg=100°C, Tc=25°C and Te=5°C, likewise the lowest COP that can be presented with a value of 0.05 under conditions of Tg=95°C, Tc=40°C and Te=5°C, this means that with the first conditions it increases twenty times more, in the second condition the COP values can be raised if the generation temperature is increased reaching a value of 0.7 with a T_g=120°C.

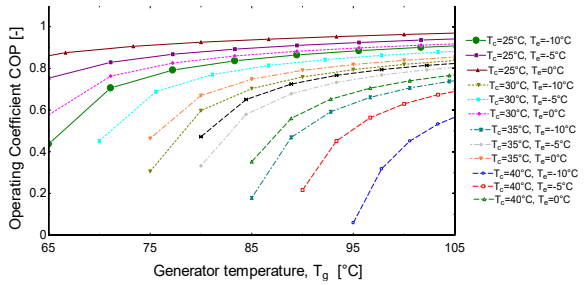

Figure 4. Coefficient of Operation against generation temperature for different condensation and evaporation temperatures, working system with lithium ammonia nitrate solution.

5. CONCLUSIONS

With the mathematical model developed in this work and the use of the *Engineering Equation Solver software (EES),* the operating conditions of a refrigeration machine to be built were determined to evaluate the performance and make possible improvements to it. Graphs were also generated based on condensation temperatures, evaporation, concentration of the solution and amount of heat removed in the evaporator.

One of the important parts of this work was that it is possible to implement an absorption refrigeration cycle that has lower temperatures in the evaporator below 0°C, in order to be able to freeze a product in which it is necessary to occupy this temperature, such as fish or meat.

Acknowledgements

The financial support of this study by the scientific research grant SIP20241776, of the National Polytechnic Institute, IPN, is greatly appreciated. The authors are also grateful for the financial support granted to graduate students by the National Council of Science and Technology, CONACYT, of Mexico.

Conflicts of interest

The authors declare no conflict of interest.

REFERENCES

[1] Quiroz, J. A. (2015). Thermal study of an adiabatic absorption refrigeration machine using the solution Ammonia - Lithium Nitrate as a working fluid. *Master's thesis*. Mexico, Federal District: National Polytechnic Institute.

[2] García L. M. (2017) Study of a low-capacity adiabatic absorption cooling system operating with solar energy, Master's Thesis, National Polytechnic Institute, Mexico.

[3] Kreith, F. (1999). *Principles of Solar Engineering*. Philadelphia: Taylor & Francis.

[4] M. Venegas, P. R. (2005). Spray absorbers in absorption systems using lithium nitrate–ammonia solution. International Journal of Refrigeration, 554–564.

[5] Ryan, W. (1995). Model development and verification of spray absorption for gas driven cooling systems. International Gas Research Conference, 1483 - 1493.

[6] G. Romage, C. Jiménez, J de J Reyes, A. Zacarías, I. Carvajal, J.A. Jiménez, J. Pineda, M. Venegas. Modeling and simulating of a hybrid compression/absorption chiller driven by Stirling engine and solar dish collector. FI: 2.47, Q1. Applied Sciences 2020 Vol. 10 (24) 9018.

[7] G Romage, C Jiménez, A Zacarías, I Carvajal, N. García, M de Vega, M. Venegas. Solar cooler by adiabatic absorption cooling using low-temperature solar energy, IX Ibero-American Congress of Cold Sciences and Techniques, April 17-19, 2022, Cartagena, Spain.

[8] G. Romage, C. Jiménez, J de J Reyes, A. Zacarías, I. Carvajal, J.A. Jiménez, J. Pineda, M. Venegas. Modeling and simulating of a hybrid compression/absorption chiller driven by Stirling engine and solar dish collector. FI: 2.47, Q1. Applied Sciences 2020 Vol. 10 (24) 9018.

[9] M. Venegas, P. R. (2005). Spray absorbers in absorption systems using lithium nitrate–ammonia solution. International Journal of Refrigeration, 554–564.

[10] S A Crepaldi, J M Cruz, C Jiménez, G L Gutiérrez, J A Jiménez, A Zacarías, A Flores, G Romage. Thermal evaluation of flat plate solar collectors with nanofluids for food drying

253-I-PO ELECTROCHEMICAL REDUCTION OF CO_2 OVER Ag@Bi AND Ag@Sn ELECTROCATALYSTS TOWARDS THE GENERATION OF FORMIC ACID AND FORMALDEHYDE

C. X. Tirado-López[1], M. Á. Soto-Mendoza[1], E. M. Arce-Estrada, A. Manzo-Robledo[2], R. G. Sánchez-Alvarado[1], A. Ezeta-Mejía[1]*

[1]Instituto Politécnico Nacional, Escuela Superior de Ingeniería Química e Indústrias Extractivas. Departamento de Metalurgia y Materiales. UPALM. Edif. 7, Av. Luis Enrique Erro S/N, Unidad Profesional Adolfo López Mateos, Zacatenco, C.P. 07738 CDMX, México.
[2]Instituto Politécnico Nacional, Escuela Superior de Ingeniería Química e Indústrias Extractivas. Laboratorio de Electroquímica y Corrosión. UPALM. Edif. Z5, Av. Luis Enrique Erro S/N, Unidad Profesional Adolfo López Mateos, Zacatenco, C.P. 07738 CDMX, México.

*Correspondence: aezetam@ipn.mx

Abstract: The electrochemical carbon dioxide reduction reaction (CO_2RR) has emerged as a promising strategy to transform CO_2 into value-added, conversion, and generation devices. In this work, Ag@Bi and Ag@Sn electrocatalysts were synthesized using the seed nucleation and growth method. The morphology, composition, and particle size were determined through scanning electron microscopy and energy dispersive spectroscopy (SEM-EDX) exhibiting the formation of nanosheets and nanoflakes with average sizes of 143 and 218 nm, respectively. The activity, area and stability of electrocatalysts was evaluated for the CO_2RR with the electrochemical techniques of cyclic voltammetry (CV) in a 0.1 M $KHCO_3$ supporting electrolyte, showing favorable results and reaching cathodic current densities of -5 and -8 $mAcm^{-2}$, respectively. The electrochemical analysis indicates a higher efficiency during the adsorption-desorption of species and reaction kinetics, linked with a lower charge-transfer resistance on the surface of the electrocatalyst. The products obtained were identified *in situ* by differential electrochemical mass spectrometry (DEMS), demonstrating selectivity towards hydrogen, formic acid, and formaldehyde.

Keywords: CO_2 electroreduction, conversion, biofuels.

1. INTRODUCTION

Global warming is strongly influenced by greenhouse gas emissions, which trap heat in the atmosphere by absorbing solar radiation reflected from the Earth's surface, increasing the effects of climate change. Global greenhouse gas (GHG) emissions come mainly from fossil fuels combustion with 75% of total emissions and almost 90% of those emissions correspond only to carbon dioxide [1-2]. In 2023, the electric sector was the major global contributor for GHG emissions releasing 15.1 $GtCO_2$ into the atmosphere, followed by the transportation sector with 8.4 $GtCO_2$, the agriculture sector with 6.5 $GtCO_2$ and the industrial sector 6.5 $GtCO_2$ [3]. There are different strategies to reduce and prevent CO_2 emissions, mainly focused on the transition and implementation of renewable energy sources, lowering the dependence on fossil fuels and allowing to meet the current energy demand. New technologies have been developed to control CO_2 emissions, such as; capture and storage processes (CCS) and capture and utilization processes (CCU). Within the CCU strategy, multiple methods have been developed for the utilization of CO_2 including biochemical, chemical,

photochemical, photo-electrochemical, and electrochemical reactions [4-6].

The electrochemical carbon dioxide reduction reaction (CO_2RR) is a promising approach to convert polluting CO_2 into a renewable energy source by utilizing the produced biofuels in direct alcohol fuel cells, as well as valuable products for the general chemical industry, which makes this approach a sustainable and carbon-neutral energy conversion system. Furthermore, CO_2RR offers several advantages such as simple synthesis methods, affordable costs, reactions at room conditions (pressure and temperature), easy control of operating parameters, and the use of several supporting electrolytes and electrocatalytic materials. The electrocatalysts performs an important role in CO_2RR, as they selectively produce the desired products and suppress side reactions, mainly the Hydrogen Evolution Reaction (HER) [7-9].

Currently, the research has focused on the development of new electrocatalysts for CO_2RR capable of promoting optimal binding of CO_2 to the electrocatalytic surfaces, controlling the generation of intermediates, long-term stability, high selectivity towards hydrocarbons, low selectivity for HER, and high electrocatalytic activity. Additionally, variables such as electrolyte, pH, concentration, among others, can be modulated to directly impact the efficiency and selectivity of CO_2RR products depending on the employed electrocatalyst [10-11]. Numerous electrocatalysts for the CO_2RR based on noble and non-noble metals, metal oxides, organometallic materials, metal alloys or nanostructures have been studied. Among the metallic materials, Cu stands out for its capability to directly reduce CO_2 to products such as carbon monoxide, methane, ethylene, and a wide variety of hydrocarbons and alcohols. Noble metals such as Ag and Au are known for their high selectivity towards CO, as the main reduction product with high faradic efficiencies. Other metals, such as In, Sn, Cd, Hg and Pb are selective to produce formic acid and formates. Particularly, Sn and Bi have been studied as electrocatalysts for CO_2RR with high efficiency depending on their structure, size, morphology and composition [12-13].

Nowadays, nanostructured materials have gained relevance for their properties, like larger number of active sites compared to bulk materials, exhibiting outstanding electrocatalytic responses [14-15]. Within the wide range of nanostructured materials, bimetallic and polymetallic structures have been known to achieve good faradic efficiency for the $RRCO_2$, allowing the modulation of the electronic structure in the electrocatalysts surface, directly influencing the chemisorption of intermediaries, the activation of CO_2^*, and the subsequent desorption of generated products, enhancing the overall electrocatalytic reaction [16].

In this work, Ag@Sn and Ag@Bi nanostructured electrocatalysts were evaluated in the CO_2RR. The electrocatalysts were obtained by chemical synthesis using the seed nucleation and growth method. The morphology, particle size and elemental identification were analyzed using the SEM-EDX characterization technique. The electrocatalytic activity and stability of the electrocatalysts in the CO_2RR were evaluated using the electrochemical technique of cyclic voltammetry (CV), and the reduction products obtained from CO_2RR were monitored and identified *in situ* by DEMS.

2. MATERIALS AND METHODS

2.1. Chemical synthesis

The synthesis of Ag@Sn and Ag@Bi electrocatalysts was carried out by the seed nucleation and growth method. $AgNO_3$, $SnCl_2$ and $BiCl_3$ were used as precursors, the cationic surfactant CTAB was used for the formation of micelles during the nucleation process. $NaBH_4$, $C_6H_8O_6$ and $Na_3C_6H_5O_7$ were used as reducing agents and assisted in the growth process for controlled particle sizes. The methodology is fully described elsewhere [17].

2.2. Preparation of Ag@Bi and Ag@Sn electrochemical inks

For the electrochemical evaluation, electrocatalytic inks were prepared by adding Ag@Bi or Ag@Sn nanoparticles obtained by chemical synthesis, Vulcan carbon as a support, Nafion® solution as a binder, and acetone as a solvent; the inks were subjected to sonication for 25 minutes to obtain a homogeneous dispersion. Finally, 1 µL of the ink was deposited on a glassy carbon electrode and the solvent was left to evaporate at room temperature for 5 minutes.

2.3. Characterization and conditions

Morphological characterization

The morphology was identified by SEM in a JEOL JSM-6701F at 10 kV using secondary electrons. In addition, EDX analysis was performed to obtain the spectrum of elements present in the electrocatalysts.

Electrochemical evaluation

Electrochemical measurements were performed in a VERSAstat 4 potentiostat/galvanostat in a conventional three-way glass electrochemical cell of 50 mL. A glassy carbon electrode of 3mm in diameter as working electrode, a reversible hydrogen electrode (RHE) as reference electrode, and a graphite rod as a counter electrode. The supporting electrolyte used was a 0.1 M aqueous solution of $KHCO_3$ saturated with N_2 and/or CO_2 (INFRA).

Products identification

The products generated during the CO_2RR were monitored and identified *in situ* using a DEMS coupled to a potentiostat. A 5 ml three-electrode microcell was used, a glassy carbon with Ag@Sn or Ag@Bi electrocatalytic ink as working electrode, a platinum wire as counter electrode and a RHE as reference electrode were used. A scan was performed using CV at a scan rate of 20 and 1 mVs^{-1}.

3. RESULTS AND DISCUSSION

Figure 1 presents the micrographs obtained for Ag@Bi showing a non-homogeneous particle distribution and an irregular flake-like morphology with an average size of 218 nm. The EDS spectrum shows the presence of Ag and Bi, the signal corresponding to Al comes from the metallic probe where the particles were dispersed.

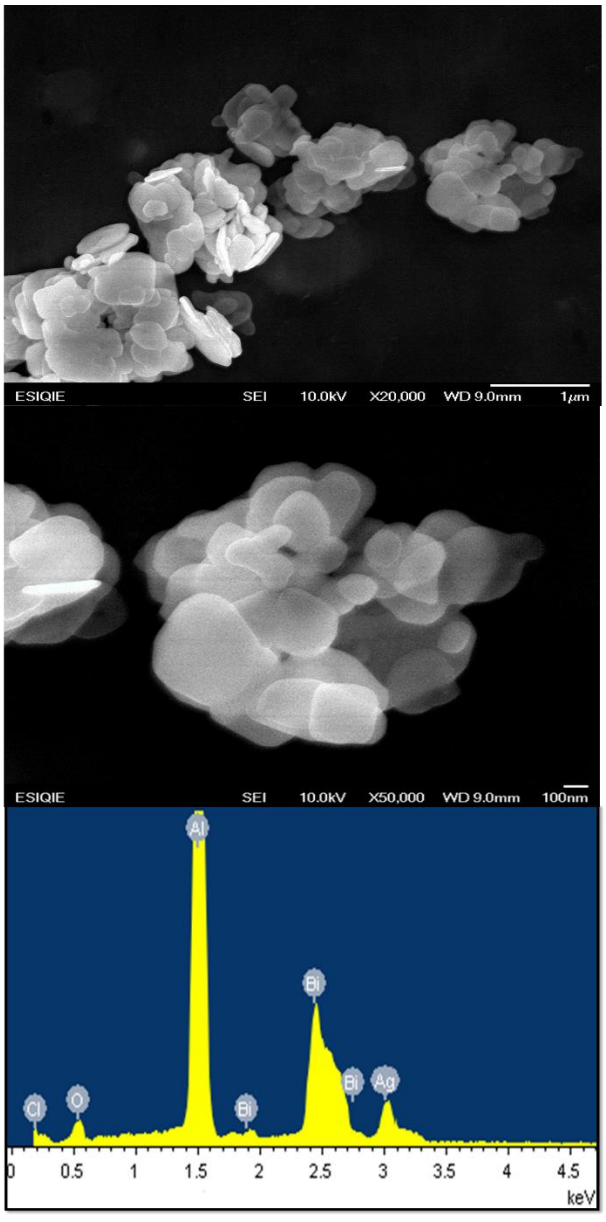

Figure 1. SEM micrographs of Ag@Bi and EDX analysis.

Figure 2 shows the micrographs obtained for Ag@Sn with multiple particle sizes and a non-homogeneous distribution with irregular

lamellar morphology and an average size of 143 nm. Additionally, a compositional analysis obtained by EDX is presented in which, the elements of interest Ag and Sn are shown. The presence of O in the spectra indicates that Ag and are in its oxidized state.

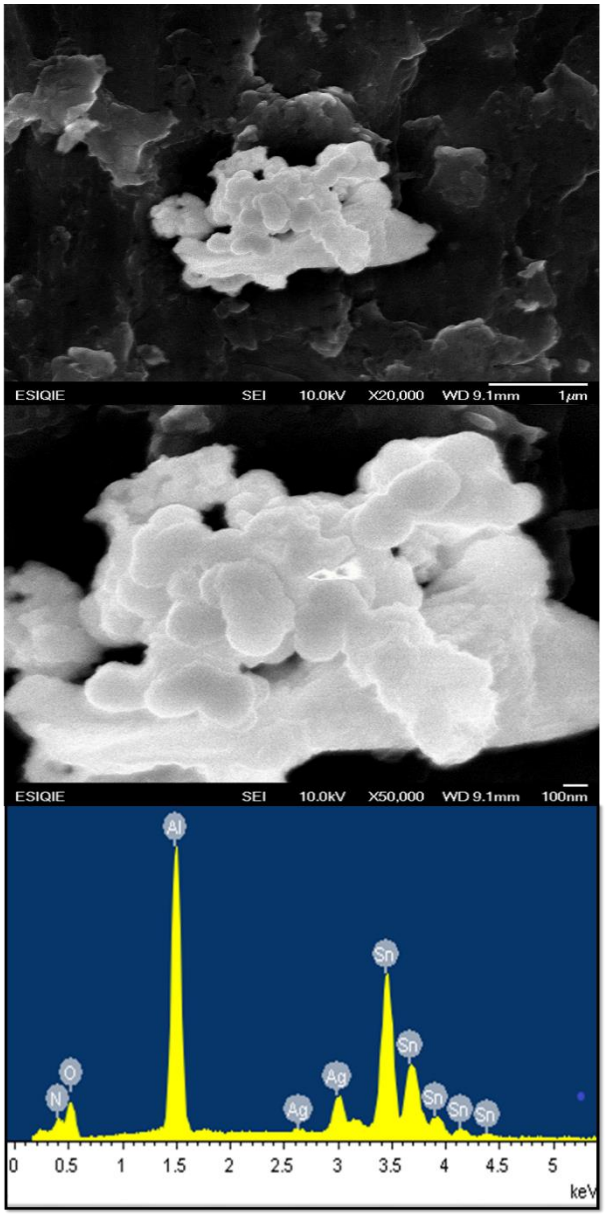

Figure 2. SEM micrographs of Ag@Sn and EDX analysis.

The electrochemical evaluation of electrocatalysts in 0.1 M $KHCO_3$ at 20 mVs^{1} is presented in Figure 3. For Ag@Bi in figure 3 a) shows the characteristic electrochemical response, observing an oxidation peak at 0 V due to the formation of Bi_2O_3 and its reduction at -0.32 V in the cathodic region, from -1.28 V, there is an increase in the current associated with the HER in the absence of CO_2. In the presence of CO_2, the current increases from -1.13 V attributed to the reduction of CO_2 and also to the HER. Figure 3 b) shows the voltammogram of Ag@Sn in the presence of N_2, showing a cathodic peak corresponding to the reduction of SnO_2 to SnO (-0.78 V) and two anodic peaks corresponding to the oxidation of Sn to SnO (-0.39V) and to SnO_2 (-0.16 V). From -1.38 V potential, an increase in the cathodic current attributed to the HER is presented. An increase in the cathodic current is presented from -1.07 V due to the development of the CO_2RR and HER reactions. In saturated CO_2 electrolyte, a change in the redox processes is shown for both materials, a shift towards electropositive potentials are associated with a change in the pH (from 8 to 7).

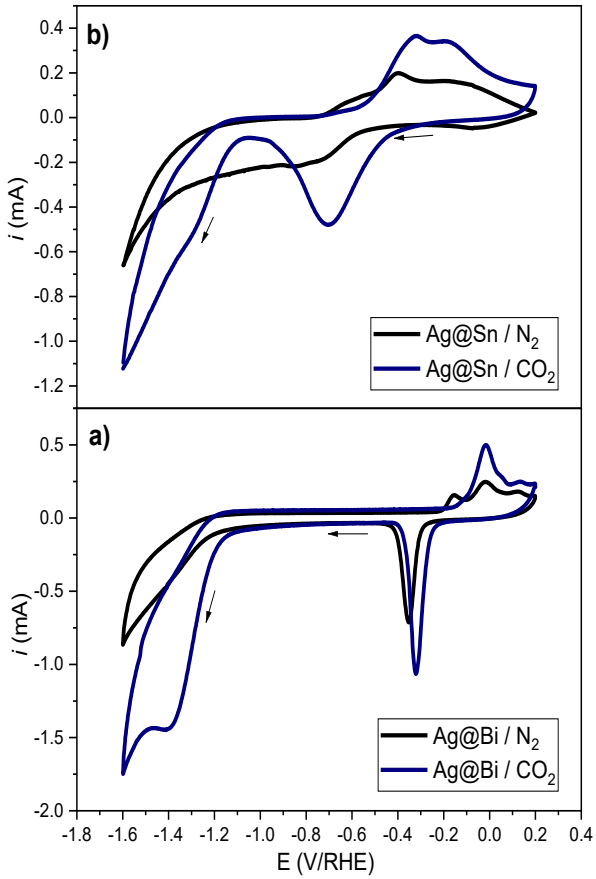

Figure 3. Electrochemical evaluation by CV of a) Ag@Bi and b) Ag@Sn electrocatalysts.

The electrochemical active surface area (ECSA) was determined for each electrocatalyst using as supporting electrolyte 1 M of NaOH and 10 mM of $K_4Fe(CN)_6$. The study was carried out using CV at different scanning rates for the analysis of the ferri/ferro redox couple. The Randles-Sevick model was used to show the current response as a function of the scanning rate. The current obtained by CV was modified by the electroactive area calculated for Ag@Bi (5.63 cm^2mg^{-1}) and Ag@Sn (4.51 cm^2mg^{-1}) in presence and absence of CO_2, the results are shown in Table 1.

Table 1. Current densities affected by ECSA.

Material	***j*** **N_2 (mAcm^{-2})**	**J CO_2 (mAcm^{-2})**
Ag@Sn	-2.93	-5.06
Ag@Bi	-3.18	-8.05

In situ identification of the generated products in CO_2RR was recorded through their mass by DEMS technique. The ionic (i_i) and faradic (i_f) currents were monitored simultaneously. Figure 4 shows the mass signals monitored by DEMS for (a) Ag@Bi and (b) Ag@Sn associated with hydrogen (m/z=2) as well as their voltamperometric profiles. Additionally, the associated signal for formaldehyde (m/z=30) and formic acid (m/z=46) were detected during CO_2RR.

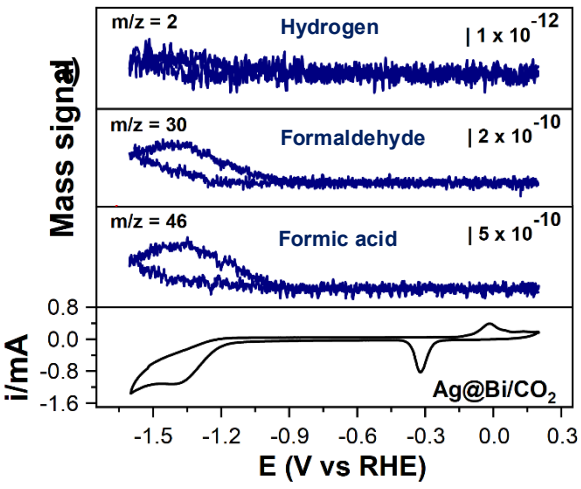

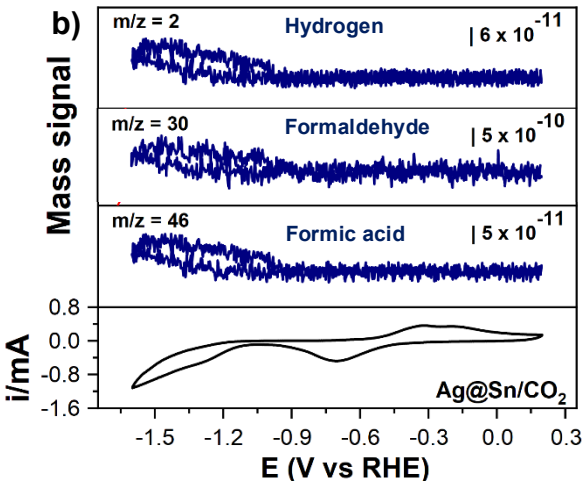

Figure 4. CV and *in situ* identification of a) Ag@Bi and b) Ag@Sn reduced species by DEMS during CO_2RR.

2. CONCLUSIONS

Chemical synthesis by seed nucleation and growth method allowed the formation of Ag@Bi nanoflakes and Ag@Sn nanosheets. The electrocatalysts exhibited a synergistic effect between Ag and Sn/Bi, as well as a higher electrocatalytic activity and higher efficiencies for CO_2RR due to the increase in the ECSA. Current densities of -8 and -5 mAcm^{-2} were achieved for Ag@Bi and Ag@Sn respectively during CO_2RR. DEMS technique allowed *in situ* identification of CO_2 reduction products generated during the cathodic polarization resulting in high selectivity towards hydrogen, formaldehyde, and formic acid.

Acknowledgements

The authors wish to thank the institutions CONAHCYT, SNI, COFAA, and SIP-Instituto Politécnico Nacional for their permanent assistance.

Conflicts of Interest

The authors declare that they have no known competing financial interests or personal relationships that could have appeared to influence the work reported in this work.

REFERENCES

[1]. Intergovernmental Panel on Climate Change (IPCC, 2021). Climate Change 2021: The Physical Science Basis. Contribution of Working Group I to the Sixth Assessment Report. Cambridge University Press. https://www.ipcc.ch/report/ar6/wg1/ Accessed 3 September 2024.

[2]. European Parliament (EUP, 2023). Climate change: the greenhouse gases causing global warming. https://www.europarl.europa.eu/topics/en/article/20230316STO77629/climate-change-the-greenhouse-gases-causing-global-warming Accessed 3 September 2024.

[3]. Olhoff, A., Christensen, J. M. (UNEP, 2024). Emissions gap report 2024. https://www.unep.org/resources/emissions-gap-report-2024 Accessed 3 September 2024.

[4]. Wang, Y., He, D., Chen, H., Wang, D. (2019). https://doi.org/10.1016/j.jphotochemrev.2019.02.002

[5]. Li, K., An, X., Park, K. H., Khraisheh, M., Tang, J. (2014). https://doi.org/10.1016/j.cattod.2013.12.006

[6]. Lim, R. J., Xie, M., Sk, M. A., Lee, J. M., Fisher, A., Wang, X., Lim, K. H. (2014). https://doi.org/10.1016/j.cattod.2013.11.037

[7]. Lu, Q., Jiao, F. (2016). https://doi.org/10.1016/j.nanoen.2016.04.009

[8]. Ting, L. R. L., Yeo, B. S. (2018). https://doi.org/10.1016/j.coelec.2018.04.011

[9]. Qiao, Jinli, Yuyu Liu, Jiujun Zhang, Electrochemical reduction of carbon dioxide: fundamentals and technologies, 1st edn. (CRC press, 2016).

[10]. Ringe, S., Clark, E. L., Resasco, J., Walton, A., Seger, B., Bell, A. T., & Chan, K. (2019). https://doi.org/10.1039/c9ee01341e

[11]. König, M., Vaes, J., Klemm, E., & Pant, D. (2019). https://doi.org/10.1016/j.isci.2019.07.014

[12]. Wang, Z. L., Li, C., & Yamauchi, Y. (2016). https://doi.org/10.1016/j.nantod.2016.05.007

[13]. Gattrell, M., Gupta, N., Co, A. (2006). https://doi.org/10.1016/j.jelechem.2006.05.013

[14]. Yin, Z., Palmore, G. T. R., Sun, S. (2019). https://doi.org/10.1016/j.trechm.2019.05.004

[15]. Yu, F., Wei, P., Yang, Y., Chen, Y., Guo, L., Peng, Z. (2019). https://doi.org/10.1016/j.nanoms.2019.03.006

[16]. Shao, Q., Wang, P., Liu, S., & Huang, X. (2019). https://doi.org/10.1039/C9TA07016H

[17]. Tirado L. C. X., Romero H. A., Arce E. E. M., Sánchez A. R. G., Ezeta M. A. (2023). https://doi.org/10.1557/s43580-023-00719-7

301-I-PP IMPACT OF ALTERNATIVE GRAVITY THEORIES ON THE LARGE-SCALE STRUCTURE OF THE UNIVERSE

E. R. García Davalos [1], D. V. Gomez-Navarro[2]

[1]Instituto Politécnico Nacional, Escuela Superior de Física y Matemáticas, Av. Instituto Politécnico Nacional S/N, C.P. 07738 CDMX, México.
[2]Instituto Politécnico Nacional, Unidad Profesional Interdisciplinaria de Ingeniería Palenque, Carretera Federal 199, tramo Catazajá - Rancho Nuevo, KM 24.5, Col. Pakal-Na, CP 29960 Palenque, Chiapas.

*Correspondence: dgomezn@ipn.mx

Abstract: General Relativity is a successful gravity theory tested in the solar system, in binary systems and in the detection of gravitational waves, but by no means is valid in all scales of the universe. Modified gravity models predict a new gravity law, modifying the interaction strength between matter and gravity. In this work we study theories of gravity beyond General Relativity, which can explain several current cosmological observations as the late-time accelerated expansion of the universe. We consider the f(R) model where a fifth force is screened at large scales and GR is recovered, while at an unscreened regime the fifth force is large. The linear power spectrum therefore is like the ΛCDM model at large-scale, and the main differences occur in the small scales of the quasi linear and nonlinear regime. We also compute the one loop power spectra of f(R) at z=0, 0.5 and 1.0, which captures interesting effects in the quasilinear regime. Galaxy surveys like DESI will yield the most precise cosmological measurements and provide a powerful tool to study the f(R) models.

Keywords: dark energy, modified gravity theories, f(R) gravity, large-scale structure of Universe

1. INTRODUCTION

Accelerated expansion of the universe is one of the biggest problems of modern cosmology. The $\Lambda\mathrm{CDM}$ model, based on the premises of general relativity (GR), has successfully explained many aspects of the universe's evolution from the primordial universe to the inhomogeneous universe of galaxies and filaments of clustered galaxies separated by giant voids that we see today (see Figure 1). The fundamental parameters of the $\Lambda\mathrm{CDM}$ model are constrained by the measurements of the cosmic microwave background (CMB), Type Ia supernovae, abundances of galaxy clusters, galaxy clustering and lensing clustering.

The $\Lambda\mathrm{CDM}$ model however cannot explain successfully the missing mass question for galaxy clusters and individual galaxies, or dark matter question, and it cannot also explain the problem of the dark energy that drives the universe's accelerated expansion. The history of the universe is characterized by three epochs, a radiation-dominated epoch, a matter-dominated epoch and finally a late-time accelerated expansion epoch (see Figure 1). For example, models like modified gravity (MG) theories have been proposed to explain the dark sector of the universe [1]. MG theories also have increased attention due to explaining the accelerated expansion and structure formation of the universe. The f(R) gravity theory is a type of MG theory which generalizes general relativity and considers a function, f, of the Ricci scalar, R. The f(R) gravity theories also suggest the existence of a fifth force of nature, leading to variations in the gravitational potential and consequently altering the evolution of the large-scale structure (LSS) of the universe. The formation of cosmological structures at large scales is

driven by gravitational collapse of cold dark matter (CDM), where baryonic matter falls into potential wells formed by the CDM, and ultimately forming the clustering of galaxies we observe with telescopes. N-body simulations are the most trustable techniques to study the process of structure formation, however they are computationally very expensive and the understanding of how this process takes place stays hidden. For these reasons, we consider approximation methods, like perturbation theory, to study the evolution of structures for MG theories.

In this work, we study the evolution of the matter power spectrum using linear and 1-loop perturbation theory in the Eulerian Standard perturbation theory (SPT) to study f(R) gravity theory. SPT is a framework to study the LSS of the universe, where it leads to significant improvements over linear theory at the weakly non-linear scales, but at $k \geq 0.3\ h/Mpc$ is a poor approximation [2]. In the nonlinear regime, the numerical simulations, or models like halo models, are essential to study the nature of dark energy and allow us to identify possible ways of constraining or ruling out some MG models.

Weak gravitational lensing allows mapping dark matter distribution around galaxies, galaxy clusters and on cosmological scales. Gravitational lensing surveys, such as Vera Rubin LSST [3] and Euclid [4], will measure the matter power spectrum at nonlinear scales, and to achieve a high precision level of their instruments, they will need to calibrate with theoretical models that reach accuracy on these scales. This will allow us to put more precise constraints on gravity models.

2. MATERIALS AND METHODS

We use Code for Anisotropies in the Microwave Background (CAMB) [5] to compute the linear matter power spectrum at $z = 0, 0.5, 1, 1.5, 2$. The greater is the value of z, the farther back in time. We also consider the cosmological parameters

$$H_0 = 67.66, \Omega_m = 0.309 \text{ and } \Omega_\Lambda = 0.691.$$

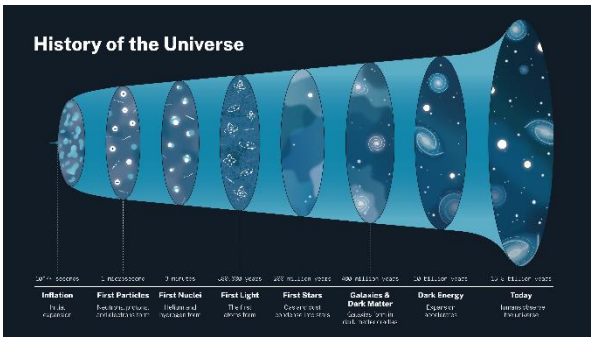

Figure 1. History of the universe [6].

2.1. f(R) gravity theories

The f(R) theories have been used to describe different aspects of modern cosmology, such as the accelerated expansion of the universe, which is obtained from GR by adding higher powers of the Ricci scalar. In this work we consider Hu-Sawicky (HS) gravity [7-9], with $f(R) = -f_{R0}\bar{R}^{n+1}/(nR^n)$, where $\bar{R}$ is nowadays value of the Ricci scalar evaluated at the background evolution, f_{R0} the derivate of $f(R)$ with respect to R evaluated today. We note that the smaller is the value f_{R0}, the smaller the effect of HS-f(R) gravity theories. While $f_{R0} = 0$ corresponds to ΛCDM model. In this paper, we consider $n = 1$ and three different values for $|f_{R0}| = 10^{-4}, 10^{-5}, 10^{-6}$ and are called F4, F5 and F6, respectively. The constraints on $f(R)$ gravity theory parameters have certain limitations, e.g. the most upper bound on $|f_{R0}|$ found to be $|f_{R0}| \leq 10^{-8}$, obtained from astrophysical scales [10]. Other cosmological constraints in the HS gravity theory come from weak-lensing mass [11], cluster abundance [12] and weak lensing peak statistics analysis [13], with significantly tighter constraints, which yield an upper bound o$|f_{R0}| \sim 10^{-5}$f.

At f(R) gravity theories, the gravitational strength modifies the evolution of density matter fluctuation. The linear growth function equation takes the following form

$$\left(\frac{d^2}{dt^2} + 2H\frac{d}{dt} - A(k)\right) D_+(k,t) = 0,$$

$$A(k) = 4\pi G\bar{\rho}\left(1 + \frac{k^2}{3k^2 + 3m_\phi^2 a^2}\right),$$

where m_ϕ is the mass of the associated scalar field. We note that we recover GR when $\mathrm{A}(\mathrm{k}=0)=4\pi\mathrm{G}\bar{\rho}$. The HS gravity theory is characterized by having an evolution very close to $\Lambda\mathrm{CDM}$ in the early universe, and main differences appear at the late-time accelerating expansion of the universe. Meanwhile there are MG theories, such as the normal branch Dvali-Gabadadze-Porrati (nDGP) gravity, where range of the fifth force is very large, and the linear growth function becomes scale-independent. The HS-f(R) gravity theory introduces a finite-range attractive "fifth force", where this fifth force behaves according to GR on the largest cosmological scales, while their effects are notable on the matter power spectrum at mildly nonlinear scales. This signature will appear above comoving wavenumbers $k \geq k_{MG}(a) \equiv am(\phi)$, where a is the scale factor of the universe. This type of MG gravity theory employs screening mechanisms (see Figure 2), which eliminates gravitational effects in populated regions and the power spectrum therefore is enhanced above k_{MG} in comparison to $\Lambda\mathrm{CDM}$ model [8, 9].

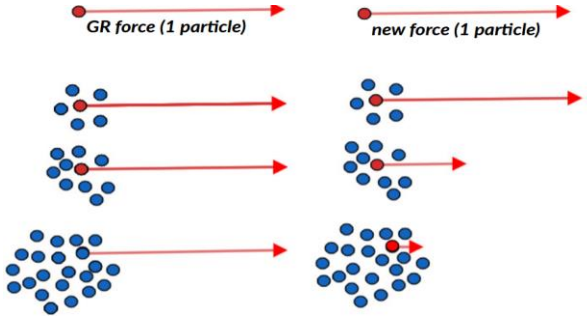

Figure 2. Screening mechanism eliminates gravitational effects in populated regions. At the top, the effect on a single particle is observed and at the bottom the effect on a system of particles.

2.2. Standard Perturbation Theory

In this section, we provide a brief description of the theory and numerical code used to compute the matter power spectrum of f(R) gravity model and $\Lambda\mathrm{CDM}$ model.

The process of structure formation can be explained by gravitational collapse in the expanding universe, where gravity holds together to matter, but also that the universe is expanding.

The matter density field is expanded as

$$\rho(\mathbf{x},\mathrm{t}) = \bar{\rho}(\mathrm{t})[1+\delta(\mathbf{x},\mathrm{t})] \qquad \text{Eq. (1)}$$

where $\bar{\rho}$ is the background matter density and δ is the matter density contrast. Standard perturbation theory (SPT, often also called Eulerian perturbation theory: EPT) solves perturbatively for the density at the observed position x [2], i.e.

$$\delta(\mathbf{x}) = \delta_1(\mathbf{x}) + \delta_2(\mathbf{x}) + \delta_3(\mathbf{x}) + \cdots. \qquad \text{Eq. (2)}$$

A good approximation to study the large-scales structures of the universe is the linear theory, where the matter power spectrum (PS) is given by

$$P_{lin}(z,k) = D_+^2(z,k)P_{lin}(k) \qquad \text{Eq. (3)}$$

with $D_+(z,k)$ is the linear growth function and is the linear power spectrum at redshift zero. In f(R) gravity theories, D_+ is a scale-dependent function due to attractive fifth force defined by the range λ of a Yukawa potential $e^{-r/\lambda}/r$, meaning that on the largest scales, GR is recovered. While in the ΛCDM model D_+ is independent of wavenumber k. In the mildly nonlinear regime, one can compute perturbative corrections to this result. The first correction is the so-called one-loop contribution, where the real space matter power spectrum is expanded as

$$P_{1-loop,SPT}(k) = P_{13}(k) + P_{22}(k), \qquad \text{Eq. (4)}$$

where both terms are given as a convolution integral,

$$P_{22}(k) = 2\int_{\boldsymbol{q}} [F_2(\boldsymbol{q},\boldsymbol{k}-\boldsymbol{q})]^2 P_{lin}(q)P_{lin}(|\boldsymbol{k}-\boldsymbol{q}|),$$

$$P_{13}(k) = 6P_{lin}(k)\int_{\boldsymbol{q}} F_3(\boldsymbol{k},-\boldsymbol{q},\boldsymbol{q})P_{lin}(q). \qquad \text{Eq. (5)}$$

The convolution kernels F_2 and F_3 are the usual perturbation theory kernels, where we use the notation $\int_{\mathbf{q}} = \int \mathrm{d}^3\mathrm{q}/(2\pi)^3$ [2]. In this work, we

do not consider the effective field theory (EFT) counterterm, which allows us to obtain quite accurate on the nonlinear matter power spectrum (PS). The EFT counterterm at this order is given by $P_{ctr}(z,k) = -2c_s^2(z)k^2P_{lin}(z,k)$, where $c_s^2(z)$ is an effective parameter and must be treated as a nuisance parameter in data analysis. SPT does not predict the c_s parameter because PT considers perfect fluid, while real physical system is a collection of particles with a gravitational effect of the small-scale fluctuations.

We use a perturbation theory code, Velocileptors code [14], which uses FFTLog methods to evaluate loop integrals. The FFTLog technique decomposes the linear power spectrum into complex power laws, where the loop integrals have an analytical solution for the power-law universes [15, 16]. This numerical method allows us to sample a large space of parameters with Monte Carlo Markov chain (MCMC) analysis, needed for galaxy surveys where use theoretical models to obtain reliable cosmological constraints.

3. RESULTS AND DISCUSSION

In Fig. 3 we show the evolution of the matter power spectrum with $|f_{R0}| = 10^{-6}$. We note that the linear power spectrum carries a k dependence due to the finite mass of the scalar field of the fifth force. As we back in time, the linear power spectra reduce to GR in the early universe, and the main differences occur at late time when the dark energy is dominant. At $0.03h/Mpc \leq k \leq 0.08h/Mpc$, there is a decrease of the 1loop PS in comparison to the linear theory due to weak nonlinear processes such as tidal forces, while at $k \geq 0.1\,h/Mpc$ the one-loop power spectrum is enhanced. However, 1-loop perturbation theory does not predict beyond $k \geq 0.3\,h/Mpc$ because of it does not take into gravitational collapse of objects like dark matter mini-haloes.

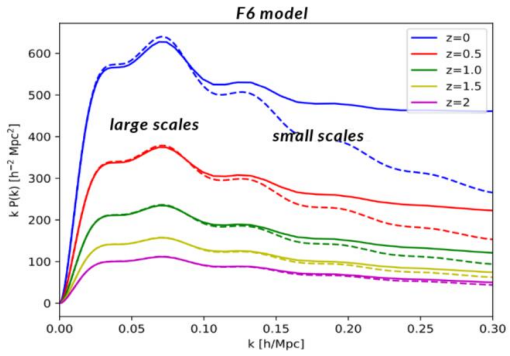

Figure 3 Evolution of the matter power spectrum for the F6 model; solid (dashed) curves show perturbation theory (linear theory) predictions.

The real system is a collection of collisionless particles; however, perturbation theory is based on treating matter as an ideal fluid. For this reason, PT does not predict an accurate on the nonlinear PS. The solution is to consider the effective field theory, where matter is treated as an effective fluid: the stress tensor σ_m^{ij} is expanding in terms of the matter density field itself. The diagonal part of the stress tensor corresponds to the pressure due to the gravitational effect of small-scale perturbations. This effective term is suppressed at small k and can be determined by N-body simulations. In future work, we shall consider effective field theory.

In Fig. 4 we show the ratios of the power spectrum from f(R) theories and ΛCDM model. The power spectrum is like the ΛCDM model at large-scale, and the main differences occur in the small scales of the quasi linear and nonlinear regime. We also compute the one loop power spectra of f(R) theories at z=0, 0,5, which captures interesting effects in the quasilinear regime.

There are many observations that indirectly probe the matter distribution, such as galaxy clustering and gravitational lensing. Redshift surveys use the spectrum of galaxies as tracers of the large-scale matter distribution, while photometric surveys take images of parts of the sky. Both measurements constrain the expansion history of the universe and the rate at which structure grows. These observations

are probes of dark energy and gravity. We expect a larger growth rate in modified gravity theories because they typically increase the strength of gravity.

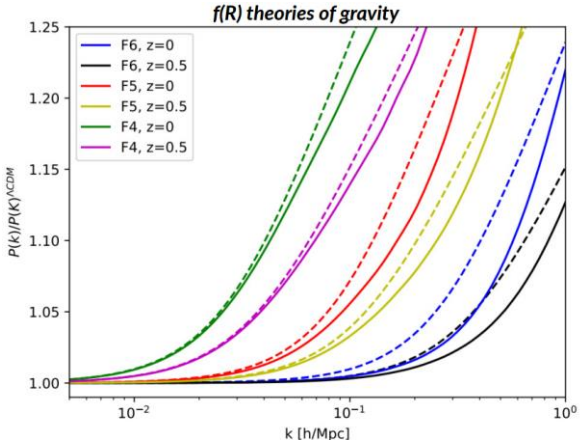

Figure 4. The ratios of the power spectrum from f(R) theories and ΛCDM model; solid (dashed) curves show perturbation theory (linear theory) predictions.

4. CONCLUSIONS

We study here f(R) theories of gravity to explain the accelerated expansion of the universe. f(R) gravity introduces a scale dependence on the growth of perturbations due to their new forces mediated by scalar field. The power spectrum therefore is enhanced above k_{MG} in comparison to that in ΛCDM model. In this work, we utilize the *Velocileptors code* to compute the one loop perturbation theory which considers power laws for the power spectrum. Approximation methods, like SPT, are important to study the evolution of the matter spectrum of MG theories at mild nonlinear scales.

Although current data is consistent with the ΛCDM model, the MG theories are also compatible with the cosmological data. The next results provided by galaxy surveys like Vera Rubin LSST and Euclid [3-4], opens new opportunities to test MG theories. These observations will need to be calibrate with theoretical models, like EFT, to achieve high accuracy on non-linear regime.

Acknowledgements

We appreciate the support provided by a CONAHCyT fellowship for the realization of this work.

Conflicts of Interest

The authors declare no conflict of interest.

REFERENCES

[1] C. M.Will, “The Confrontation between General Relativity and Experiment,” Living Rev. Rel. 17, 4 (2014) https://doi.org/10.12942/lrr-2014-4

[2] F. Bernardeau, S. Colombi, E. Gaztañaga, R. Scoccimarro, Large-scale structure of the Universe and cosmological perturbation theory, Physics Reports, 367, 1–3, 2002, https://doi.org/10.1016/S0370-1573(02)00135-7

[3] Vera Rubin Observatory collaboration. See the Universe in action. http://www.lsst.org/ Accessed 02 October 2024.

[4] Euclid Consortium. A space mission to map the Dark Universe. https://www.euclid-ec.org/_Accessed 02 October 2024.

[5] CAMB (Code for Anisotropies in the Microwave Background). https://camb.readthedocs.io/en/latest/ Accessed 02 October 2024.

[6] National Aeronautics and Space Administration (NASA, 2022) https://science.nasa.gov/resource/history-of-the-universe/ Accessed 02 October 2024

[7] W. Hu and I. Sawicki, “Models of f(R) Cosmic Acceleration that Evade Solar-System Tests,” Phys. Rev. D 76, 064004 (2007) https://doi.org/10.1103/PhysRevD.76.064000 [arXiv:0705.1158 [astro-ph]].

[8] J. Khoury and A. Weltman, “Chameleon cosmology,” Phys. Rev. D 69, 044026

(2004) https://doi.org/10.1103/PhysRevD.69.044026 [arXiv:astro-ph/0309411 [astro-ph]].

[9] C. Burrage and J. Sakstein, "Tests of Chameleon Gravity," Living Rev. Rel. 21, no.1, 1 (2018) https://doi.org/10.1007/s41114-018-0011-x [arXiv:1709.09071 [astro-ph.CO]].

[10] R. G. Landim, H. Desmond, K. Koyama and S. Penny, Testing screened modified gravity with SDSS-IV-MaNGA, Mon. Not. Roy. Astron. Soc. 534 (2024) 349–360, [2407.08825].

[11] SPT, DES collaboration, S. M. L. Vogt et al., Constraints on f(R) gravity from tSZE-selected SPT galaxy clusters and weak lensing mass calibration from DES and HST, 2409.13556.

[12] E. Artis et al., The SRG-eROSITA All-Sky Survey: Constraints on f(R) Gravity from Cluster Abundance, 2402.08459.

[13] X. Liu et al., Constraining f(R) Gravity Theory Using Weak Lensing Peak Statistics from the Canada-France-Hawaii-Telescope Lensing Survey, Phys. Rev. Lett. 117 (2016) 051101, [1607.00184].

[14] Velocity-based perturbation theory (both Lagrangian (LPT) and Eulerian (EPT) formulations) expansions of redshift-space distortions and velocity statistics. https://github.com/sfschen/velocileptors Accessed 02 October 2024.

[15] A. J. S. Hamilton, Uncorrelated modes of the nonlinear power spectrum, Mon. Not. Roy. Astron. Soc. 312 (2000) 257 [astro-ph/9905191].

[16] M. Simonović, T. Baldauf, M. Zaldarriaga, J. J. Carrasco and J. A. Kollmeier, Cosmological perturbation theory using the FFTLog: formalism and connection to QFT loop integrals, JCAP 1804 (2018) 030 [1708.08130]

312-I-PO EVALUATION OF FLAT PLATE SOLAR COLLECTORS USING SIMPLE NANOFLUIDS (COPPER OXIDE (CuO) AND FULLERENE (C60)

J. Michael Cruz[1,2], G Gutierrez-Urueta[3], A. Zacarías[1]*, G. Romage[1], J. G. Sánchez[4], E. E. Barrera[4], C. Jiménez[1]

[1]Instituto Politécnico Nacional, Escuela Superior de Ingeniería Mecánica y Eléctrica, Unidad Azcapotzalco, Av. de las Granjas 682, Col. Santa Catarina, CP 02250 CDMX, México.
[2]Universidad Autónoma de Tlaxcala, Facultad de Ciencias Básicas, Ingeniería y Tecnología, San Luis Apizaquito, C.P. 90401 Tlaxcala, México.
[3]Universidad Autónoma de San Luis Potosí, Facultad de Ingeniería, C.P. 78290 San Luis Potosí, México.
[4]Instituto Politécnico Nacional, Centro de Investigación en Ciencia Aplicada y Tecnología Avanzada, Unidad Querétaro, Cerro Blanco 141, Colinas del Cimatario, C.P. 76090 Querétaro, México.

*Correspondence: azacarias@ipn.mx

Abstract: This study evaluates flat plate solar collectors using simple nanofluids based on metallic oxides and carbon compounds. A solar collector with riser tubes was employed, characterized by the circulation of the working fluid (heat transfer fluid) through tubes coupled to the absorber surface. The analysis was conducted using two nanofluids: copper oxide (CuO) and fullerene (C60). Modeling and simulation results that, for a mass flow rate of 0.08 kg/s and a volume fraction of 0.15, the collector efficiency with CuO and C60 nanofluids was found to be 0.6792 and 0.6818, respectively, which is attributed to the changes in the thermophysical properties of the fluids. The results of the use of CuO and C60 nanofluids in a solar collector has been reported and compared to the base fluid (H_2O), which under identical conditions has an efficiency of 0.67.

Keywords: Nanofluids; Thermal efficiency; Flat plate solar collectors; Heat removal factor.

1. INTRODUCTION

Flat plate solar collectors (FPCs) have long been widely employed in applications such as water heating and space heating, which require low to moderate temperatures [1,2]. Despite extensive research over the years, these systems still demonstrate fairly low efficiency. In [3] and [4] the authors classified the efficiency losses in traditional flat plate collectors into two main types: optical losses, related to the angles at which solar radiation strikes the collector surface, and thermal losses, which increase substantially as the working temperature rises. Nevertheless, FPCs have the unique benefit of capturing both direct and scattered solar radiation, which helps enhance their efficiency, especially at lower temperatures, as shown by [5]. Research on these collectors indicates that improving efficiency involves maximizing energy capture and minimizing environmental heat losses. Additionally, it was observed in [6] that efficiency can be further improved by enhancing heat transfer from the absorbing plate to the heat transfer fluid and subsequently to the final application. Prior studies [7, 8, 9, 10] have proposed various techniques to improve the thermal efficiency of flat plate collectors. One such approach includes the addition of nanoparticles with high thermal conductivity, such as those made from carbon, metals, or metal oxides, into the heat transfer fluid, thereby increasing the fluid's overall thermal conductivity. Given the low thermal conductivity of water, alternatives

are sought to optimize collector performance. Recent advancements in nanotechnology have introduced nanofluids—a new type of fluid containing nanoscale particles suspended within a base liquid. Thus, in efforts to enhance the efficiency of solar collectors, conventional heat transfer fluids have been increasingly replaced by nanofluids.

Among the nanoparticles studied in flat plate solar collectors are Fe_3O_4, Al_2O_3, MgO, CuO, TiO_2, SiO_2, ZrO_2, CeO_2, ZnO, MWCNT, SWCNT, and graphene. In this work, FPCs are evaluated using simple nanofluids of CuO and C60, the latter being a type of carbon nanoparticle that is beginning to be utilized in these components.

2. MATERIALS AND METHODS

The mathe7matical model is established based on Figure 1, with detailed explanations and validation provided in [11] and supported by prior studies [12-18]:

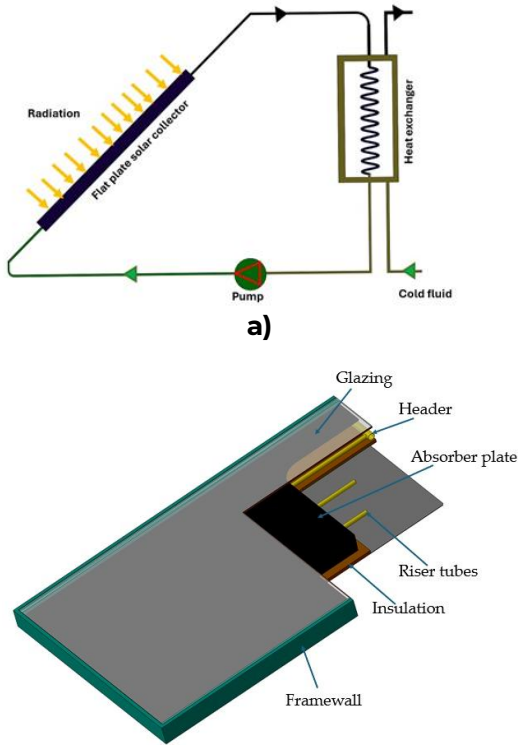

Figure 1. a) Flat-plate solar thermal system; b) Cross-sectional diagram of the flat plate solar collector.

2.1. Solar Energy Collector

According to [11], the useful heat is determined by the following expression:

$$Q_u = A_C F_R[I\tau\alpha - U_L(T_i - T_a)], \qquad \text{Eq. (1)}$$

where Ac, I, $\tau\alpha$, represent the collector area, irradiance, and the product of transmittance and absorptance, respectively. T_i and T_a denote the inlet temperature and the ambient temperature, respectively. The heat removal factor, also known as the heat dissipation factor F_R, is determined as:

$$F_R = \frac{\dot{m}Cp}{A_C U_L}\left[1 - exp\left(\frac{U_L F' A_C}{\dot{m}Cp}\right)\right], \qquad \text{Eq. (2)}$$

The efficiency factor of the flat-plate solar collector, F', is calculated using the eq. (3) presented in [12]

$$F' = \frac{1/U_L}{W\left[\frac{1}{U_L[D_o + (W - D_o)F]} + \frac{1}{C_b} + \frac{1}{\pi D_{in} h_{fi}}\right]} \qquad \text{Eq. (3)}$$

where W, D_{in}, and D_o represent the distance between fins and the internal and external diameters of the pipes, respectively. The conductance at the joints is denoted as C_b.

The standard fin efficiency, F, is determined by Eq. (4):

$$F = \frac{\tanh[m(W - D_o)/2]}{m(W - D_o)/2}, \qquad \text{Eq. (4)}$$

The convective heat transfer coefficient, h_{fi} is calculated as:

$$h_{fi} = \frac{Nuk}{D_i} \qquad \text{Eq. (5)}$$

where the Nusselt number is determined as suggested in [14]:

Laminar Flow: $Nu = 0.4328(1 + 11.285\phi^{0.754}Pe^{0.218})Re^{0.333}Pr^{0.4}$ Eq. (6)

Turbulent Flow: $Nu = 0.0059(1 + 7.6286\phi^{0.6886}Pe^{0.001})Re^{0.9238}Pr^{0.4}$ Eq. (7)

This relationship is valid for *Re≤2300* in laminar flow and Re > 2300 in turbulent flow.

The overall heat loss coefficient, U_L is calculated by:

$$U_L = U_t + U_b + U_\theta \qquad \text{Eq. (8)}$$

where U_t, U_b and U_q and are the top, bottom, and side loss coefficients, respectively. These loss coefficients are determined as:

$$U_t = \left\{ \frac{\frac{1}{N}}{\frac{C}{T_P\left[\frac{T_P - T_a}{N+f}\right]^{0.33} + \frac{1}{h_a}}} \right\} + \left\{ \frac{\sigma(T_P + T_a)(T_P^2 + T_a^2)}{\varepsilon_p + 0.5N(1-\varepsilon_p) + \frac{2N+f-1}{\varepsilon_g}} \right\} \qquad \text{Eq. (9)}$$

$$U_b = k_b / x_b \qquad \text{Eq. (10)}$$

$$U_e = A_e / A_C \qquad \text{Eq. (11)}$$

The collector efficiency, η is calculated by

$$\eta = F_R\left[\tau\alpha - \frac{U_L(T_i - T_a)}{I}\right], \qquad \text{Eq. (12)}$$

2.2. Simple nanofluids

The specific heat capacity of the nanofluid is determined as suggested in [15], using the eq. (13):

$$Cp_{nf} = \frac{Cp_{bf}\rho_{bf}(1-\emptyset) + Cp_{np}\rho_{np}\emptyset}{\rho_{nf}} \qquad \text{Eq. (13)}$$

where Cp, ρ, ⌀ represent the specific heat capacity, density, and volume fraction, respectively. The subscripts n_f, n_p, b_f refer to nanofluid, nanoparticle, and base fluid, respectively.

The nanofluid density is determined as proposed in [16]:

$$\rho_{nf} = (1-\emptyset)\rho_{bf} + \emptyset\rho_{np} \qquad \text{Eq. (14)}$$

The Brownian motion of the nanoparticles was considered in the study by [11] and in this work to estimate the thermal conductivity of the nanofluid, k_{nf}, with spherical nanoparticle:

$$k_{nf} = \left[\frac{k_{np} + 2k_{bf} - 2\emptyset(k_{bf} - k_{np})}{k_{np} + 2k_{bf} + \emptyset(k_{bf} - k_{np})} + \frac{\rho_{np}\phi Cp_{np}}{2k_{nf}}\sqrt{\frac{k_B T_m}{3\pi r_c \mu_{nf}}}\right] k_{bf} \qquad \text{Eq. (15)}$$

For cylindrical nanoparticles, the thermal conductivity of the nanofluid, k_{nf}, was estimated with n=6:

$$k_{nf} = \left[\frac{k_{np} + 2k_{bf} - 2\emptyset(k_{bf} - k_{np})}{k_{np} + 2k_{bf} + \emptyset(k_{bf} - k_{np})}\right] k_{bf} \qquad \text{Eq. (16)}$$

The developed model was implemented using Engineering Equation Solver (EES) software [19]. The simulation was performed with a nanoparticle volume fraction of 0.15 for the CuO and C60 nanofluids. This latest nanofluid was selected due to its low production cost and its potential to enhance heat transfer, as demonstrated by the results presented by Barrera et al. [20]. Base fluid properties were sourced from the data given in [20], while the nanoparticle characteristics were specified as outlined in Table 1. The full set of parameters employed in the simulation is presented in Table 2.

Table 1. Thermophysical properties of nanoparticles at 20 ° C.

Nano-particles	□ (kg/m³)	**Cp** (J/kg K)	**K** (W/mK)	**Ref.**
CuO	6000	551	33	[16]
Fullerene, C_{60}	1720	506.7	0.4	[20]

Table 2. Parameters used in the simulation.

Parameters	**Value**
FPSC inclination, β [°] [17]	20
Inlet temperature, Ti [°C]	30, 40 y 50
Mass flow rate, $\dot{m}$, [kg⁄s]	0.01–0.085

3. RESULTS AND DISCUSSION

In Figure 2, it is observed that the removal factor (FR) increases as the volume fraction rises, which holds true for both nanofluids (CuO and C60). The figure also shows that at a 0.15 volume fraction, the FR for the C60 nanofluid is 0.8825, slightly higher than that of the CuO nanofluid, which has an FR of 0.879. The FR integrates the thermophysical properties of the fluid and represents the ratio of the actual useful energy gain of a collector to the useful gain if the entire collector surface were at the fluid inlet temperature. Therefore, an increase in FR would correspond to an increase in both useful heat and thermal efficiency of the solar collector. Additionally, the increase in the removal factor with the C60 nanofluid can be attributed to its relatively smaller reduction in specific heat compared to CuO nanofluids. For a volume fraction of 0.1, the specific heat values are 3324 J/kg·K for C60 and 2311 J/kg·K for CuO.

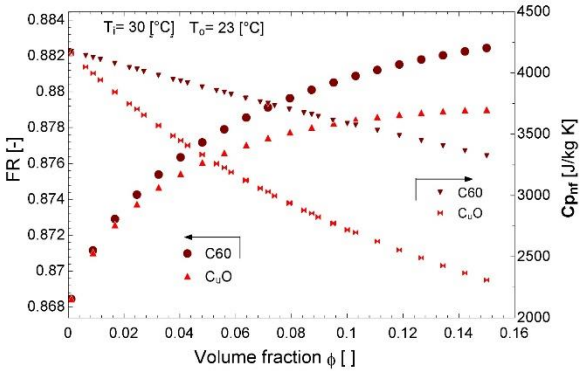

Figure 2. Removal factor (FR) and specific heat (Cp) as a function of volume fraction for copper oxide and fullerene nanofluids.

In Figure 3, the useful heat with respect to the volume fraction of the nanofluids is shown. It reveals that useful heat increases with the addition of nanoparticles for the nanofluids studied (CuO and C60). Fullerene demonstrates a very slightly higher useful heat production compared to copper oxide, with values of 577.9 kW for C60 and 575.6 kW for copper oxide at a 0.15 volume fraction.

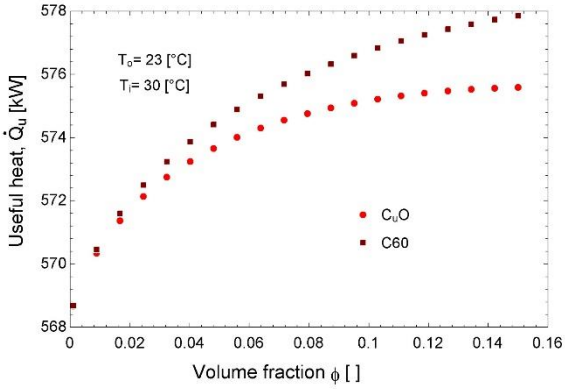

Figure 3. Useful heat as a function of volume fraction for copper oxide (CuO) and fullerene (C60) nanofluids.

Figure 4 shows thermal efficiency with respect to the volume fraction of the nanofluids. The efficiency rises with the addition of nanoparticles for the nanofluids considered (CuO and C60). Fullerene exhibits also a little higher thermal efficiency than copper oxide, with 577.9 kW for C60 and 575.6 kW for copper oxide at a 0.15 volume fraction. Additionally, it can be noted that thermal efficiency would increase further for C60 with additional nanoparticles, while CuO would begin to reach a steady line.

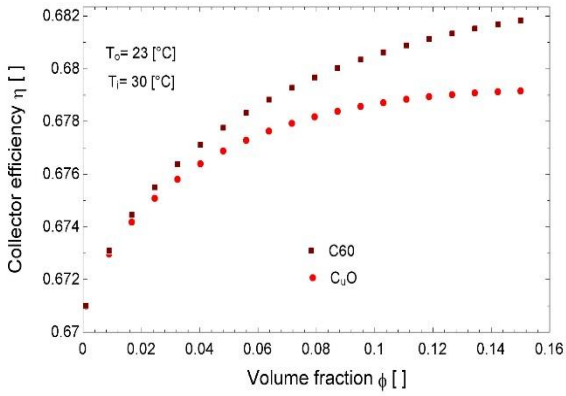

Figure 4. Collector efficiency as a function of volume fraction for copper oxide (CuO) and fullerene (C60) nanofluids.

The relevance of the results presented lies in the fact that the investigated nanofluid (C60) represents a relatively novel option for application in flat-plate solar collectors and has not been studied before. The findings show

that its use leads to a 1.76% increase in efficiency compared to the base fluid (water).

4. CONCLUSIONS

It can be concluded that the C60 nanofluid shows a slight superior FR, useful heat production, and thermal efficiency compared to CuO, due to its higher specific heat at comparable volume fractions. At a volume fraction of 0.15, C60 achieves an FR of 0.8825 and a useful heat output of 577.9 kW, and CuO, which reaches 0.879 and 575.6 kW, respectively. This is also reflected in the thermal efficiency trend, where C60 continues to improve with additional nanoparticles, while CuO reaches stable values. The significance of the presented results is that the investigated nanofluid (C60) offers a relatively novel approach for application in flat-plate solar collectors, representing an area that has not been previously explored.

Acknowledgements

We thank the Instituto Politécnico Nacional, IPN, for the financial support received from the scientific research grant SIP20240435. The authors also acknowledge the financial support given to the postgraduate students by the National Board of Science and Techmology, CONACYT, of Mexico.

Conflicts of Interest

The authors declare no conflict of interest

REFERENCES

[1] Belessiotis, V., Kalogirou, S., & Delyannis, E. Thermal Solar Desalination. Methods and Systems (AP, 2016), https://doi.org/10.1016/C2015-0-05735-5

[2] Duffie JA, Beckman WA. Solar engineering of thermal processes (Wiley, New York, 1991), 10.1002/9781118671603

[3] Venegas, M.; García-Hernando, N.; Zacarías, A.; De Vega, M., Applied Sciences (2020). https://doi.org/10.3390/app10082761

[4] Dincer, Y. Bicer, PV-Based energy conversion systems, iCompr. Energy Syst. (2018), https://doi.org/10.1016/B978-0-12-809597-3.00430-2

[5] H. Bhowmik, R. Amin, Energy Reports (2017) https://doi.org/10.1016/j.egyr.2017.08.002

[6] F.S. Javadi, R. Saidur, M. Kamalisarvestani, Renewable and Sustainable Energy Reviews (2013), https://doi.org/10.1016/j.rser.2013.06.053

[7] X.Q. Wang, A.S. Mujumdar, International Journal of Thermal Sciences (2007) http://dx.doi.org/10.1016/j.ijthermalsci.2006.06.010

[8] L. Godson, B. Raja, D.M. Lal, S. Wongwises, Renewable and Sustainable Energy Reviews (2010) https://doi.org/10.1016/j.rser.2009.10.004

[9] Pandey KM, Chaurasiya R. A, Renewable and Sustainable Energy Reviews (2017). https://doi.org/10.1016/j.rser.2016.09.078

[10] I. Wole-osho, E.C. Okonkwo, S. Abbasoglu, D. Kavaz, International Journal of Thermophysics (2020). https://doi.org/10.1007/s10765-020-02737-1

[11] Cruz J.M. et al. Applied Sciences (2024) https://doi.org/10.3390/app14198732

[12] Goswami D.Y, Principles of Solar Engineering, 4th edn. (CRC Press, 2022). https://doi.org/10.1201/9781003244387

[13] Kalogirou S.A., Solar Energy Engineering. Processes and Systems (AP, 2023). https://doi.org/10.1016/C2021-0-02041-1

[14] Sint, N.K.C. et al. Solar Energy (2017) https://doi.org/10.1016/j.solener.2017.06.055

[15] Alawi, O.A.; et al. Journal of Cleaner Production (2021). https://doi.org/10.1016/j.jclepro.2020.125725

[16] Pak, B.C.; Cho, Y.I. Experimental Heat Transfer (1998), doi:10.1080/08916159808946559.

[17] Hawwash, A.A.; et al. in *IEEE* (2021) https://doi.org/10.1109/ACCESS.2021.3060004

[18] Xuan, Y.; Li, Q.; Hu, W. AIChE Journal (2023). https://doi.org/10.1002/aic.690490420

[19] Klein, S.A. (2018). Engineering Equation Solver, 1992-2015, f-Chart Software, https://fchartsoftware.com/ees/

[20] Barrera, E.E.; et al. Applied Sciences (2022). https://doi.org/10.3390/app12063161

366-I-PO EVALUATION OF THE INFLUENCE OF MICROSTRUCTURAL CHARACTERISTICS ON SUSCEPTIBILITY TO STRESS CORROSION CRACKING IN API 5L STEELS IN NEAR-NEUTRAL PH ENVIRONMENTS

D. M. González Fong[1], D. I. Rivas López[1]*, M. A. Beltrán Zúñiga[1]

[1]Instituto Politécnico Nacional, Escuela Superior de Ingeniería Química e Industrias Extractivas Departamento de Ingeniería en Metalurgia y Materiales, Av. Luis Enrique Erro S/N, Unidad Profesional Adolfo López Mateos, Zacatenco, C.P. 07738 CDMX, México.

*Correspondence: drivasl@ipn.com.mx

Abstract: This study evaluated the effect of microstructural characteristics on the susceptibility to Stress Corrosion Cracking (SCC) in low-carbon pipe-grade steels, using pipe segments specified as API 5L [1].

The results show the formation of atypical morphology pits with cracks observed at the bottom, which are associated with the initial stage of the SCC mechanism. It was observed that a higher pearlitic microconstituent content reduces the formation of these pits, as does homogeneity in the microstructure, due to the distribution of anodic and cathodic sites. Additionally, the steel with larger grain size exhibited the highest number of pits. Results also showed that pit formation depends on the magnitude of the applied stress; greater stress led to more pits. Photographic evidence indicates that the cracks formed are associated with non-classical SCC, characterized by their transgranular nature and location at the bottom of atypical morphology pits.

Keywords: Stress Corrosion Cracking, microstructure, susceptibility, pipelines.

1. INTRODUCTION

The transportation of hydrocarbons is mostly carried out through carbon steel pipelines that fulfill the regulations described in the API 5L standard specifications. This form of transportation is considered economical, effective, and safe; however, the main concern is that various damage mechanisms occasionally develop in these types of pipelines [2-14]. Stress Corrosion Cracking (SCC) is one such mechanism, occurring when a component is subjected to stress below the material's yield stress point over prolonged periods in a mildly corrosive environment [2, 15-19].

Although SCC is primarily found in environments with a pH greater than 9 [3-5], multiple studies indicate that SCC can also occur in environments with near-neutral pH characteristics [3-7]. This has been reported for various types of steel; however, due to the wide range of possible material-environment-stress combinations, there is no consensus on the effect that certain metallurgical factors have on this phenomenon, such as microstructure [2,3,8,9,15,16].

For this reason, this work investigates which microstructural factors promote susceptibility to stress corrosion cracking by applying different static load values to API 5L steel samples, which were metallurgically and mechanically characterized and exposed to an NS4 solution.

2. MATERIALS AND METHODS

The methodology of this study was conducted in two stages. The first stage allowed us to establish parameters that helped analyze the results more precisely for the second stage.

In the first stage, six API 5L steels from decommissioned pipelines, labeled A1, A2, A3, A4, A5, and A6, were metallurgically and mechanically characterized in three directions as shown in Figure 1, according to ASTM standards E-415, E-112, E-407, E-3 and E-8. For each steel, two rectangular specimens of 117x65x43mm (4.6x2.5x1.69in) were prepared by grinding with sandpaper of grades 180 to 2000, mechanically polishing with 1.0, 0.3, and 0.05µm alumina.

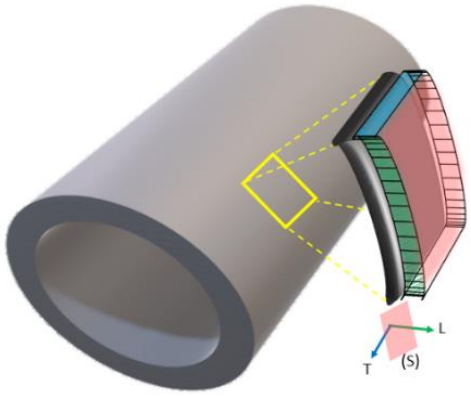

Figure 1. Representation of Section Cuts of the Material Used.

For the proposed SCC test: one specimen from each steel was subjected to a load of 80% of the yield strength point (YS) by using a three-point bending test with the mechanism shown in Figure 2., while the other had no applied load. Bending was calculated by using Eq. 1

$$\delta_{max} = \frac{YSl^2}{6Et} \qquad \text{Eq. (1)}$$

Where:

δ_{max} = Maximum bending

YS= Yield strength

l= Distance between span points

E= Young's Modulus

t= Sample thickness

An NS4 solution was used to control the solution's pH, and specimens were placed in an autoclave for 720 hours at a temperature of 80°C ± 5°C. The solution was purged with a gas mixture of 5% CO_2 and 95% N_2 every 24 hours. Preliminary results were obtained after removing the specimens from the autoclave by counting pit appearance on each specimen using a metallographic microscope, OLYMPUS model GX51 and watching these pits on SEM.

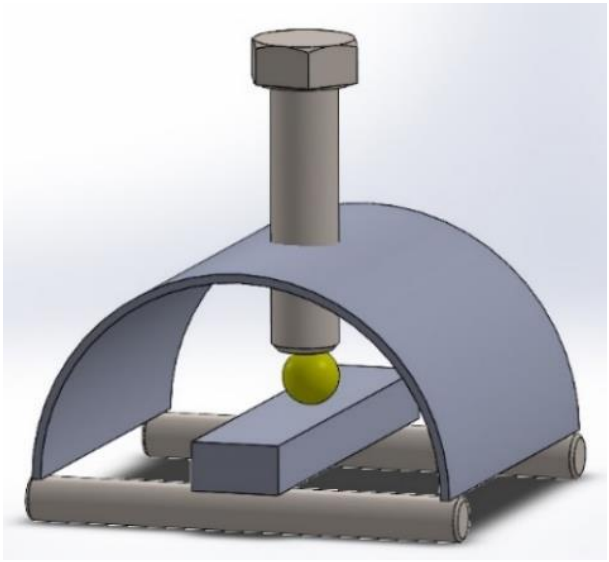

Figure 2. Diagram of the Sample Holder Used for Three-Point Bending.

Based on the first stage results and by following the same SCC proposed test and results analysis method, the second stage was performed in the same way, but the number of steels studied was reduced, and the "no load" condition was removed. Steels A1 and A3 were evaluated under progressive stress of 30%, 50%, 80%, and 110% of YS for steel A1, and 61%, 102%, 163%, and 225% of YS each one. The exposure time for the test in the second stage was extended to 4320 hours; the first 2160 hours the autoclave maintained an 80°C ± 5°C temperature, the next 2160 hours the test was performed on environmental conditions. The autoclave used is a device specifically designed for SCC generation tests; this design is not commercially available. This apparatus is shown in Figure 3.

Figure 3. Used autoclave.

3. RESULTS AND DISCUSSION

According to the chemical and microstructural characterization, the main differences of the six used steels are presented on Table 1.

Table 1. Microstrucutal and chemical characterization results.

Specimen	%C	%Perlite		%Inclusions		Grain size
		(L)	(T)	(L)	(T)	
A1	0.141	1.09	2.22	0.24	0.12	9.0
A2	0.100	5.12	5.98	0.16	0.16	11.0
A3	0.136	8.21	7.62	0.11	0.14	10.0
A4	0.166	10.98	9.53	0.17	0.15	11.5
A5	0.298	31.72	30.80	0.09	0.14	10.0
A6	0.242	23.39	22.15	0.06	0.04	10.0

Micrographs of used steel are presented in Figures 4-9, where it can be observed that all the steel used consists of a ferrite-pearlite matrix. The surface microstructures of steels 1 and 2 have a homogeneous distribution, while steels 3, 4, 5, and 6 display a heterogeneous distribution with bands of the pearlitic microconstituent.

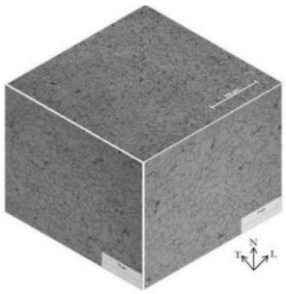

Figure 4. Steel A1 micrograph.

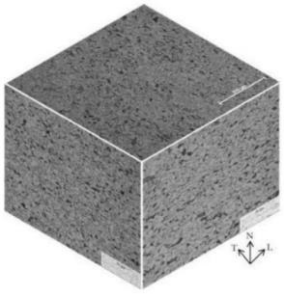

Figure 5. Steel A2 micrograph.

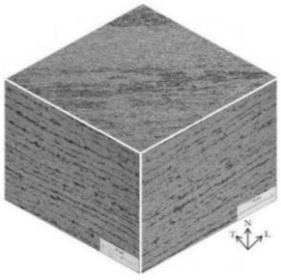

Figure 6. Steel A3 micrograph.

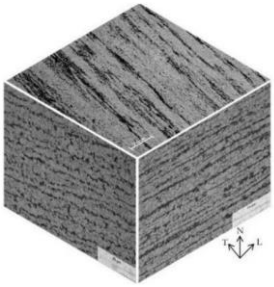

Figure 7. Steel A4 micrograph.

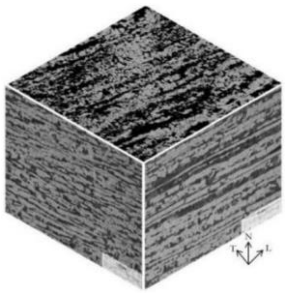

Figure 8. Steel A5 micrograph.

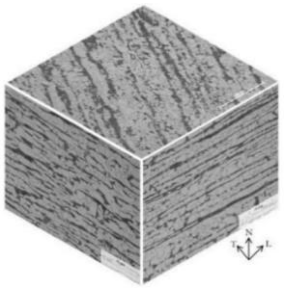

Figure 9. Steel A6 micrograph.

The tensile test results are shown in Table 2. These results show that the steels exhibit different yield strength (YS) and ultimate tensile strength (UTS), with Steel 2 displaying the highest YS and Steel 6 the lowest YS.

Table 2. Tensile test results.

Specimen	YS [MPa]	UTS [MPa]
A1	454	460
A2	468	508
A3	446	549
A4	445	559
A5	438	603
A6	400	560

Figures 10 and 11 show the specimens right after the first stage of SCC test, the surfaces show a loss of their mirror-like finish, suggesting the presence of pits. Photographic evidence of the polished surfaces reveals that the bent steels were more reactive, as they lost their mirror finish compared to the specimens without bending. The surfaces of the unbent steels exhibit an earthy appearance and show little adhesion of the corrosion product.

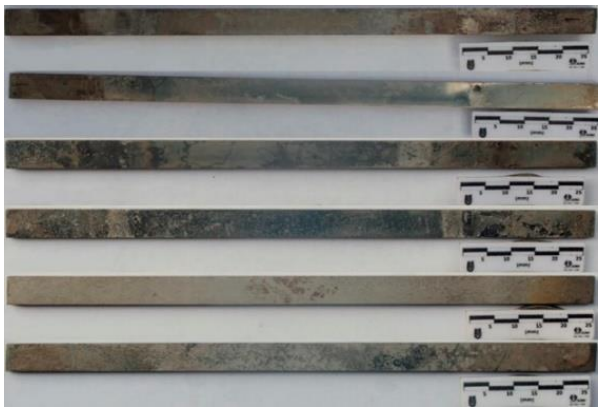

Figure 10. Unbent steels right after SCC test.

Figure 11. Bent steels right after SCC test.

Through metallographic microscopy, it was observed that the specimens contained surface pits. The number of pits per unit area was quantified. In Figure 12, where a bar graphic is presented, it is possible to see a significant difference in the number of pits per unit area between the tests with and without bending. This confirms that the steels respond differently based on their microstructural characteristics. The predominant presence of pits on the surfaces of loaded samples suggests stress corrosion cracking originating from pits. Additionally, this clearly demonstrates that the applied load promotes localized corrosion.

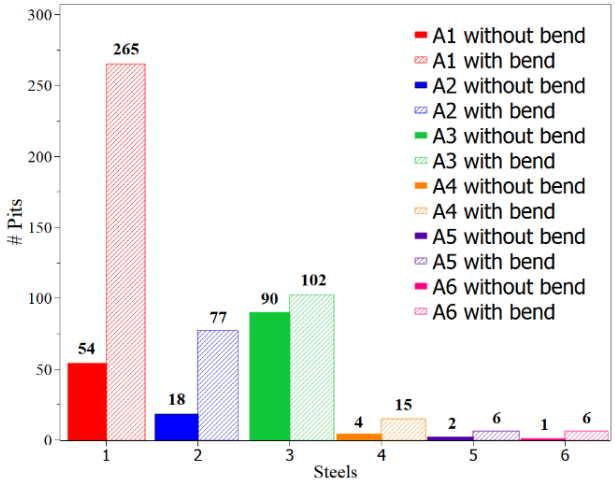

Figure 12. Number of pits per unit area.

Figure 13 shows pits observed on the surface of one of the steels, viewed through SEM. It is appreciable that the pits exhibit high internal chemical activity. Figure 14 is a side view of a specimen, where internal cracking is visible, both intergranular and transgranular.

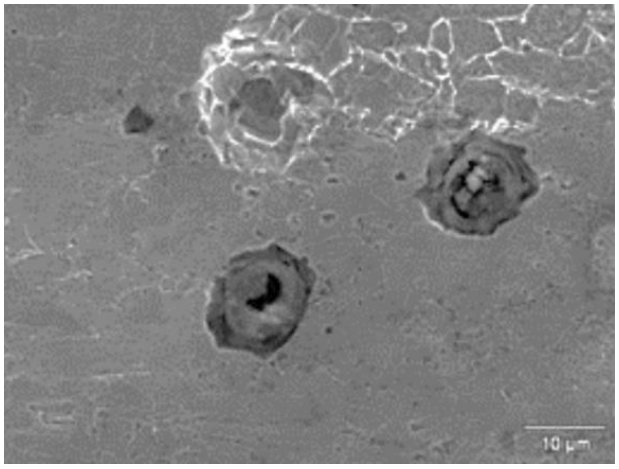

Figure 13. Superficial pits.

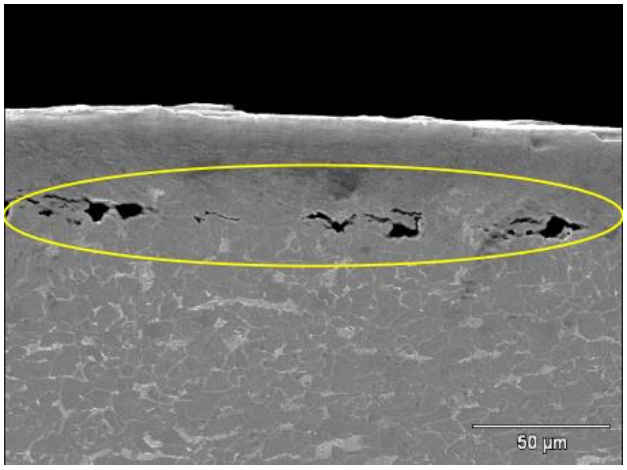

Figure 14. Side view of specimen on SEM.

After evaluating these results, the second stage of experimentation was conducted, focusing on Steels A1 and A3, as they exhibited the highest number of pits under load conditions. Figures 15 and 16 show the specimens after the 4320-hour test, where the increased presence of an orange oxide layer is notable compared to stage one of the experimentation.

Figure 15. Steel A1 right after 3620 hours SCC test.

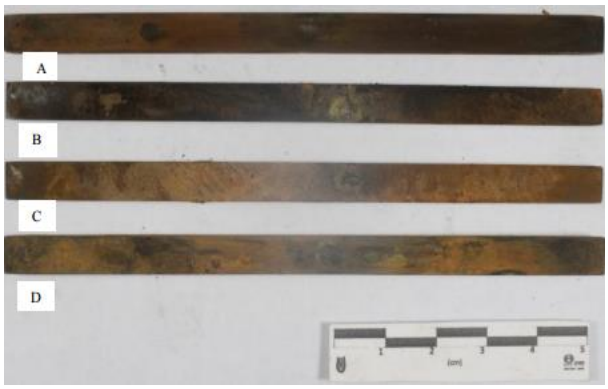

Figure 16. Steel A 3 right after 3620 hours SCC test.

As in stage 1, the pits were counted, and the number of pits per unit area in relation to the applied load percentage of YS is shown in the bar chart in Figure 17. It can be observed that the incidence increased with the applied load percentage, with the number of pits exponentially maximized when the YS is exceeded.

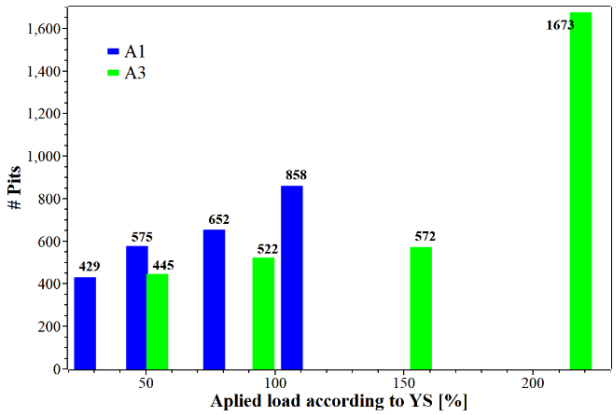

Figure 17. Pits vs applied load.

Finally, Figures 18 and 19 show the pits observed via SEM, where the typical semi-spherical shape of an electrochemical corrosion pit has been lost, suggesting that these pits may be associated with SCC. It is also evident that there was increased chemical activity leading to a non-uniform detachment of material from the pit walls. For this reason, the pits were examined at higher magnifications, revealing the presence of both intergranular (highlighted in blue) and transgranular (highlighted in green) internal

cracks associated with SCC in near-neutral pH environments, as shown in Figures 20 and 21.

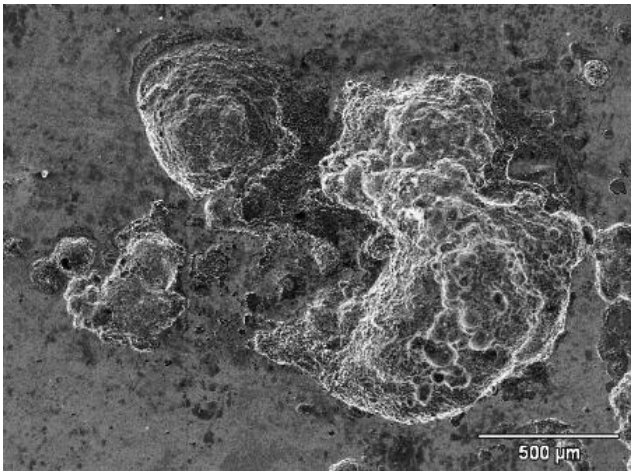

Figure 18. Pit on A1 surface observed on SEM.

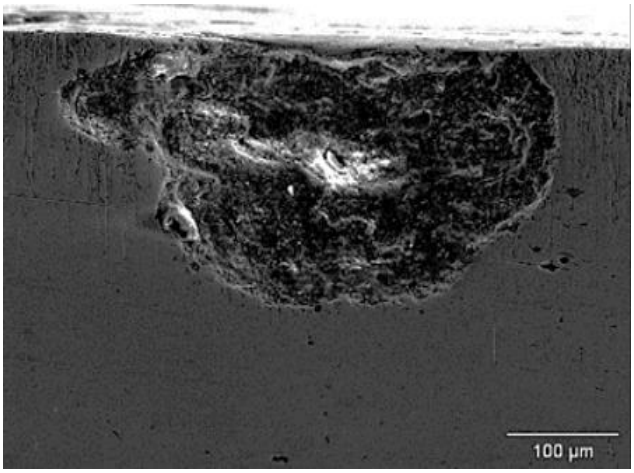

Figure 19. A2 pit side view on SEM.

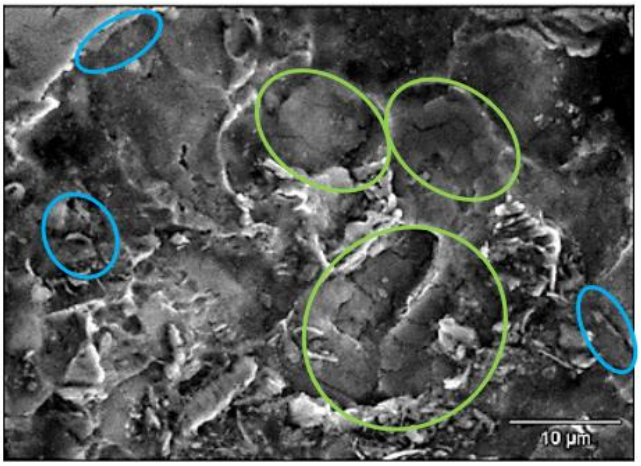

Figure 20. Cracks observed inside A1 pit.

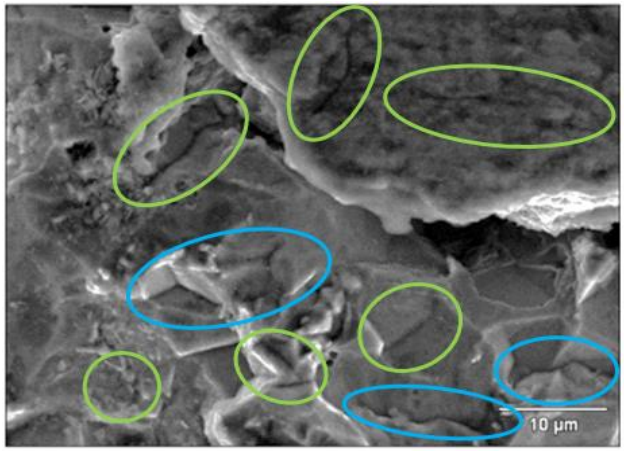

Figure 21. Cracks observed inside A2 pit.

4. CONCLUSIONS

Based on the evidence generated in this study on the relationship between microstructure and SCC susceptibility, and the analysis conducted, the following conclusions can be drawn:

1. This experimentation revealed the development of the initial stage of SCC, with the formation of pits with atypical morphology, featuring transgranular cracks at their base.

2. The applied stress on a component is linked to the number of SCC pits. Higher stress correlates with a greater presence of pits.

3. Non-metallic inclusions are considered stress concentrators, where a higher number of inclusions results in an increased number of pits.

4. An increase in the pearlitic microconstituent content reduces the likelihood of pit formation due to the distribution and proximity of anodic and cathodic sites.

5. Steel A1 shows a larger grain size but fewer cracks, suggesting that larger grain size reduces susceptibility to the initial stages of SCC. This is attributed to grain boundaries being active sites that reduce corrosion resistance.

6. The cracks observed in this study are associated with non-classical SCC, as they are identified as transgranular and located within pits of atypical morphology.

Acknowledgments

The authors wish to thank the IPN, ESIQIE and CONAHCYT.

Conflicts of Interest

The authors declare that they have no known competing financial interests or personal relationships that could have appeared to influence the work reported in this paper. “The authors declare no conflict of interest.”

REFERENCES

[1] American Petroleum Institute. (2018). API SPECIFICATION 5L 46th. Line Pipe.

[2] González V, J. (2017). Fractografía y análisis de falla. Ciudad de México: Edición del Autor.

[3] Khidir, E., Basha, S., & Al-Assadi, H. (2017). Analysis of Stress Corrosion Cracking of X65 Oil Pipeline. International Journal of Mechanical Engineering and Technology, 212-222.

[4] Bogdanov, R., Gutman, E., Ryakhovskikh, I., & et al. (2019). Stress corrosion cracking of pipeline steels in near-neutral-pH solutions: the role of mechanochemical and chemomechanical effects. Colección científica y técnica · NOTICIAS DE CIENCIA DEL GAS, N° 3 (40).

[5] Chen, W. (2015). An overviwe of near-neutral pH Stress Corrosion Cracking in pipelines and mitigation strategies for its initiation and growth. NACE International, 1938-159X.

[6] Liu, Z., Li, X., Du, C., & et al. (2009). Effect of inclusions on initiation of stress corrosion cracks in X70 pipeline steel in an acidic soil environment. Corrosion Science 51, 895-900.

[7] Zhao, J., Chen, W., Yu, M., & et al. (2017). Crack Growth Modeling and Life Prediction of Pipeline Steels Exposed to Near-Neutral pH Environments: Stage II Crack Growth and Overall Life Prediction. METALLURGICAL AND MATERIALS TRANSACTIONS A, 1641-1652.

[8] Abubakar, S., Mori, S., & Summer, J. (2022). A Review of facotrs affecting SCC initiation and propagation in pipelines carbon steels. Metals, 12, 1397.

[9] Bueno, A., & Gomes, J. (2009). Environmentally Induced Cracking of API Grade Steel in Near-Neutral pH Soil. ABCM, 97-104.

[10] Beavers, J., Johnson, J., & Sutherby, R. (2000). Materials factors influencing the initiation of near-neutral pH SCC on underground pipelines. IPC, 979-988.

[11] Nyrkova, L. (2020). Stress-corrosion cracking of pipe steel under complex influence of factors. Engineering Failure Analysis, 104757.

[12] Chen, W. (2016). An overview of near-neutral pH SCC in pipelines and mitigation strategies for its initiation and growth. Corrosion, 1-117.

[13] Fang, B., Han , E., & Wang, J. (2007). Stress corrosion cracking of X-70 pipeline steel in near neutral pH solution subjected to constant load and cyclic load testing. Corrosion Engineering, Science and Technology, 123-129.

[14] Wang, Z., Wang, J., & Han, E. (2007). Influence of intermittent loading on SCC behavior for an X70 pipeline steel in a near-neutral pH solution. Materials and Corrosion, 583-587.

[15] Perez, N. (2004). Electrochemestry and Corrosion Science. Boston: Kluwer Academic Publishers.

[16] Pedeferri, P. (2018). Corrosion Science and Engineering. Milan: Springer.

[17] Muraleedharan, P. (2002). Metallurgical Influences on Stress Corrosion Cracking . Indira Gandhi Centre for Atomic Research, 139-165.

[18] Boven, G., Chen, W., & Rogge, R. (2007). The role of residual stress in neutral pH stress corrosion cracking of pipeline steels. Part I: Pitting and cracking occurrence. Acta Materialia 55, 29-42.

[19] Zhang, C., Ran, M., Wang, Y., & Zheng, W. (2022). Microestructural effects in the development of near-neutral pH Stress Corrosion Cracking. Materials, 15, 4372.

[20] Baker, M. (2004). Understanding Stress Corrosion Cracking (SCC) in Pipelines. OPS TTO8 – Stress Corrosion Cracking Study, 15

395-I-PO INFLUENCE OF COMPUTATIONAL PARAMETERS ON RANS-BASED PREDICTIONS OF AXIAL-FLOW COMPRESSOR PERFORMANCE

O. Hernández Alonso[1]*, M. Toledo Velazquez[1], D. Mimic[2]

[1]Instituto Politécnico Nacional, Escuela Superior de Ingeniería Mecánica y Eléctrica, Unidad Zacatenco, Sección de Estudios de Posgrado e Investigación –Mecánica Laboratorio de Ingeniería Térmica e Hidráulica Aplicada, Av. Instituto Politécnico Nacional S/N, C.P. 07738 CDMX, México.

[2]Leibniz Universität Hannover, Institut of Turbomachinery and Fluid Dynamics, An der Universität 1, Gebäude 8141, 30823, Garbsen, Germany.

*Correspondence: omar.hernandez1710@gmail.com

Abstract: This study investigates the impact of various methodologies on extending the predictive capability of a four-and-a-half-stage high-speed axial flow compressor simulation near the surge region. Conducted within the TRACE Computational Fluid Dynamics (CFD) framework, the simulation utilizes steady-state Reynolds-Averaged Navier-Stokes (RANS) equations coupled with the k-ω Shear Stress Transport (SST) turbulence model. The investigation focuses on three specific parameters: the number of simulated passages, the extent of the inlet and outlet domains, and the incorporation of a converging nozzle at the compressor outlet. Additionally, the influence of incorporating a proportional-integral-derivative (PID) controller within the simulation framework is assessed.

Keywords: Multi-Stage Axial Compressor, Operating map, Numerical Stability, Surge Limit, Computational Fluid Dynamics.

1. INTRODUCTION

The successful design of compressors depends on accurately predicting performance parameters across their full operational range, particularly near stability limits. Advanced steady-state simulation techniques are essential for modeling such unsteady conditions. Numerous studies have investigated various aspects of compressor simulation. For instance, Davis R. et al. [1] analyzed how geometric configurations and boundary conditions influence the prediction of aerodynamic performance in the NASA Stage 35 single-stage axial flow compressor under stall conditions. Similarly, Vahdati M. et al. [2] studied the implementation of a variable nozzle downstream, which enabled the simulation to capture the hysteresis loop and surpass the stall condition. These studies underscore the importance of accurate boundary condition and geometric modeling in improving the fidelity of compressor performance predictions.

Achieving a high-fidelity simulation requires meticulous consideration of several critical factors: selecting the appropriate turbulence model, accurately defining the simulation domain size, implementing optimal inlet and outlet boundary conditions, and, where necessary, incorporating a variable nozzle at the compressor outlet alongside a PID controller to enhance numerical stability.

The primary aim is to analyze how these parameters affect the fidelity of simulations in capturing compressor performance across its operating range, especially near the surge region. By systematically assessing these parameters, the study seeks to determine whether these modifications improve the predictive accuracy of simulations while accounting for their inherent limitations. The outcomes are expected to advance simulation methodologies for high-speed axial flow compressors, contributing to the design and

optimization of these critical components in aerospace and power generation applications.

Critical parameters include the number of computational fluid passages, which enhances flow field resolution, and the extension of inlet and outlet domains to ensure adequate flow development. Incorporating a converging nozzle at the compressor outlet significantly alters pressure and velocity distributions. Additionally, a PID controller is integrated into the simulation framework to dynamically regulate outlet pressure during reduced mass flow rates, enabling more realistic replication of operating conditions. These enhancements aim to provide a comprehensive evaluation of compressor performance.

2. METHODOLOGY

This investigation uses the four-and-a-half stage high-speed axial compressor from the Institute of Turbomachinery and Fluid Dynamics at Leibniz University Hannover as the test case.

Franke et al. [3] demonstrated that the k-ω SST turbulence model, when combined with the stagnation-point anomaly correction by Kato and Launder [4], the approach for rotational effects by Bardina et al. [5], and the transition model by Langtry and Menter [6], delivers satisfactory performance in predicting the behavior of multi-stage axial compressors while ensuring numerical stability. Thus, this model is applied in the present study.

Table 1. Four-and-a-half stage high-speed axial compressor key characteristics. Taken from [3].

Rotor speed	18000 RPM
Mass-flow rate	7.93 kg/s
Power	952 kW
Total pressure ratio	2.72
Inlet total pressure	60 kPa

The reference geometry used in this study follows the configuration established by Mimic et al. [7], as illustrated in Figure 1.

The study aims to minimize the mass flow rate to approach the surge region and extend the performance prediction curve. Starting at 7.9 kg/s, the mass flow rate was systematically reduced by increments of 1 g/s until the simulation reached a point of non-convergence, indicating instability.

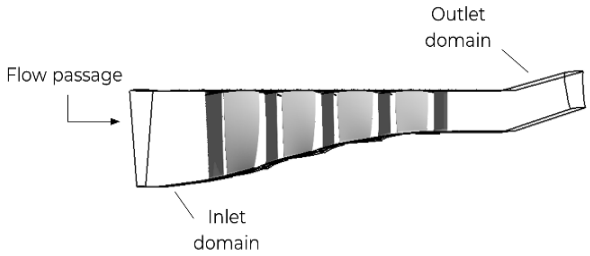

Figure 1. Compressor model employed in the present study.

Several modifications to the computational domain were implemented to evaluate numerical stability as the compressor's operating conditions approached the surge limit. Three distinct strategies were assessed independently: (i) increasing the number of simulated flow passages, (ii) extending both the inlet and outlet sections, and (iii) incorporating a converging nozzle at the outlet. Additionally, the effectiveness of employing a Proportional-Integral-Derivative (PID) controller to regulate outlet pressure was examined. The combination of two or more strategies in this study was not possible due to the time and resources available.

To evaluate the impact of simulated flow passages, four configurations were tested: (a) one passage, (b) two passages, (c) four passages, and (d) eight passages as shown in Figure 2. To evaluate the impact of domain extent, four computational configurations were examined: the first extended the inlet domain by one chord length from the mid-span blade of the first-stage rotor, while the second configuration doubled this extension; the outlet domain was extended in an analogous way, corresponding to the third and fourth configuration, respectively. The

influence of an outlet nozzle was examined by integrating a converging nozzle designed for a smooth transition, minimizing the effects of sudden geometric changes on the flow field. Figure 3 illustrates the domain configurations.

The effectiveness of a Proportional-Integral-Derivative (PID) controller in regulating outlet pressure was evaluated using seven configurations, each with unit gains, to analyze simulation behavior.

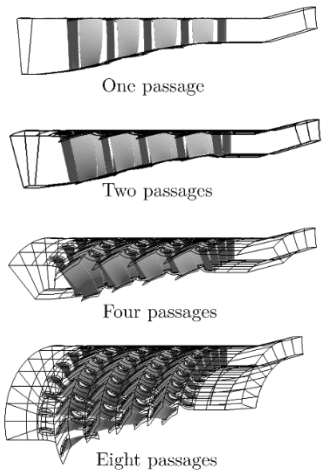

Figure 2. Passage extension configurations.

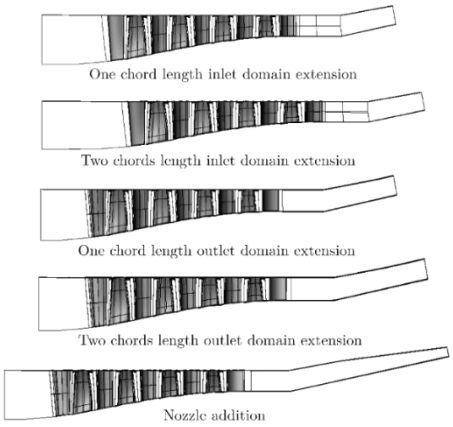

Figure 3. Domain extension configurations.

All simulations were performed in steady-state mode, using the turbomachinery flow solver TRACE 9.4.8 developed by the German Aerospace Center (DLR) and MTU Aero Engines.

2.1. Numerical Setup and Boundary conditions

This study is based on the numerical setup established in references [3, 7], which employs a Fromm scheme combined with a van Albada-square limiter and a second-order finite-volume spatial discretization to compute the state variables. The governing equations are solved using an incomplete lower-upper (ILU) factorization method. A turbulent Prandtl number of 0.9 is assumed for heat flux calculations. To ensure consistency with the experimental conditions reported by Mimic et al. [7], the inlet total pressure and total temperature at the mid-span were set to 60 kPa and 288.15 K, respectively. Additionally, all simulations are conducted at 95% of the design speed. In all instances, a converged simulation was used to initialize the subsequent simulations.

The structured mesh was generated using NUMECA Autogrid5. The configuration and parameterization of the base mesh corresponds to that used by Franke et al [3], with a node-to-node connection in the circumferential direction. All boundary layers are resolved with a nondimensional wall distance of y + <1.

3. RESULTS AND DISCUSSION

3.1. Number of simulated passages

All investigated configurations exhibited similar pre-convergence characteristics, with the observed discrepancies between them being minimal and considered negligible for the purposes of this study (see Figure 4). Additionally, a direct proportionality was observed between the number of simulated flow passages and the computational cost per iteration. This finding aligns with established principles, as increasing the model complexity by incorporating additional flow passages necessitates a commensurate increase in computational resources to maintain solution fidelity.

Overall, the two-passage simulation provides a more realistic representation of the flow

behavior within the compressor, showing interactions that a single-passage model cannot capture. However, this increased accuracy comes with greater computational complexity. The two-passage configuration achieved a stable solution with a mass flow rate of 7.865 kg/s, while the four- and eight-passage configurations were unviable due to their high computational cost.

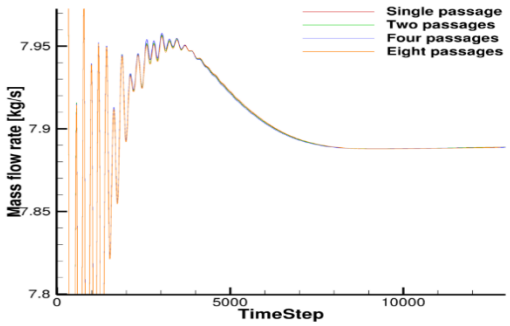

Figure 4. Results of the passage extension simulation with a mass flow rate of 7.89 kg/s, after 12,000 iterations. TimeStep and iteration count are effectively interchangeable in this steady-state setup. Thus, each time step corresponds to a single iteration in the numerical simulation.

Table 2 provides a comparison between this two-passage case and the reference single-passage case, with data extracted from the final 1000 iterations of the simulation for analysis.

Table 2. Simulation results comparison of the two-passage configuration and the reference case at 7.865 kg/s mass flow rate. Data extracted from the final 1000 iterations of the simulation.

Parameter	One passage (reference)	Two passages
Target mass flow rate [kg/s]	7.865	7.865
Average mass flow rate [kg/s]	7.831244	7.864981
Mass flow rate standard deviation	2.34E-03	3.34E-06

This suggests that the two-passage configuration provides a more stable and consistent simulation, with reduced fluctuations in mass flow rate. In contrast, the one-passage configuration shows a loss of numerical stability at that mass flow rate, emphasizing the benefit of using multiple passages for improved accuracy and reliability in simulations close to operational limits, albeit with increased computational cost.

3.2 Domain extension

After the initial 72-hour simulation period, notable differences emerged in the behavior of the various domain extension configurations.

Outlet domain extensions displayed significantly larger mass flow rate oscillations during the transient phase than Inlet domain extensions. Transient phase corresponds to the period during which the mass oscillates until it reaches a stable value. However, as the simulation progressed, these fluctuations decreased, and all configurations converged to a steady-state mass flow rate. Notably, Outlet domain extensions required more iterations over the simulated 72-hour period, with the nozzle configuration taking the longest to achieve a stable mass flow rate.

Figure 5 depicts the convergence trajectory of three different outlet domains. The plot illustrates the relationship between the mass flow rate and the compressor pressure ratio for three different simulation configurations near the surge limit: two outlet extension configurations (Configurations 1 and 2) and a nozzle at the outlet section, corresponding to the last 3 configurations shown in Figure 3, respectively.

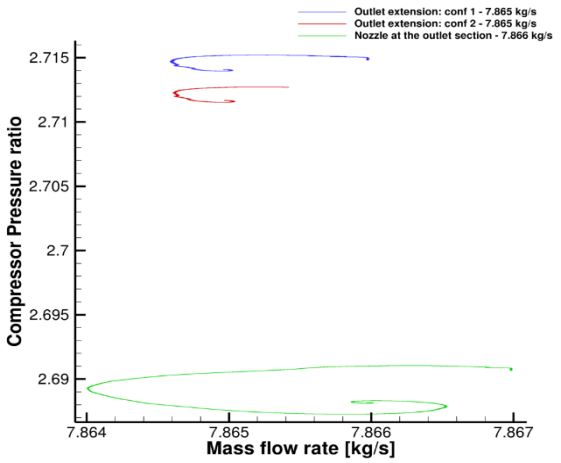

Figure 5. Compressor convergence trajectories of the different outlet extension configurations.

Inlet domain modifications are excluded from Figure 5 due to significant variations, making it difficult to distinguish the converged cases. Outlet extensions (blue line for one chord and red line for two chords) maintain a relatively steady compressor pressure ratio around a mass flow rate of 7.865 kg/s. In contrast, the nozzle configuration (green line) exhibits more pronounced fluctuations, indicating greater instability and non-linear behavior in the compressor pressure ratio as the mass flow rate changes, highlighting its reduced stability compared to the outlet extension configurations.

Table 3 shows the comparison of the three cases stated before with the reference case. The two-chord length outlet extension configuration attained an average mass flow rate closer to the target (7.865 kg/s) with the smallest standard deviation among the outlet extensions, indicating enhanced stability in the simulation. This aligns with the plot showing that this configuration maintains a relatively stable compressor pressure ratio with minimal fluctuations.

The nozzle configuration, while having a low standard deviation, displayed a broader range of behavior in terms of mass flow rate and pressure ratio, as seen in Figure 5. This implies that while it might achieve good stability in certain aspects, the overall pressure characteristics are more varied, which could impact the overall performance. The one-chord outlet extension had a higher standard deviation compared to the other configurations, indicating greater fluctuations in mass flow rate and less consistency.

Table 3. Simulation results comparison of the outlet domain extension configurations and the reference case at 7.865 kg/s mass flow rate. Data extracted from the final 1000 iterations of the simulation.

Parameter	Reference Case	One chord Outlet extension	Two chords Outlet extension	Nozzle
Target mass flow rate [kg/s]	7.865	7.865	7.865	7.865
Average mass flow rate [kg/s]	7.831244	7.865003	7.864980	7.864959
Mass flow rate standard deviation	2.34E-03	6.83E-06	3.89E-06	7.45E-06

Overall, the two-chord outlet extension configuration appears to provide the best balance between maintaining a stable mass flow rate and consistent pressure ratio, demonstrating its effectiveness for extending the domain while maintaining stability near the operational limits.

The domain extension approach facilitated the execution of a broader spectrum of simulations due to its lower computational expense compared to increasing the number of simulated flow passages. Additionally, the introduction of a nozzle resulted in a lower pressure ratio than configurations using only outlet extensions, with the convergence trajectory of the nozzle simulations showing greater variation.

3.3 PID Controller

The target mass flow rate for the PID controller was set to 7.865 kg/s. Configurations with zero gains for the proportional and integral components resulted in system instability, consistent with the limitations of a purely derivative controller, which lacks corrective influence from the other terms. When only the proportional gain was active, the system behaved similarly to scenarios without a PID

controller, indicating that the proportional term alone is insufficient for effective control. Figure 6 illustrates the simulation results for different gain combinations.

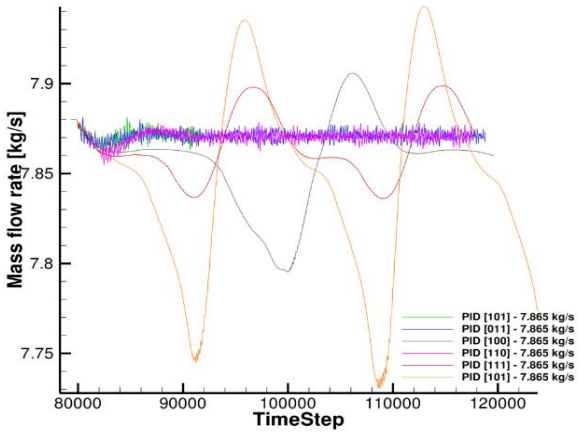

Figure 6. PID Pressure control. Different combinations of gains was studied, employing a mass flow rate of 7.865 kg/s.

Simulations with combinations of proportional-derivative and proportional-integral gains produced smoother and more stable results, suggesting these configurations are more effective. Further improvements could be achieved by applying formal tuning methods such as Ziegler-Nichols or Cohen-Coon [8].

4. CONCLUSIONS

Extending the number of simulated passages had minimal impact on simulation results compared to extending the inlet and outlet domains at the same mass flow rate. However, the computational cost increased significantly with more passages. The four-passage configuration required approximately 310% more time per iteration than the reference case, while the eight-passage configuration required around 465%, even when the simulations remained in a stable state. This underscores the substantial rise in computational expense with increasing passage numbers.

Inlet domain modifications, such as extending the inlet length, had little effect on prediction accuracy or simulation stability. In fact, these configurations performed worse than other modifications, exhibiting instabilities under conditions where other setups achieved stability at the same mass flow rate. Conversely, extending the outlet domain enabled the attainment of lower mass flow rates, though the results varied significantly across configurations. This variation underscores the need for a more detailed analysis to ensure the simulations accurately represent the underlying physical phenomena.

Further exploration of the PID pressure controller, potentially in conjunction with the approaches examined, could result in notable improvements in the ability to predict the compressor performance map.

Acknowledgements

The authors would like to express their sincere gratitude to the Leibniz Universität Hannover, particularly the Institut of Turbomachinery and Fluid Dynamics, for granting access to their facilities and the axial compressor test case, which were instrumental in the success of this project. The authors also acknowledge the contributions of the DLR Institute of Propulsion Technology and MTU Aero Engines AG for providing the TRACE software. Appreciation is further extended to the Leibniz University Hannover IT Services (LUIS) for supplying the necessary computational resources. Special thanks to the Instituto Politécnico Nacional and CONAHCYT for its invaluable support and resources throughout this research. We would also like to thank Prof. Dr.-Ing. Jörg Seume and Prof. Dr.-Ing. Miguel Toledo Velazquez.

Conflicts of Interest

The authors declare no conflict of interest.

REFERENCES

[1] R. L. Davis, J. Yao, J. Propuls. Power (2012). https://doi.org/10.2514/1.15463

[2] M. Vahdati, A.I. Sayma, C. Freeman, M. Imregun, J. Turbomach (2005). https://doi.org/10.1115/1.1861912

[3] P. Franke, M. Nyhuis, L. Wein, D. Mimic, in *Proc.* ETC15 (2023). https://doi.org/10.29008/ETC2023-175

[4] M. Kato, B. Launder, in *Proc. 9th Symp. Turbulent Shear Flows,* 16 (1993).

[5] J. Bardina, P. Huang, T. Coakley, Turbulence Modeling Validation, Testing, and Development, NASA Technical Memorandum 110461 (NASA Langley Research Center, Hampton VA, 1997), pp. 14-16

[6] F. Menter, M. Kuntz, R.B. Langtry, Turbulence, Heat and Mass Transfer 4, 625 (2003)

[7] D. Mimic, P. Sauer, J. R. Seume, in *Proc.* GPPS Xi'an21 (2022). https://dx.doi.org/10.33737/gpps21-tc-337

[8] Duarte Valério, José Sá da Costa, Signal Processing 86, (2006). https://doi.org/10.1016/j.sigpro.2006.02.020

HORIZONTES
de Investigación y Desarrollo

II

Medical-biological sciences

7-II-PO CHARACTERIZATION OF MACROPHAGE POLARIZATION IN EARLY STAGES OF SYSTEMIC LUPUS ERYTHEMATOSUS: ANALYSIS IN A MOUSE MODEL INDUCED WITH LIPID PARTICLES

R. Ramos-Monteagudo[1], C. Wong-Baeza[1], G. Barrera-Aveleida[1], E. Galarce-Sosa[1], E. Rundquist-Sánchez[1], A. Reséndiz-Mora[1], I. Baeza-Ramírez[1]*

[1]Instituto Politécnico Nacional, Escuela Nacional de Ciencias Biológicas, Laboratorios de Biomembranas y de Enzimología, Departamento de Bioquímica, Prolongación de Carpio y Plan de Ayala S/N, C.P. 11340, Ciudad de México, México.

*Correspondence: isabelbeza@yahoo.com

Abstract: Macrophages are essential cells of the innate immune system that can polarize into two main phenotypes, M1 and M2, which enable pro-inflammatory and regulatory functions, respectively. Dysfunction in these cells can lead to autoimmune responses and loss of immune tolerance, as observed in systemic lupus erythematosus (SLE). This study focuses on assessing macrophage polarization in a mouse model induced with lipid particles. Fluorochrome-labeled antibodies will be used to identify the total macrophage population through markers such as CD68 and F4/80. M1 macrophages will be identified by CD80 and CD40, while M2 macrophages will be marked by CD206 and MGL. Cytokines associated with each phenotype will be measured, including IL-6 and IL-12 for M1, and IL-10, TGF-β, and Arg-1 for M2. A Cytek® Aurora flow cytometer will be employed for these analyses.

Keywords: Macrophage, SLE, lipid particles.

1. INTRODUCTION

Systemic lupus erythematosus (SLE) is an autoimmune pathology characterized by chronic inflammation, the production of autoantibodies targeting self-antigens, and damage to healthy tissues by the deposition of immunocomplexes [1]. Macrophages are phagocytic immune cells that play a vital role in maintaining homeostasis and recognizing and eliminating foreign pathogens [2]. Macrophages exhibit polarization and differentiation into distinct phenotypes in diverse inflammatory milieus. Macrophages can polarize into pro-inflammatory macrophages (M1) or anti-inflammatory macrophages (M2). M2 macrophages may be split into four subtypes: M2a, M2b, M2c, and M2d. M1 and M2 will coexist and be in balance under normal circumstances [2, 3].

Recent studies have observed that macrophages are essential in SLE pathogenesis, specifically in defective apoptotic cell clearance. This leads to persistent inflammation and autoimmune reactions to self-antigens, leading to self-antibody production [4]. It is also observed that the disruption of the delicate balance between M1/M2 phenotypes is associated with the pathogenesis of SLE [4, 5].

Several mouse models have been created to further research SLE. Our research group has developed a systemic lupus erythematosus model that can be produced in BALB/c, C57BL/6, and NIH mouse strains by directly administering lipid particles (NPA's) [6,7]. The anionic lipids cardiolipin, phosphatidylserine, diacylglycerol, and phosphatidylethanolamine are arranged in a tubular Hexagonal II (H_{II}) phase to form these NPA's, which are temporary intermediate structures [6,7]. Divalent cations and drugs like chlorpromazine can both cause NPA's production. This type is distinguished by the early development of anti- NPA's antibodies, which are followed by the identification of anti-cardiolipin, anti-histone, anti-nuclear, and anticoagulant autoantibodies about one

month following the appearance of anti- NPA's IgG antibodies [7, 8]. This study will assess macrophage polarization into M1 and M2 phenotypes in the early stages of a mouse model induced with NPAs to investigate their role in SLE pathogenesis.

2. MATERIALS AND METHODS

2.1 Liposome preparation, NPA's induction and characterization

The lipids from egg yolk L-α-phosphatidylcholine and L-α-phosphatidic acid (SIGMA) were used to generate smooth liposomes in a molar ratio of 2:1 using the reverse phase evaporation method described previously [6]. The induction of NPAs was performed by adding chlorpromazine (SIGMA) to smooth liposomes, followed by incubation at 37°C for 30 minutes. To determine the optimal chlorpromazine concentration for NPA induction, concentrations of 1, 2, 3, 4, and 5 mM were tested. Flow cytometry analysis using a Cytek Aurora confirmed the generation of NPAs. Characterization was performed only once, and results were reported as liposome numbers, SSC histograms, and FSC vs SSC dot plots on logarithmic scales. The Kolmogorov–Smirnov test was applied to compare SSC histograms between smooth liposomes and NPA-bearing liposomes. D values greater than 0.5 were considered statistically significant.

2.2 Generation of a SLE model triggered by NPA's in BALB/c mice

Six six-week-old female BALB/c mice (n=6) were administered with 100 µL of complete Freund's adjuvant (Sigma Aldrich), diluted 1:2 in TS buffer (10 mM Tris-HCl, 1 mM NaCl, pH 7), via intraperitoneal injection on Day 0. This was followed by intrasplenic administration of 50 µL of NPA-bearing or TS solution on Day 1 and an intraperitoneal injection of 100 µL of TS or NPA-bearing liposomes on Day 2. Mice were euthanized four days after the first intrasplenic injection. Spleens and mesenteric lymph nodes were harvested from the euthanized mice and disaggregated to obtain cell suspensions in Dulbecco's Modified Eagle Medium (DMEM) (GIBCO) supplemented with 5% bovine fetal serum (Biowest) for subsequent flow cytometry assays.

2.3 Macrophage polarization and cytokine production assessment by flow cytometry

Fluorochrome-labeled antibodies were used to identify the total macrophage population with markers such as CD68 and F4/80. M1 macrophages were distinguished using CD80 and CD40, while CD206 and MGL were used for M2 macrophages. Intracellular staining was performed with the GolgiStop™ kit to inhibit cytokine release and enable intracellular detection using specific antibodies. Pro-inflammatory cytokines (IL-6 and IL-12 for M1) and anti-inflammatory cytokines (IL-10, TGF-β, and Arg-1 for M2) were analyzed. Marker expression was assessed with a Cytek® Aurora flow cytometer, and data were processed using FlowJo™ software to evaluate macrophage composition and cytokine production. All fluorochrome-labeled antibodies were titrated at concentrations ranging from 1:100 to 1:800. Further details on the flow cytometry panel and antibody concentrations are provided in (Table 1).

Table 1. Flow cytometry panel for macrophage polarization markers and cytokines.

Extracellular staining	
Marker	**Dilution**
α-CD68-APC	1:400
α-F4/80-PE DAZZLE 594	1:200
α-CD80-APC FIRE 750	1:200
α-CD40-PACIFIC BLUE	1:400
α-MGL-PE Cy 7	1:400
α-CD206-AF 700	1:800
Intracellular staining	
α-IL-6-PE	1:200
α-IL-10-FITC	1:200
α-ARG-1-PE	1:200
α-TGF-β-PerCP Cy 5.5	1:400

2.3 Ethical statements

All animal procedures followed the principles of the "Guide for the Care and Use of Laboratory Animals" from the US National Institute of Health [9]. In addition, the procedures were approved by the bioethics

committee of the National School of Biological Sciences of the National Polytechnic Institute (CEI-ENCB-025).

3. RESULTS AND DISCUSSION

Flow cytometry characterization of NPA-bearing liposomes revealed increased bilayer complexity (measured as side scatter, SSC) as chlorpromazine concentration rose to 3 mM, Figure 1 C, E, G. However, at 4 and 5 mM Figure 1 I, K, liposome size and complexity were reduced. These findings align with the results of the Kolmogorov–Smirnov test, which yielded the following D values at the specified chlorpromazine concentrations: 1 (D=0.25) (D), 2 (D=0.52) (F), 3 (D=0.68) (H), 4 (D=0.55) (J), and 5 mM (D=0.35) (L). Since a D value ≥ 0.5 is considered statistically significant, the optimal concentration of chlorpromazine for induction is 3 mM. These observations align with previous studies [6,7]. In those studies, different inducers were analyzed, including promazine, hydralazine, manganese, and calcium. Notably, chlorpromazine at a concentration of 3 mM appears to be the optimal inducer for generating NPA-bearing liposomes. The simultaneous increase in bilayer complexity (SSC) and liposome size (FSC) with rising inducer concentration is linked to NPA formation. NPAs play crucial roles in various cellular processes, such as phagocytosis, membrane junctions, ion transport, and membrane fusion during exocytosis and endocytosis, as well as protein insertion and the formation of polar pores and compartments [10]. Therefore, the observed increase in size likely results from liposome fusion facilitated by the presence of NPAs.

In this study, following the previously outlined procedure, the assessment focused on macrophage polarization in the NPA group four days after intrasplenic administration of NPA-bearing liposomes. (Figure 2) presents dot plot graphics depicting the M1 markers of the cells recovered from the spleen. The analysis included the following events: individual events (Figure 2A), the total cellular population (Figure 2B) viable cells (Figure 2C), the macrophage population identified by the CD68 and F4/80 markers (Figure 2D), and the selection of M1 macrophages (CD80+ and CD40+) (Figure 2E), along with their expression of the pro-inflammatory cytokine IL-6 (Figure 2F).

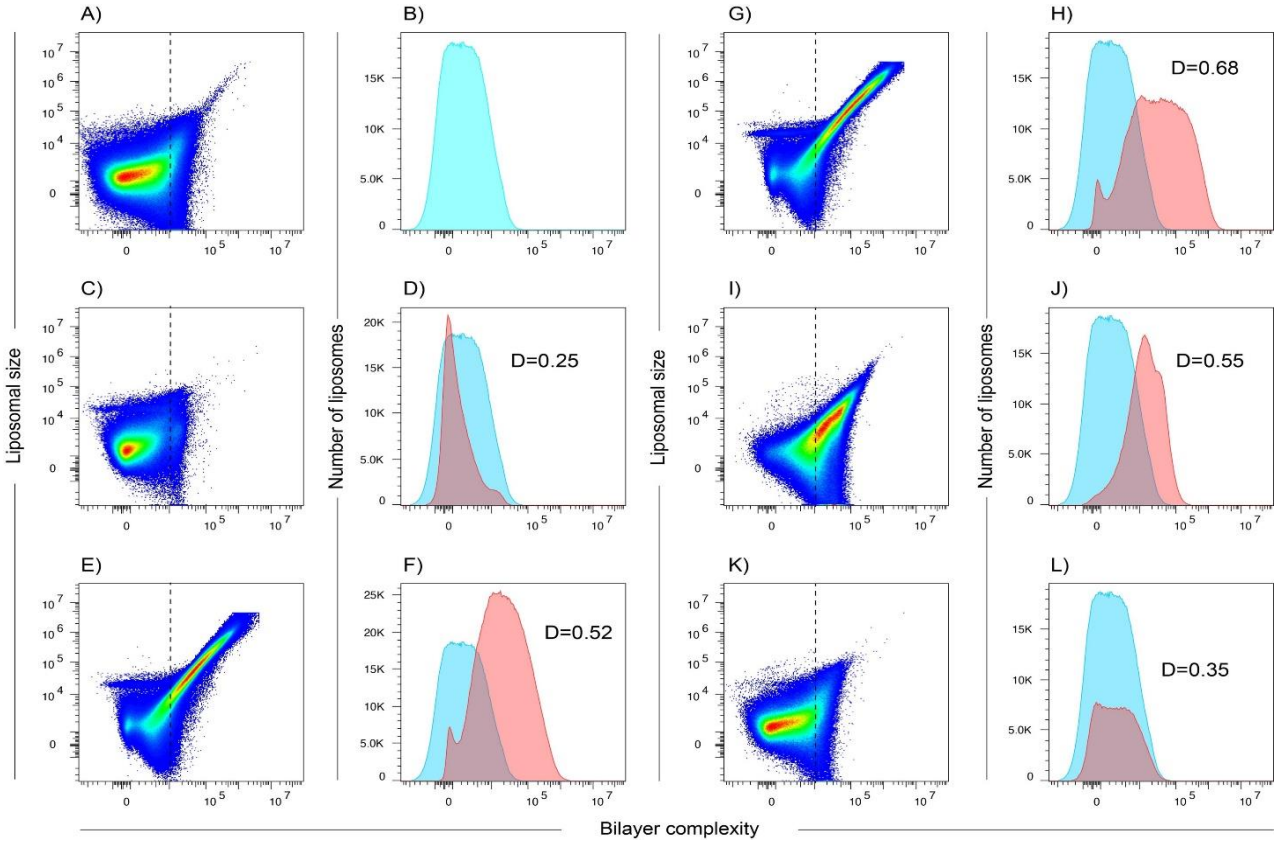

Figure 1. Flow cytometry characterization of liposomes bearing lipid particles. Liposomal size and bilayer complexity increase upon induction with chlorpromazine at different concentrations (1, 2, 3, 3, 4, and 5 mM). Smooth liposomes (A) exhibit uniform size and complexity. As the chlorpromazine concentration increases to 1, 2, and 3 mM (C, E, and G), a progressive increase in size and complexity is observed. However, at higher concentrations (4 and 5 mM; I and K), these values begin to decrease. To determine if changes in bilayer complexity are significant, the histogram of smooth liposomes (B) was compared with liposomes induced at different concentrations (D, F, H, J, and L) using the Kolmogorov–Smirnov test. A D-value greater than 0.5 indicates a statistically significant difference, confirming the presence of lipid particles in the liposomes.

Of the approximately 100,000 total events, only 4.69% were identified as macrophages. Among these, 11.1% were classified as M1 macrophages, and only 4.15% of these M1 macrophages expressed IL-6.

Conversely, Figure 3 displays the M2 macrophage graphics, using the same approach for M1 to select the cellular population. Individual events Figure 3A, the total cellular population Figure 3B, viable cells Figure 3C, and the macrophage population identified by the CD68 and F4/80 markers **(**Figure 3D) are shown; in this case, M2 macrophages were identified based on $CD206^{+}$ and MGL^{+} expression Figure 3E.

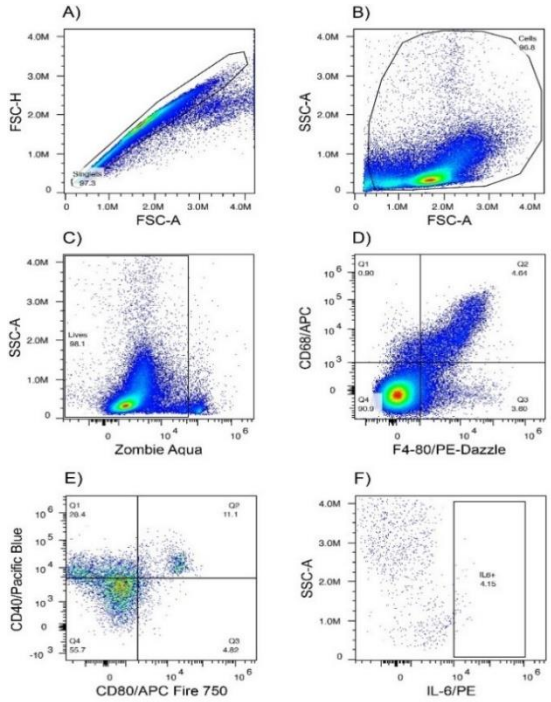

Figure 2. Flow cytometry strategy for identifying and characterizing M1 macrophages in the spleen from mice administered with liposomes bearing NPAs.

They also produce the anti-inflammatory cytokines TGF-β Figure 3F and IL-10 Figure 3G, as well as the enzyme Arginase 1 Figure 3H.

For M2 macrophages, a greater percentage of events were positive for macrophages (7.25%) compared to M1 macrophages. However, the percentage of M2 macrophages was lower at 7.03%, while M1 accounted for 11.1%. The expression of cytokines in M2 macrophages was as follows: TGF-β (0.92%), IL-10 (2.20%), and Arg-1 (3.67%).

As these results are part of ongoing research, it is necessary to observe macrophage polarization at different time points within this model and compare it to the control group (administered with TS). The current hypothesis suggests that the M1 phenotype may be more prevalent due to the inflammatory response induced by the model. The presence of both M1 and M2 phenotypes aligns with existing literature on polarization, which indicates that both phenotypes actively participate in the inflammatory process [11, 12]. However, as the model progresses, a shift in the balance of these phenotypes is anticipated. Comparisons with the control group remain essential to fully understand these dynamics.

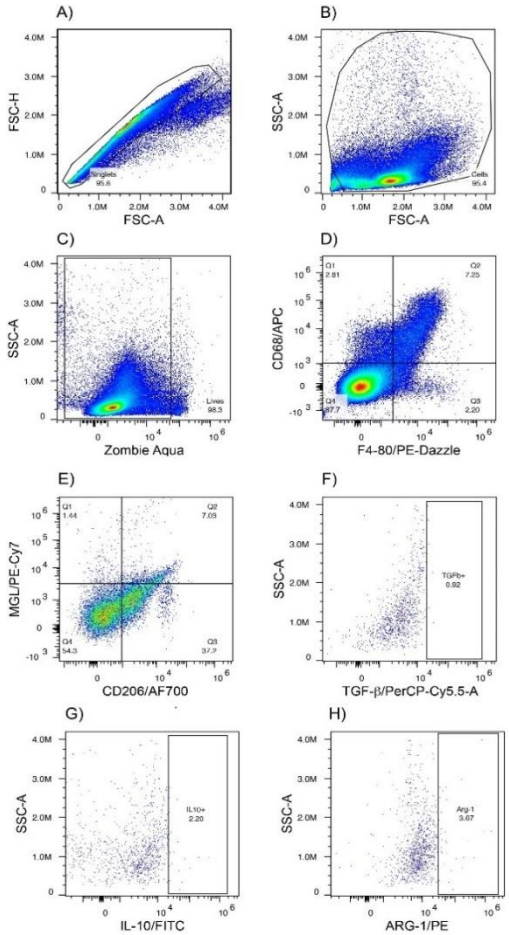

Figure 3. Flow cytometry strategy for identifying and characterizing M2 macrophages in the spleen from mice administered liposomes bearing NPAs.

3. CONCLUSIONS

Systemic lupus erythematosus (SLE) is a chronic autoimmune disease affecting diverse populations worldwide. Developing animal models is essential to better understand its pathogenic mechanisms. Macrophage polarization plays a key role within the complex interplay of cellular, genetic, and environmental factors contributing to lupus. In this study, the generation of NPAs was confirmed to be using chlorpromazine, with an optimal concentration determined to be 3 mM. This initial analysis provides a foundation for clarifying the landscape of macrophage polarization in this model.

Contrary to what might be assumed, both phenotypes coexist under normal conditions; however, the balance shifts toward M1 during inflammatory events, as represented by this model, although eventually, the M2 phenotype should become more prevalent. Furthermore, the presence of macrophages with a mixed phenotype expressing markers of both M1 and M2 has been documented. While a higher presence of M1 has been observed in lupus due to the chronic inflammation they generate, M2 macrophages have gained attention as a potential therapeutic target, as their induction with various molecules has been shown to improve symptoms and reduce inflammation in other animal models. Therefore, it is crucial to observe whether the balance of polarization is disrupted and, even more importantly, to understand the reasons behind this change.

Acknowledgements

The research and postgraduate section of the Instituto Politécnico Nacional (IPN) and the Consejo Nacional de Humanidades, Ciencia y Tecnología (CONAHCYT) are acknowledged for funding this research project

Conflicts of Interest

The authors declare no conflicts of interest related to this study.

REFERENCES

[1] Chen Y, et al. Prednisone combined with Dihydroartemisinin attenuates systemic lupus erythematosus by regulating M1/M2 balance through the MAPK signaling pathway. Molecular Immunology. (2024). https://doi.org/10.1016/j.molimm.2024.04.011

[2] Luo M, Zhao F, Cheng H, Su M, Wang Y. Macrophage polarization: an important role in inflammatory diseases. Frontiers in Immunology. (2024). https://doi.org/10.3389/fimmu.2024.1352946

[3] Wang LX, Zhang SX, Wu HJ, Rong XL, Guo J. M2b macrophage polarization and its roles in diseases. Journal of Leukocyte Biology. (2018). https://doi.org/10.1002/jlb.3ru1018-378rr

[4] Játiva S, Torrico S, Calle P, Poch E, Muñoz A, García M, et al. The phagocytosis dysfunction in lupus nephritis is related to monocyte/macrophage CPT1a. Immunology Letters. (2024). https://doi.org/10.1016/j.imlet.2024.106841

[5] Ma C, Xia Y, Yang Q, Zhao Y. The contribution of macrophages to systemic lupus erythematosus. Clinical Immunology. (2019). https://doi.org/10.1016/j.clim.2019.06.009

[6] Baeza I, Leyva E, Campos B, Lara M, Ibáñez M, Farfán N, et al. Antibodies to non-bilayer phospholipid arrangements induce a murine autoimmune disease resembling human lupus. European Journal of Immunology. (2004). https://doi.org/10.1002/eji.200324177

[7] Wong-Baeza C, Hernández-Pando R, Reséndiz A, Tescucano A, Bustos I, Ibáñez M, et al. Molecular organization of the non-bilayer phospholipid arrangements that induce an autoimmune disease resembling human lupus in mice. Molecular Membrane Biology. (2012). https://doi.org/10.3109/09687688.2012.667577

[8] Reséndiz-Mora A, Wong-Baeza C, Nevárez-Lechuga I, Landa-Saldívar C,

Molina-Gómez E, Hernández-Pando R, et al. Interleukin 4 deficiency limits the development of a lupus-like disease in mice triggered by phospholipids in a non-bilayer arrangement. Scandinavian Journal of Immunology. (2020). https://doi.org/10.1111/sji.13002

[9] National Research Council. Guide for the Care and Use of Laboratory Animals; National Academies Press: Washington, WA, USA, 2011; Volume XXV, p. 220

[10] Reséndiz-Mora A, Tescucano A, Barrera-Aveleida G, Sotelo-Rodríguez A, Nevárez-Lechuga CI, Galarce-Sosa I, et al. Anti-Non-Bilayer Phospholipid Arrangement Antibodies Trigger an Autoimmune Disease Similar to Systemic Lupus Erythematosus in Mice. IntechOpen. (2022). https://doi.org/10.5772/intechopen.106373

[11] Yang S, Zhao M, Jia S. Macrophage: Key player in the pathogenesis of autoimmune diseases. Frontiers In Immunology. (2023). https://doi.org/10.3389/fimmu.2023.1080310

[12] Murray PJ. Macrophage polarization. Annual Review Of Physiology. (2016). https://doi.org/10.1146/annurev-physiol-022516-034339

59-II-PP COMPARISON OF THE CHANGE OF MICROBIOTA IN BILE FLUID IN PATIENTS WITH CHOLELITHIASIS AND CHOLANGITIS

M. A. Vazquez-Avila [1], M. Á. López-Luis [2], A. Méndez-Tenorio [2], A. Rojas-Bernabé [1], G. Ibáñez-Cervantes[1*]

[1]Instituto Politécnico Nacional, Escuela Superior de Medicina, Sección de Estudios de Posgrado e Investigación, Plan de San Luis y Díaz Mirón S/N, C.P. 11340, Ciudad de México, México.

[2]Instituto Politécnico Nacional, Escuela Nacional de Ciencias Biológicas, Laboratorio de Biotecnología y Bioinformática, Prolongación de Carpio y Plan de Ayala S/N, C.P. 11340, Ciudad de México, México.

*Correspondence: gabrielaibanezcervantes@gmail.com

Abstract: Cholelithiasis, gallstone formation, is a common disease of the biliary tract, influenced by genetic, dietary and metabolic factors. It can lead to serious complications such as cholangitis, a gallstone-associated infection of the bile ducts. Microbial dysbiosis, an imbalance of the biliary microbiota, is linked to the progression of liver diseases, such as cholangitis and gallbladder cancer. Recent research suggests that altering the biliary microbiome exacerbates inflammation and liver damage. This study explores the relationship between microbiota dysbiosis and the development of cholelithiasis and cholangitis, looking for therapeutic strategies.

Keywords: Cholangitis, cholelithiasis, microbiome, dysbiosis.

1. INTRODUCTION

Cholelithiasis, defined as the formation of gallstones in the gallbladder, is a multifactorial disease influenced by genetic, dietary and metabolic elements. It is one of the most common bile duct conditions, affecting 10% to 20% of the adult population and increasing prevalence at younger ages due to changes in diet and lifestyles [1]. Cholelithiasis is not only associated with gallstone formation but can also lead to serious complications such as cholangitis. Cholangitis is an inflammation and infection of the bile ducts that occurs when stones obstruct the flow of the bile, allowing bacteria to ascend from the gut to the biliary system [1]. This condition can be life-threatening and is characterized by fever, abdominal pain, and jaundice. Recent research has shown how alteration of the biliary microbiome may play a role in the pathogenesis of cholangitis, exacerbating the inflammatory response and complicating the clinical course of the disease [2]. Factors such as being overweight, a high-carbohydrate, low-fiber diet, and genetic predisposition have also been shown to contribute significantly to its development [3]. In addition, cholangitis, like cholelithiasis, has been linked to microbial dysbiosis, underscoring the importance of a balance in the microbiota to maintain bile duct health and prevent complications [4].

The biliary microbiome is an essential component of liver health, and its dysregulation is associated with multiple liver diseases. Dysbiosis of biliary microbiota has been linked to the progression of diseases such as cholangitis and gallbladder cancer. Recent research has revealed how specific bacteria, such as *Proteobacteria* and *Prevotella*, correlate with chronic inflammation and liver damage, contributing to the development of disorders such as primary sclerosing cholangitis and primary biliary cirrhosis [5]. Altered microbial composition can influence the host's immune

response and foster an inflammatory environment that exacerbates the progression of chronic liver diseases [6]. Metagenomic analysis of the biliary microbiota has been proposed as a promising tool to better understand the pathogenesis of these conditions and develop therapeutic strategies based on microbiome modulation [7]. These findings suggest that microbiota should be considered both as a diagnostic marker and as a potential treatment target in gallbladder-related liver diseases [5-7].

The aim of this study was to identify biliary microbiota dysbiosis in cholelithiasis and cholangitis. Through a detailed analysis of microbial composition in bile fluid biopsies.

1. MATERIALS AND METHODS

1.1 Sample collection

Samples from patients over 18 years of age were used, obtained from colonoscopy biopsy booth tests performed on patients treated at the Hospital Juárez de México for the detection of gallbladder cancer, cholelithiasis and cholangitis, ruling out those positive for cancer.

Approximately 25 mg of bile tissue from each patient was used to obtain metagenomic DNA. Metagenomic DNA was obtained using the DNeasy Blood & Tissue kit (QIAGEN, Venlo, Netherlands).

1.2 Microbiome metagenomic analysis

Amplification of the hypervariable regions V2, V3, V4, V6, V7, V8 and V9 of the 16S gene was performed using the Ion 16STM (Thermo Fisher Scientifi) metagenomics kit, following the manufacturer's protocol. The quantification of the libraries was carried out with the QubitTM equipment, using the dsDNA HS Assay High Sensitivity (Invitrogen) kit.

The sequencing of the libraries was carried out using the Ion ChefTM system (Cat. No. 4484177), with the Ion Torrent instrument and the automated Ion Torrent™ server station. To do this, the Chef Ion 510TM, Ion 520™ and Ion 530™ (Thermo Fisher Scientific) reagents were used. The configuration and control of the process were carried out through the Torrent Suite™ software for data acquisition and analysis. Once the sequencing was complete, the generated files were stored directly on the Ion Torrent™ server.

1.3 Sequence quality control

The sequencing files are in FASTQ format and contain nucleotide sequences. Prior to a detailed analysis, a quality check was performed to verify the reliability of the data. To do this, the FASTQC tool was used, which generates reports on the quality of the sequences, detecting problems such as low-quality bases, contaminants or adapters present.

1.4 Flow Data Processing

Raw Ion Torrent streams were analyzed with QIIME2 (version 2021.11) [8]. Quality filtering, chimera removal, and sequence clustering in ASV were carried out with the DADA2 algorithm [9].

1.5 Taxonomic composition

From the classification of ASVs, the relative abundance of microorganisms by patient and disease was calculated.

1.6 Diversity analysis

The alpha and beta diversity analyses were performed with the microbiome and filoseq libraries using Rstudio.

1.7 Ethical considerations

In accordance with the provisions of Article 17 of the General Health Law on research, this study is classified as low risk (CDHCU, 2014). The protocol was presented and approved by the hospital committees, with registration number: HJM 041/23-I.

2. RESULTS AND DISCUSSION

A total of 31 biliary biopsy specimens were obtained that met the inclusion criteria. In the analysis of the population studied, several relevant trends were observed in terms of

demographics and health factors that could be associated with cholelithiasis and cholangitis conditions.

Table 1. Demographic and health distribution of the patients in the study: percentages of gender and diagnosis.

Variables	Percentage
Female	55%
Male	45%
Cholelithiasis	39%
Cholangitis	61%
Female with Cholelithiasis	26%
Male with Cholelithiasis	13%
Female with Cholangitis	29%
Male with Cholangitis	32%

The distribution by sex revealed that 55% of the patients are women, while 45% are men (Table 1). This slight predominance in the female gender suggests that the pathologies studied may have a higher incidence in this group, or that women are more prone to various factors in relation to biliary problems. It was identified that 61% of the patients had cholangitis, while the remaining 39% were diagnosed with cholelithiasis. 64% of the patients were overweight and an additional 16% were classified as obese. The high proportion of overweight and obesity in this population is significant, as these conditions are recognized as risk factors for the development of biliary diseases, including cholelithiasis.

In relation to the identification of the microbial genera identified in the microbiota of the patients studied, they showed the presence of bacteria considered pathogenic such as Pseudomonas (Table 2). Other studies have identified different phylum such as *Actinobacteria, Bacteroidetes, Firmicutes, Proteobacteria and Verrucomicrobia* [10-11].

Table 2. The most relevant bacterial genera in patients with cholelithiasis and cholangitis.

Bacterial genera
Streptococcus
Pseudomonas
Fusobacterium
Bacteroides
Atopobium
Staphylococcus
Enterococcus
Anaerococcus
Veillonella
Morganella

In relation to biliary microbial dysbiosis, the results obtained in this study, in patients with cholelithiasis and cholangitis, a significant diversity in bacterial composition was identified. In particular, the genera *Streptococcus* and *Pseudomonas* predominate notably in this group. In addition to these predominant genera, others such as *Fusobacterium* and *Atopobium were identified*.

In the study conducted by Dan et al. [11], it is suggested that the presence of bacteria commonly found in the gastrointestinal tract in the biliary microbiota may be due to the fact that intestinal bacteria can migrate retrograde into the bile space. Based on this hypothesis, our results support that bile bacteria originate in a retrograde infection of intestinal bacteria. With respect to the presence of the genus *Streptococci,* it is closely associated with inflammatory processes, which can affect both the integrity of the biliary mucosa and the metabolic function of the host. On the other hand, *Pseudomonas* has shown a link with the modulation of the immune response, suggesting its possible role in protecting against bacterial infections and stabilizing the microbial environment in the gallbladder (Table 2).

According to Ozdirik et al. [12], patients with cholangitis have decreased bacterial diversity and overrepresentation in the genera *Enterococcus, Fusobacterium* and *Lactobacillus*.

The abundance of *Enterococcus* present in samples from patients with cholangitis is associated with an increase in proinflammatory bile acid [1]. The biliary microbiome presents an increase in *Enterococcus spp*. causing damage to the

epithelial barrier and reaffirming mucosal inflammation [13].

Various bile-related disorders, such as cholelithiasis, have been shown to have a significant impact on the composition of the microbiota of the biliary tract and gallbladder. In particular, Petrov et al. [14], have shown that the presence of gallstones is associated with notable changes in the abundance of certain bacterial families in the bile of affected patients. An increase in the concentrations of bacteria belonging to the families *Bacteroidaceae*, *Prevotellaceae*, *Porphyromonadaceae* and *Veillonellaceae have been observed*. These changes in the microbiota could have relevant implications for the pathophysiology of cholelithiasis and other biliary disorders.

The present study has several limitations that should be considered when interpreting the results. First, the sample size may have been insufficient to capture all the variability of the microbiota in the different groups. A larger sample size could have allowed for more robust analysis and better generalizability of the findings to the general population.

Despite these limitations, the study's findings offer several directions for future research. An important area of exploration is the effect of dietary interventions on the microbiota in patients of different weight categories. Longitudinal studies examining how specific dietary changes influence microbial composition and metabolic health could provide valuable insights.

3. CONCLUSIONS

This study shows that biliary disorders such as cholelithiasis and cholangitis are associated with changes in the biliary microbiota. In particular, patients with cholangitis have a higher abundance of potentially pathogenic bacteria. These results suggest that the alteration of microbiota could influence the progression of these diseases, which opens up new therapeutic possibilities.

On the other hand, progress in the typing of microbiota in specific pathologies is crucial to better understand its role in the development and progression of various diseases. Detailed characterization of microbial profiles could identify key biomarkers for early diagnosis, personalized treatment, and disease prevention, contributing significantly to improving public health and designing more effective intervention strategies.

Acknowledgements

I want to express my sincere gratitude to the Juárez Hospital of Mexico for its invaluable support during the development of this research. I thank my internal directors, who provided their guidance and expertise, as well as the Higher School of Biological Sciences and the Higher School of Medicine of the National Polytechnic Institute (IPN) for providing a nurturing academic environment.

Conflicts of interest

The authors declare that they have no conflict of interest.

REFERENCES

[1] Zhang K, Wang Y, Cui X, et al. Characteristics of metabolite changes in disease evolution in cholecystolithiasis. *Dig Dis Sci*. 2023; https://doi.org/10.1007/s10620-023-08134-6

[2] Haritonova L, Kucherya TV. The role of the gut microbiota in the genesis of gallstone formation in childhood. *Exp Clin Gastroenterol*. 2024; https://doi.org/10.31146/1682-8658-ecg-221-1-53-61

[3] Chen H. Analysis of the effect of laparoscopic versus open cholecystectomy in patients with cholelithiasis and the effect on CRP and IL-1β levels. *J Clin Nurs Res*. 2024; https://doi.org/10.26689/jcnr.v8i7.7868

[4] Xu Z, Wang J, Feng Y, et al. Evaluation of the influence of air pollution on

cholelithiasis formation and blood lipid levels: a Mendelian randomization study of two samples. *Prepress*. 2024; https://doi.org/10.21203/rs.3.rs-4811191/v1

[5] Xie M, Zhang XL, Wu Y, et al. Alterations of the biliary and intestinal microbiota in relation to gallstone formation. *J Clin Trans. Res*. 2024; https://doi.org/10.36922/jctr.23.00118

[6] Shukla R, Tsuchiya Y, Behari A, et al. Metagenomic analysis of biliary microbial flora in patients with gallbladder cancer or chronic gallstone-associated cholecystitis. *Cancer Research*. 2024; https://doi.org/10.1080/07357907.2024.2361305

[7] Komorniak N, Pawlus J, Gaweł K, et al. Cholelithiasis, gut microbiota and bile acids after bariatric surgery: can cholelithiasis be prevented by modulating the microbiota? *Nutrients*. 2024; https://doi.org/10.3390/nu16152551

[8] Bolyen E, Rideout JR, Dillon MR, Bokulich NA, Abnet CC, Al-Ghalith GA, et al. Reproducible, interactive, scalable, and extensible microbiome data science using QIIME 2. Nat Biotechnol. August 2019; 37(8):852-7. Available in: https://doi.org/10.1038/s41587-019-0209-9

[9] Callahan BJ, McMurdie PJ, Rosen MJ, Han AW, Johnson AJ, Holmes SP. ADA2: Inference of high-resolution samples from Illumina amplicon data. Métodos Nat. July 2016; 13(7):581-3. Available in: https://doi.org/10.1038/nmeth.3846

[10] Dan WY, Yang YS, Peng LH, Sun G, Wang ZK. Gastrointestinal microbiome and cholelithiasis: Current status and perspectives. World J Gastroenterol. 2023 Mar 14; 29(10):1589-1601. https://doi.org/10.3748/wjg.v29.i10.1589 PMID: 36970590; PMCID: PMC10037248.

[11] Li ZJ, Gou HZ, Zhang YL, Song XJ, Zhang L. Role of intestinal flora in primary sclerosing cholangitis and its potential therapeutic value. World J Gastroenterol. 2022 Nov 28; 28(44):6213-6229. https://doi.org/10.3748/wjg.v28.i44.6213 PMID: 36504550; PMCID: PMC9730442.

[12] Özdirik B, Müller T, Wree A, Tacke F, Sigal M. The Role of Microbiota in Primary Sclerosing Cholangitis and Related Biliary Malignancies. Int J Mol Sci. 2021 Jun 28; 22(13):6975. https://doi.org/10.3390/ijms22136975 PMID: 34203536; PMCID: PMC8268159.

[13] Quast C, Pruesse E, Yilmaz P, Gerken J, Schweer T, Yarza P, et al. The SILVA ribosomal RNA gene database project: Improving data processing and web-based tools. Nucleic Acids Res. 2012; 41 Available in: https://doi.org/10.1093/nar/gks1219

[14] Petrov VA, Fernández-Peralbo MA, Derks R, Knyazeva EM, Merzlikin NV, Sazonov AE, Mayboroda OA, Saltykova IV. Biliary Microbiota and Bile Acid Composition in Cholelithiasis. Biomed Res Int. 2020 Jul 1;2020:1242364. https://doi.org/10.1155/2020/1242364 PMID: 32714973; PMCID: PMC7352139.

84-II-PP VALIDATION OF THE TWO BEST SURROGATE INSULIN RESISTANCE AND OBESITY MARKERS TO IDENTIFY METABOLIC SYNDROME IN MEXICAN ADULTS

A. Flores-Miranda[1], I. F. Contreras-Hernández[2], L. R. García-Cortes[3], R. Romero-Nava[4], M. E. Ocharan-Hernández[4], D.-L. Cruz Vargas[1,4]*

[1]Hospital Juárez de México, División de Investigación, Av Instituto Politécnico Nacional 5160, C.P. 07760, Ciudad de México, México.
[2]Instituto Mexicano del Seguro Social, Unidad de Medicina Familiar 75, Delegación 15 Oriente, Estado de México 57500, México.
[3]Instituto Mexicano del Seguro Social, Jefatura de Servicios de Prestaciones Médicas, Órgano de Operación Administrativa Desconcentrada Regional Oriente Estado de México, 54060, México.
[4]Instituto Politécnico Nacional, Escuela Superior de Medicina, Sección de Estudios de Posgrado e Investigación, Laboratorio de Modelación Bioestadística para la Salud, Plan de San Luis y Díaz Mirón S/N, C.P. 11340, Ciudad de México, México.

*Correspondence: leoncruz82@yahoo.com.mx

Abstract: Metabolic syndrome is a cluster of chronic metabolic diseases closely related to diabetes and cardiovascular diseases. This study aims to validate the two best surrogate markers of MetS in Mexican adults MetS in Mexican adults: the triglyceride-glucose index (TyG) and the lipid accumulation product (LAP). Based on the Adult Treatment Panel III (ATP III) MetS criteria, a total of 4,137 Mexican data from ENSANUT 2021-2022 were analyzed.

Accuracy measures (sensitivity and specificity) were calculated, and their confidence intervals were determined. The Youden Index (YI) was calculated by summing sensitivity and specificity, then subtracting 1, to identify the best biomarker between TyG and LAP. LAP was found to be the most effective biomarker for women aged 20 to 39, while the triglyceride-glucose index (TyG) was the best in the group of women aged 40 to 59 and those aged 60 and above.

In men, LAP was the best biomarker for the 20 to 39 age group and those aged 60 and older, while TyG and LAP were similar for men aged 40 to 59. The most effective biomarker for diagnosing MetS in Mexican adults varies by sex and age group, but LAP appears to be a more reliable biomarker than TyG, particularly in younger populations and in men of all ages. Both LAP and TyG are accessible and useful at the primary care level.

Keywords: hypertension, hyperglycemia, obesity, dyslipidemia, insulin resistance**.**

1. INTRODUCTION

The constellation of metabolic diseases such as diabetes, obesity, hypertension, and dyslipidemia forms the term metabolic syndrome (MetS). Metabolic Syndrome (MetS) is a term that includes risk factors that contribute to the progression of cardiovascular diseases and type 2 diabetes [1]. According to the harmonized definition, the prevalence of MetS among Mexican adults was recorded at 40.2% in 2006, 57.3% in 2012, 59.99% in 2016, and 56.31% in 2018 [2]. This reflects an approximate percentage change of 40.04% from 2006 to 2018, indicating a significant increase over time that poses a pressing public health concern nationally.

Given this context, it is essential to identify MetS at the primary care level, where screening for glucose, triglyceride and total cholesterol levels is recommended for

individuals over 20 years old. A study in Mexico comparing traditional and novel surrogate markers for identifying MetS found that the two most effective markers in the adult Mexican population are the triglyceride-glucose index (TyG) and the lipid accumulation product (LAP) [3].

However, it is important to validate the cut-off values for TyG and LAP obtained in [3] using an independent sample and to assess the diagnostic performance of these indices. This study aims to validate TyG and LAP as tools for identifying Metabolic Syndrome in Mexican adults.

The TyG and LAP indices utilize glucose (Glu), triglycerides (Tri), and waist circumference (WC) in a quantitative manner, making them practical tools for primary care settings.

2. MATERIALS AND METHODS

a. Study selection

We extracted the data from the national health survey (ENSANUT CONTINUA 2021 and 2022), which is a transversal, probabilistic, grouped sampling, and stepped wedged designed survey that offers a view of the health in Mexico.

A thorough explanation of the survey methodology and sampling techniques has already been published [4,5].

The collected variables included height (m), weight (kg), sex, waist circumference (cm), fasting serum glucose (Glu), serum triglycerides (mg/dL), total serum cholesterol (mg/dL), HDL-C (mg/dL), and medication treatment for elevated triglyceride levels, high cholesterol levels, elevated blood pressure, and diabetes mellitus.

The inclusion criteria were Mexican females and males adults, stratified by sex and group of age (20 a 39, 40 a 59 and 60 or more).

In contrast, exclusion criteria were data with triglycerides levels over than 1200 mg/dL and/or less than 70 mg/dL, while the incomplete or absent information were filtered.

2.2 Definition of Metabolic Syndrome

This project relied on the definition of MetS established by the ATP III criteria, which identifies MetS as being present when three or more of the following parameters are met in a single patient: WC≥ 102 cm (men) or ≥88 cm (women); Glu ≥ 110 mg/dL or being on treatment of elevated glucose; Tri ≥ 150 mg/dL, being by elevated triglyceride treatment; blood pressure ≥ 130/85 mmHg, being on treatment for hypertension; high-density lipoprotein cholesterol < 40 mg/dL (men) and <50 mg/dL (women) been on treatment for low HDL cholesterol.

2.3 Surrogate markers

TyG and LAP formulas [6,7]:

$$\mathbf{LAP_{Women}} = (\mathbf{WC} - \mathbf{58}) \times \mathbf{Tri}, \quad \text{Eq. (1)}$$
$$\mathbf{LAP_{Men}} = (\mathbf{WC} - \mathbf{65}) \times \mathbf{Tri},$$

WC is measured in centimeters, and triglycerides are measured in mmol/L.

$$\mathbf{TyG} = \frac{1}{2}\mathbf{In}\,(\mathbf{Tri} \times \mathbf{Glu}), \quad \text{Eq. (2)}$$

Both glucose and triglycerides are measured in mg/dL.

2.4. Validation

For validation, we will use the cutoff points for TyG and LAP obtained from by Contreras-Hernández et. al [3], categorized by sex and age, as follows (Table 1):

Table 1. Cut off points from LAP and TyG.

Group age	Surrogate Marker	Women	Men
20-39 years	TyG	≥4.73	≥4.87
	LAP	≥56.01	≥65.22
40-59 years	TyG	≥4.77	≥4.90
	LAP	≥60.23	≥70.75
Over 60 years	TyG	≥4.75	≥4.80
	LAP	≥ 51.79	≥55.83

2.5 Data Analysis

The following measures of accuracy, along with their 95% confidence intervals, were provided: sensitivity and specificity. Confidence intervals for sensitivity, and specificity were computed with the "exact" Clopper–Pearson confidence intervals. The Youden Index (YI) was calculated by summing sensitivity and specificity, then subtracting 1, to identify the best biomarker between TyG and LAP.

Sensitivity and specificity were calculated using the Diagnostic Test Evaluation Calculator in MedCalc Software.

2.6 Ethical Considerations

The present study is aligned with the principles of the Declaration of Helsinki and the General Health Law. Also, has the approbation of the institutional Committee of Research, Ethics, and Biosafety of Hospital Juárez de México, registered under the number HJM 013/22-1.

3. RESULTS AND DISCUSSION

The (Table 2) provides a comprehensive overview of the study population's characteristics, differentiated by sex. In terms of BMI, the third quartile for women (33.1) exceeds the cutoff value of 30, indicating obesity. The WC in the third quartile is above the ATP III cutoff values for both women (104 cm) and men (106 cm), indicating an elevated risk in both groups. Regarding blood pressure, the third quartile for women (129 mmHg) approaches the cutoff for systolic pressure, while the third quartile for men (136 mmHg) surpasses it, indicating hypertension. The HDL cholesterol levels for men in the third quartile (47 mg/dL) are close to the risk threshold, while women are also at the lower limit. For triglycerides, the third quartile for men (231 mg/dL) exceeds the cutoff of 150 mg/dL, suggesting an elevated risk.

Table 2. Biochemical and anthropometric characteristics of 4137 Mexican adults in the ENSANUT 2021-2022.

Variables	Women n=2523 median (Q1, Q3)	Men n=1614 median (Q1, Q3)
Age (years)	34 (46,58)	32 (46,60)
Body Mass Index (kg/m2)	25.9 (29.4, 33.1)	24.8 (27.9,31.3)
WC (cm)	88 (96,104)	90 (98,106)
Systolic pressure (mmHg)	105 (115,129)	115 (124,136)
Diastolic pressure (mmHg)	65 (72,80)	68 (76,83)
Cholesterol (mg/dL)	137 (166,193)	141 (169,19)
HDL-cholesterol (mg/dL)	37 (43.6,50.5)	34.3 (40,47)
Triglycerides (mg/dL)	98 (137.5,195.0)	106 (153, 231)
Glucose (mg/dL)	84 (92, 104)	84 (92,102)

Q1: Quartile 1; Q3: Quartile 3

(Table 3) summarizes the sensitivity and specificity for two surrogate markers, TyG and LAP, in women across three age groups: 20-39 years, 40-59 years, and over 60 years. In the 20-39 age group, LAP achieved a higher YI of 70.8% compared to TyG's 67.4%, indicating that LAP may be a more effective biomarker in this age group. In the 40-59 age group, TyG demonstrated a slightly better YI of 63.6% versus LAP's 56.7%, suggesting that TyG is relatively more reliable in this category. In the over 60 age group, TyG again outperformed LAP, with a YI of 54.5% compared to LAP's 45.2%.

Table 3. Sensitivity and specificity of TyG and LAP to identify metabolic syndrome in Mexican adult women.

Group age	Surrogate Marker	Se 95% CI	Sp 95% CI
20-39 years (n=887)	TyG	83.0 (78.0, 87.3)	84.4 (81.3, 87.2)
	LAP	88.2 (83.7, 91.8)	82.6 (79.4, 85.5)
40-59 years (n=1062)	TyG	81.6 (78.2, 84.7)	82.0 (78.3, 85.3)

	LAP	83.4 (80.1, 86.3)	73.3 (69.1, 77.1)
Over 60 years (n=574)	TyG	77.0 (72.2, 81.2)	77.5 (71.4, 82.8)
	LAP	84.4 (80.1, 88.0)	60.8 (54.0, 67.3)

The (Table 4) presents the sensitivity and specificity for two surrogate markers, TyG and LAP, in men across three age groups: 20-39 years, 40-59 years, and over 60 years. In the 20-39 age group, LAP showed the highest YI at 63.3%, indicating it may be a more effective biomarker for this age group compared to TyG, which had a YI of 49.0%. In the 40-59 age group, the indices were closer, with LAP at 49.8% and TyG at 47.5%, suggesting that both markers have similar effectiveness in this age group. In the over 60 age group, LAP again outperformed TyG, with a YI of 52.4% compared to 42.7% for TyG.

Table 4. Sensitivity and specificity of TyG and LAP to identify metabolic syndrome in Mexican adult men.

Age Group	Surrogate Marker	Se 95% CI	Sp 95% CI
20-39 years (n=600)	TyG	71.3 (63.4, 78.4)	77.7 (73.6, 81.5)
	LAP	86.0 (79.4, 91.1)	77.3 (73.18,81.1)
40-59 years (n=607)	TyG	67.5 (61.5, 73.2)	80.0 (65.9, 75.7)
	LAP	79.1 (73.7, 83.9)	70.7 (65.6,75.4)
Over 60 years (n=407)	TyG	76.8 (70.0,82.7)	65.9 (59.4,72.1)
	LAP	81.2 (74.7,86.6)	71.2 (64.8,77.1)

The results regarding the YI of LAP indicate that this biomarker is particularly effective in young women (20-39 years), where our result (YI = 70.8) slightly surpasses that of (YI = 70.5) [3]. However, in women aged 40-59, the performance of LAP decreases slightly in our sample (YI = 56.7) compared to that of (YI = 58.0) [3]. In the group over 60 years, we observe a more significant decrease in the effectiveness of LAP, with a YI of 45.2 compared to 53.1 from the study by [3]. In men, LAP also shows superior performance in the 20-39 age group (YI = 63.3 compared to 54.6 from [3]), but its effectiveness diminishes in the other age groups, especially in those over 60 years (YI = 52.4 compared to 60.8 from Contreras-Hernández et al.). The results of YI for TyG reveal that in young women (20-39 years), our result (YI = 67.4) surpasses that of the study by Contreras-Hernández et al. [3]. (YI = 65.5). However, in women aged 40-59, the performance of TyG is significantly better in our sample (YI = 63.6) compared to [3]. (YI = 58.3). In the group over 60 years, we observe a decrease in its effectiveness, with a YI of 54.5 compared to 60.0 from the study by [3]. In men, the performance of TyG is also superior in the 20-39 age group (YI = 49.0 compared to 43.9), but its effectiveness declines in the 40-59 age groups (YI = 47.5 compared to 43.7 from [3]) and over 60 years (YI = 42.7 compared to 57.8 from [3]).

Despite these numerical differences in the YI between our validation study and the study where the cutoff values were obtained [3], the superiority of the YI between TyG and LAP across age groups and sex remains similar in both studies. This suggests that, although the exact performance metrics may vary, the relative effectiveness of these biomarkers in identifying conditions holds, indicating a robust pattern that can be reliably observed in the Mexican population.

The limitations of the study include its cross-sectional design, which prevents establishing causal relationships between the biomarkers and metabolic syndrome. The reliance on self-reported data for certain variables and the lack of longitudinal follow-up also represent limitations. Lastly, factors such as diet, physical activity, and other social determinants of

health were not considered. These limitations highlight the need for longitudinal studies to confirm the findings in the Mexican population.

4. CONCLUSIONS

The effectiveness of the markers varies by sex and age group. In women under 40 years old, LAP is superior; in women aged 40-59 and over 60, TyG is better. In men, LAP is superior in the 20-39 and over 60 age groups, while both are similar in the 40-59 age group. Therefore, LAP suggests that it may be a more reliable biomarker than TyG, especially in younger populations and in men regardless of age.

Our validation demonstrates that both LAP and TyG are reliable indicators for the diagnosis of metabolic syndrome (MetS) in adults. Moreover, since only serum triglyceride and glucose levels are needed to calculate TyG, or WC and serum triglycerides to establish LAP, their calculation is straightforward, accessible for healthcare professionals to request in patient laboratories, and cost-effective for primary care.

All these findings provide doctors with a valuable tool for the diagnosis of MetS, thereby facilitating early diagnosis and treatment of the condition. It is essential to incorporate TyG and LAP into our lipid profile reports.

Acknowledgements

Flores-Miranda acknowledges for the support received through the BEIFI scholarship (Beca de Estímulo Institucional de Formación de Investigadores by its Spanish acronym).

Conflicts of Interest

The authors of the study declares no conflict of interest.

REFERENCES

[1] Expert Panel on Detection, Evaluation, and Treatment of High Blood Cholesterol in Adults. Executive Summary of the Third Report of the National Cholesterol Education Program (NCEP) Adult Treatment Panel III. *JAMA*. 2001;285(19):2486–2497. https://doi.org/10.1001/jama.285.19.2486

[2] Rojas-Martínez R, Aguilar-Salinas CA, Romero-Martínez M, Castro-Porras L, Gómez-Velasco D, Mehta R. Trends in the prevalence of metabolic syndrome and its components in Mexican adults, 2006–2018. *Salud Publica Mex*. 2021;63(6):713–724. https://doi.org/10.21149/12835

[3] Contreras-Hernández IF, Vargas-De-León C, García-Cortes LR, Flores-Miranda A, Romero-Nava R, Ocharán-Hernández ME. Comparison of ten surrogate insulin resistance and obesity markers to identify metabolic syndrome in Mexican adults. *Metabolites*. 2024;14(7):358. https://doi.org/10.3390/metabo14070358

[4] Romero-Martínez M, Barrientos-Gutiérrez T, Cuevas-Nasu L, Bautista-Arredondo S, Colchero MA, Gaona-Pineda EB, et al. Metodología de la Encuesta Nacional de Salud y Nutrición 2021. *Salud Publica Mex*. 2021;63(6):813–818. https://doi.org/10.21149/13348

[5] Romero-Martínez M, Barrientos-Gutiérrez T, Cuevas-Nasu L, Bautista-Arredondo S, Colchero MA, Gaona-Pineda EB, et al. Metodología de la Encuesta Nacional de Salud y Nutrición 2022 y planeación y diseño de la Ensanut Continua 2020–2024. *Salud Publica Mex*. 2022;64(5):522–529. https://doi.org/10.21149/14186

[6] Guerrero-Romero F, Villalobos-Molina R, Jiménez-Flores JR, Simental-Mendia LE, Méndez-Cruz R, Murguía-Romero M, et al. Fasting triglycerides and glucose index as a diagnostic test for insulin resistance in young adults. *Arch Med Res*. 2016;47(5):382–387. https://doi.org/10.1016/j.arcmed.2016.08.012

[7] Kahn HS. The lipid accumulation product performs better than the body mass index for recognizing cardiovascular risk: a population-based comparison. *BMC Cardiovasc Disord*. 2005;5(1):26. https://doi.org/10.1186/1471-2261-5-26

115-II-PP EVALUATION OF 2-AMINOBENZOTHIAZOLE DERIVATIVES AS ALDOSE REDUCTASE INHIBITORS IN DIABETES TREATMENT AND THEIR MICRO- AND MACROVASCULAR COMPLICATIONS

N. Reyes-Vallejo[1], M. Valdes-Guevara[1], A. Reyes-Ramírez[2], A. Cruz[3], J. Mendieta-Wejebe[1*]

[1]Instituto Politécnico Nacional, Escuela Superior de Medicina, Sección de Estudios de Posgrado e Investigación, Laboratorio de Biofísica y Biocatálisis, Plan de San Luis y Salvador Díaz Mirón S/N C.P. 11340, Ciudad de México, México.
[2]Universidad Nacional Autónoma de México, Facultad de Estudios Superiores Zaragoza Campus II, Unidad Multidisciplinaria de Investigación Experimental Zaragoza, Laboratorio de Síntesis Farmacéutica, Batalla 5 de Mayo S/N, C.P. 09230, Ciudad de México, México.
[3]Instituto Politécnico Nacional, Unidad Profesional Interdisciplinaria de Biotecnología, Laboratorio de Química Supramolecular y Nanociencias, Av. Acueducto S/N, C.P. 07340, Ciudad de México, México.

*Correspondence: jemw2009@gmail.com

Abstract: Diabetes has become the epidemic of the 21st century due to its increasing prevalence and serious health consequences, which is why searching for new therapeutic options that control blood glucose levels and prevent future complications is a priority. In this context, aldose reductase (ALR2) has gained significant relevance, as it is strongly associated with developing of microvascular diabetic complications as retinopathy, nephropathy, and neuropathy.

Previous research has utilized benzothiazoles within the structure of ALR2 inhibitors, such as zopolrestat, and has explored this structure as a pharmacophore for various conditions, including diabetes. Our research group recently demonstrated that 2-aminobenzothiazole-derived compounds could reduce blood glucose, glycated hemoglobin (HbA1c), and triglycerides without causing liver damage or increasing polyphagia. Based on this evidence, this project aims to evaluate the ALR2 inhibitory capacity of 2-aminobenzothiazole derivatives linked to guanidines, ureas, and isothioureas with possible antihyperglycemic activity. This will begin with *in silico* screening, followed by synthesis, characterization, and *in vitro* evaluation of the most promising molecules.

The process has shown promise, as the analyzed structures possess physicochemical and pharmacological properties suitable for oral administration and affinity for the amino acid residues of the ALR2 active site. The synthesis and purification conditions have also been optimized to facilitate production in sufficient quantities for further evaluation. At *in vitro* tests, these compounds have demonstrated significant inhibition at a concentration of 1 µM, without intervening in the oxidation of the NADPH cofactor, and finally, we confirmed that its LD_{50} values exceed 1750 mg/kg.

Keywords: Benzothiazole, Aldose reductase, Diabetes, Diabetic complications, polyol pathway

1. INTRODUCTION

Diabetes is a chronic and complex disease due to its different implications in metabolic processes and its serious repercussions on health that generate disability and early death, so the apparent glycemic control resulting from current commercial treatments may not

be enough, as this does not imply that peripheral organs are not being affected by the activation of metabolic pathways such as polyols [1]. This pathway, and more specifically the ALR2 enzyme, is the main theory of the appearance of complications such as retinopathy, nephropathy, and diabetic neuropathy, since when metabolizing glucose, it triggers a state of oxidative stress due to the depletion of NADPH and NAD+, a state of osmotic stress due to the accumulation of sorbitol and an increase in the generation of advanced glycation products. In addition to this damage, there is the activation of the NF-kB and AP-1 pathway when the enzyme contributes to the metabolism of lipid peroxidation products [2]. Because of all these repercussions, the ALR2 enzyme has become an important target in the development of new drugs for the treatment of diabetes and the prevention of its micro- and macrovascular complications.

The research carried out so far agrees that hydantoins and carboxylic acids are the pharmacophores to which the inhibition of this pathway is attributed, however, both structures represent toxicological and pharmacokinetic disadvantages, therefore, the proposal is to take as a structural basis another structure that is repeated within the molecules that have already been described in the literature with this activity, benzothiazole, since it has been studied as pharmacophores in a wide range of conditions, among which diabetes stands out, and, by merging this structure with other functional groups, more specific biological activities can be obtained.

In previous work, the use of guanidines has allowed obtaining antihyperglycemic properties related to the agonism of the peroxisome proliferator-activated receptor gamma (PPAR-gamma) and it is expected that on this occasion by fusing 2-aminobenzothiazole with different amino acids forming ureas and isothioureas, a dual activity will be obtained, antihyperglycemic and ALR2 inhibitory [3]. Well, products have already been reported that have amino acid fragments and that act on important targets in the treatment of diabetes such as α-glucosidase, PTP 1B, and DPP IV [4].

2. MATERIALS AND METHODS

This project is a preclinic, prospective, comparative, and longitudinal study consisting of *in silico*, *in vitro*, and *in vivo* evaluations.

An in silico screening of a series of 2-aminobenzothiazole derivatives bound to guanidines or amino acids was carried out by analyzing their physicochemical, pharmacokinetic, and toxicological properties on online platforms such as Molinspiration, SwisADME, preADMET, and Protox, in addition, a directed and blinded molecular coupling study was carried out on the ALR2 enzyme with its cofactor NADPH (PDB ID: 4JIR); optimizing the molecules in Avogadro by MMFF94 force field, running the calculation in Autodock4 and choosing the cluster with the highest number of conformations. The interactions analysis was completed in Discovery studio obtaining values of binding energy (ΔG), inhibition constant, type, the distance of the interactions, and amino acid residues involved.

With these results, a score was assigned to each molecule, and the best ones were chosen to be synthesized based on the methodology previously reported [5]. Modifications were made to the reaction and purification conditions to decrease reaction times and obtain purer products.

The resulting products were characterized by physical and spectroscopic techniques and were subsequently evaluated as inhibitors of the ALR2 enzyme using a Colorimetric kit ab283360 at six different concentrations (1 nM, 10 nM, 100 nM, 1 µM, 10 µM and 100 µM), using Epalrestat as a reference (the only ALR2 inhibitor marketed for the treatment of diabetic neuropathy). In this experiment, the oxidation of the cofactor was observed as a function of time by measuring the absorbance at 340 nm in kinetic mode for 60-90 minutes at 37°C.

Acute oral toxicity was probed in female Wistar rats by "up and down" procedure in accordance with OECD protocol 425 [6]. The organs were analyzed macroscopically to observe changes in color or structure, and data were statistically analyzed using the program GraphPad Prim with the one-way ANOVA analysis method and the results were expressed as the mean ± standard error of the mean.

3. RESULTS AND DISCUSSION

Based on previous results, we consider guanidine-benzothiazoles **4x** and **4y** due to their potential affinity with ALR2, but, as its molecules lack a recognized pharmacophore, we had to compare them with other kinds of compounds.

As was mentioned, carboxylic acid is one of the pharmacophores that allow the inhibition of ALR, however, this functional group is protonated at physiological pH, so for the present work the evaluation of acid derivatives, such as esters and amides, from amino acids treated under conventional reaction conditions was proposed.

The results of the *in silico* evaluation were favorable because all the compounds comply with the Lipinski rules and the other filters of medicinal chemistry, which indicates that they are good.

Candidates to be administered orally. Most of them have ideal logP and TPSA values that suggest that they will be able to cross the gastrointestinal barrier without reaching the blood-brain barrier. On the other hand, it is predicted that they will not be P-glycoprotein substrates or inhibitors of the main CYP450 isoforms that metabolize xenobiotics, indicating that their pharmacokinetics will not be affected. In addition, they did not present structural characteristics that conferred serious toxicity as hepatotoxicity, tumorigenicity, irritation or reproductive effects. Some of these data are presented below in (Figure 1).

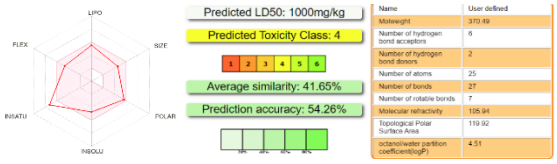

Figure 1. Description *In silico* analysis results using online platforms (SwisADME and ProTox).

The results of the docking, shown in (Table 1), were encouraging because the ΔG values are like those found for the reference drugs and endogenous ligands.

Table 1. Some of the results of molecular docking. Data of **4y** (guanidine), **5d** (isothioureas with carboxylic acid), **12d** (isothioureas with amide); Epalrestat (reference drug), and an endogenous ligand.

	4y	**5d**	**12d**	**Epa**	**Endog**
ΔG	-8.28	-7.97	-8.40	-8.54	-7.42
Ki (μM)	0.792	0.589	0.166	0.328	0.383

It also showed that the molecules are related to the active site of the enzyme since both in blind and targeted docking, the ligands remain in the pockets of the active site. Specifically, benzothiazole is the one that interacts with catalytic amino acid residues and the cofactor through hydrophobic interactions of the π-π, π-alkyl or π-sulfur type at 3.5 – 5 Å. Nonetheless, a notable preference for the selectivity pocket is observed, as shown in (Figure 2).

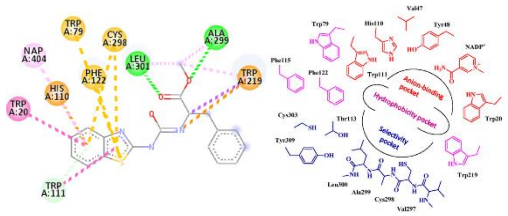

Figure 2. Results of molecular docking. Interactions and position of amino acid residues from the active site of ALR2.

However, we observed a different behavior than expected, because zopolrestat shows interaction with the selective pocket in the benzothiazole region and interaction with the anion-binding pocket of its carboxylic acid [2].

It should be noted that this process was validated from a re-docking with the co-crystallized ligand obtaining RMSD of 1.4754 and 0.9948 Å, respectively.

Among the ligands evaluated, guanidinbenzothiazoles (**4x** and **4y**) and benzothiazoles bound to phenylglycine and phenylalanine stand out, with some modifications in the carbonyl group (**8c**, **8d**, **11c**, **11d** and **12d**) since it is observed that the presence of aromatic rings implies a greater number of hydrophobic interactions. For this reason, the reaction conditions of these compounds were optimized, decreasing the reaction time and increasing the yields and purity of the products as is present in (Figure 3). In addition, the characterization of these compounds was completed since some parameters such as the melting point are not presented in the literature.

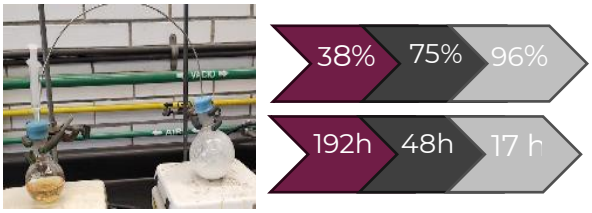

Figure 3. Methodology and achievements of optimizing synthesis conditions.

In vitro evaluations show that at a concentration of 1µM, the products can relatively inhibit the action of the enzyme in a percentage like epalrestat, however, the inhibitory behavior of guanidines is not linear or proportional to the concentration as is the behavior of compounds that have carbonyl groups. For this reason, it has not yet been possible to calculate the inhibitory concentrations 50, but the evaluations will be carried out using another methodology to verify the results already obtained.

As can be seen in (Figure 4), guanidine 4y can inhibit ALR2 at a concentration of 0.01 µM, a lower concentration than that obtained by amino acid-derived molecules, so despite its behavior at different doses, it is still being considered for future evaluations.

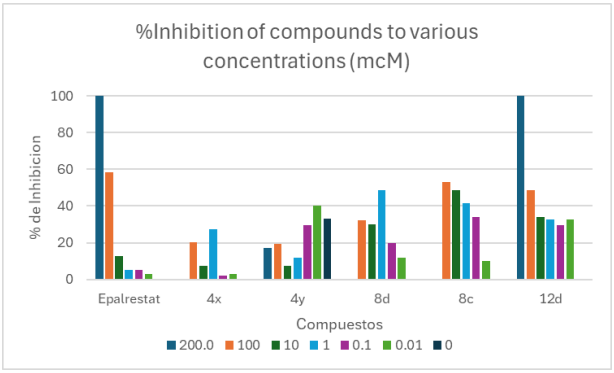

Figure 4. Graph of compound inhibition percentages at different concentrations compared to epalrestat.

Finally, **4x**, **4y**, **8c**, **8d,** and **12d** were orally administrated at 175, 550, and 1750 mg/kg in Wistar rats according to the up-and-down procedure. These compounds did not cause death or significant toxic effects on the individuals at any of the doses (Table 2.), and, through macroscopic analysis, it was determined that they do not cause change in size, color, or damage to any organ. There was not a significant difference in the weight of each organ in the distinct groups.

With this, it was determined that its LD_{50} is >1750 mg/Kg and corresponds to category 4 according to the OECD.

Table 2. Acute oral toxicity results of compound 4x.

Doses (mg/Kg)	% Deaths	Toxic effects
175	0	No observed
550	0	No observed
1750	0	Sleepiness

4. CONCLUSIONS

2-Aminobenzothiazole derivatives are potential ALR2 inhibitors that may be developed as safe oral treatments for diabetic complications caused by the activation of this enzyme. Nevertheless, the results obtained so far suggest that a carbonyl group is necessary to obtain a better biological response. However, further preclinical trials are needed to demonstrate the antidiabetic effect of these compounds.

This project, for the time being, may provide more information on the structural requirements for the interaction with ALR2. However, the evaluation of these compounds in a STZ-induced Wistar rat model is still being considered to see if they are capable of lowering blood glucose levels while preventing the formation of microvascular complications. If so, this would be important to solve a major problem in the diabetic population, as prophylactic drugs for these complications could be developed.

Acknowledgements

The authors would like to thank the Secretaría de Investigación y Posgrado of the Instituto Politécnico Nacional (grant numbers: SIP20240101; SIPMULTI20242297) for supporting this research.

Conflicts of Interest

The authors declare no conflict of interest.

REFERENCES

[1] S. Thakur, S.K. Gupta, V. Ali, P. Singh, M. Verma, Arch. Pharm. Res. (2021). https://doi.org/10.1007/s12272-021-01343-5

[2] A. Kousaxidis, A. Petrou, V. Lavrentaki, M. Fesatidou, I. Nicolaou, A. Geronikaki, EJMECH. (2020) https://doi.org/10.1016/j.ejmech.2020.112742

[3] J.A. Alvarado-Salazar, M. Valdes, A. Cruz, B. Moreno-De-Jesús, D. Patiño-González, I.M. Olivares-Corichi, F. Tamay-Cach, J.E. Mendieta-Wejebe, Preprint (2024) https://doi.org/10.20944/preprints202408.2205.v1

[4] A. Hamdi, M. Yaseen, W.A. Ewes, M.A. Bhat, N.I. Ziedan, H.W. El-Shafey, M.M. Elbadawi, J Enzyme Inhib Med Chem (2023) https://doi.org/10.1080/14756366.2023.2231170

[5] Padilla-Martínez, J.M. González-Encarnación, E.V. García-Báez, A. Cruz, A.A. Ramos-Organillo, Molecules. (2019) https://doi.org/10.3390/molecules241833391

[6] OECD, (2022) https://doi.org/10.1787/9789264071049-en

160-II-PP *IN SILICO* EVALUATION OF BASIC AMINO ACID BOROXAZOLIDONES AS INHIBITORS OF BACTERIAL ENZYMES

J. R. Moran Diaz[1,2]*, A. B. Guzmán Urbieta[3], J. A. Guevara Salazar[2], J. G. Trujillo Ferrara[3]*

[1]Instituto Politécnico Nacional, Centro de Investigación en Ciencia Aplicada y Tecnología Avanzada-Unidad Legaria, Laboratorio de Química Orgánica del Doctorado en Tecnología Avanzada, Calz Legaria 694, C.P. 11500 Ciudad de México, CDMX, México México.
[2]Instituto Politécnico Nacional, Escuela Superior de Medicina, Departamento de Farmacología, Plan de San Luis y Salvador Díaz Mirón S/N C.P. 11340, Ciudad de México, México.
[3]Instituto Politécnico Nacional, Escuela Superior de Medicina, Laboratorio de Bioquímica Médica I, Plan de San Luis y Salvador Díaz Mirón S/N C.P. 11340, Ciudad de México, México.

*Correspondence: jmorand@ipn.mx, jtrujillo@ipn.mx

Abstract: Antimicrobial resistance (AMR) is a global health emergency, the World Health Organization (WHO) estimates that by 2050 it will be the leading cause of death, and it was in its latest report in May 2024 that it establishes as a priority to investigate new ways to mitigate AMR, the objective of this research was to predict (*in silico*) physicochemical, pharmacokinetic and toxicological properties of boroxazolidones derived from basic amino acids (L-arginine, L-ornithine, L-citrulline, L-lysine and L-histidine), as inhibitors of the polyamine pathway (involved in bacterial growth), the enzyme ornithine decarboxylase (ODC) and arginine decarboxylase (ADC). Regarding the rules of medicinal chemistry (Muegge, Lipinski, GSK, Ghose, Pfizer, Veber, Egan), boroxazolidones derived from L-arginine and L-ornithine met all evaluated as molecular weight (PM g / mol) = 339.21 and 297.17, partition coefficient (logP) = -0.30 and -0.48, hydrogen bond acceptors (HBA) = 2 and 2, hydrogen bond donors (HBD) = 4 and 2, topological polar surface area (TPSA Å) = 106.55 and 70.55, regarding the absorption process in the permeability of caco-2 cells and the logP must be lipophilic between 0.5 and 1, there is a correlation in all pharmacokinetic processes and the logP, the best candidates were compounds 3a and 3f, linear regression values were found Since the r^2 count is greater than 0.5, it is finally suggested to perform the molecular coupling and molecular dynamics of compounds 3a and 3f with the ODC and ADC enzymes.

Keywords: Bacterial resistance, polyamine pathway, DIFAC, medicinal chemistry, pharmacokinetics.

1. INTRODUCTION

On May 17, 2024, the World Health Organization (WHO) published its new list of priority bacterial pathogens resistant to antibiotics, classified into critical, high and medium priority microorganisms, in addition, new evidence and information provided by experts were incorporated, for research (R) and the development of new antiotiocos (D). The pathogens that are on the critical and high priority list are bacteria such as, Enterobacterales third-generation cephalosporin-resistant, and carbapenem - resistant *Salmonella typhi* fluoroquinolone - resistant, *Shigella spp.* fluoroquinolone - resistant and *Pseudomonas aeruginosa* carbapenem-resistant which cause resistance mechanisms, one of which is biofilm production [1]. The National Institutes of Health revealed that among all microbial and chronic infections, about 80% are associated with biofilm formation [2,3], this causes

antimicrobial drugs to not reach the molecular target in the bacteria. Biofilm formation is a complex process involving: 1. Adhesion to a living or non-living surface, 2. Formation of a microcolony, 3. Three-dimensional structures and maturation, and 4. Dispersal (Figure 1) [4].

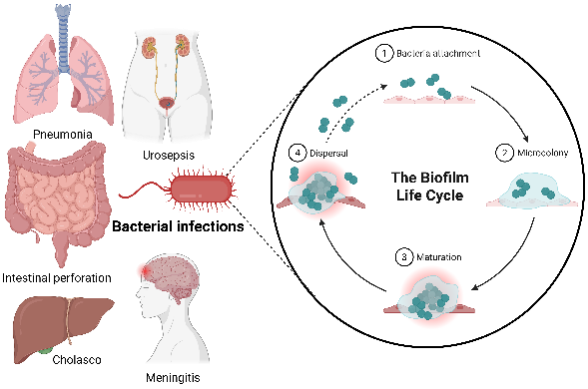

Figure 1. Main infections caused by gram-negative bacteria and the biofilm life cycle.

Bacterial biofilm has been associated with the polyamine pathway, specifically with decreased putrescine and increased spermidine [5-8]. Therefore, the objective of this study was to predict (*in silico*) the physicochemical, pharmacokinetic, and toxicological properties of boroxazolidones derived from basic amino acids (L-arginine, L-ornithine, L-citrulline, L-lysine, and L-histidine) as inhibitors of the polyamine pathway (involved in bacterial growth), ornithine decarboxylase (ODC), and arginine decarboxylase (ADC) enzymes, with the aim of proposing a novel pathway to mitigate AMR.

2. MATERIALS AND METHODS

2.1 Softwares: ChemSketch [9], ChemDraw v 21.0 [10].

2.2 Search engines and platforms: PubChem [11], IUPHAR [12], Molinspiration cheminformatics [13], SwissADME [14], ProTox-3.0 - Prediction of TOXicity of chemicals [15], ADMETlab 3.0 [16], Molsoft L.L.C. [17], Protein Data Bank (PDB) [18].

2.3 Borated compound library and controls: (Figure 2).

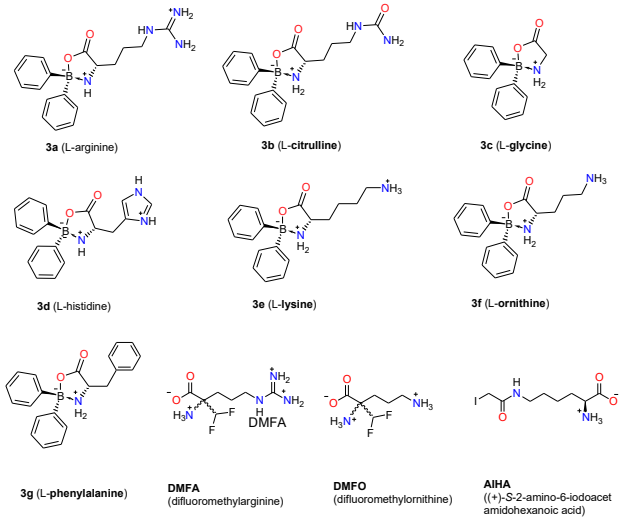

Figure 2. Borated compound library and controls.

2.4 Chemoinformatics prediction*:* The canonical SMILE code was obtained from the chemical library with the ChemSketch software and subsequently used on the following platforms: Molinspiration cheminformatics [13], SwissADME [14], ProTox-3.0 - Prediction of TOXicity of chemicals [15], ADMETlab 3.0, [16], Molsoft L.L.C. [17], SMARTCyp: Site of Metabolism prediction for Cytochrome P450s [19], correlations were performed, and the statistical analysis was carried out using the simple linear regression method. The value of $r^2 \geq 0.5$ was considered significant [20].

3. RESULTS AND DISCUSSION

3.1 Medicinal chemistry*:* The main rules were used to establish the similarity to drugs such as: Muegge, Lipinski, GSK, Ghose, Pfizer, Veber and Egan, boroxazolidones 3a (L-arginine) and 3f (L-ornithine), DMFA (difluoromethylarginine), DMFO (difluoromethylornithine) comply with the main parameters evaluated by these filters (Table 1).

Table 1. Control parameters and boroxazolidones.

Parámetros	DFMA	DFMO	3a	3f
Molecular weight (MW g/mol)	225.21	183.17	339.21	297.17
Partition coefficient (logP o/w)	-2.31	-2.45	-0.30	-0.48
Hydrogen-bond donors (HBA)	4	4	2	2
Hydrogen-bond acceptors (HBD)	4	2	4	2
Topological polar surface área (TPSA Å)	131.41	95.41	106.55	70.55
Number of rotatable bonds	7	5	7	5
Number of rings	0	0	3	3
Number of carbons	7	6	18	17
Number of heteroatoms	8	6	7	5
Molar refractivity	49.47	95.41	105.48	94.87
Atoms	15	12	25	22

3.2 Predicción in silico de la Farmacodinamia*:* The results of the Molinspiration Bioactivity Score were on the following types of receptors: GPCR ligand, ion channel modulator, kinase inhibitor, nuclear receptor ligand, protease inhibitor and enzyme inhibitor, the latter being the one that obtained the best score, considering that ODC and ADC are enzymes.

3.3 In silico prediction of Pharmacokinetics: Regarding *absorption*, boroxazolidones are required to have a logP between 0.5 and 1 like compounds 3f and 3e, the lipophilicity of a molecule is crucial for its absorption, and in the case of intestinal bacterial infections where a biofilm exists, this suggests that these compounds can reach the enzymes of interest. (Figure 3).

The boiled egg diagram was obtained that correlates the logP as a function of the TPSA (Å), where the compounds that enter the egg yolk are likely to reach the central nervous system (CNS), and the compounds that remain in the egg white are likely to have intestinal absorption by the enterocytes, with respect to the basic amino acid boroxazolidones, 3g, 3c, 3d, 3e, and 3f, they would probably cross the membranes and reach the CNS (Figure 4).

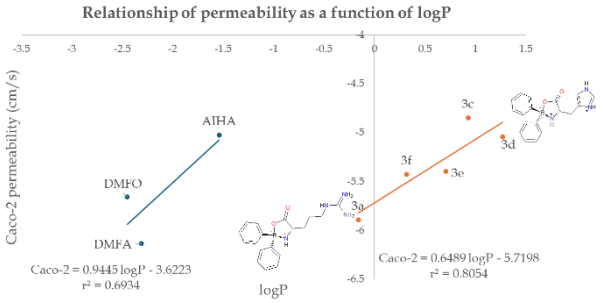

Figure 3. Relationship of caco-2 permeability (cm/s) as a function of logP of controls and basic amino acid boroxazolidones.

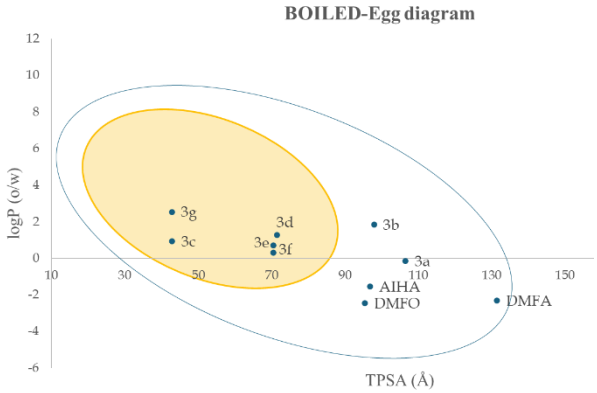

Figure 4. Relationship of logP as a function of TPSA (Å) of controls and basic amino acid boroxazolidones.

Regarding distribution, the pharmacokinetic parameter that indicates its distribution in the body is the volume of distribution (Vd), which can be expressed in L/kg or in L, considering the total body water and the respective compartments, therefore there is a correlation between the logVd as a function of the logP of the controls and basic amino acid boroxazolidones (Figure 5).

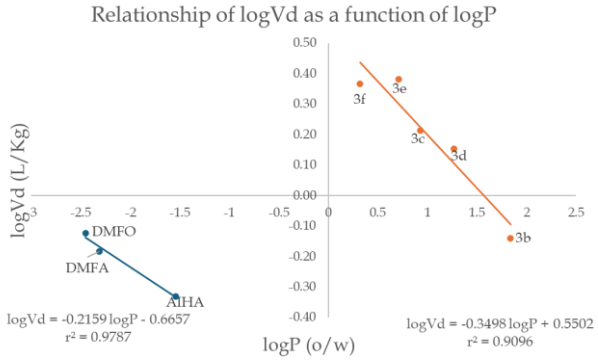

Figure 5. Relationship of logVd (L/Kg) as a function of logP (o/w) of controls and basic amino acid boroxazolidones.

Regarding biotransformation, the SMARTCyp platform was used: Site of Metabolism prediction for cytochrome P450s, the results show the probable site where the biotransformation reaction by the 3A4, 2D6, and 2C9 isoforms of cytochrome P450 can occur (Figure 6 and 7).

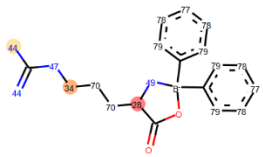

3A4 Ranking	Atom	3A4 Score	Energy
1	C.18	28.4	32.8
2	C.21	34.0	41.1
3	N.25	44.0	54.1
4	N.24	44.1	54.1

Figure 6. Probable site where the biotransformation reaction by the cytochrome P450 isoform 3A4 of compound 3a can occur.

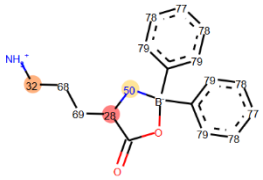

3A4 Ranking	Atom	3A4 Score	Energy
1	C.18	27.6	32.8
2	C.21	32.5	41.1
3	N.17	49.8	54.1
4	C.20	68.4	75.9

Figure 7. Probable site where the biotransformation reaction by the cytochrome P450 isoform 3A4 of compound 3f can occur.

Regarding elimination, it is a process that mainly occurs in the kidney, however it can be through secretions such as sweat, tears, breast milk, sweat, where drugs can be eliminated, regarding $t_{1/2}$ there is a correlation with the logP of controls and basic amino acid boroxazolidones

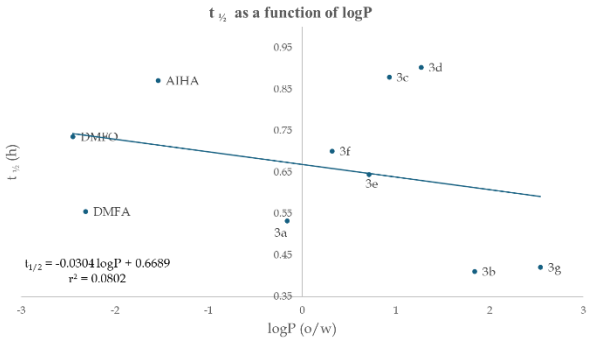

Figure 8. Relationship of $t_{1/2}$ (h) as a function of logP (o/w) of controls and basic amino acid boroxazolidones.

Regarding toxicity, borated compounds are in category 3 and 4, specifically 6 is the safest, this based on the values of the predicted lethal dose 50 (LD50), the values obtained for the safest were for compound 3d (911 mg/kg) and for the most unsafe was for compound 3e (200 mg/kg).

In silico pharmacokinetics, pharmacodynamics and toxicology estimates are crucial for screening the chemical library and selecting the best molecule with the best physicochemical, pharmacokinetic, and pharmacodynamic properties.

Acknowledgements

JRMD, JAGS, JGTF are supported by the Multidisciplinary and Transdisciplinary Projects of Scientific Research and Technological Development grant # 2305, and SIP project (# 20241006 and # 20240792) of the Instituto Politécnico Nacional. J.R. Moran-Diaz thanks the Secretaría de Ciencia, Humanidades, Tecnología e Innovación (SECIHTI, grant # 889474) for the National Scholarship received.

Conflicts of Interest

The authors declare no conflict of interest.

REFERENCES

[1] Report. (WHO bacterial priority pathogens list, 2024: Bacterial pathogens of public health importance to guide research, development and

strategies to prevent and control antimicrobial resistance) https://www.who.int/publications/i/item/9789240093461 Accessed May 2025

[2] J.A. Guevara-Salazar, J.R. Moran-Diaz, E, Ramírez-Segura, J.G. Trujillo Ferrara, Expert Rev Anti Infect Ther. (2020) https://doi.org/10.1080/14787210.2021.1839418

[3] K. K. Jefferson, FEMS Microbiol. Lett. (2004) https://doi.org/10.1111/j.1574-6968.2004.tb09643.x

[4] K. Sauer, P. Stoodley, D. M. Goeres, L. Hall-Stoodley, M. Burmølle, P. S. Stewart, T. Bjarnsholt, Nat. Rev. Microbiol. (2022) https://doi.org/10.1038/s41579-022-00767-0

[5] P. Shah, E. Swiatlo, Mol. Microbiol. (2008) https://doi.org/10.1111/j.1365-2958.2008.06126.x

[6] A.Ö. Gevrekci, World J Microbiol Biotechnol (2017) https://doi.org/10.1007/s11274-017-2370-y

[7] M. Inouye, A. B. Pardee, J. Bacteriol. (1970) https://doi.org/10.1128/jb.101.3.770-776.1970

[8] D. H. Kwon, C. D. Lu, Antimicrob Agents Chemother, (2007) https://doi.org/10.1128/aac.01472-06

[9] ACD/ChemSketch, Advanced Chemistry Development, Inc. Toronto, Ontario, Canada 2025. https://www.acdlabs.com/ Accessed May 2025

[10] ChemDraw 21.0, Revvity Signals Software. https://cloud.info.revvitysignals.com/SCD-trial Accessed May 2025

[11] PubChem, https://pubchem.ncbi.nlm.nih.gov/ Accessed May 2025

[12] IUPHAR/BPS Guide to pharmacology, an expert-curated resource of pharmacological targets and the substances that act on them, https://www.guidetopharmacology.org/ Accessed May 2025

[13] Molinspiration cheminformatics, https://www.molinspiration.com/ Accessed May 2025

[14] A. Daina, O. Michielin, V. Zoete, Sci. Rep. (2017) https://doi.org/10.1038/srep42717

[15] Banerjee, E. Kemmler, M. Dunkel, R. Preissner, Nucleic Acids Res. (2024) https://doi.org/10.1093/nar/gkae303

[16] G. Xiong, Z. Wu, J. Yi, L. Fu, Z. Yang, C. Hsieh, M. Yin, X. Zeng, C. Wu, A. Lu, X. Chen, T. Hou, D. Cao, Nucleic Acids Res. (2021) https://doi.org/10.1093/nar/gkab255

[17] Molsoft L.L.C. molecules *in silico*, https://www.molsoft.com/ Accessed May 2025

[18] PubMed, https://pubchem.ncbi.nlm.nih.gov/ Accessed May 2025

[19] SMARTCyp: Site of Metabolism prediction for Cytochrome P450s, https://smartcyp.sund.ku.dk/mol_to_som Accessed May 2025

[20] J. RM. Moran-Diaz, F. Neveros-Juárez, M. G. Arellano-Mendoza, D. Quinatana-Zavala, O. Lara-Salazar, J. G. Trujillo-Ferrara, J. A. Guevara-Salazar, Mol. Diver. (2023) https://doi.org/10.1007/s11030-023-10730-7

162-II-PP LIGAND-RECEPTOR ANALYSIS BY DOCKING OF ANTHRANILIC ACID-DERIVATED DIELS-ALDER ADDUCTS ON COX-1 AND 2

E. S. Cruz Ruiz[1], J. G. Trujillo Ferrara[1], J. R. Morán Díaz[1,2], M. G. Arellano Mendoza[3], J. A. Guevara Salazar[1,2,3*]

[1]Instituto Politécnico Nacional, Escuela Superior de Medicina, Laboratorio de Bioquímica Médica I, Maestría en Ciencias en Farmacología, Plan de San Luis y Salvador Díaz Mirón S/N C.P. 11340, Ciudad de México, México.
[2]Instituto Politécnico Nacional, Escuela Superior de Medicina, Academia de Farmacología, Plan de San Luis y Salvador Díaz Mirón S/N C.P. 11340, Ciudad de México, México
[3]Instituto Politécnico Nacional, Escuela Superior de Medicina, Laboratorio de enfermedades crónico-degenerativas, Plan de San Luis y Salvador Díaz Mirón S/N C.P. 11340, Ciudad de México, México.

*Correspondence: jguevaras@gmail.com

Abstract: Actually, anti-inflammatory drugs (NSAIDs) have significant adverse effects, or may not be effective for some patients, highlighting the importance of having diverse therapeutic options. Therefore, the development of new anti-inflammatory drugs is crucial to improve the quality of life of patients.

The team designed new chemical entities, selecting the lead compound through pharmacophore-based design, starting from salicylic acid, whose bioisostere is anthranilic acid. After completing the design, two series of compounds were generated: series 5, consisting of *N*-phenylmaleamic acids monosubstituted in the *-ortho, -meta* and *-para* positions with carboxylic acid; while serie 6, consisting of *N*-phenylmaleimides monosubstituted in the same positions with carboxylic acid. We proposed to evaluate these compounds by a molecular docking study directed to the catalytic site of COX-1 and COX-2 enzymes to predict the binding of Diels-Alder adducts on these enzymes. Stereoisomers of each adduct were evaluated, and NSAIDs such as acetylsalicylic acid, mefenamic acid, indomethacin and celecoxib were used as positive controls.

Keywords: NSAIDs, Docking, Correlation, Diels-Alder.

1. INTRODUCTION

In contemporary medical practice, Nonsteroidal Anti-Inflammatory Drugs (NSAIDs) represent a fundamental pillar in the treatment of various painful and inflammatory conditions. Since their discovery and subsequent commercialization in the mid-20th century, these drugs have revolutionized the management of chronic and acute pain, as well as inflammatory diseases such as rheumatoid arthritis and osteoarthritis. However, its wide use is not exempt from critical considerations due to its potential adverse effects, particularly at the gastrointestinal and cardiovascular levels, which have motivated a constant search for safer and more effective formulations [1,2].

Historically, the development of new NSAIDs has been driven by the need to improve the safety and tolerability of these drugs, as well as the search for alternatives for patients with specific contraindications. The introduction of COX-2 selective NSAIDs, such as celecoxib, marked a milestone in this regard by demonstrating a significant reduction in the incidence of gastrointestinal ulcers and bleeding compared to non-selective NSAIDs. However, even COX-2 selective NSAIDs are not without risk, as evidenced by the withdrawal of

rofecoxib from the market due to concerns about its cardiovascular safety [3,4,5,6].

The group developed new chemical entities, choosing a lead compound using a pharmacophore-based design approach, starting with salicylic acid, whose bioisostere is anthranilic acid, (Figure 1).

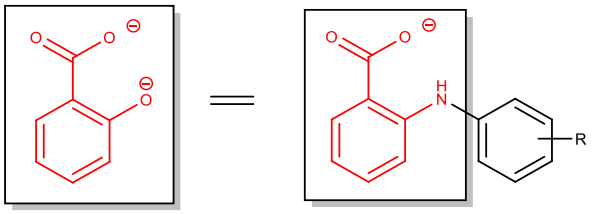

Figure 1. Salicylic acid is bioisosteric is anthranilic acid.

Once the design was completed, two series of compounds were generated: series 5, which includes *N*-phenylmaleamic acids monosubstituted at the *ortho-*, *meta-* and *para*-positions with carboxylic acid; (Figure 2),

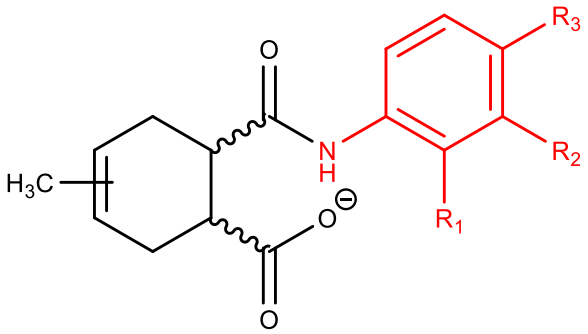

Figure 2. Serie 5 compounds.

and series 6, which is integrated by *N*-phenylmaleimides monosubstituted at the same positions with carboxylic acid, (Figure 3).

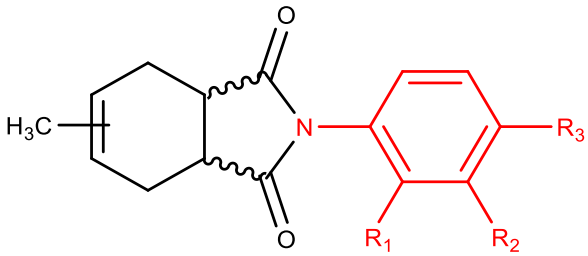

Figure 3. Serie 6 compounds.

In this work we evaluated the binding of novel ligands on COX-1 and COX-2 and predicted their biological activity through a study.

The design of new NSAIDs, using SAR or QSAR, allows the creation of drugs with better biological activity, more selectivity to COX-2 and less toxic effects.

2. MATERIALS AND METHODS

2.1 Preparation of the protein (receptor)

Searching and obtaining the three-dimensional structure of the protein in the Protein Data Bank platform [7], the following criteria were considered: that it was obtained by experimental techniques (such as X-ray crystallography or NMR), that it is co-crystallized with an endogenous ligand, a resolution value equal to or less than 2 Å. The following crystals were selected: for COX-1:3N8Z [8], and COX-2: 3PGH [9]. After obtaining the protein, in Autodock Tools [10], water molecules and other substances were removed from the protein structure with which it was crystallized and the endogenous ligand, leaving only the binding site of the latter. Subsequently, the file was saved in *.pdbqt format.

2.2 Ligand preparation

The structures of the compounds were drawn in their ionized form, in ChemSketch [11], a pre-optimization was performed, making explicit the hidrogens in a three-dimensional structure, to save the file in *.mol, and then take the ligand to GaussView 6.0. 16 and Gaussian 16 [12], where the optimization was carried out at a DFT level, with the files in *.pdb format, in Autodock tools, the parameters were added to the ligands to ensure that it is in a conformation suitable for Docking and the files were obtained in *.pdbqt format.

2.3 Validation

Molecular docking was validated by "redocking" of the co-crystallized ligand flurbiprofen onto the COX-1 and -2 proteins. The Figures 4 and 5 show the overlay view of the docked conformation and the reference

ligand. The RMSD (Root Mean Square Distance) of both docked ligands are within the reliable range of 2 Å, with a value for both of 0.00 Å, verifying that flurbiprofen can interact with the 3N8Z and 3PGH crystal structures in a similar manner to the pre-existing co-crystallized flurbiprofen.

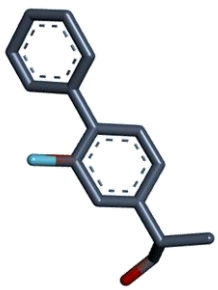

Figure 4. Re-docking pose and RMSD value of 0.000 Å (Red = Original, Gray = Docked) COX-1.

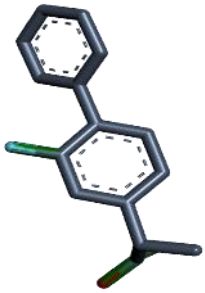

Figure 5. Re-docking pose and RMSD value of 0.000 Å (Green = Original, Gray = Docked) COX-2.

2.4 Grid generation and docking algorithm

It was decided that targeted molecular docking would be carried out, so a three-dimensional grid was defined with the following dimensions: 66x66x66, 0.375 Å spacing, center Grid Box: X center: 8.833, y center: -5.250, Z center: 24. 833, for COX-1, while for COX2: They were used with the following dimensions: 66x66x66, 0.375 Å spacing, center Grid Box: X center: -19.500, y center: -9.333, Z center: -21.528, which formed the grid around the receptor binding site, where ligand complementarity was assessed. These grids guided the search for the ligand within the search space. The Lamarckian algorithm was applied to explore the possible conformations of the ligand at the binding site. After performing the simulation, the results were analyzed in autodock tools 1.5.6 software where the values of K_d, Gibbs free energy (ΔG) and root mean square were obtained, and the intermolecular interactions established between the proposed molecules and positive controls with the amino acid residues of the hydrophobic channel of the COXs were analyzed, and from this study the compound with the best binding characteristics to the COXs was selected.

With the E_{HOMO} and E_{LUMO} values, calculations were performed to elucidate the ligand-receptor recognition, in addition, with the previous *in silico* study of the physicochemical and molecular properties of the compounds, correlations were sought with the predicted biological activity for both COX. To find out if there is a structure-activity relationship.

3. RESULTS AND DISCUSSION

The **6b** compound, the most promising of the 6 serie, which is the best being the one substituted in *-meta* position in its *endo* configuration on COX-1, with a ΔG value of -8.35 kcal/mol, which established links with ARG120, of the salt bond type, Charge-Charge and hydrogen bond type, also with SER530 with which it established a hydrogen bond type link, as shown in Figure 6.

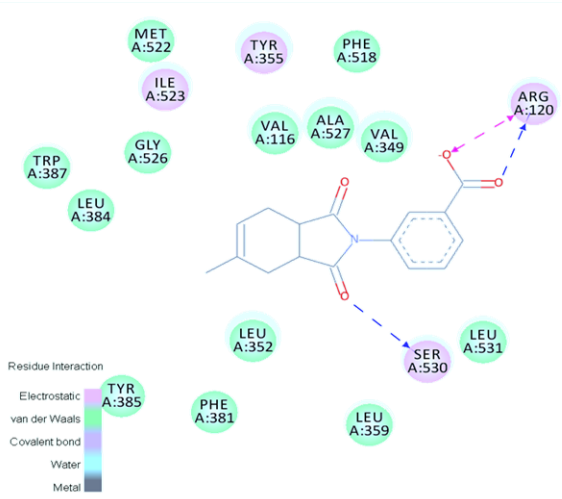

Figure 6. The compound **6b**, is the best candidate for binding to COX-1.

on the other side for COX-2, likewise, were the compounds of the 6 series (**6c**), being the best the one substituted in *para* in its *exo* configuration with a ΔG value of -8.57 kcal/mol, where likewise hydrogen bond and Charge-Charge bonds were established with ARG120, as shown in (Figure 7).

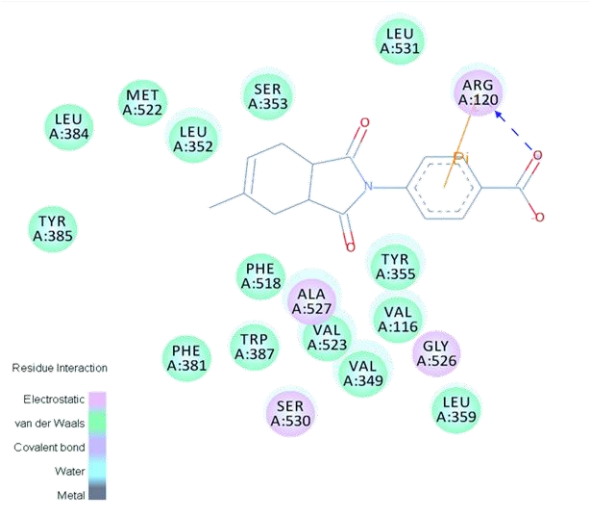

Figure 7. The compound **6c**, is the best candidate for binding to COX-2.

The controls used in docking were acetylsalicylic acid, mefenamic acid, celecoxib and indomethacin; their ΔG values are shown in (Table 1).

Table 1. ΔG values of compounds and controls.

	ΔG (kcal/mol)	
LIGAND	**COX-1**	**COX-2**
6b	-8.35	-8.31
6c	-8.18	-8.57
Acetylsalicylic acid	-5.38	-5.45
Mefenamic acid	-6.97	-7.15
Celecoxib	-7.77	-9.37
Indomethacin	-7.03	-7.13

In COX-1, the best compound is **6b**, surpassing the control drugs, especially those derived from acetates and phenamates. In COX-2, celecoxib was the best compound, surpassing **6c**; however, they are comparable to each other, with celecoxib being almost 10 times more affine than compound 6c, these being the best in this isoenzyme.

Serie 6 is the most promising on both COX and performs interactions with amino acids of the catalytic site, only changes the conformation in COX-1 is *endo*, and on the other side in COX-2 is *exo*, hence the importance of the shape of the compounds, to recognize amino acids and make links.

Using the results of the physicochemical properties obtained from the *in silico* study, the HOMO and LUMO values of the best candidates for both enzymes and arginine, which was the amino acid in which both enzymes showed binding, were taken to elucidate ligand-receptor recognition.

Table 2. HOMO-LUMO analysis.

	E_{HOMO} (eV)	E_{LUMO} (eV)	GAP (eV)	Electro-chem. potencial μ (eV)
6b	-4.8398	2.458	-7.2978	-1.1909
6c	-4.8346	2.2016	-7.0362	-1.3165
Arg	-0.4081	3.7078	-4.1159	1.4498

	Electrone-gativity c (eV)	Global chemical hardness η	Global chemical softness S	Electrop hilicity index ω
6b	1.1909	3.6489	0.2740	0.1943
6c	1.3165	3.5181	0.2842	0.2463
Arg	-1.4458	2.0579	0.4859	0.5078

The HOMO-LUMO recognition analysis, was made by a series of calculations of revealed that the GAP value (eV) of arginine is -4.1159, in contrast to the compounds, that have a value lower than -7, which makes them more unstable and reactive than arginine, therefore they have a greater tendency to form bonds, as for m (eV), arginine has a value of 1.4498, therefore it is more viable to electron density exchange, unlike the compounds that have negative values, which represents the opposite, in terms of hardness, the compounds present greater resistance to electron exchange than arginine, in terms of softness, arginine shows the greatest tendency to give up electrons, having the highest value of the three, therefore in both cases, arginine acts as a nucleophile, giving up electrons, while the tested compounds behave as electrophiles, accepting electrons. This relationship is key to

understanding the molecular interactions involved in biological activity. It is illustrated in Figure 8.

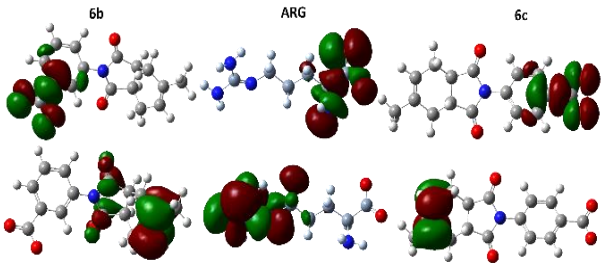

Figure 8. Analysis of ligand-receptor recognition of compounds **6b** and **6c** with arginine.

Using the *in silico* study of the compounds, their physicochemical and molecular properties were estimated, correlations of these properties with the K_d values estimated by docking, correlations were performed and sought, however only resulting in positive linear correlations between the dipole moment (m) and the molecular volume of the compounds with respect to the predicted biological activity on both COXs. As shown in (Figures 9) and 10. However, a slight selectivity of the compounds on COX-2 can be observed, in addition to the fact that COX-1 is more sensitive to changes in the volume of the molecules. This suggests that both m and molecular volume are relevant factors that could influence the efficacy of the proposed compounds.

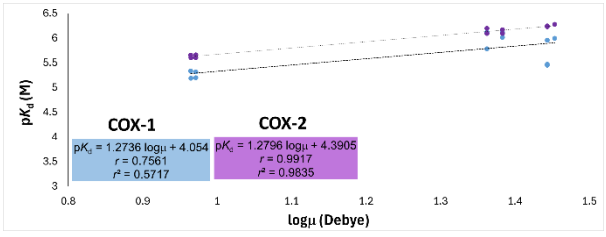

Figure 9. Correlation of the compounds, dipole moment (m) with pK_d (M) on COX-1 and COX-2.

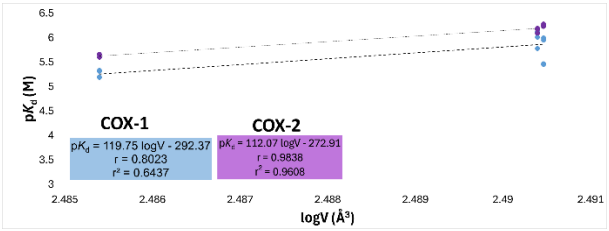

Figure 10. Correlation of the compounds, volume with pK_d (M) on COX-1 and COX-2.

4. CONCLUSIONS

These findings provide a solid basis for future research and the design of new compounds with ligand-receptor binding potential toward both COX. The identification of structural properties that contribute to biological activity can guide the optimization of new candidates for COX recognition. In this case the dipole moment and volume, while increasing as well, predicted biological activity, however volume changes are more sensitive to COX-1, and the compounds tend to selectively bind to COX-2. In this particular case, the *in silico* study affirms that the compounds can recognize and bind to COXs and that the best candidates with the best physicochemical and molecular properties would be amides with substitution at the para position, followed by *in vitro* and then *in vivo* evaluation for biological activity.

Acknowledgements

The authors would like to thank the Multidisciplinary and Transdisciplinary Projects of Scientific Research and Technological Development of the IPN 2024 (#2305), the Projects of the Secretary of Research and Graduate Studies of the IPN (#20241006 and 20240792), the Project of the National Council of Humanities, Sciences and Technologies (CONAHCyT, #257364), the Institutional Program for the Training of Researchers (PIFI) and its component Scholarship for Institutional Stimulus for the Training of Researchers (BEIFI).

Conflicts of Interest

The authors declare no conflict of interest.

REFERENCES

[1] Rao, P., & Knaus, E. E. (2008). Evolution of nonsteroidal anti-inflammatory drugs (NSAIDs): cyclooxygenase (COX) inhibition and beyond. Journal of Pharmacy & Pharmaceutical Sciences: A Publication of the Canadian Society for Pharmaceutical Sciences, Societe Canadienne Des Sciences Pharmaceutiques, 11(2), 81s–110s. https://doi.org/10.18433/j3t886

[2] Montinari, M. R., Minelli, S., & De Caterina, R. (2019). The first 3500 years of aspirin history from its roots – A concise summary. Vascular Pharmacology, 113, 1–8. https://doi.org/10.1016/j.vph.2018.10.008

[3] Asirvatham, S., Dhokchawle, B. V., & Tauro, S. J. (2019). Quantitative structure activity relationships studies of non-steroidal anti-inflammatory drugs: A review. Arabian Journal of Chemistry, 12(8), 3948–3962. https://doi.org/10.1016/j.arabjc.2016.03.002

[4] Delgado, C. (2005). Introduccion a la Quimica terapeutica. Diaz de Santos.

[5] James, D. (1999). The multisystem adverse effects of NSAID therapy. The Journal of the American Osteopathic Association, 99(11), 1-7. https://doi.org/10.7556/jaoa.1999.02

[6] Sostres, C., Gargallo, C. J., Arroyo, M. T., & Lanas, A. (2010). Adverse effects of non-steroidal anti-inflammatory drugs (NSAIDs, aspirin and coxibs) on upper gastrointestinal tract. Best Practice & Research. Clinical Gastroenterology, 24(2), 121–132. https://doi.org/10.1016/j.bpg.2009.11.005

[7] Protein Data Bank, https://www.rcsb.org/ Accessed March 2025.

[8] La estructura 3N8Z del PDB, depositada por Sidhu, R.S., fue utilizada en este estudio https://doi.org/10.2210/pdb3N8Z/pdb. El acceso a los datos se realizó a través de RCSB PDB http://www.rcsb.org

[9] La estructura 3PGH del PDB, depositada por Kurumbail, R., Stallings, W., fue utilizada en este estudio https://doi.org/10.2210/pdb3PGH/pdb. El acceso a los datos se realizó a través de RCSB PDB http://www.rcsb.org

[10] Morris, G. M., Huey, R., Lindstrom, W., Sanner, M. F., Belew, R. K., Goodsell, D. S., & Olson, A. J. (2009). AutoDock4 and AutoDockTools4: Automated docking with selective receptor flexibility [AutoDock Suite https://autodocksuite.scripps.edu/citing/ Journal of Computational Chemistry, 30(16), 2785-2791.

[11] ACD/ChemSketch, Advanced Chemistry Development, Inc. Toronto, Ontario, Canada 2025. https://www.acdlabs.com/ Accessed May 2025.

[12] GaussView, versión 6.1, R. Dennington, T. A. Keith, J. M. Millam, Semichem Inc., Shawnee Mission, KS, 2016

166-II-PP *IN SILICO* DESIGN AND EVALUATION OF NEW LACTONES WITH DUAL ANTIMICROBIAL ACTIVITY

E. D. Rodríguez Rojas[1], J. A. Guevara Salazar[2], C. M. Jácome Gordillo[2], J. G. Trujillo Ferrara[1]*, J. R. Morán Diaz[2]*

[1]Instituto Politécnico Nacional, Escuela Superior de Medicina, Maestría en Ciencias en Farmacología, Laboratorio de Bioquímica Médica I, Salvador Díaz Mirón y Plan de San Luis S/N, C.P. 11340, Ciudad de México, México.
[2]Instituto Politécnico Nacional, Escuela Superior de Medicina, Departamento de Farmacología, Salvador Díaz Mirón y Plan de San Luis S/N, C.P. 11340, Ciudad de México, México.

*Correspondence: jmorand@ipn.mx, jtrujillo@ipn.mx

Abstract: Antimicrobial resistance (AMR) is a global health emergency. The World Health Organization (WHO) estimates that it will be the leading cause of death by 2050. It has also established the need to investigate new inhibition pathways, making bacterial communication attractive for exploration. The objective of this investigation was to design and evaluate *in silico* new lactones for evaluation against clinically important strains. Fifteen receptor-based molecules (LasROC12 HSL from *Pseudomonas aeruginosa* (PDB 3IX3) and 14α-demethylase from *Candida albicans*, in complex with VN12 Benzamide (PDB 5TZ1)) and ligand-based molecules (homosein lactone and ketoconazole) were obtained. Regarding *in silico* screening by means of coupling, the values of the FD4-Z interactions with the A chain of the LasR protein were as follows: ΔG = −8.6 kcal/mol, K_d = 506.68 nM, with bond lengths for tyrosine 56 (5.28 A˚), tyrosine 64 (5.80 A˚) and aspartate 73 (3.19 A˚). The interactions of FD8-Z with the A chain of the 14-□-demethylase protein were as follows: ΔG = −9.06 kcal/mol, K_d = 227.1 nM, with bond lengths for tyrosine 118 (3.48 A˚), glycine 307 (3.24 A˚), leucine 307 (5.32 A˚) and HEM (4.60 A˚), with respect to the chemoinformatic analysis (ADME-Tox), the rules of medicinal chemistry are met (Muegge, Lipínski, GSK, Ghose, Pfizer, Veber, Egan), it is suggested to continue with more experiments to establish the reaction conditions of compounds FD4-Z and FD8-Z.

Keywords: Resistance, lactones, *in silico*, *Quorum sensing*.

1. INTRODUCTION

Antimicrobials are medications used to prevent and treat infectious diseases in humans, animals, and plants. Antimicrobial resistance occurs when bacteria, viruses, fungi, and parasites no longer respond to antimicrobial medications. As a result of drug resistance, antibiotics and other antimicrobial medications become ineffective, and infections become difficult or impossible to treat, increasing the risk of spreading diseases, severe illnesses, disability, and death. Antimicrobial resistance is a natural process that occurs over time through genetic changes in pathogens. Its emergence and spread are accelerated by human activities, primarily the misuse and overuse of antimicrobials to treat, prevent, or control infections in humans, animals, and plants [1].

Susceptibility and resistance are usually measured as a function of minimum inhibitory concentration (MIC), the minimal concentration of drug that will inhibit growth of the bacteria. The susceptibility is a range of the average MICs for any given drug across the same bacterial species. If that average MIC for a species is in the resistant part of the range,

the species is considered to have intrinsic resistance to that drug. Bacteria may also acquire resistance genes from other related organisms, and the level of resistance will vary depending on the species and the genes acquired [2]. Mechanism of resistance: Antimicrobial resistance mechanisms fall into four main categories:1. limiting uptake of a drug, 2. modifying a drug target, 3. inactivating a drug, 4. active drug efflux. Intrinsic resistance may make use of limiting uptake, drug inactivation, and drug efflux; acquired resistance mechanisms used may be drug target modification, drug inactivation, and drug efflux [3].

Bacteria Quorum sensing (QS) is a cell-density-dependent communication system employed by bacteria to coordinate their behavior and regulate gene expression. QS governs a wide array of pathogenic processes, including antibiotic resistance, biofilm formation, and cell adhesion. Given the extensive range of QS-regulated phenotypes, this system presents a promising target for the development of novel compounds aimed at modulating bacterial behavior. While both Gram-positive and Gram-negative bacteria utilize QS, Gram-negative bacteria primarily rely on N-acyl-homoserine lactones (AHSLs) as signaling molecules [4,5].

Fungi ergosterol biosynthesis pathway, lanosterol and its derivatives serve as substrates for the 14α-lanosterol demethylase enzyme. Inhibition of this enzyme results in the accumulation of 14α-methyl sterols, specifically 14α-methyl fecosterol and 14α-methyl-diolergosta-8,24(28)-dien-3β,6α-diol. These sterols can disrupt membrane fluidity and function in azole-treated cells, leading to growth arrest. However, *Candida albicans* have developed mechanisms to tolerate this accumulation. Recent research indicates that the accumulation of the diol compound also inhibits *C. albicans* growth, but a mutation in the ERG3 gene, encoding C-5 sterol desaturase, can mitigate these toxic effects, conferring resistance to azoles and moderate resistance to amphotericin B. The 14α-lanosterol demethylase enzyme is encoded by the CYP51/ERG11 gene, a member of the CYP51 gene family. Numerous genetic alterations associated with the *C. albicans* ERG11 gene have been identified [6].

Problem Statement: Antimicrobial resistance is a serious threat to global public health. Antibiotic-resistant infections are more difficult to treat and can cause more complications, which may lead to death. Additionally, treating antibiotic-resistant infections is more costly than treating antibiotic-sensitive infections. Therefore, the development of new antibiotics and treatments for antibiotic-resistant infections is of paramount importance. New antibiotics must be effective against bacteria resistant to existing antibiotics and must be safe for patients [7].

Research Objectives: The objective of this investigation was to design and evaluate *in silico* new lactones for evaluation against clinically important strains.

Significance of the Study: This work aims to provide basic structures for the development of new drugs that can help mediate the drug-resistant activity of two clinically relevant microorganisms: fungi and bacteria.

2. MATERIALS AND METHODS

The ChemSketch software [8], was utilized to generate and visualize the three-dimensional structures of the novel lactones. Subsequently, ChemDraw v 21.0 [9], was employed to derive the SMILES representations of the new lactone family. These SMILES codes were then leveraged to conduct literature searches and predict a range of pharmacokinetic, pharmacodynamic, and physicochemical properties using various databases such as: Molinspiration cheminformatics [10], SwissADME [11], ProTox-3.0 - Prediction of TOXicity of chemicals [12], ADMETlab 3.0, [13], Molsoft L.L.C. [14], GausView 6 and Gaussian 16W [15], was instrumental in optimizing the geometries of the newly designed lactones, thereby generating suitable ligand files for molecular docking simulations. Molecular docking experiments were carried out using

Autodock Tools 1.5.7 [16], with crystal structures of the 14α-demethylase and LasR proteins, retrieved from the Protein Data Bank (PDB), serving as the protein targets. The accuracy of the docking results was validated by computing the root mean square deviation (RMSD) using Pymol [17], the molecular interactions resulting from the docking simulations were meticulously analyzed using Discovery Studio Visualizer Software, Version 4.0 [18].

2.1 Study Design: This study was designed to be conducted experimentally. By leveraging the capabilities of the software and databases, the thermodynamic parameters ΔG, K_d, and bond distances were computed to facilitate the interpretation and approximation of the drug-receptor interactions involving the proposed compounds and their respective molecular targets.

2.2 Data Collection: The data retrieved from multiple databases was tabulated to facilitate a comprehensive comparative analysis of physicochemical, pharmacokinetic, and toxicological properties. The physicochemical properties evaluated included density, topological polar surface area (TPSA), molecular weight, and hydrogen bond donor/acceptor counts. Pharmacokinetic parameters such as volume of distribution, clearance, half-life, and lipophilicity (logP) were also assessed. Toxicological properties, including estimated lethal dose (LD_{50}) and organ-specific toxicity scores (heart, kidneys, lungs, liver), were determined. Molecular docking results, specifically ΔG and K_d values, were compared with those of co-crystallized ligands to evaluate the binding affinities of the proposed compounds. The accuracy of the molecular docking results was assessed by calculating the root mean square deviation (RMSD) using Pymol. The RMSD analysis enabled the validation of the predicted binding pose of the ligand within the receptor binding site. These results were then compared with the experimentally determined crystal structure obtained from the Protein Data Bank (PDB).

3. RESULTS AND DISCUSSION

Analyzing the results, the eight compounds proposed as new lactones, the family was designed taking as reference the structure of the 3-O-C12-HSL from the autoinductors family form *P. aeruginosa*. The lactone ring was proposed as the central group for the new family of compounds and starting from that point we did some molecular modifications from halogenation, ring addition till alkylation (Figure 1).

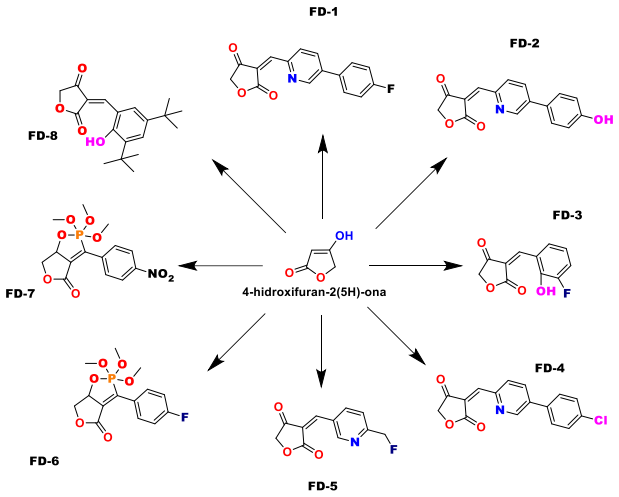

Figure 1. Design of the new lactones.

After the design of the new compounds, the physico-chemical properties and pharmacokinetics parameters obtained from the *in silico* study in diverse databases of medicinal chemistry. We focused on those properties that are considered in the medicinal chemistry rules. Mainly APH, DPH, MW, logP and Molar Refractivity. As we can see in table 3, we have the results of the analyze of the new family of lactones considering this seven rules of the medicinal chemistry. The first screening of the results showed that the compounds FD4 and FD8 could not be accepted for the Pfizer rule and the GSK rule for the FD8. Pzifer rule considers than a logP higher than 3 and TPSA higher than 75 is optimal for the development of new drugs, outside these parameters the compound are likely to be toxic. For the GSK rule a compound with a MW equal or less than 400 g/mol and logP value equal or less than 4 is acceptable for

the development for new drugs to have a good ADMET profile (Figure 2).

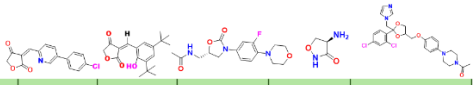

Properties	FD4	FD8	Linezolid	Cycloserine	Ketoconazole
Molecular weight (MW, g/mol)	**299.7**	**316.3946**	337.40	102.04	530.15
Partition coefficient (logP, o/w)	**2.266**	**4.529**	2.44	-2.09	4.17
Hydrogen-bond acceptors (HBA)	**4**	**4**	5	4	5
Hydrogen-bond donors (HBD)	**0**	**1**	1	3	0
Topological surface area (TPSA, Å)	**56.26**	**63.6**	71.11	64.35	69.06
Rotatable bonds	**2**	**3**	5	0	8
Rings	**3**	**2**	3	1	5
Carbon atoms	**16**	**19**	16	3	25
Heteroatoms	**5**	**4**	8	4	10
Molar refractivity	**78.53**	**89.61**	91.06	22.47	139.11
Atoms	**21**	**23**	24	12	36

Figure 2. Main parameters evaluated in medicinal chemistry.

After that analysis, we did the docking experiment with the entire family of new compounds. First, we had to validate the experiment with the calculation of RMSD value to compare the poses of the ligands in the catalytic site of the proteins of interest LasR and 14α-demethylase. The values obtained were: 1.304 for LasR protein and 1.362 for 14α-demethylase Figures 2-6. This value means that the pose of the compound at the moment of being simulated the ligand-receptor interaction by the software was very similar to the original pose of the ligand co-crystalized in the PDB file of the protein [7,8].

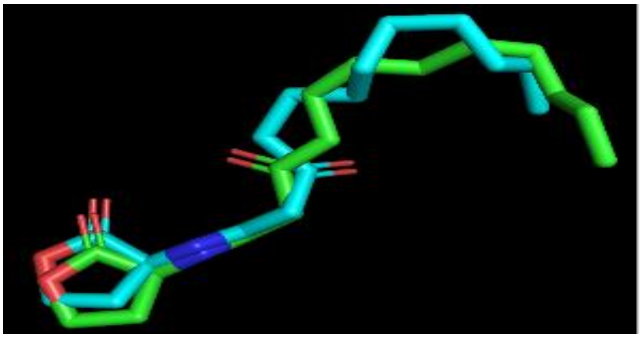

Figure 3. Validation of *N*-3-oxo-dodecanoyl-L-Homoserine lactone with the A chain of the ROC12 HSL of *P. aeruginosa* (PDB 3IX3), RMSD = 1.304.

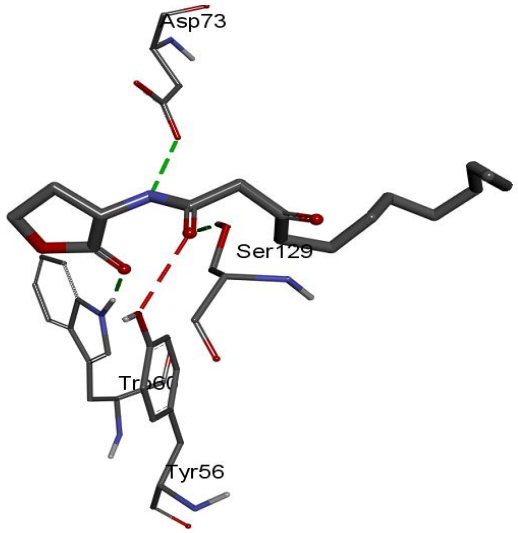

Figure 4. Molecular interactions of *N*-3-oxo-dodecanoyl-L-Homoserine lactone at the catalytic site of the with the A chain of the ROC12 HSL of *Pseudomonas aeruginosa* (PDB 3IX3), with amino acids; W60, Y56, S129, D73.

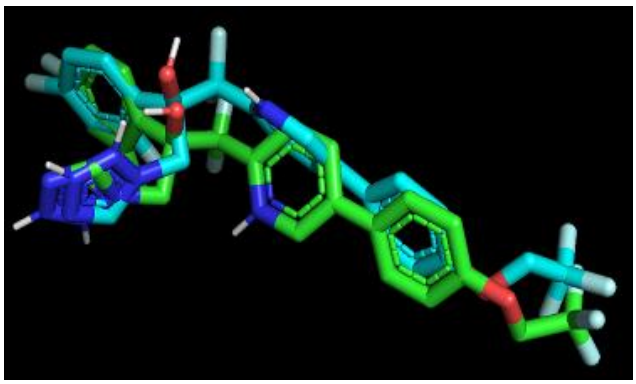

Figure 5. Validation VN12 Benzamide with the A chain of the enzyme lanosterol 14α-demethylase from *Candida albicans* (PDB 5TZ1), RMSD = 1.362.

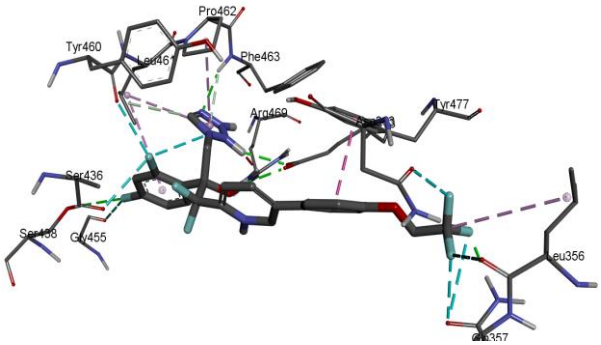

Figure 6. Molecular interactions VN12 Benzamide at the catalytic site of the enzyme lanosterol 14α-demethylase from *Candida albicans* (PDB 5TZ1), with amino acids Q357, L356, S436-438, G455, Y460, L461, P462, F463, R469, Y477.

After the validation of docking experiment, we did an individual assay for every compound proposed, analyzing all the data obtained by the *in silico* assay we decided to take the compound FD4 and the compound FD8 this because in the interaction ligand receptor we saw that the best parameters obtained were to LasR protein FD4-*Z* with chain A of the LasR protein ΔG value of -8.6 kcal/mol, K_d = 506.68 nM, with bond lengths of tyrosine 56 (5.28 Å), tyrosine 64 (5.80 Å) and aspartate 73 (3.19 Å) (Figure 7, 8).

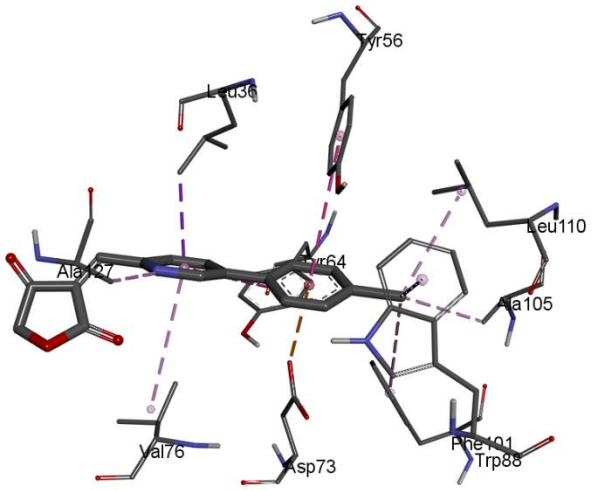

Figure 7. The interactions of FD4*Z* with the A chain of the ROC12 HSL of *P. aeruginosa* (PDB 3IX3), ΔG = -8.6 kcal/mol K_d = 506.68 nM, with interaction lengths of Y 56 (5.28 Å), Y 64 (5.80Å) and D 73 (3.19Å).

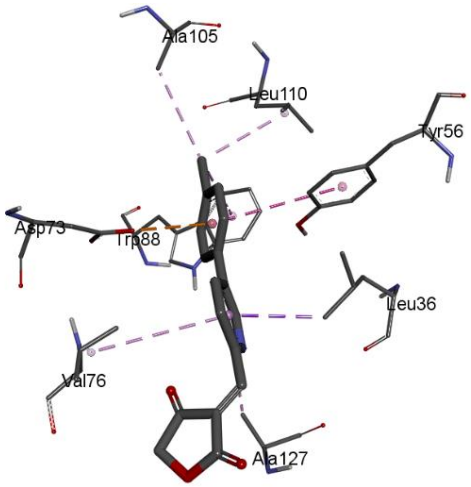

Figure 8. The interactions of FD4E with the A chain of the ROC12 HSL of *P. aeruginosa* (PDB 3IX3), ΔG=-8.51 kcal/mol K_d = 576.24 nM, with interaction lengths of Y 56 (5.24 Å) and D 73 (3.27Å).

For the 14α-demethylase was the compound FD8-Z with chain A of the 14α-demethylase with a ΔG value of -9.06 kcal/mol, K_d = 227.1 mM with bond lengths: tyrosine 118 (3.48 Å), glycine 307 (3.24 Å), leucine 307 (5.32 Å), HEM (4.60 Å). These results suggest that these compounds has a favorable binding energy with the receptor and we were able to see the interactions with aminocids reported in the literature that are important for each ortosteric site of the proteins from the family proposed.

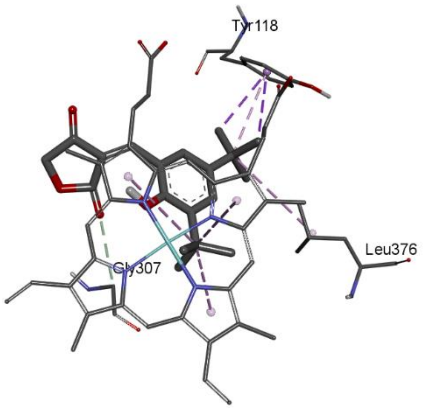

Figure 9. The interactions of FD8Z with chain A of the enzyme lanosterol 14α-demethylase from *Candida albicans* (PDB 5TZ1), ΔG = -9.06 kcal/mol K_d = 227.1 nM with interaction lengths: Y 118 (3.48 Å), G 307 (3.24 Å), L 307 (5.32 Å), HEM (4.60 Å).

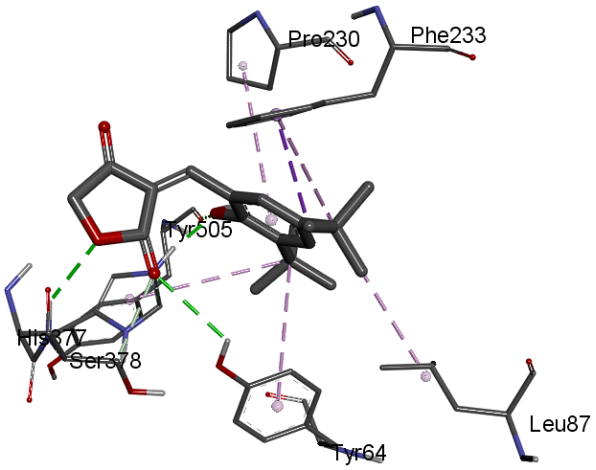

Figure 10. The interactions of FD4E with chain A of the enzyme lanosterol 14α-demethylase from *Candida albicans* (PDB 5TZ1), ΔG = -8.51 kcal/mol K_d = 576.24 nM, with interaction lengths of Y 56 (5.24 Å) and D 73 (3.27 Å).

With this results the next step in the job is to scale the project to organic synthesis of FD4 and FD8 to do the corresponding structural elucidation and characterization of the compounds, and after that, the *in vitro* assay to confirm the antibiotic and antimicotic activity.

4. CONCLUSIONS

Compounds FD4 and FD8 were selected due they performance in the Docking assay considering the ΔG values of both compounds, according to the Rules of the medicinal chemistry the new family of lactones proposed are between the parameters of the seven rules considered so, all of them is considered as potential new structures with possible antimicrobial activity.

Acknowledgements

JRMD, JAGS, JGTF are supported by the Multidisciplinary and Transdisciplinary Projects of Scientific Research and Technological Development grant # 2305, and SIP project (# 20241006 and # 20240792) of the Instituto Politécnico Nacional. E.D. Rodríguez-Rojas thanks the Secretaría de Ciencia, Humanidades, Tecnología e Innovación (SECIHTI, grant # 991877) for the National Scholarship received and the program of the Beca de Estímulo Institucional de Formación de Investigadores (BEIFI, grant # 2023, registration 3316) for additional support.

Conflicts of Interest

The authors declare no conflict of interest.

REFERENCES

[1] J.A. Guevara-Salazar, J.R. Moran-Diaz, E, Ramírez-Segura, J.G. Trujillo Ferrara, Expert Rev Anti Infect Ther. (2020) https://doi.org/10.1080/14787210.2021.1839418

[2] Report. (WHO bacterial priority pathogens list, 2024: Bacterial pathogens of public health importance to guide research, development and strategies to prevent and control antimicrobial resistance) https://www.who.int/publications/i/item/9789240093461 Accessed May 2025

[3] J.A. Guevara-Salazar, J.R. Moran-Diaz, J.G. Trujillo Ferrara, Gen Rep. (2024) https://doi.org/10.1016/j.genrep.2024.101882

[4] M.B. Miller, B.L. Bassler, Annu. Rev. Microbiol. (2001) https://doi.org/10.1146/annurev.micro.55.1.165

[5] C. Spaggiari, C. Yamukujije, M. Pieroni, G. Annunziato, Expert Opin. Ther. Pat. (2025) https://doi.org/10.1080/13543776.2025.2491382

[6] L.E. Cowen, J.B. Anderson, L.M. Kohn, Annu. Rev. Microbiol. (2022) https://doi.org/10.1146/annurev.micro.56.012302.160907

[7] J.A. Guevara-Salazar, J.R. Moran-Diaz, J.G. Trujillo Ferrara, Expert Opin. Drug Discov. (2021) https://doi.org/10.1080/17460441.2022.1985459

[8] ACD/ChemSketch, Advanced Chemistry Development, Inc. Toronto, Ontario, Canada 2025. https://www.acdlabs.com/ Accessed May 2025

[9] ChemDraw 21.0, Revvity Signals Software. https://cloud.info.revvitysignals.com/SCD-trial Accessed May 2025

[10] Molinspiration cheminformatics, https://www.molinspiration.com/ Accessed May 2025

[11] A. Daina, O. Michielin, V. Zoete, Sci. Rep. (2017) https://doi.org/10.1038/srep42717

[12] P. Banerjee, E. Kemmler, M. Dunkel, R. Preissner, Nucleic Acids Res. (2024) https://doi.org/10.1093/nar/gkae303

[13] G. Xiong, Z. Wu, J. Yi, L. Fu, Z. Yang, C. Hsieh, M. Yin, X. Zeng, C. Wu, A. Lu, X. Chen, T. Hou, D. Cao, Nucleic Acids Res. (2021) https://doi.org/10.1093/nar/gkab255

[14] Molsoft L.L.C. molecules *in silico*, https://www.molsoft.com/ Accessed May 2025

[15] GaussView, versión 6.1, R. Dennington, T. A. Keith, J. M. Millam, Semichem Inc., Shawnee Mission, KS, 2016.

[16] G. M. Morris, R. Huey, W. Lindstrom, M. F. Sanner, R. K. Belew, D. S. Goodsell, A. J. Olson, J. Comput. Chem. (2009) https://doi.org/10.1002/jcc.21256

[17] L. Schrödinger, L, M. DeLano, (2020). *PyMOL*. Retrieved from http://www.pymol.org/pymol

[18] Discovery Studio Visualizer Software, Version 4.0 https://www.3ds.com/products/biovia/discovery-studio/visualization Accessed May 2025

171-II-PO HUMAN PAPILLOMAVIRUS AS A RISK FACTOR IN THE DEVELOPMENT OF PROSTATE CANCER

B. I, Rodríguez Romero[1, 2], R. M. Ordóñez Razo[3], V. Sánchez Monroy[4*]

[1]Instituto Politécnico Nacional, Escuela Superior de Medicina, Programa de Doctorado en Investigación en Medicina, Plan de San Luis y Díaz Mirón S/N, C.P. 11340, Ciudad de México, México.
[2]Instituto Mexicano del Seguro Social, UMAE Hospital de Traumatología "Dr. Victorio de la Fuente Narváez", Av Fortuna 101, Magdalena de las Salinas, Gustavo A. Madero, 07760 Ciudad de México, Ciudad de México, México.
[3]Instituto Mexicano del Seguro Social, Centro Médico Nacional Siglo XXI, Hospital de Pediatría, Unidad de Investigación Médica en Genética Humana, Av Cuauhtémoc 330, C.P. 06720, Ciudad de México, México.
[4]Instituto Politécnico Nacional, Escuela Superior de Medicina, Laboratorio de Biomedicina Molecular y Bioingeniería, Plan de San Luis y Díaz Mirón S/N, C.P. 11340, Ciudad de México, México.

*Correspondence: vsanchezm@ipn.mx

Abstract: The association between Prostate Cancer (PCa) and Human Papillomavirus (HPV) infection has been well documented worldwide, however, few studies in Mexico have been documented. This research links HPV infection in 117 biopsy samples with PCa and 60 with benign prostatic hyperplasia (BPH) from Mexican patients in 2023. HPV infection was detected in 109 (93%) of the samples with PCa and in 40 (67%) of the samples with BPH. In both cases, multiple infection and high-risk genotypes predominated. Evidenced of HPV infection was associate with PCa (odds ratio 6.8, 95% CI 2.77–16.69, *p*<0.0001).
This research is part of the preliminary results. The investigation is continuing with the analysis of the effect of human papillomavirus proteins on cellular gene expression in prostate cancer, since further studies are required to establish a role of the virus in the pathogenesis to implement specific prevention strategies in PCa.

Keywords: human papilloma virus, prostate cancer, benign prostatic hyperplasia.

1. INTRODUCTION

Background Information: The human papillomavirus (HPV) has been considered a causal factor of prostate cancer (PCa); it is the most frequent sexually transmitted viral infection in the sexually active population and can cause chronic inflammation of the prostate [1-6]. As HPV infections can be prevented by vaccination, investigation of HPV genotypes and their potential role in PCa is of critical importance for reduce the risk of developing PCa.Problem Statement: There are discrepant results between populations regarding the role of HPV as an etiologic agent of PCa; recent meta-analyses point to HPV as a risk factor for the development of the disease [7-10]; it is necessary to elucidate the mechanisms to relate the modulation of cellular gene expression in PCa by viral infection, to contribute to intensifying the prevention of PCa through infection control.

Research question: What is the risk of developing prostate cancer if there is human papillomavirus infection in the Mexican population?

Research Objectives: To evaluate the human papillomavirus as a risk factor in the development of prostate cancer.

Hypothesis: Human papillomavirus infection in the Mexican population is a risk factor for the development of prostate cancer.

Significance of the Study: This research aims to investigate the role of HPV infection and the most common type in the Mexican population. The results may contribute to preventing infection control and the development of PCa.

2. MATERIALS AND METHODS

Study Design: Quantitative, cross-sectional, descriptive, correlational research.

Materials/Participants: Paraffin-embedded samples from the pathology service of a hospital in Mexico City; 117 with PCa and 60 with BPH.

Data Collection:

- Identification in the computer system of patients with PCa with samples from the pathology service at the participating third-level hospital.
- Search for paraffin-embedded samples in the pathology service archive.
- Obtaining sections from the paraffin block of each identified sample.

Sample processing: Deparaffinization was performed with xylene and DNA extraction with phenol-chloroform-isoamyl alcohol.

Detection and genotyping of 23 HPV genotypes was performed by real-time polymerase chain reaction (qPCR) with the Sansure Biotech - Human Papillomavirus DNA Kit (PCR-Fluorescence Probing)

Data Analysis: Quantitative and qualitative variables were categorized; IBM SPSS Statistics 25 was used for data analysis.

Ethical Considerations: The procedures carried out in accordance with the Regulations of the General Health Law on Health Research are considered risk-free research [7].

3. RESULTS AND DISCUSSION

Results: High frequency of HPV was detected in both study groups 40/60 (67%) in BPH and 109/117 (93%) in PCa, and the presence of HPV was associated with PCa OR 6.8 (CI 2.8-16.7, p<0.0001).

A higher frequency of multiple infection in PCa (64%) than in BPH (35%) (p<0.01) was detected. (Table 1).

The most frequent genotypes were in PCa: 16, 11, 18, 6 and 39, and in HPB: 16, 11, 6, 39, 33 and 18. A higher frequency of genotypes 16 (15% vs 45%), 18 (31% vs 8%) and 11 (43% vs 8%) (p<0.01) in the PCa group than the BPH group were detected, while a higher frequency of genotype 58 (12.5% vs 2%) was detected in the HPB group than the PCa group (p<0.01).

Table 1. HPV infection type in studied samples.

Samples	HPV infection		
	Without	**Single**	**Multiple**
BPH	20(33%)	19 (32%)	21 (35%)
PCa	8 (7%)	31 (26%)	78 (67%)
Total	28(16%)	50 (28%)	99 (56%)

Discussion:

In this study similar to numerous case-control studies and meta-analyses [9-16]. association between HPV infection and PCa was detected.

Moreover, high-risk HPVs were detected in both study groups, which suggest that HPV oncogenic activity and is concordant with Glenn et al., who detected high-risk HPVs in prostate tissues from patients with benign prostatic hyperplasia who developed PCa 10 years later, detecting the same genotypes, suggesting that HPV oncogenic activity is an early phenomenon in prostate tumorigenesis and can be considered as an important risk factor for PCa [14].

Limitations: The use of tissue with BPH as a control can influence the results [14]. Recent meta-analyses have shown that there is a greater association between HPV and PCa

when healthy tissue is used as a control group [16], and even an association may not be detected when considering BPH as a control. In addition, it is well documented that high-risk HPV is present in benign tissues before the development of PCa [17].

However, it is very difficult to obtain biopsy samples of healthy prostate tissue, since the indication for a biopsy is based on pre-existing symptoms and is not indicated in healthy patients.

Future: Research related to the expression of viral proteins E2, E6 and E7, as well as cellular proteins could expand or develop the findings regarding the development of HPV-induced PCa [18-20].

4. CONCLUSIONS

Summary of Findings: There is a risk of developing PCa if there is HPV infection in Mexican population; the high frequency of infection in HPB by high-risk HPV suggests oncogenic activity of HPV as an early phenomenon in oncogenesis.

Contribution to the Field: The finding is support for promoting vaccination in the male population.

Practical Implications: Male vaccination may help to decreasing the risk of developing PCa.

Recommendations: The analysis of the virus in PCa pathogenesis could contribute to implement specific prevention strategies in PCa.

Acknowledgements

The work was supported by the National Polytechnic Institute Project: SIP 20240195 and by the National Council of Humanities, Sciences and Technologies (CONAHCYT) with the CVU number: 927388.

Conflicts of Interest

The authors declare no conflict of interest.

REFERENCES

[1] Bleyer, Q., Spreafico, F., Barr, R. (2020). Prostate Cancer in Young Men: An Emerging Young Adult and Older Adolescent Challenge. Cancer, 126:46-57. https://doi.org/10.1002/cncr.32498

[2] Anic, G., Lee, J., Stockwell, H., Rollison, D., Wu, Y., Papenfuss, M. (2011). Incidence and human papillomavirus (HPV) type distribution of genital warts in a multinational cohort of men: The HPV in men study. The Journal of Infectious Diseases, 204, 1886–92. https://doi.org/10.1093/infdis/jir652

[3] Álvarez, A., Sepúlveda, J., Siller, F. (2015). Carcinogénesis inducida por el virus del papiloma humano. Investigaciones andina, 24 (14): 130. https://doi.org/10.33132/01248146.278

[4] Basulto, M., Flores, J., Conde, L., Esuqeda, A., Kantun, N., Gómez, J., Gonzalez, M. (2022). Detección molecular del virus de Papiloma humano en pacientes con Hiperplasia prostática benigna y cáncer. Urología Oncológic,.75 (1), 27-33.

[5] Medel-Flores, O., Valenzuela-Rodríguez, V., Ocadiz-Delgado, R. (2018). Association between HPV infection and prostate cancer in a Mexican population. Genetics and Molecular Biology, 41 (4), 781-789. http://dx.doi.org/10.1590/1678-4685-GMB-2017-0331

[6] Yin, B., Liu, W., Yu, P., Liu, C., Chen, Y., Duan, X., Liao, Z., Chen, Y., Wang, X., Pan, X., & Tao, Z. (2017). Association between human papillomavirus and prostate cancer: A meta-analysis. Oncology letters, 14(2), 1855–1865. https://doi.org/10.3892/ol.2017.6367

[7] Multhoff, G., Molls, M., & Radons, J. (2012). Chronic inflammation in cancer development. Frontiers in immunology, 2, 98. https://doi.org/10.3389/fimmu.2011.00098

[8] Sadri Nahand, J., Esghaei, M., Hamidreza Monavari, S., Moghoofei, M., Jalal Kiani, S., Mostafaei, S., Mirzaei, H., & Bokharaei-Salim, F. (2020). The assessment of a possible link between HPV-mediated

inflammation, apoptosis, and angiogenesis in Prostate cancer. International immunopharmacology, 88, 106913. https://doi.org/10.1016/j.intimp.2020.106913

[9] Tsydenova, I. A., Ibragimova, M. K., Tsyganov, M. M., & Litviakov, N. V. (2023). Human papillomavirus and prostate cancer: systematic review and meta-analysis. Scientific reports, 13(1), 16597. https://doi.org/10.1038/s41598-023-43767-7

[10] Russo, G. I., Calogero, A. E., Condorelli, R. A., Scalia, G., Morgia, G., & La Vignera, S. (2020). Human papillomavirus and risk of prostate cancer: a systematic review and meta-analysis. The aging male: the official journal of the International Society for the Study of the Aging Male, 23(2), 132–138. https://doi.org/10.1080/13685538.2018.1455178

[11] Moghoofei, M., Keshavarz, M., Ghorbani, S., Babaei, F., Nahand, J. S., Tavakoli, A., Mortazavi, H. S., Marjani, A., Mostafaei, S., & Monavari, S. H. (2019). Association between human papillomavirus infection and prostate cancer: A global systematic review and meta-analysis. Asia-Pacific journal of clinical oncology, 15(5), e59–e67. https://doi.org/10.1111/ajco.13124

[12] Opeyemi Bello, R., Willis-Powell, L., James, O., Sharma, A., Marsh, E., Ellis, L., Gaston, K., & Siddiqui, Y. (2023). Does Human Papillomavirus Play a Causative Role in Prostate Cancer? A Systematic Review Using Bradford Hill's Criteria. Cancers, 15(15), 3897. https://doi.org/10.3390/cancers15153897

[13] Lawson, J. S., & Glenn, W. K. (2020). Evidence for a causal role by human papillomaviruses in prostate cancer - a systematic review. Infectious agents and cancer, 15, 41. https://doi.org/10.1186/s13027-020-00305-8

[14] Glenn, W. K., Ngan, C. C., Amos, T. G., Edwards, R. J., Swift, J., Lutze-Mann, L., Shang, F., Whitaker, N. J., & Lawson, J. S. (2017). High risk human papilloma viruses (HPVs) are present in benign prostate tissues before development of HPV associated prostate cancer. Infectious agents and cancer, 12, 46. https://doi.org/10.1186/s13027-017-0157-2

[15] Ahmed, M. Y., Salman, N. A., Sandhu, S., Cakir, M. O., Seddon, A. M., Kuehne, C., & Ashrafi, G. H. (2023). Detection of high-risk Human Papillomavirus in prostate cancer from a UK based population. Scientific reports, 13(1), 7633. https://doi.org/10.1038/s41598-023-34734-3

[16] Tsydenova, I. A., Ibragimova, M. K., Tsyganov, M. M., & Litviakov, N. V. (2023). Human papillomavirus and prostate cancer: systematic review and meta-analysis. Scientific reports, 13(1), 16597. https://doi.org/10.1038/s41598-023-43767-7

[17] Opeyemi Bello, R., Willis-Powell, L., James, O., Sharma, A., Marsh, E., Ellis, L., Gaston, K., & Siddiqui, Y. (2023). Does Human Papillomavirus Play a Causative Role in Prostate Cancer? A Systematic Review Using Bradford Hill's Criteria. Cancers, 15(15), 3897. https://doi.org/10.3390/cancers15153897

[18] Chen, X. Zheng, D. Kang, B. Yan, X. Liu, Y. Gao, K. Zhang. (2012). Apoptosis and expression of the Bcl-2 family of proteins and P53 in human pancreatic ductal adenocarcinoma. Medical Principles and Practice, 21 (1), 68–73.

[19] Morka, N., Joseph, M., Norris, M., Kelly, D. (2021). Prostate cancer and the human papilloma virus: causative association, role of vaccines, and the impact of the COVID-19 pandemic. Prostate Cancer and Prostatic Diseases, 25, 55–57.

[20] Williams, M. Filippova, U. Soto, P.J. Duerksen-Hughes. (2011). HPV-DNA integration and carcinogenesis: putative roles for inflammation and oxidative stress. Future Virology. 6 (1), 45–57.

172-II-PP DIFFERENTIAL EXPRESSION OF NRF2 TARGET GENES AFTER EXPOSURE TO INORGANIC ARSENIC IN HEPATOCELLULAR CARCINOMA CELLS (HEPG2)

J. A. Alcocer Zuñiga[1], P. López Sánchez[1], E. J. Córdova Alarcón[2], A. Hernández Zavala[1]*

[1]Instituto Politécnico Nacional, Escuela Superior de Medicina, Sección de Estudios de Posgrado e Investigación, Plan de San Luis y Díaz Mirón S/N, C.P. 11340, Ciudad de México, México.
[2]Instituto Nacional de Medicina Genómica, Departamento de Investigación Clínica, Laboratorio Consorcio de Oncogenómica, Periférico Sur 4809 C.P. 14610, Ciudad de México, México.

*Correspondence: ahernandezza@ipn.com

Abstract: Arsenic is a carcinogenic contaminant for humans. Its biotransformation process takes place in the liver, organ where the AS3MT enzyme is predominantly expressed. This enzyme generates monomethylated and dimethylated organic metabolites with a toxicity mechanism different from that of inorganic arsenic. Nrf2 is a transcription factor that, by regulating the expression of various antioxidant and detoxifying proteins, represents a response mechanism against oxidative stress, providing cellular protection against various xenobiotics.

To determine the effect of arsenic exposure on the transcriptional activation of Nrf2 target genes in hepatocarcinoma (HepG2) cells.

A concentration-response curve (0, 0.1, 1, 2.5, and 5 µM arsenic) was conducted, and cell viability of hepatocarcinoma (HepG2) cells was determined using the MTT assay. Subsequently, using the 5 µM concentration, a time-course curve (0, 3, 6, 9, 12, and 24 h) was conducted to evaluate the transcript levels of some Nrf2 target genes using RT-qPCR.

Statistical analysis revealed a decrease in cell viability corresponding to the increase in arsenic concentration. An increase in some Nrf2 target genes was found proportional to the duration of exposure in the time-course curve.

These findings demonstrate the role of Nrf2 as a defense mechanism against arsenic and its generated metabolites, showing the dual nature of this transcription factor in providing cytoprotection in both healthy and cancerous cells.

Keywords: arsenic, Nrf2, liver, AS3MT, biotransformation.

1. INTRODUCTION

Inorganic arsenic is classified as a carcinogen to humans by the International Agency for Research on Cancer (IARC). It can enter the body through oral, inhalator and dermal via. However, its primary toxicokinetic process is biotransformation, as the resulting methylated metabolites exhibit a distinct toxicity mechanism compared to inorganic arsenic [1]. Inorganic arsenic is metabolized by arsenite methyltransferase (AS3MT), an enzyme primarily expressed in the liver. This enzyme catalyzes an oxidative methylation reaction to produce monomethylarsonic acid (MMA), whose reduced form serves again as a substrate for AS3MT to generate dimethylarsinic acid (DMA), which is subsequently also reduced to its trivalent form [2]. (Figure 1).

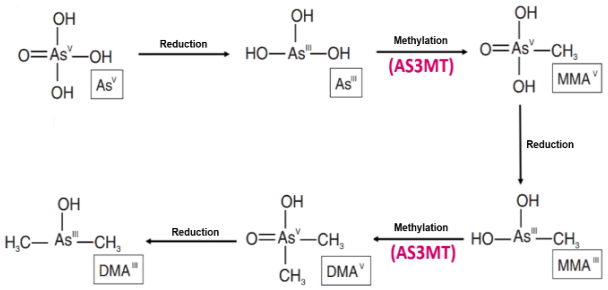

Figure 1. Arsenic biotransformation.

Nrf2 is a transcription factor that acts as a cellular defense mechanism by regulating various antioxidant genes (e.g., *HMOX1*, *NQO1*, *TXN*), genes for glutathione synthesis (*GCLM*, *GCLC*), xenobiotic conjugation genes (*GST*s), excretion genes (*ABCC1*, *ABCC2*, *ABCB6*), and numerous other cell response genes (e.g., *FTL*, *SQSTM1*). Oxidative stress from xenobiotic exposure triggers Nrf2 dissociation from Keap1, its main inhibitor, enabling translocation to the nucleus. Here, it binds to antioxidant response element (ARE) sequences in target gene promoters to regulate their expression [3].

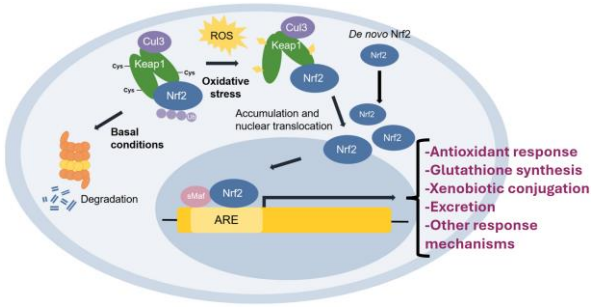

Figure 2. Nrf2 system.

Since there is limited information on how arsenic biotransformation affects Nrf2 activation, it is logical to investigate the behavior of this transcription factor in cancer cells capable of metabolizing arsenic.

Thus, the aim of this study is to assess Nrf2 transcriptional activation in HepG2 cells by analyzing the expression of strategic target genes following exposure to an appropriate arsenic concentration.

This study could contribute to the comprehension of molecular mechanisms implicated in Nrf2 system, liver cancer and arsenic toxicology.

2. MATERIALS AND METHODS

HepG2 cells were cultured using Minimum Essential Medium Eagle (Sigma-Aldrich, M0268-1L,) supplemented with 10% fetal bovine serum.

To determine the appropriate arsenic concentration, 500,000 cells were seeded, and after 24 hours, they were treated with arsenic at concentrations of 0.1, 1, 2.5, and 5 µM for a 24-hour exposure period. An MTT assay (Thermo Scientific, M6494) was then conducted to calculate cell viability as a percentage (%).

For gene expression analysis, 500,000 cells were seeded, and 5 µM arsenic was added after 24 hours. Total RNA was extracted using Trizol reagent (Thermo Scientific, 15596026;) at 3, 6, 9, 12, and 24 hours of exposure. These RNAs were then used for cDNA synthesis (Thermo Scientific, K1622) followed by qPCR using SYBR Green (Thermo Fisher Scientific, 4367659) to assess the expression of the strategic target genes *TXN* (thioredoxin) an antioxidant gene; *GCLM* (glutamate-cysteine ligase modifier subunit) a glutathione synthesis gene; *GST* (glutathione S-transferase) a xenobiotic conjugation gene; *ABCC1* (MRP1) an excretion gene; *FTL* (ferritin light chain) an iron homeostasis gene; and *SQSTM1* (p62) an autophagy gene. The sequences of the oligos are shown in (Table 1). The expression was normalized to constitutive *GAPDH* and is expressed as $2^{-\Delta\Delta C_T}$.

Table 1. Sequences of oligos.

TXN	
F	GTGAAGCAGATCGAGAGCAAG
R	CGTGGCTGAGAAGTCAACTAACTA
GCLM	
F	TGCCTCCTGCTGTGTGATGCC
R	CAGTAGCCACAGCGGCACC
GST	
F	GCCTTTGAAAAAGTCTTAAAGAGCC
R	GTTTTCAGGGCCTTCAGCAGA
ABCC1	
F	TGCATCGTTCTGTTTGCTGC

R	TCAAGTACGTGGTGACCTGC
FTL	
F	CCGCACGGACCCCCATCTCT
R	AGTCGCTGGGCTCAGAAGGC
SQSTM1	
F	GCCGGGTGGGAATGTTGAGGG
R	CCTGGGAGGGGTCCAGAGAGC
GAPDH	
F	CATCTCTGCCCCCTCTGCTGA
R	GGATGACCTTGCCCACAGCCT

Three independent assays were performed with three technical replicates. SigmaPlot software (Dundas Data Visualization, v15.0.0.13), one-way ANOVA test and $p<0.05$ value as statistical significance were used.

3. RESULTS AND DISCUSSION

After conducting statistical analysis, a decrease in cell viability was observed corresponding to the increase in inorganic arsenic concentration. Significant differences were found at concentrations of 1, 2.5, and 5 µM compared to untreated cells. (Figure 3)

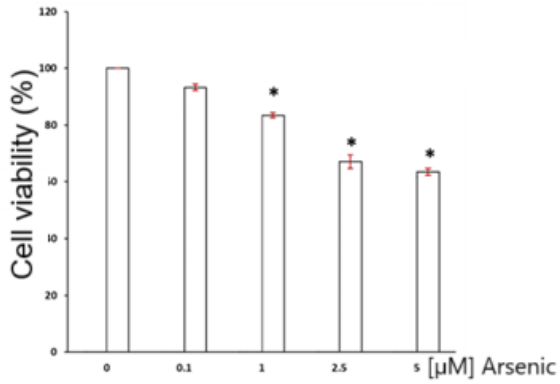

Figure 3. Effect of arsenic in cell viability (%) by MTT assay. There is a significant decrease in 1, 2.5 and 5 µM arsenic. 3 independent experiments analysis.

A 5 µM concentration of arsenic was used for the time-course assay. No significant differences in the transcript expression levels of *TXN*, *GST* and *ABCC1* were observed at any time exposure. (Figure 4).

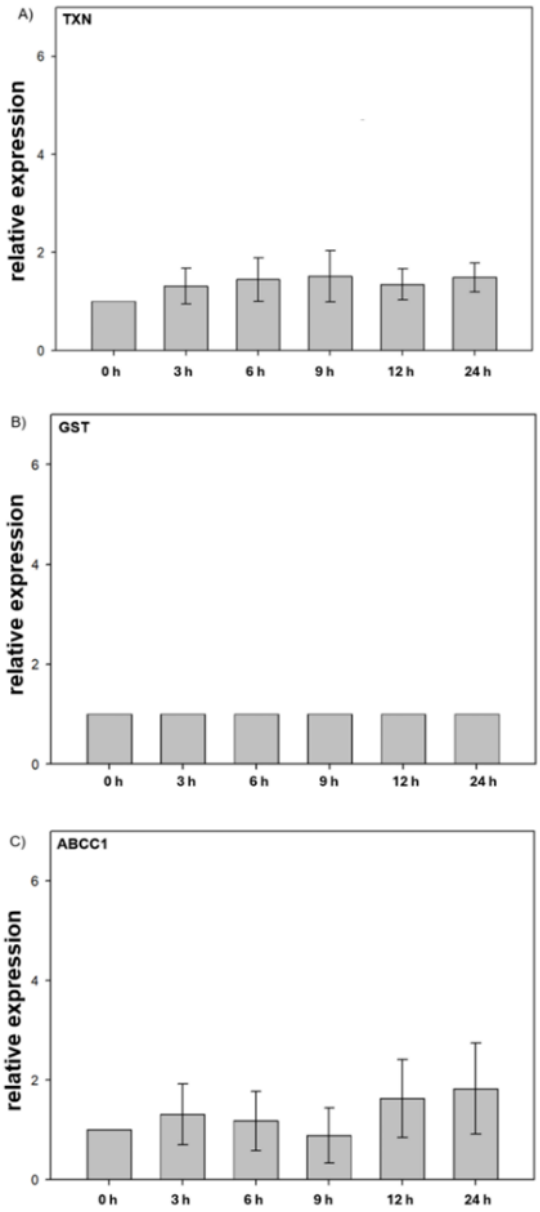

Figure 4. Time-course assay: relative expression analysis of A)*TXN*, B)*GST* and C)*ABCC1*. There is no significant difference at any exposure time. 3 independent experiments analysis each.

In contrast, the transcript expressions levels of *GCLM*, *FTL* and *SQSTM1* showed marked increases. (Figure 5). Specifically, *GCLM* expression was significantly induced at 6, 9, 12 and 24 h of arsenic exposure compared to the control (0 h exposure), additionally significant differences were also found at 9, 12 and 24 h when compared to the 3 h exposure time. For *FTL* an increase in expression was observed

exclusively at 12 h of arsenic exposure. Finally, *SQSTM1* showed significant upregulation at 9, 12 and 24 hours of exposure to arsenic.

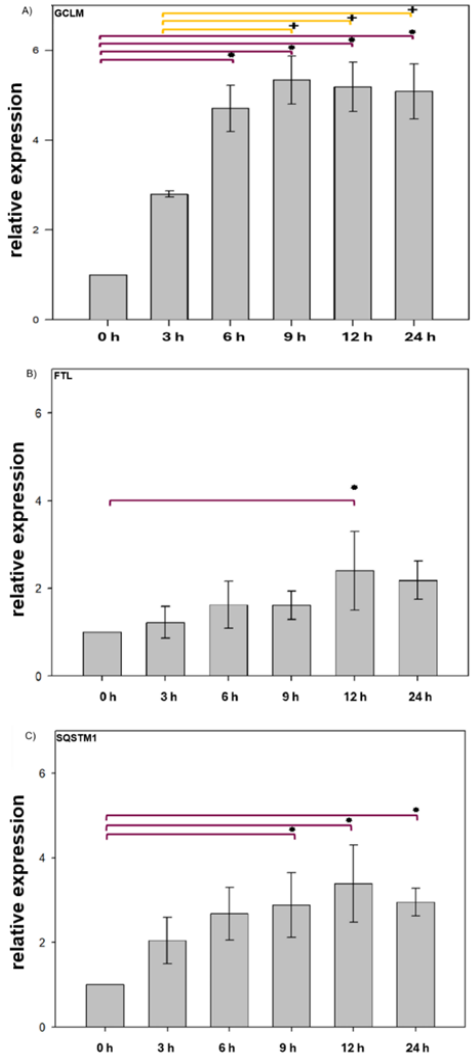

Figure 5. Time-course assay: relative expression analysis of A)*GCLM*, B)*FTL* and C)*SQSTM1*. 3 independent experiments analysis each.

It is very important to note that the differential expression of Nrf2 target genes may be influenced by several factors, including variations in the number of ARE sequences within promoter regions, simultaneous regulation by other transcription factors, interaction with miRNA's or other epigenetic processes [4]. These factors could explain why certain Nrf2 target genes showed increased expression while others did not.

Regarding *TXN* (Figure 4A), Hu and colleagues reported a slight increase in *TXN* expression in fibroblast cells following exposure to arsenic 5 µM for 24 h [5], a finding that contrasts with our results. However, the literature indicates that research is more focused on using thioredoxin inhibitors to increase arsenic sensitivity in cancer cells [6]. This suggests that *TXN* activation and sustained overexpression may occur constitutively without the need for a stimulus like arsenic. This could explain the lack of observed expression changes at any exposure time in our experimental model.

For *GST* (Figure 4B), no Ct values were recorded during amplification. A study with the same cell type has reported an increase in the expression of this gene but using concentrations of 50 to 250 µM of arsenic [7], which suggests that the conditions used in this study may not have been sufficient to induce such an increase. On the other hand, evaluation in another cell line or under different conditions would help confirm the proper functioning of the oligos used.

Similarly, for *ABCC1* (Figure 4C), the fact that no differences in expression were found may be due to the involvement of other excretion genes, Lee and collaborators observed no changes in *ABCC1* expression after arsenic exposure in resistant lung adenocarcinoma cells, however they also reported a marked increase in *ABCC2* expression [8].

GCLM gene exhibited the most significant increase in expression (Figure 5A), and this arsenic-induced upregulation is well-supported by several studies. For example, Bourdonnay using a macrophage cell line found substantial increases in *GCLM* expression after 8 h of exposure to arsenic 1 µM, with the induction continuing to rise with prolonged exposure times [9]. Similarly, Huerta-Olvera observed comparable results in the same cell line (HepG2), his team found an increase in the *GCLM* transcript level at 8h of arsenic exposure, although using the high concentration of 50 µM [10].

The observed increase in *FTL* expression at 12 hours of arsenic exposure (Figure 5B) is

consistent with findings reported in the literature, for example, Huang and colleagues documented an upregulation of *FTL* expression after 4 h of exposure to arsenic 10 µM in keratinocytes [11]. This is possibly due to the important role of ferritin in iron homeostasis, because an intracellular excess of this trace element promotes the generation of reactive species, a condition that would exacerbate cellular stress [12,13].

Finally, for *SQSTM1* (Figure 5C), many other studies have reported similar findings, resembling the pattern observed for *GCLM*. Shah reported an increase in *SQSTM1* transcript level in a keratinocytes cell line exposed to arsenic 8 µM, with significant differences detected as early as 3 h of exposure [14]. Regarding cancer cells, Lee and Oh found that p62 protein levels were induced in a lung cancer cell line under both concentration-response and time-course assays after arsenic exposure [15]. The sustained induction of expression through time could be due to the positive feedback loop between p62 and Nrf2 system. In this process, p62 binds to Keap-1, reducing the formation of the Nrf2–Keap-1 complex, thereby decreasing the degradation of Nrf2 and enhancing its transcriptional activity in the nucleus (non-canonical activation of Nrf2) [16].

Based on the statistical analysis, it is evident that an increase in the number of independent assays is necessary to improve the standard deviation and draw more reliable conclusions from the obtained results.

Furthermore, we strongly believe that it would be worthwhile to directly analyze the effect of arsenic metabolites on the expression of genes regulated by Nrf2, making the determination of these molecules a highly valuable outcome.

4. CONCLUSIONS

In this study, we observed significant increases in the expression of several Nrf2 target genes, such as *GCLM* (glutathione synthesis gene), *FTL* (ferritin light chain subunit) and *SQSTM1* (p62), following arsenic exposure in HepG2 cells.

These results highlight Nrf2's role as a cellular defense mechanism, activating the expression of a wide range of genes that mitigate the stress caused by xenobiotic exposure. This defense is facilitated through the translation of corresponding proteins, which operate through various strategies, including the antioxidant response, glutathione synthesis, xenobiotic conjugation, excretion, intracellular iron regulation, and p62-mediated autophagy regulation, among others.

Thus, this transcriptional activation is crucial not only in healthy cells but also in cancer cells, where it has been linked to chemoresistance processes. Furthermore, given that hepatocarcinoma cells have a high biotransformative capacity for arsenic, it is possible to correlate the various metabolites generated over time with the differential Nrf2 response to xenobiotics. Only through the analytical determination of these metabolites can these phenomena be properly correlated.

The results obtained here contribute to the growing trend of positioning Nrf2 as a potential therapeutic target in cancer cells. However, due to its dual nature, it is advisable not to generalize or take such categorical stances regarding its functional roles. Further research is definitely needed in this regard.

Acknowledgements

The authors acknowledge the support provided by CONAHCYT, as well as that provided by the Instituto Politécnico Nacional (IPN) through the PIFI program.

Conflicts of Interest

The authors declare no conflict of interest.

REFERENCES

[1] DJ. Thomas, Toxicology 15, 457 (2021)
[2] JP. Buchet, R. Lauwerys, H. Roles, Int. Arch. Occup. Environ. Health. 48, 1 (1981).
[3] V. Ngo, ML. Duennwald, Antioxidants (Basel) 27, 11 (2022).
[4] MV Medina, D Sapochnik, M Garcia Solá, O Coso. Antioxid. Redox Signal. 32, 14 (2020)

[5] Y. Hu, X. Jin, E. T. Snow, Toxicol. Lett. 133, 1 (2002).
[6] Y. Tan, L. Bi, P. Zhang, F. Wang, F. Lin, W. Ni, J. Wu, L. Jiang, Int. J. Clin. Exp. Pathol. 7, 8 (2014).
[7] D. B. Tully, B. J. Collins, J. D. Overstreet, C. S. Smith, G. E. Dinse, M. M. Mumtaz, R. E. Chapin, Toxicol. and Appl. Pharmacol. 168, 2 (2000).
[8] T. C. Lee, I. C. Ho, W. J. Lu, J. D. Huang, J. Biol. Chem. 281, 27 (2006).
[9] E. Bourdonnay, C. Morzadec, O. Fardel, L. Vernhet, J. Cell. Biochem. 107, 3 (2009).
[10] S. G. Huerta-Olvera, J. Macías-Barragán, M. E. Ramos-Márquez, J. Armendáriz-Borunda, F. Díaz-Barriga, F. Siller-López, Environ. Toxicol. Pharmacol. 29, 2 (2010).
[11] B. W. Huang, P. D. Ray, K. Iwasaki, Y. Tsuji, FASEB J. 27, 9 (2013).
[12] C. Martin-Chouly, C. Morzadec, M. Bonvalet, M. D. Galibert, O. Fardel, L. Vernhet Mol. Imm. 48, 6-7 (2011).
[13] M. Valenzuela, C. Glorieux, J. Stockis, B. Sid, J. M. Sandoval, K. B. Felipe, M. R. Kviecinski, J. Verrax, P. B. Calderon, Br. J. Cancer 111, 5 (2014).
[14] P. Shah, E. Trinh, L. Qiang, L. Xie, W. Y. Hu, G. S. Prins, J. Pi, Y. Y. He, Molecules 22, 2 (2017).
[15] H. Y. Lee, S. H. Oh, Biochem. Biophys. Res. Commun. 587, 16-23 (2022).
[16] Y. Katsuragi, Y. Ichimura, M. Komatsu, Curr. Opin. Toxicol. 1, 54-61 (2016).

259-II-PP EVALUATION OF GABA AMINOTRANSFERASE INHIBITOR DIELS-ALDER ADDUCTS WITH POTENTIAL ANTICONVULSANT ACTIVITY

M. F. Camacho Merino[1*], J. G. Trujillo Ferrara[1*], J. A. Guevara Salazar[1,2*]

[1]Instituto Politécnico Nacional, Escuela Superior de Medicina, Laboratorio de Bioquímica Médica I, Doctorado en Investigación de Medicina, Plan de San Luis y Salvador Díaz Mirón S/N, C.P. 11340, Ciudad de México, México.
[2]Instituto Politécnico Nacional, Escuela Superior de Medicina, Academia de Farmacología, Plan de San Luis y Salvador Díaz Mirón S/N, C.P. 11340, Ciudad de México, México.

*Correspondence: jtrujillo@ipn.mx, jguevaras@ipn.mx

Abstract: Globally is estimated that approximately 1% of the population has epileptic-type seizures and if we complement it with the recurrence of non-epileptic seizures, the incidence rate increases. To deal with this problem, numerous drugs with the ability to reduce the magnitude and even prevent the appearance of seizures and their symptoms, has been used.

In the present work it is intended to evaluate the pharmacological profile, as well as the potential anticonvulsant activity of Diels-Alder adducts that previously proved to be non-competitive inhibitors of GABA aminotransferase, since by preventing the catabolism of GABA they could have the ability to enhance synaptic inhibition and thus conclude in a possible anticonvulsant activity.

Keywords: GABA-AT, Diels-Alder adduct, anticonvulsive, molecular docking, epilepsy

1. INTRODUCTION

Epilepsy is described as a disorder of episodic brain dysfunction characterized by unpredictable, spontaneous and recurrent seizures [1].

In order to treat and control seizure disorders there are different pharmacological alternatives used in modern clinical practice and the choice of the drug to be used is made depending on the type of seizure manifested by the patient [2].

Anticonvulsant drugs may interact with one or more targets in the CNS. There is a great interest in GABA-AT inhibition, due to the relationship of the neurotransmitter GABA in different neurological disorders, such as Huntington, Parkinson, Alzheimer and epilepsy to mention a few; for which GABA-AT becomes important as it is the key enzyme in the regulation of GABAergic activity [3].

There are anticonvulsant drugs such as valproic acid (VPA) and vigabatrin (VGB), which share as pharmacological target the GABA-AT enzyme, responsible for the degradation of the neurotransmitter GABA. Both inhibit this enzyme, increasing the permanence of GABA in the synaptic space; however [4], VPA is not specific to this mechanism of action and its use is related to adverse teratogenic effects [5], while VGB, an irreversible inhibitor of GABA-AT, has the capacity to develop blindness due to retinal atrophy with its chronic use [6].

The research of new molecules as inhibitors of GABA-AT is of great interest, therefore in 2020 the research group synthesized, characterized and analyzed kinetically a series of Diels-Alder adducts derived from maleic acid, isoprene and *para*-substituted anilines Figure 1.

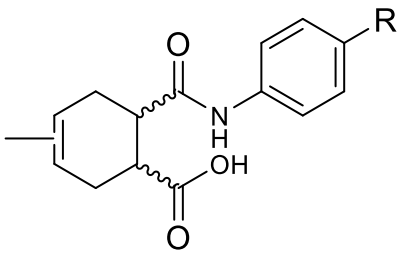

R= -H,-CH_3, -OCH_3, -NO_2,-I, -Br, -Cl, -F, -COOH, -COOEt

Figure 1. Synthesized Diels-Alder adduct series.

As a result, it was reported that the proposed compounds were found to exhibit non-competitive inhibition against GABA-AT; the adducts of the series with -I, -Br and -COOEt substituents stood out with the highest percentage of inhibition.

2. MATERIALS AND METHODS

A QSAR study was performed in order to correlate experimental inhibitory activity with changes in the structure of a series of non-competitive GABA-AT inhibitory Diels-Alder adducts. Subsequently, an enzyme-ligand interaction assay was performed on a GABA-AT protein homologue from *P. fluorescens* and *H. sapiens*. Finally, *in vivo* studies were performed for anticonvulsant evaluation on a murine model of generalized seizures induced with PTZ, as well as an acute toxicity assay to determine the LD_{50} by the modified Lorke method.

Table 1. Software and platforms used in the *in silico* study.

Physicochemical and molecular properties	ChemDraw Pro 12.0, Chemsketch, Molinspiration (property calculation), OSIRIS Property Explorer, Spartan 18, Gaussian 16.
Pharmacokinetic properties	SwissADME, ADMETlab 2.0, AdmetSAR
Pharmacodynamic properties	Molecular Docking: Chemsketch, Gaussian 16, PDB, AutodockVina, Spartan 18, Molinspiration (Bioactivity prediction)
Toxicological properties	Toxtree, ProTox-II, ADMETlab 2.0

Table 2. Materials and reagents employed in the *in vivo* study

Determination of the LD_{50} of the Diels-Alder adducts with the highest percentage inhibition of GABA-AT (-Br, -I and -COOEt) by the modified Lorke method.	Male CD-1 mice, mouse cages, biotherapeutic grade pine sawdust, pellets, distilled water, Saline, Diels-Alder adducts with p-substituted anilines (-Br, -I and -COOEt), 1 mL syringes.
Determination of anticonvulsant activity of Diels-Alder adducts with higher percentage inhibition of GABA-AT (-Br, -I and -COOEt) by PTZ-induced seizure model.	Male CD-1 mice, mouse cages, biotherapeutic grade pine sawdust, pellets, distilled water, Saline, Diels-Alder adducts with p-substituted(-Br, -I and COOEt), valproic acid, vigabatrin, pentylenetetrazole, 1 mL syringes.

3. RESULTS AND DISCUSSION

QSAR

Structural physicochemical parameters were calculated for the 10 Diels-Alder adducts and then related to the percentage of experimental inhibition on GABA-AT. Molar refractivity (MR) and polarizability (α) were selected for the QSAR analysis because the correlation coefficients obtained were the most appropriate; the multiparametric equation was calculated using multiple linear regression to obtain the final QSAR model; dividing the series of compounds into two groups, those with a substituent that provides the structure with an electronic inductive effect (-I, -Br, -CH_3, -Cl, -F) (EIE) and an electronic resonance effect (-COOEt, -NO_2, -COOH, -OCH_3,) (ERE).

Table 3. Multiparametric QSAR equations for Diels-Alder adducts of *N*-phenylmaleamic acid and isoprene with p-substituted anilines with respect to inhibitory activity on GABA-AT enzyme.

	EIE	ERE
Multiparametric QSAR equation	%inhibition = 3888 log RM - 2869 log α - 3088	%inhibition = 473.5 log RM - 108.8 log α - 709.1

After the validation of the equation, it was conclusively shown that the increase in molar

refractivity and polarizability in the molecule means an increase in inhibitory activity on the GABA-AT enzyme.

MOLECULAR DOCKING

The SwissModel platform was used to obtain a GABA-AT homologue for Pseudomonas fluorescens using the 1SF2 crystal from *Escherichia coli* using its FASTA sequence. After protein optimization, molecular docking was performed using AutodockVina software [7], where blind docking was performed on the whole protein using the ten Diels-Alder adducts of *N*-phenylmaleamic acid and isoprene with *p*-substituted anilines as ligands. The RMSD and ΔG values of the docking were obtained as shown in table 4, as well as the amino acids with which the ligands were shown to interact.

When analyzing the amino acids with which the ligands interacted Figure 2, using the software BIOVIA Discovery Studio [8] it is observed that there are residues in common, which may indicate the allosteric site where the Diels-Alder adducts can bind in the macromolecule, where this is described by the amino acids ILE25, ILE22, ILE386, LEU388, VAL35, TYR 43 and ALA47, which confer a lipophilic nature to the jointing site.

Table 4. Values obtained from molecular docking of Diels-Alder adducts of N-phenylmaleamic acid and isoprene with p-substituted anilines on the GABA-AT from Pseudomonas fluorescens.

Adduct substituted by	RMSD	ΔG (kcal/mol)	Amino acids with interaction
-COOH	0.2831	-8.1	ILE22, ILE25,LEU388, GLN50, ALA47, ILE386, VAL35, TYR43
-Br	0.02379	-7.9	ILE22, ILE25, ILE386, VAL35, TYR43, ASP45
$-CH_3$	0.0485	-7.9	ILE22,ILE25, GLN21, HIS23, LEU388, ILE386, VAL35, TYR43
-Cl	0.0312	-7.8	ILE25, VAL35, TYR43, ILE 386, ASP45, HIS57, GLY49, GLN50
-COOET	0.5368	-7.8	ILE22, ILE25, TYR43, VAL35, ASP45, ILE386, ALA47, LEU388
-F	0.0975	-8	ILE22, ILE25, TYR43, VAL35, ILE386, HIS23, GLN21, LEU388
-H	0.00139	-8.1	ILE22, ILE25, TYR43, VAL35, ILE386, ALA47, LEU388
-I	0.224	-7.8	ILE22, ILE25, ILE386, VAL35, TYR43
$-NO_2$	0.2636	-8.2	ILE22, ILE25, ILE386, VAL35, TYR43, ALA47, LEU388
$-OCH_3$	0.0524	-8.2	ILE22, ILE25, ILE386, VAL35, TYR43, ALA47, LEU388, GLN50

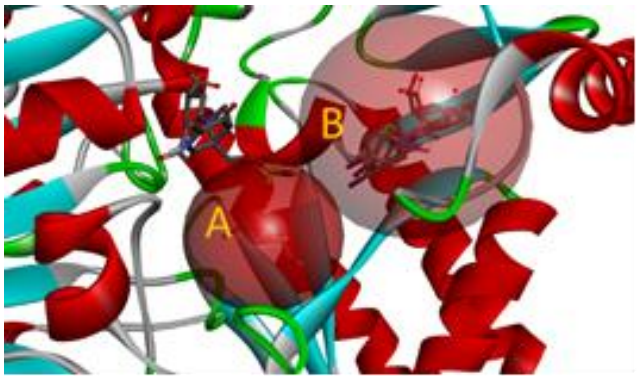

Figure 2. A) Binding site between GABA and GABA-AT of *Pseudomonas fluorescens*. B) Binding site between the Diels-Alder adduct series and GABA-AT of *Pseudomonas fluorescens*.

APPROXIMATION OF THE LD_{50}

For this acute toxicity test, groups and doses were divided according to table 5.

Table 5. Doses employed for phases I and II for the approximation of the LD_{50} by the modified Lorke method.

Adduct substituted by	LD_{50} (mmol/kg)
-Br	1.2010
-I	1.7220
-COOEt	0.4040

Using for the first phase a logarithmic dose scale and then adjusting this scale for the second phase taking as criteria the group with the last dose in which all subjects survive and the first dose in which death is observed in the whole group, the approximation of the LD_{50} was determined with the geometric mean equation (Table 6).

Table 6. Approximation of LD LD_{50} by the modified Lorke method.

Adduct substituted by	Phase	Dose (mg/kg)	n	Phase	Dose (mg/kg)	n
-Br	**I**	10 100 1000	3	**II**	300 550 800	1
-I		10 100 1000	3		300 550 800	1
-COOEt		10 100 1000	3		30 55 80	1

It is shown that the most toxic compound according to the approach is the adduct substituted with -COOEt; as well as, the least toxic is the one substituted with -I.

DETERMINATION OF ANTICONVULSANT ACTIVITY

Taking into regard the approximation calculation of the LD_{50}, the dose intervals tested of each of the adducts were selected for the model of tonic-clonic seizure induction with pentylenetetrazole (PTZ).

After PTZ administration, the number of generalized tonic-clonic seizures, as well as the latency time were registered over a period of one hour Figure 3.

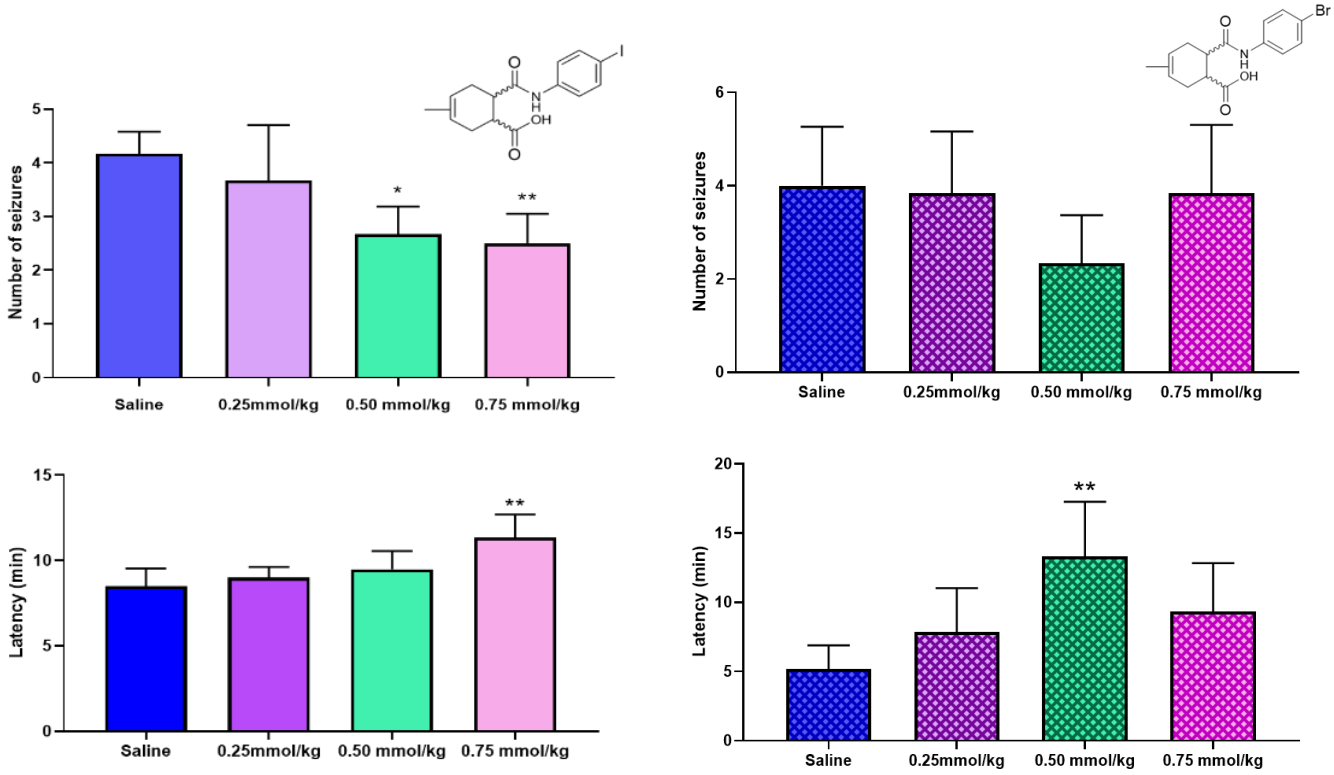

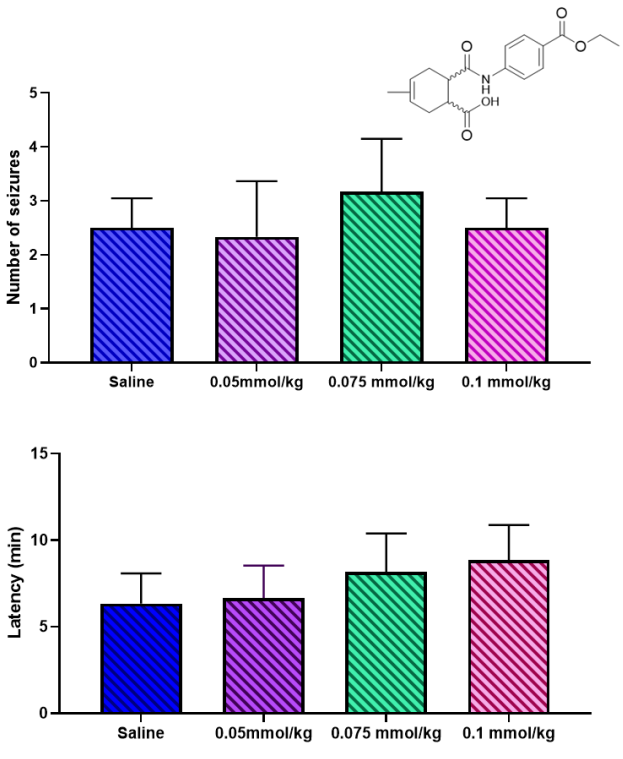

Figure 3. Number of seizures and latency time (min) for the groups treated with Diels-Alder adducts derived from isoprene and maleic anhydride substituted with -I,-COOEt and -Br, and saline as negative control using the PTZ-induced seizure model. Kruskal-Wallis and Dunn's test where * $p < 0.05$.

The Diels-Alder adduct derived from 4-iodophenylmaleamic acid and isoprene proved to be the most promising by demonstrating a significant difference in the number of generalized tonic-clonic seizures in comparison with the control group treated with Saline, by the groups treated with the doses of 0.75 mmol/kg and 0.5 mmol/kg and a statistically significant increase in latency time was found only in the group administered with the 0.75 mmol/kg dose. In comparison with the results obtained from treatment with the Diels-Alder adducts substituted with both -COOEt and -Br, where we did not find significant anticonvulsant activity at the doses employed.

4. CONCLUSIONS

The Diels-Alder adducts, non-competitive inhibitors of GABA-AT, showed a directly proportional relationship between their physicochemical properties related to the dimensions of the molecule and the activity on the enzyme according to the QSAR study; their interaction with GABA-AT taking place in an allosteric site. Specifically, the Diels-Alder adduct derived from 4-iodophenylmaleamic acid and isoprene according to its LD_{50} approximation turned out to be the compound with the lowest toxicity compared to the adducts substituted with -Br and -COOEt, as well as, it was shown to have the highest capacity to decrease the number of seizures and to increase the latency time in a model of generalized tonic-clonic seizures induced by PTZ in a murine model.

Of the non-competitive GABA-AT inhibitors tested, the Diels-Alder adduct derived from 4-iodophenylmaleamic acid and isoprene demonstrated the ability to emerge as a new anticonvulsant drug candidate with the potential for decreased toxicity related to its use.

Acknowledgements

The authors would like to thank the Multidisciplinary and Transdisciplinary Projects of Scientific Research and Technological Development of the IPN 2024 (#2305), the Projects of the Secretary of Research and Graduate Studies of the IPN (# 20241006 and 20240792), the Project of the National Council of Humanities, Sciences and Technologies (CONAHCyT, # 257364), the Institutional Program for the Training of Researchers (PIFI) and its component Scholarship for Institutional Stimulus for the Training of Researchers (BEIFI).

Conflicts of Interest

The authors declare no conflict of interest.

REFERENCES

[1] Fisher, R. S., Cross, J. H., French, J. A., Higurashi, N., Hirsch, E., Jansen, F. E., . . . Zuberi, S. M. (2017). Operational classification of seizure types by the International League Against Epilepsy: Position Paper of the ILAE Commission for Classification and Terminology. Epilepsia, 58(4), 522-530.

[2] Cheolsu Shin, M., & James O. McNamara, M. (1994). MECHANISM OF EPILEPSY. Annual review of medicine, 379-389.

[3] Bormann, J. (2000). The 'ABC' of GABA receptors. Trends in pharmacological sciences, 21(1), 16-19.

[4] Löscher, W. (1980). Effect of inhibitors of GABA transaminase on the synthesis, binding, uptake and metabolism of GABA. Journal of neurochemistry, 1603-1608.

[5] Tomson, T., Battino, D., & Perucca, E. (2016). Valproic acid after fi ve decades of use in epilepsy: time to reconsider the indications of a time-honoured drug. The Lancet Neurology, 15(2), 210-218.

[6] Rod Foroozan, M. (2018). Vigabatrin: Lessons Learned From the United States Experience. Journal of Neuro-Ophthalmology, 38(4), 442-450.

[7] J. Eberhardt, D. Santos-Martins, A. F. Tillack, and S. Forli. (2021). AutoDock Vina 1.2.0: New Docking Methods, Expanded Force Field, and Python Bindings. Journal of Chemical Information and Modeling.

[8] BIOVIA, Dassault Systèmes, Discovery Studio, 2019, San Diego: Dassault Systèmes,

302-II-PP EVALUATION OF THE DIETARY PATTERN IN MORBIDLY OBESE ADULTS

E. A. Davila del Rio[1]*, J. M. Acevedo[1], M. A. Castro Reyes[1], E. S. Aguilar Barrera[1]

[1]Instituto Politécnico Nacional, Centro Interdisciplinario de Ciencias de la Salud Unidad Milpa Alta, Carretera Xochimilco-Oaxtepec Km 39.5 C.P. 12000, Ciudad de México, México.

*Correspondence: erickdavila619@gmail.com

Abstract: According to data obtained by ENSANUT 2022, it was estimated that between 6% and 8% of adults in Mexico suffer from morbid obesity, this represents a significant group of people whose BMI is equal to or greater than 40 kg/m². It has been observed in the literature that the positive relationship between dietary patterns and the development of obesity, where an energetic imbalance is evidenced. The objective is to establish the relationship between dietary patterns and the development of morbid obesity in patients of the Rubén Leñero and General Hospital of Tláhuac, in the CDMX. Material and methods: A standardized food consumption frequency questionnaire was applied, and dietary patterns were determined by principal component analysis. Results: The main pattern is characterized by a high consumption of cereals, representing 30% of the recommended 22%. Likewise, consumption of high-fat foods of animal origin of 13% compared to the recommended 8%, and of oils and fats, representing 18% in contrast to the suggested 5%, were observed. The consumption of vegetables and fruits only reached 3% compared to the recommended 50%, as did the consumption of legumes, which was zero compared to the recommended 15%. In addition, foods not included in the "Plato del bien comer", such as Mexican food, represent 21% of total consumption, together with sugars, 15%. Conclusion: The dietary pattern influences the development of morbid obesity, characterized by high consumption of high-energy foods, such as fats and sugars. This caloric imbalance, where calories consumed exceed, calories expended, is the main cause of weight gain.

Keywords: Obesity, Dietary Patterns, Frequency of consumption.

1. INTRODUCTION

According to data obtained by ENSANUT 2022, it was estimated that between 6% and 8% of adults in Mexico suffer from morbid obesity, this represents a significant group of people whose Body Mass Index (BMI) is equal to or greater than 40 Kg/m². It has been observed in literature the positive relationship between dietary patterns and the development of obesity, where an energy imbalance is evidenced. [1]

Diet is one of the main factors in the overall burden of disease, as it is associated with an increased risk of chronic degenerative diseases and several micronutrient deficiencies. Consumption of non-recommended food groups such as processed meats, high sodium foods, and sweetened beverages have been associated with increased mortality, and increased risk of being overweight and obesity, respectively. [2]

The main objective of this study establishes the relationship between dietary patterns and the development of morbid obesity. This study highlights a significant health problem that affects a considerable part of the population by establishing a relationship between dietary patterns and morbid obesity.

2. MATERIALS AND METHODS

The present investigation is a cross-sectional, observational, descriptive study. It was conducted in the obesity clinic in two hospital institutions: Hospital Rubén Leñero and Hospital General Tláhuac. The study consisted of two phases:

In the first phase, the sample was selected. Patients with a BMI equal to or greater than 40 Kg/m^2 were included. Also, dietary indicators were determined using the Food Consumption Frequency Questionnaire of the National Institute of Public Health (INSP), with the aim of finding the dietary pattern that corresponds to each hospital.

For the second phase, principal component analysis (PCA) was applied to determine the dietary pattern of the population studied, where a relationship was established between the established dietary pattern and the alteration of nutritional status. This analysis was carried out using IBM SPSS Statistics software version 25.0 and XLS STAT version 2024.

3. RESULTS AND DISCUSSION

To identify the food pattern, the PCA generates new variables called components. For each component, there is a factor loading that shows the contribution of each variable, in this case food, to the formation of the component. A cut-off value of ±0.5 was used for the factor loading, which made it possible to establish the set of foods that were part of the dietary pattern.

The main dietary pattern identified in it was called 'cereal diet', since cereals constitute the food group most consumed by the population studied.

The main pattern is characterized by a high consumption of cereals, representing 30% of the recommended 22%. Likewise, consumption of high-fat foods of animal origin was 13% compared to the recommended 8%, and of oils and fats, which represented 18% in contrast to the suggested 5%. The consumption of vegetables and fruits only reached 3% compared to the recommended 50%, as well as the consumption of legumes, which is at zero consumption compared to the recommended 15%.

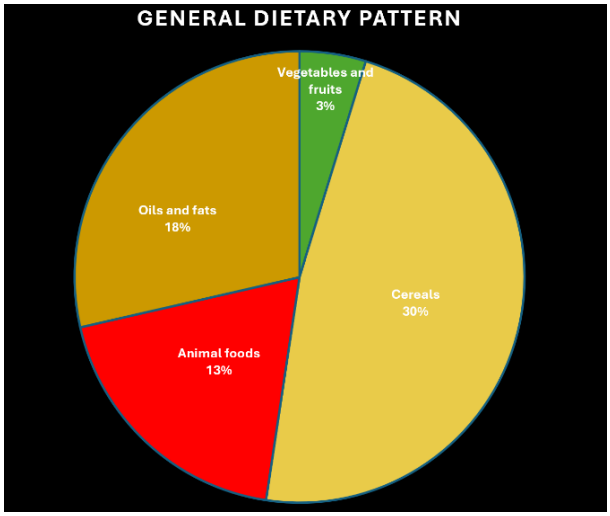

Figure 1. "Food consumption according to the groups established in the ''Plato del bien comer''.

In addition, foods that are not included in the ''Plato del bien comer'', such as Mexican food, represent 21% of total consumption, along with sugars 15%.

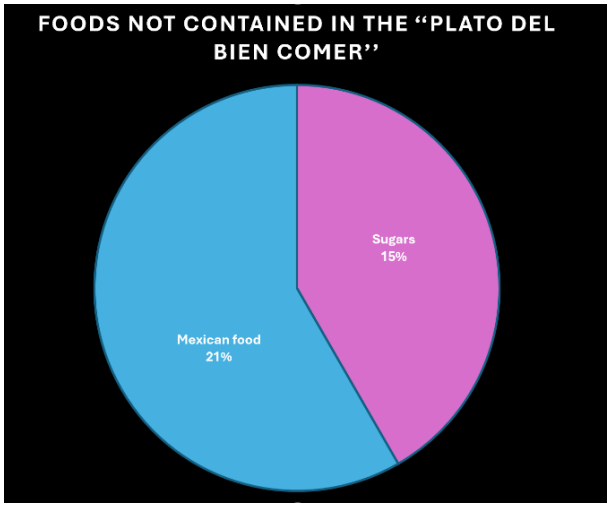

Figure 2. "Consumption of food groups, including those not contemplated in the ''Plato del bien comer''.

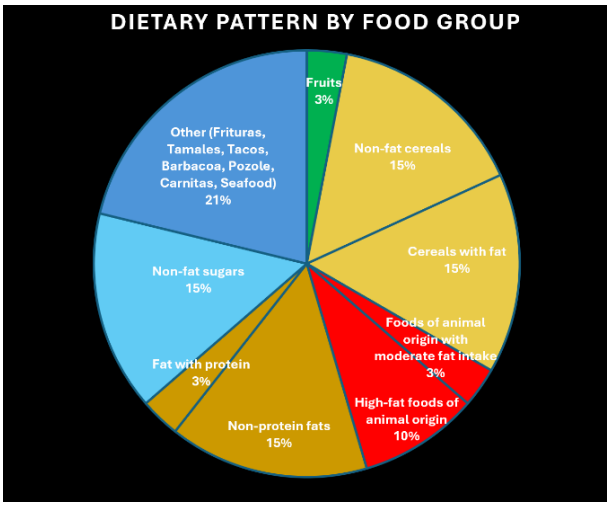

Figure 3. "Food consumption according to the groups established by the Sistema Mexicano de Alimentos Equivalentes. (SMAE)'".

The results highlight a worrying dietary pattern: on the one hand, high consumption of cereals of 30% over the recommended 22%, high-fat foods of animal origin of 13% over the recommended 8%, oils and fats of 18% over 5%. This is completed with a minimum consumption of vegetables and fruits of 3% over the recommended 50% and zero consumption of legumes compared to the recommended 15%.

In addition, the consumption of foods not included in the ''Plato del bien comer'', such as Mexican food, represented 21% and sugars 15% of the total intake. This shows that dietary patterns may be contributing factors to the development of morbid obesity.

The results clearly support the fact that unbalanced dietary patterns are related to the development of morbid obesity. Excessive consumption of low nutrient and energy-dense foods combined with low contribution of healthy foods provides strong evidence that current dietary choices are aligned with the obesity environment observed in the population.

Based on the findings, it is recommended that health professionals implement nutrition education programs that raise awareness among the population of the importance of maintaining a balanced and healthy diet. Likewise, it is suggested that policy makers review and reinforce the regulations that regulate the advertising of unhealthy foods, especially aimed at vulnerable populations. In accordance with previous research that, based on studies on the high-energy, high-fat, low-fiber dietary pattern related to fruit and vegetable intake, establishes the relationship between similar diets and metabolic dysfunctions [2, 3, 4], subsequent studies such as the one mentioned on dietary patterns and cardio metabolic health support the observation that a diet rich in fat and poor in essential nutrients correlates with metabolic disorders.

One of the interesting findings was the null consumption of legumes and the high consumption of high-energy foods such as Mexican dishes. This finding could also be related to cultural factors influencing food selection and the inadequate level of nutrition education provided to the research participants. In addition, the level at which people are encouraged to eat their traditional foods, rather than the new healthy eating habits found, could be responsible.

Further research on the relationship between cultural determinants and dietary intake is also recommended. The practical implications of these findings are clear. It is crucial to promote food policies that encourage greater consumption of fruits, vegetables and legumes, and to reduce the intake of products high in sugars and fats. In addition, public health interventions should focus on nutrition education, highlighting the importance of following balanced dietary patterns.

This research is fundamental for the field of nutrition and public health, as it provides concrete evidence on the dietary habits prevalent in a population with a high incidence of morbid obesity. It contributes to the understanding of the relationship between unbalanced diets and health problems.

Studying has several limitations that should be recognized. First, the sample size may be

insufficient to generalize the results. In addition, the methodology used for the accumulation of dietary data may be biased by the participants' memory, as it is based on the participants' own statements. Finally, factors such as access to a healthy diet, socioeconomic status, and cultural difference may impact the results and should be considered and analyzed in future studies.

According to the limitations already mentioned, one of the new areas of research would be: studies on the relationship between demographic variables of gender, age, socioeconomic level, ethnicity and, in addition, the association of psychological well-being with dietary patterns. Another area of study could be qualitative studies that address cultural and social perceptions about food in the population.

4. CONCLUSIONS

In conclusion, the development of morbid obesity is closely related to the dietary patterns adopted. Excessive consumption of energy-rich foods, particularly those high in fats and sugars, contributes significantly to caloric imbalance. When caloric intake consistently exceeds energy expenditure, it inevitably results in weight gain and progressively leads to morbid obesity. This underscores the importance of promoting balanced and conscious eating habits as a crucial strategy to prevent and manage morbid obesity, emphasizing the need for education and lifestyle modifications that favor energy balance.

This study not only provides a clear diagnosis of current dietary patterns in the population but also highlights the urgency of coordinated actions to improve the nutritional health of Mexicans and combat the growing epidemic of morbid obesity.

Acknowledgements

I would like to thank all the people and the Instituto Politécnico Nacional who have supported this research. Special thanks to Doctora en Ciencias en Alimentos Jocelyn Madrigal Acevedo, Maestro en Ciencias en Manejo de Recursos Marinos Marco Antonio Castro Reyes, Maestro en Ciencias de la Salud Eliud Salvador Aguilar Barrera, for their contribution and support in conducting this study.

Conflicts of interest

The authors declare that they have no conflicts of interest.

REFERENCES

[1] Campos-Nonato I, Galván-Valencia O, Hernández-Barrera L, Oviedo-Solís C, Barquera S. Prevalence of obesity and associated risk factors in Mexican adults: results of the Ensanut 2022. *Salud Publica Mex* 2023;65. https://doi.org/10.21149/14809

[2] Gaona-Pineda EB, Rodríguez-Ramírez S, Medina-Zacarías MC, Valenzuela-Bravo DG, Martínez-Tapia B, Arango-Angarita A. Consumidores de grupos de alimentos en población mexicana. Ensanut Continua 2020-2022. *Salud Publica Mex* 2023;65. https://doi.org/10.21149/14785

[3] Wang W, Liu Y, Li Y, Luo B, Lin Z, Chen K, Liu Y. Dietary patterns and cardiometabolic health: clinical evidence and mechanism. *MedComm* 2023;4(1). https://doi.org/10.1002/mco2.212

[4] Jordan I, Hebestreit A, Swai B, Krawinkel MB. Dietary patterns and breast cancer risk among women in northern Tanzania: a case-control study. *Eur J Nutr* 2013;52(3):905–15. https://doi.org/10.1007/s00394-012-0398-1

[5] Parri Bonet A, Villatoro Moreno M, Benaiges Boix D, Ramon Moros JM, Flores Le Roux JA, Goday Arno A. Characterization of the pattern of food consumption in severely obese patients prior to bariatric surgery. *Nutr Hosp* 2018. https://doi.org/10.20960/nh.2239

402-II-PO CYTOTOXICITY OF IMMUNOSTIMULANT MOLECULES WITH POTENTIAL ADJUVANT ACTIVITY

J. C. López-Vázquez[1], K. Delgadillo-Gutiérrez[1], J. Luna-Herrera[1]*

[1]Instituto Politécnico Nacional, Escuela Nacional de Ciencias Biológicas, Laboratorio de Inmunoquímica II, Departamento de Inmunología, Prolongación de Carpio y Plan de Ayala S/N, C.P. 11340, Ciudad de México, México

*Correspondence: jlunah@ipn.mx

Abstract: Adjuvants are essential components of vaccines; they are classified into immunostimulants and delivery systems. The immunostimulants are signaling molecules that lead to the activation and maturation of Antigen Presenting Cells (APC) by targeting Toll Like Receptors (TLR) and other Pattern Recognition Receptors (PRR) to promote antigenic signals and co-stimulators signals, which improve the adaptive immune response. Delivery systems facilitate antigen presentation by prolonging the bioavailability of loaded antigens as well as by targeting antigens to lymph nodes or APC. In this work evaluated the biological activity of molecules with potential adjuvant activity. We selected two molecules derived from triterpenes, molecules with immunostimulatory activity. Triterpenes are distributed widely in plants and are of interest because of their structural diversity and broad range of bioactivities: anti-inflammatory, antiviral, antitumor. The candidate molecules were identified as: molecule A and molecule B (an isomer of molecule A). The results indicate that molecule A exhibits cytotoxic effect, and molecule B shows an apparent proliferative activity was observed. It is important to determine whether cell death significantly impacts the adjuvant activity of the selected molecules.

Keywords: Adjuvant, immunostimulants, triterpenes, vaccine, cytotoxicity.

1. INTRODUCTION

Adjuvant comes from the Latin "*adiuvare*" which means to assist or to help [1]. In immunology, it is defined as a substance or component that enhances the immunogenicity of a vaccine when administered along with the vaccine antigen [2].

Adjuvants are classified according to their function into immunostimulants and delivery systems. There are several reasons to incorporate adjuvants into vaccines for human and veterinary use: a) increase the immune response to the immunogen; b) promote an effective and long-lasting protective state against various diseases, with particular interest in populations with suppressed immune response capability; c) require lower concentrations of antigen; d) reduce the number of vaccine doses, improving population acceptance and reducing costs and logistical requirements for the storage and distribution of biologicals [2,3].

Adjuvants are an essential component of vaccines that allow the induction of an effective protective response with an adequate safety profile [4].

Currently, there is a limitation in the use of adjuvants in vaccines, mainly due to their reactive effects. The rational design of adjuvants will allow the development of new adjuvants that meet efficacy and safety standards, that is, an effective protective response and an adequate safety profile [5].

COVID-19 has brought with it great challenges for public health worldwide in the prevention and control of infectious diseases, which highlights the importance of developing not only new effective and safe vaccines against emerging pathogens and re-emerging with pandemic potential, but also new and better adjuvants.

The purpose of this work is to evaluate the safety of adjuvants in immune system cells to determine their immunological properties that provide a broad overview for the rational design of adjuvants with application in different vaccines of public health interest.

2. MATERIALS AND METHODS

Cell cytotoxicity and proliferation assays are used for drug screening to detect if the test molecules have cytotoxic effects or cell proliferation [6].

Cytotoxicity is one of the main endpoints to be assessed in any toxicological investigation. The Alamar blue assay is widely used to investigate cytotoxicity and cell proliferation [7].

In the present study, the adjuvant capacity of two compounds derived from triterpenes is analyzed by Alamar blue assay.

2.1. Cell line

The J774A.1 mouse macrophage was cultured at 37°C, 5% CO_2 in Dulbecco's Modified Eagle Culture Medium (DMEM) added with 7% of Fetal Bovine Serum (FBS), 100 IU/mL penicillin, 100 µg/mL streptomycin and 1% L-Glutamine.

2.2. The Alamar Blue assay

A 96-well plate was inoculated with $1X10^4$ J774A.1 mouse macrophages the day before exposure. Candidate molecules A and B were added at different concentrations: 1.562, 3.125, 6.25, 12.5 and 25 µg/mL in dimethyl sulfoxide (DMSO), the plate was incubated at 37°C, 5% CO_2. Cytotoxicity was determined at 24 and 72 hours by Alamar blue reagent (1X) to a final concentration of 10%. After adding Alamar blue reagent, incubated at 37 °C for 2 h, at the end of the incubation time, the Alamar blue signal read in fluorometer at 590 nm. The negative control was untreated cells. Data is expressed as mean ± standard deviation from three replicates, a coefficient of variation <20 per test and analyzed with two-way ANOVA (Analysis of variance) ($p < 0.01$*).

3. RESULTS AND DISCUSSION

The study of molecules of natural or synthetic origin with potential adjuvant effect represents a strategic factor in the development of new vaccines against emerging and re-emerging pathogens with pandemic potential. We propose two candidate adjuvant molecules, which have already been described as molecules with immunomodulatory activity. Analysis of the minimum cytotoxic concentrations will allow us to select the appropriate concentration to evaluate their response at the cellular level in a murine macrophage model by gene expression studies and to establish the profile of the two candidate adjuvant molecules for use in vaccines.

The Alamar blue assay is based on the fluorometric redox indicator resazurin. The conversion of resazurin to resorufin is mediated by intracellular diaphorases, with NADPH or NADH as reductant. The test molecule is considered cytotoxic if the signal in the cells treated with the test molecule is reduced at least by 20% compared to the negative control [8].

Cytotoxicity analyses were performed on two candidate molecules: A and B. Molecule A did not show cytotoxic effect at concentrations 1.562, 3.125 y 6.25 µg/mL at 24 hours, but it was cytotoxic from the concentration 12.5 µg/mL at 24 hours with a viability percentage of 66%. And the cytotoxic effect was greater from the concentration 3.125 µg/mL at 72 hours with a percentage of less than 50% viability.

Molecule B did not show cytotoxic effect at the concentrations analyzed at 24 hours, but apparent proliferative activity was observed. Nevertheless, it was cytotoxic at the

concentration 25 µg/mL at 72 hours with a percentage of 58% viability. (Figure 1).

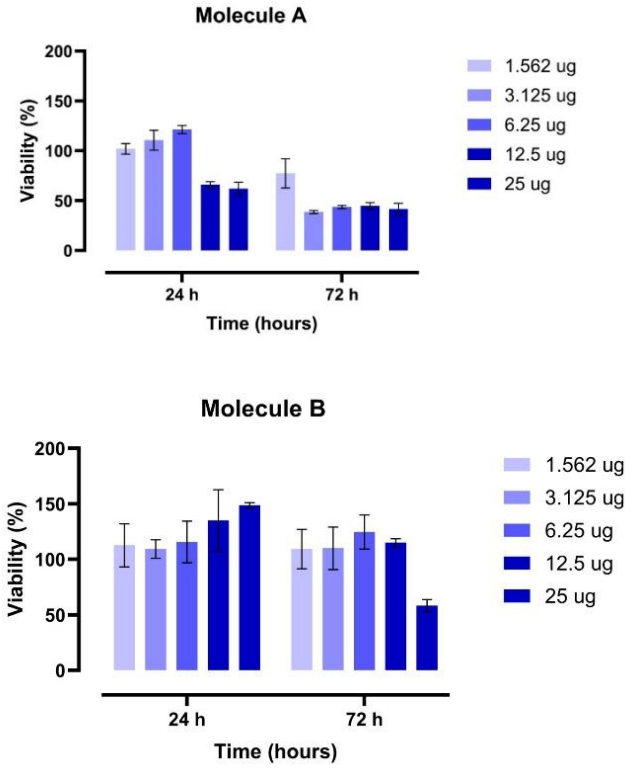

Figure 1. Cytotoxicity of molecule A and molecule B by Alamar blue assay. The J774A.1 mouse macrophages cell line was exposed to molecule A and B at different concentrations: 1.562, 3.125, 6.25, 12.5 and 25 µg/mL for 24 and 72 hours.

Many molecules have the potential as adjuvants from mineral components, water-in-oil or oil-in-water emulsions, synthetic or natural toxins derived from bacteria, and molecules of natural origin. Despite this, the specific mechanisms of these molecules are not known due to the complexity of the immune response. Therefore, based on our results it is important to determine whether cell death significantly impacts the adjuvant activity of the selected molecules.

4. CONCLUSIONS

- Candidate A presents cytotoxicity from 12.5 µg /mL at 24 hours on the J774 A.1 mouse macrophage cell line.
- Candidate B is not cytotoxic at the concentrations analyzed at 24 hours and exhibits an apparent proliferative effect on the J774 A.1 mouse macrophage cell line.
- Candidate B presents cytotoxicity at 25 µg /mL at 72 hours on the J774 A.1 mouse macrophage cell line.

Acknoeledgements

The authors are grateful for support for this work from the Instituto Politécnico Nacional with SIP- 20251343 and 20251363.

Conflicts of Interest

The authors declare no conflict of interest.

REFERENCES

[1] A. Cárdenas-Vargas, E. Q. Pedroza-Roldán. Adyuvantes pa ra vacunas: tipos, aplicaciones y modos de acción. Rev Mex Ciencias Farm. 47(3), 29–47 (2016).

[2] T. Zhao, Y. Cai, Y. Jiang, X He, Y Wei, Y Yu, *et al*. Vaccine adjuvants: mechanisms and platforms. Signal Transduct Target Ther. (2023). https://doi.org/10.1038/s41392-023-01557-7

[3] B. S. Pulendran, P. Arunachalam, D.T. O'Hagan. Emerging concepts in the science of vaccine adjuvants. Nat Rev Drug Discov. (2021). http://dx.doi.org/10.1038/s41573-021-00163-y

[4] X Chen. Emerging adjuvants for intradermal vaccination. Int J Pharm. (2023). https://doi.org/10.1016/j.ijpharm.2022.122559

[5] Y Tian, Q Hu, R Zhang, B Zhou, D Xie, Y Wang. *et al*. Rational design of innate defense regulator peptides as tumor vaccine adjuvants. npj Vaccines. (2021). http://dx.doi.org/10.1038/s41541-021-00334-3

[6] A. Aysun, Y. B. Yağmur Kiraz. Cell Proliferation and Cytotoxicity Assay. Curr Pharm Biotechnol. (2016). http://dx.doi.org/10.2174/1389201017666160808160513

[7] E. M. Longhin, N El Yamani, E Rundén-

Pran, M Dusinska. The alamar blue assay in the context of safety testing of nanomaterials. Front Toxicol. (2022). https://doi.org/10.3389/ftox.2022.981701

[8] J O'Brien, I. Wilson, T Orton, F. Pognan. Investigation of the Alamar Blue (resazurin) fluorescent dye for the assessment of mammalian cell cytotoxicity. Eur J Biochem. (2000). https://doi.org/10.1046/j.1432-1327.2000.01606.x

HORIZONTES
de Investigación y Desarrollo

III

Social and administrative sciences

17-III-PP HUMAN CAPITAL MANAGEMENT FOR THE MANAGEMENT OF PSYCHOSOCIAL RISKS IN MEXICAN SMES

V. de la C. Díaz Valdes [1]*, J. Patiño Ortiz [1]

[1]Instituto Politécnico Nacional, Escuela Superior de Ingeniería Mecánica y Eléctrica, Unidad Zacatenco, Unidad Profesional Adolfo López Mateos, Zacatenco, C.P. 07738, Ciudad de México, México.

*Correspondence: vdiazv2200@alumno.ipn.mx

Abstract: This research proposes the design and development of a viable model for human capital management in Mexican small and medium-sized enterprises (SMEs), focused on the identification and management of psychosocial risks that affect the mental and physical health of employees, in accordance with NOM-035-STPS-2018. The study addresses work stress, a factor that negatively impacts worker well-being and organizational productivity.

The model, based on organizational cybernetics and system dynamics, uses a theoretical framework relevant to physical and mental health for a comprehensive analysis of psychosocial risks. This approach is essential to ensure that interviews and surveys, aligned with NOM-035-STPS-2018, provide an accurate diagnosis of working conditions and the factors that generate stress. The data obtained will allow the construction of a causal diagram that visualizes the main causes and effects of work stress, which will facilitate the simulation of different scenarios with the aim of finding more effective interventions.

Keywords: human capital management, psychosocial risks, work stress, system dynamics, NOM 035.

1. INTRODUCTION

Any event or life situation can become stressful due to various factors: personal relationships, family life, work, and the place where it takes place. Every year, many people suffer from stress due to events experienced in the work environment. Work stress can originate from different components that generate concerns in the individual, such as fear of losing one's job or position, interest in a promotion or significant increase in salary, role conflicts that may arise perhaps between a supervisor, boss and employee, overload of responsibilities or heavy work, among other aspects no less significant that can lead to the emergence of this disorder [1].

In the field of Administrative Sciences, the management of work stress represents a critical challenge and an opportunity to improve organizational health and productivity in small and medium-sized enterprises (SMEs) [2]. Small and medium-sized enterprises (SMEs) represent a fundamental pillar of the economy, this is because they contribute significantly to the GDP, in addition to being one of the main sources of employment in a country. Likewise, due to the limited resources they have at an organizational, economic and technological level, they tend to present high levels of work stress in general within their organizations [3].

In Mexico, work-related stress represents both a social and economic problem, since this phenomenon affects workers' health and therefore their productivity, which influences business sustainability when workers' stress levels are high [4]. To avoid this situation and preserve workers' health, the Mexican government established Mexican Standard 035 of the Ministry of Labor and Social Welfare in 2018 (NOM – 035 – STPS - 2018), which constitutes a series of questionnaires and guidelines to detect levels of work-related stress and its causes within companies. Although this standard has been in place for

years, it has not yet been sufficient to mitigate this phenomenon, which is why it is imperative to explore new innovative strategies that support more effective management of work-related stress.

In recent years, there have been several authors who have been interested in this topic and the study of this phenomenon, since they recognize the rise of work stress in Mexico and the adverse implications that it brings as a consequence. The Autonomous University of Mexico (UNAM) has carried out several of these studies and has concluded that Mexico is among one of the countries with the highest level of work stress globally. By 2019, 40% of the Mexican population presented high levels of work stress, leading to Burnout Syndrome (chronic stress). After COVID-19, in 2021, after carrying out another analysis, these figures increased to 63%, a quite alarming value.

According to the Mexican Social Security Institute (IMSS), approximately 75% of Mexican workers suffer from work-related stress. This figure is higher than in countries such as China and the United States, and is associated with health problems such as gastrointestinal disorders, sleep disturbances, headaches and a higher risk of cardiovascular and psychological diseases [5].

Despite the existence of NOM – 035 – STPS - 2018, many SMEs in Mexico have failed to effectively implement the measures necessary to manage work-related stress. This may be due to the lack of predictive models adapted to the particular characteristics of SMEs, as well as a limited understanding of psychosocial factors. specific ones that predominate in this sector. Workplace stress remains a persistent problem that negatively affects the mental and physical health of workers, as well as the productivity and competitiveness of companies [2].

1.1 Research question

How can the development of a viable model based on system dynamics principles improve the management of Human Resources in Mexican SMEs in a way that promotes a healthy and sustainable work environment?

1.2 Research Objective

To design a viable model for the proper management of human resources in Mexican SMEs, which allows for optimizing personnel management, reducing work-related stress, and improving employee well-being and productivity, through the integration of systemic approaches and organizational cybernetics strategies.

1.3 Importance of the study

This study is of great economic and social relevance, since, as previously stated, SMEs are a fundamental pillar of the economy, which have a positive impact on the Gross Domestic Product (GDP) of a country. However, these companies face constant challenges because they often have limited resources, are located in informal markets, and their organizational structures are not strong enough to remain in the global market.

The capacity of SMEs to generate employment makes this significant increase possible within the economy, but at the same time, they also influence the social level within the country. Work stress affects the health of workers, in such a way that it affects their productivity, as well as generating absenteeism because workers with high levels of work stress are unable to maintain a high flow of work and sometimes have to take leave due to medical incapacity.

The proposed viable model resolves a gap in research, because although there are already several studies that highlight the importance of work-related stress in Mexico and the use of NOM – 035 – STPS – 2018 as a tool for analyzing and detecting psychosocial risks, no studies have yet been detected that promote the use of system dynamics and organizational cybernetics in order to maintain the sustainability and viability of the study of this phenomenon. This project proposes a Viable Model based on the Viable System Model (MVS) of Stafford Beer, which is capable of

adapting to the conditions of Mexican SMEs, aligning itself with the regulations proposed by the government, the NOM – 035, in order to achieve more effective management of work-related stress, and promote the improvement of employee well-being, a healthy work environment, and business sustainability and stability.

2. MATERIALS AND METHODS

2.1 Materials and participants

The target population for this research is comprised of small and medium-sized enterprises in Mexico. SMEs will be initially identified through commercial databases, chambers of commerce and industry associations. Companies will then be contacted to verify their willingness and eligibility to participate, sending them an invitation letter explaining the objectives and benefits of the study. Finally, confirmed companies will be stratified by geographic region, size, industrial subsector and level of innovation, ensuring balanced representation across all strata.

Simulation tools will be used to design causal loop diagrams, such as Ithink software. These diagrams will allow you to visualize the complex interrelationships between the selected variables, identifying feedback loops and time delays that affect work stress.

2.2 Study design

The methodological framework of this research is designed to comprehensively address the phenomenon of work stress in Mexican SMEs. This study employs a mixed approach, combining quantitative and qualitative methods, to capture the complexity of work stress and evaluate the effectiveness of a dynamic compliance model based on organizational cybernetics and system dynamics. By using questionnaires, interviews, and advanced simulation tools, the aim is to obtain accurate and relevant data that will contribute to this study and make it possible to meet the stated research objective.

(Table 1) summarizes the general aspects that make up the methodological design of this study.

Table 1. Methodological design of the research.

Type and scope	Description
By object of study:	Technological
By depth:	Correlational and descriptive
By primary sources of information:	Questionnaires, interviews.
From secondary sources of information:	Review of literature, commercial databases and statistics.
By approaching the object:	Mixed, inductive and deductive.

2.3 Data collection

Semi-structured interviews and focus groups will be conducted to obtain qualitative data. Structured surveys will also be distributed based on Reference Guides I, II and III proposed by NOM – 035 – STPS – 2018.

2.4 Data Analysis

Quantitative data collected through the questionnaires will be analyzed using statistical software such as SPSS or Excel. Descriptive measures such as means, medians, standard deviations and frequencies will be calculated to understand the distribution of stress indicators among employees.

Correlations between different variables will be explored using statistical tests such as Pearson or Spearman. This analysis will help to identify significant relationships between psychosocial risk factors and the level of work stress.

Using tools such as IBM SPSS Modeler, predictive models will be developed to identify factors that predict stress. These models will be based on the integration of quantitative and qualitative data, allowing the prediction of work stress under different conditions and scenarios.

In Figure 1, a brief summary of the methods used and the materials in each corresponding case is made.

Methods	Tools
Literature review, interviews, questionnaires.	Academic databases, survey tools and NOM-035-STPS-2018
Causal loop diagrams, preliminary simulations, pilot study.	Ithink simulation software, dynamic simulation tools.
Data collection, interviews, focus groups.	Online questionnaires based on NOM - 035, Videoconferencing tools.
Descriptive statistical analysis, correlational analysis, predictive modeling.	Statistical software SPSS, Excel, Pearson tests, IBM SPSS Modeler.

Figure 1. Correlation of Materials and Methods.

2.5 Ethical considerations

Ethical considerations for this study include ensuring the confidentiality and anonymity of participants by obtaining their informed consent prior to data collection. Participation will be guaranteed to be voluntary and employees will be able to withdraw from the study at any time without consequences. In addition, data handling will be in accordance with information protection regulations, and results will be presented in a way that does not identify any participating individual or company.

3. RESULTS AND DISCUSSION

3.1 Results

After obtaining the variables through an exhaustive review of the literature and integrating them with the psychosocial factors proposed in NOM – 035, a causal map has been created in which all the relationships and correlations between them are contemplated. Knowing that positive relationships influence the variables proportionally and negative relationships are inversely proportional. See Figure 2.

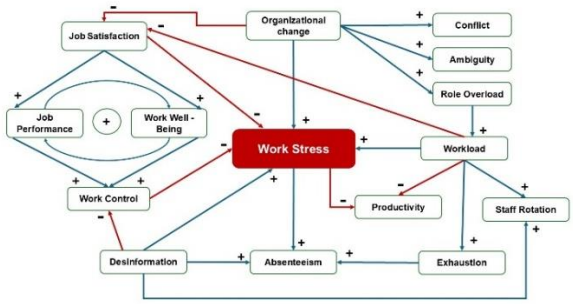

Figure 2. Causal Diagram of Work Stress.

Once the causal diagram of work stress has been obtained, the model is designed in the think software. To do this, it is decided to establish Work Stress as the central variable, then the remaining variables are classified and placed in five main categories: Job Satisfaction, Change Organizational, Work Overload, Absenteeism and Environment. Both the Job Satisfaction category and the Organizational Change category has subcategories that define the positive aspects that produce a decrease in stress, as well as the negative aspects that cause an increase.

Once the categories have been established and the variables that correspond to them have been defined, it is decided that the categories that cause an increase in stress are located on the left side of our central axis in the Forester Diagram design and those that produce a decrease on the right side.

A first design of the model is carried out in which only the connections of the variables are established according to their nature or category and their impact on work stress. See Figure 3.

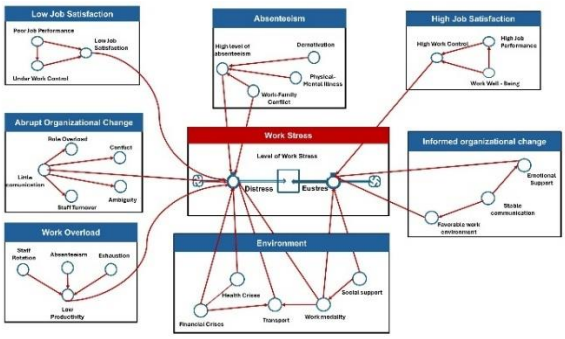

Figure 3. Forester diagram of simple connections.

Subsequently, in order to understand the complexity of the model, another diagram design is developed in which, in addition to showing the simple connections shown in Figure 3, the correlations of the variables are established regardless of their nature or category, so that the incidence of one with another can be understood independently of whether they affect work stress directly or indirectly. See Figure 4.

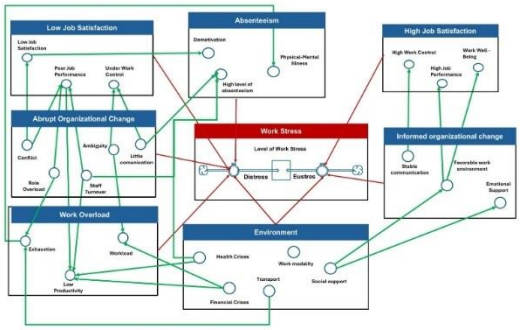

Figure 4. Forester diagram of complex connections.

By designing these diagrams, it was possible to understand the complexity of the variables and their impact on the phenomenon. Once this was understood, it was necessary to identify how it could influence the systems proposed by Beer in the Viable System Model, which is why it was decided to integrate both models.

Once these influences have been determined, these variables are inserted into the relevant systems of the Viable System Model proposed by Stanford Beer. This model has five systems, which allow a system to be viable, due to their connections between themselves and the characteristics of the current and future environment. See Figure 5.

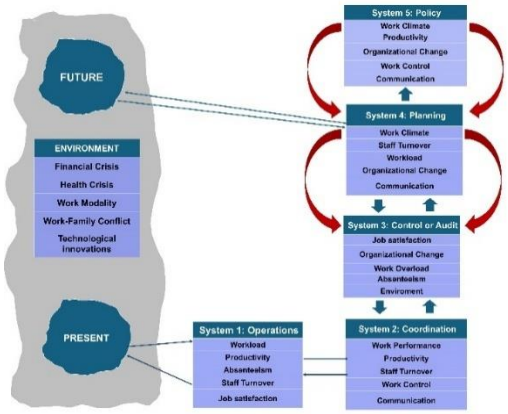

Figure 5. Viable System Model for Human Capital Management in SMEs.

If system 3 in Figure 5 is analysed in detail, it becomes clear that the psychosocial factors or variables that affect it are the union of the different categories that were proposed at the beginning of the model for the development of its simulation. This relationship is due to the fact that system 3 functions as the central axis of the rest of the systems and therefore all the variables that have been proposed for the development of the model and the detection of the level of work stress that companies may have converge or derive from it.

3.2 Discussion

Stratifying variables such as organizational change, job satisfaction, work overload, and absenteeism allows us to analyze how these interact and affect work stress. Using the Cause-Effect Diagram in Ithink dynamically visualizes these relationships, highlighting both positive and negative effects. Integrating these variables into Beer's Viable System Model provides a framework for assessing the feasibility of interventions to mitigate work stress, underscoring the importance of centralized management in this process.

The discussion of the results highlights the complexity of work-related stress and the need for a multidisciplinary approach to its management. In addition to regulatory

compliance such as NOM-035, it is necessary to develop organizational policies and wellness programs that promote healthy work environments. When comparing the results with previous studies in Mexico, the use of Beer's Viable System Model offers a more complete view of work-related stress management. In conclusion, the integration of these findings reinforces the importance of preventive strategies that improve both employee well-being and organizational success.

As a limitation of this study, it is necessary to highlight that the implementation of the dynamic model depends on data that may not fully capture the complexity of work stress in all organizational contexts, as well as the application of NOM-035-STPS-2018 may vary between companies, which may influence the effectiveness of the proposed interventions.

Future methodological research could explore advanced simulation models and artificial intelligence to obtain more accurate predictions on work stress in SMEs. On a theoretical level, organizational resilience could be investigated as a mediator between organizational change and work stress, and the impact of organizational culture on stress management. In practical terms, the development of intervention programs and flexible work policies to improve workplace well-being is recommended, especially in the context of remote work.

4. CONCLUSIONS

The study identified factors such as organizational change, job satisfaction and work overload as key factors in work stress in SMEs, using the Viable System Model. It also contributes to the field by providing a systemic approach to managing work stress in SMEs, providing new methodological tools. The results serve to create strategies to improve work well-being and reduce stress in organizations. Finally, it is suggested to implement interventions focused on change management and improving organizational culture.

Acknowledgements

We would like to thank the National Polytechnic Institute, through the Secretariat for Research and Postgraduate Studies, the Higher School of Mechanical and Electronic Engineering (ESIME), and the National Council of Humanities, Sciences and Technologies (CONAHCYT) for providing the necessary facilities for this work.

Conflict of Interest

The authors declare that they have no conflict of interest.

REFERENCES

[1] Brito Ortíz, J., Balderas, G., & Lago, A. (2021). Validation and internal consistency of the questionnaire to identify psychosocial risk factors of NOM-035-STPS-2018.

[2] Herrera, RA, Patricia, C., Picón, O., Díaz González, CL, Daniela, A., & Escobar, J. (2020). Occupational stress in the workplace in Mexico (case study), in correlation with the approach of NOM-035-STPS 2018. Innovation and Technological Development, 20 (4). http://www.imss.gob.mx/salud-en-linea/estres-laboral.

[3] IMSS. (2024). Work Stress. https://imss.gob.mx/salud-en-linea/estres-laboral

[4] OECD. (2017). Enhancing the Contributions of SMEs in a Global and Digitalized Economy. Meeting of the OECD Council at Ministerial Level.

[5] Pienkowski, T., Keane, A., Castelló and Tickell, S., de Lange, E., Hazenbosch, M., Khanyari, M., Arlidge, WNS, Baranyi, G., Brittain, S., Kapoor, V., Smit, IPJ, & Milner-Gulland, EJ (2023). Supporting conservationists' mental health through better working conditions. Conservation Biology, 37 (5). https://doi.org/10.1111/cobi.14097

[6] UNAM. (2022, April 15). Mexicans, the most stressed in the world. https://www.dgcs.unam.mx/boletin/bdboletin/2022_305.html

21-III-PP GREEN BONDS TO IMPROVE THE GROWTH OF THE BIOENERGY MARKET IN MEXICO

C. A. Salinas Olivo[1*], M. Á. Martínez García[1**], J. C. Trejo García[1***]

[1]Instituto Politécnico Nacional, Escuela Superior de Economía, Calle Plan de Agua Prieta 73, C.P. 11350, Ciudad de México, México.

Correspondence: csalinasco1700@alumno.ipn.mx, mmartinezga@ipn.mx**, jtrejog@ipn.mx***

Abstract: Mexico's growing population and industrial energy demand have put pressure on conventional energy sources. According to the Instituto Mexicano para la Competitividad [1], energy consumption in Mexico will grow by 2.5% annually between 2023 and 2037, reaching 480,000 GWh in 2037, 44% more than in 2022. Therefore, clean energy sources, such as bioenergy, are being explored to meet this demand. The objective of this research is to compare the strategies and economic and social impacts of Green Bonds in Germany, China, Spain and the United States, using financial and non-financial indicators to promote the growth of the bioenergy market in Mexico. The methodology included descriptive and comparative statistical analysis, using Pearson's correlation coefficient to identify similarities and differences in the use and issuance of these bioenergy bonds in the countries studied. An increase in the use of bioenergy in Mexico was estimated for 2030, in line with the European Union's *Fit for 55* legislative package, which aims to reduce greenhouse gas emissions by 55% by 2030 compared to 1990 levels. The results showed that the use of Green Bonds, following their international counterparts and with a correlation of 0.80 between GDP and renewable energy generation in Mexico, can increase the bioenergy market by 37% with respect to current production.

Keywords: Green Bonds, Bioenergy, Renewable Energy, Sustainability, ESG Criteria.

1. INTRODUCTION

Mexico's energy consumption is constantly growing, so much so that conventional energy sources have been compromised in meeting the energy needs of the population, so new alternative energy sources such as renewable energy, clean energy and/or bioenergy have been studied to promote their use and thus help reduce this energy demand. Nevertheless, the main obstacle to the adoption of bioenergy is the need to demonstrate its viability and sustainability as a mitigation measure. In addition, they face economic and social acceptance challenges that require a favorable public policy framework to stand out as a viable alternative for the decarbonization of the energy sector [2].

In 2007, the European Investment Bank (EIB) introduced a financial tool that revolutionized the existing model, called Green Bonds (a bond whose proceeds are used exclusively for the financing or refinancing, in whole or in part, of new and/or existing eligible green projects.). In Mexico, in 2015, Nacional Financiera issued a green bond for the first time, [3]. However, to date, Mexico has not had any green bond issuance in the bioenergy sector. The hypothesis is that the comparison of strategies and projects financed by Green Bonds in Germany, China, Spain, and United States will help to expand the bioenergy market in Mexico.

Therefore, Green Bonds could be considered as an alternative to promote the growth of the Mexican bioenergy market. Through an

analysis of the period from 2016 to 2023, we aim to generate guidelines to promote the growth of the bioenergy market. In addition, it aims to provide useful information for entrepreneurs, SMEs, other countries interested in strengthening this sector, and for investors who want to allocate resources to environmentally conscious projects. In this way, it promotes the country's economic growth and stimulates its energy sovereignty.

2. MATERIALS AND METHODS

In order to fulfill the main objective of this research, and due to the scarcity of data on Green Bonds in the bioenergy sector in Mexico, a descriptive and comparative statistical analysis methodology is used in relation to the use and issuance of Green Bonds in the field of bioenergy. This allows comparison of the frequency, volume and number of emissions, as well as the environmental and social impact of the financed projects. Successful strategies and policies that have been implemented and the challenges overcome in each country are highlighted, to offer valuable guidance for the implementation of similar initiatives that encourage the growth of the bioenergy market in Mexico.

This methodology uses the collection of two or more samples to observe how a given variable behaves, while statistically controlling for other variables that could affect the variable under study [4].

This research will be enriched with case studies focusing on the issuance of Green Bonds in the bioenergy sector, specifically in Germany, China, Spain and the United States. The choice of these countries as a reference for comparison with Mexico in the field of bioenergy Green Bonds is based on the international experience they have accumulated in the implementation of programs and policies related to renewable energy production and the use of Green Bonds.

The aim is to analyze in detail how these countries have optimized their energy production and generated positive social, environmental and governance impacts through the implementation of these bonds, with the aim of identifying lessons learned and best practices that can serve as a guide for Mexico as it moves towards a greener economy.

The proposed overall design of the comparative descriptive methodology for this research can be schematized as follows:

$$\begin{array}{ccccccccccc} & & & & & & & & & & \\ O_1 & \approx & O_2 & \approx & O_3 & \approx & O_4 & \approx & O_5 & \approx & O_6 \\ & \neq & & \neq & & \neq & & \neq & & \neq & \end{array}$$

$$\begin{array}{ccccccccccc} & & & & & & & & & & \\ O_7 & \approx & O_8 & \approx & O_9 & \approx & O_{10} & & & & \\ & \neq & & \neq & & \neq & & & & & \end{array}$$

$$\begin{array}{c} M_1 - O_1 \\ M_2 - O_2 \\ M_3 - O_3 \\ M_4 - O_4 \\ M_5 - O_5 \\ M_6 - O_6 \\ M_7 - O_7 \\ M_8 - O_8 \\ M_9 - O_9 \\ M_{10} - O_{10} \end{array}$$

$M_x =$ Work Samples
$M_1 =$ Volume of issues in Green Bonds
$M_2 =$ Amount of Green Bond issuances
$M_3 =$ Priority areas for investment
$M_4 =$ Estimated reduction of Co_2 emissions (ton/year)
$M_5 =$ Contribution to energy production through renewable energy sources
$M_6 =$ Estimated energy savings
$M_7 =$ Gross Domestic Product
$M_8 =$ Bioenergy generation
$M_9 =$ Bioenergy projects financed by Green Bonds
$M_{10} =$ ESG Indices
$O_x =$ Sample observations

On the other hand, the application of a Pearson correlation analysis in this study will allow us to describe the linear relationship between the GDP variable and the contribution to energy production by renewable energy generation, with the objective of obtaining a quantitative measure that shows the association between these elements through a correlation coefficient.

This coefficient varies in a range from +1 to -1, where a value equal to or greater than +1 indicates a perfect positive relationship, while a value less than zero suggests an inverse relationship between the variables.

Eq. (1)

$$r = \frac{n(\Sigma xy) - (\Sigma x)(\Sigma y)}{\sqrt{[n\Sigma x^2 - (\Sigma x)^2][n\Sigma y^2 - (\Sigma y)^2]}}$$

Where:

n = number of data pairs

x = GDP values

y = values of the contribution to the production of renewable energy

3. RESULTS AND DISCUSSION

Through the analysis of the CBI database and the review of reports and briefings, (Table 1) was elaborated in detail, highlighting the Green Bonds allocated to projects focused on the generation, use and promotion of bioenergy per country.

Table 1. Summary of Bioenergy Green Bonds allocation by country 2016 – 2023.

Country	Green Bonds for bioenergy	Amount issued in dollars	Installed capacity (MW)	Energy production (GWh)	CO^2 emissions avoided (ton/year)
Germany	21	$ 5,171,536,214	4,135	12,225	13,926,372
China	9	$ 1,488,514,047	1,827	3,291	1,544,797
USA	13	$ 3,008,195,000	2,010	7,026	7,899,252
Spain	5	$ 2,168,603,805	1,008	2,140	1,289,836
Mexico	0	0	0	0	0

Source: Own elaboration based on Climate Bonds Initiative 2023.

It should be noted that Germany has committed a significant amount of funding to bioenergy projects, averaging around $246 million per project, and is the country that avoids the most CO_2 emissions annually, demonstrating its crucial role in the transition to more sustainable energy sources and in the fight against climate change.

China's efforts have resulted in a remarkable impact on installed renewable energy capacity, registering just over 1800 MW from 2016 to 2023, which has a direct impact on reducing carbon dioxide emissions, avoiding the release of approximately 1,544,797 tonnes per year.

US bioenergy production reflects progress in total bioenergy production of 7026 GWh. In addition, this expansion has played a key role in reducing the country's greenhouse gas emissions by avoiding 7,899,252 tonnes per year. This means that, in absolute terms, the emissions avoided by the United States as a result of the measures implemented in the projects are 411.08% higher than those of China.

Finally, Spain has several bioenergy projects with an average financing of $434 million, which is higher than Germany, although it has fewer projects. The average installed capacity per project in Spain is 202 MW, slightly higher than Germany's 197 MW, suggesting a focus on higher capacity installations. These differences may reflect differences in efficiency, technologies, and deployment policies between the two countries, despite being part of the European Union.

(Table 2) shows the correlation between each country's GDP and its renewable energy production. The coefficient of determination R^2 was obtained using a simple linear regression model, while the adjusted R^2 comes from a multiple linear regression model that includes additional variables to improve the accuracy of the analysis.

Table 2. Descriptive statistics of GDP variables and renewable energy generation by country 2016-2023.

Regression statistics	Germany	China	USA	Spain	Mexico
Multiple correlation coefficient	0.97	0.98	0.97	0.73	0.8
Coefficient of determination R^2	0.94	0.96	0.95	0.53	0.65
R^2 adjusted	0.94	0.95	0.94	0.45	0.59
Standard error	14.73	52.48	14.73	80676.61	3.56

Source: Own elaboration 2024.

However, even though Spain has a more mature economy and a more consolidated energy policy, the ratio between economic growth and renewable energy generation (0.73) is slightly lower than in Mexico. This difference could be due to recent global conditions, such as increased investment in green infrastructure and international pressure to reduce emissions, which have had a greater impact in Mexico. This difference could be due to recent global conditions, such as increased investment in green infrastructure and international pressure to reduce emissions, having a more significant impact in Mexico.

Figure 1 shows a forecast of bioenergy growth for 2030, obtained using the exponential smoothing method. This method gives more weight to more recent data and less weight to older data, allowing for more accurate estimates. In particular, it highlights the significant increase that Mexico could experience if it adopted the strategies implemented by the United States and China, such as the issuance of Green Bonds to finance bioenergy projects.

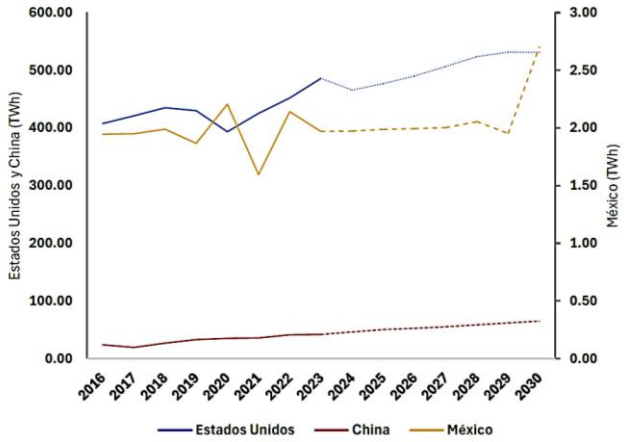

Figure 1. Estimation of the growth of the bioenergy market with the use of Green Bonds by 2030.
Source: Own elaboration 2024.

According to projections based on data from 2016 to 2023, bioenergy production is expected to grow by 14% in the United States, by a staggering 41% in China and by a remarkable 37% in Mexico by 2030.

With the data obtained, it is certain that in the short-term bioenergy production will continue to be a segment with strong growth in the Mexican Republic, given the volume of projects underway and the favourable policies implemented for its expansion. It is shown that Mexico could look to the experience of the US and China in issuing Green Bonds to develop strategies adapted to its national context, from diversifying energy sources to promoting and researching bioenergy production technologies, in order to encourage significant growth in this sector.

This is in line with an investigation that suggest that it is possible to increase the efficiency and effectiveness of the energy matrix through an appropriate technological and financial innovation procedure that serves as a guide for the adoption of bioenergy production technologies with a clean technology approach [5]. It is also in line with another item, where at a global level, environmental concerns act as a moderator between Green Bonds and sustainable investments [6].

If Mexico chooses to use Green Bonds to finance different projects in the bioenergy sector, as the US and China have done, this would have a strong impact on the Mexican energy matrix, not only in terms of promoting the use of renewable energy, but also in terms of annual CO_2 reductions.

4. CONCLUSIONS

This study highlights the wide range of renewable energy resources available in Mexico. Bioenergy, as part of these resources, is presented as an alternative with a great real potential to contribute to the decarbonization of the energy sector. In addition, the contribution of Green Bonds in the investment market has proven to be an excellent option as a financial instrument that seeks to mitigate or adapt to future situations.

In relation to the hypothesis is accepted by observing that the comparison of strategies and projects financed by Green Bonds in countries such as Germany, China, the United

States and Spain offers a significant boost to the bioenergy market in Mexico. A 37% increase in bioenergy production is projected, suggesting that by integrating lessons from these countries and taking into account relevant social, economic and political factors, Mexico has the potential to transform its energy landscape in the coming years.

Internationally, all countries are exposed to the conflicts that can arise as a result of climate issues, and given the impending consequences of increased energy consumption, many companies have already prioritised the use of Green Bonds as a sustainable investment tool.

Mexico has demonstrated that, even without a national green taxonomy, it has been able to successfully issue 32 Green Bonds through the use and enforcement of existing regulations and standards, so the publication of the Mexican Sustainable Taxonomy in 2023 will further benefit the development of projects that contribute to the environment. It has also been established that the country's GDP growth rate from 2016 to 2023 is 60% in relation to the production of renewable energy generated by investments in this type of project.

However, it is necessary for the private and public sectors to work together to create more support programs for sustainable projects, to have a better energy efficiency programme and to strengthen the policies, tax incentives and financing strategies that are currently available, so that the positive effects of these improvements are diversified and felt in the economic, social and environmental areas of Mexico.

It is particularly important to continue working on the continuous improvement of the country's current infrastructure so that the proposal made in this research can be implemented efficiently. In addition, the implementation of these renewable sources could be faster if companies in the public sector were the main players, since having the knowledge and, above all, the means to produce them would make it easier to achieve a sustainable transition. Therefore, as investments continue to be made in the issuance of more Green Bonds for bioenergy production, Mexico will continue to see greater social and economic benefits, underscoring the need to highlight the importance of this energy sector through this work.

Acknowledgements

The authors would like to thank the Graduate Studies and Research Section of the School of Economics, and the Secretariat of Research and Graduate Studies of the National Polytechnic Institute, for the support granted through the registered research '20240282 and 20240364'.

Conflicts of Interest

The authors declare no conflict of interest.

REFERENCES

Online document

[1] Instituto Mexicano para la Competitividad. El PRODESEN 2023-2037 incrementa artificialmente las cifras de generación de energía limpia en México. 2023. https://imco.org.mx/el-prodesen-2023-2037-incrementa-artificialmente-las-cifras-de-generacion-de-energia-limpia-en-mexico/ Accessed 31 may 2024

[2] Martínez-Bravo RD, Masera O. Perspectivas de disminución de emisiones de carbono en México por el uso de la bioenergía: Panorama actual. Elementos para Políticas Públicas. 2020;4(1):27-42. https://www.elementospolipub.org/ojs/index.php/epp/article/view/28 Accessed 26 April 2024

[3] Consejo Consultivo de Finanzas Verdes. Caso de estudio. Bono verde NAFF 16V. 2016. https://www.mexico2.com.mx/uploadsmexico/file/Caso%20de%20Estudio%20-%20NAFF%2016V.pdf Accessed 12 January 2024

Book

[4] Sánchez, H., & Reyes, C., Metodología y diseños en la investigación científica (Business Support Aneth, 2015), pp. 45-46

Journal article

[5] Muto Lubota D, González Suárez E, Hernández Pérez G, Miño Valdés JE. Modelo conceptual y procedimientos para asimilar tecnologías de producción de bioenergéticos de biomasa residual. Centro Azúcar. 2016;43(3):29-38

[6] Wang F, Liu J. Green bond and corporate environmental investment: The moderating effect of environmental concern. Finance Res Lett. 2024;65

44-III-PO COMPETITIVE AND INNOVATIVE STRATEGIES IMPLEMENTED BY MSMES IN SOUTHERN MEXICO CITY TO SURVIVE THE COVID-19 CRISIS

A. V. Pérez Domínguez[1]*, E. F. Galicia Haro[1], I. C. Ortega Moreno[1]

[1]Instituto Politécnico Nacional, Escuela Superior de Comercio y Administración, Unidad Tepepan, Periférico Sur 4863, C.P. 16020, Ciudad de México, México.

*Correspondence: aperezd1401@alumno.ipn.mx, smile_av@hotmail.com

Abstract: The objective of the work was to establish what competitive and innovative strategies were implemented by some of the MSMEs of the Tlalpan and La Magdalena Contreras mayor's office during March 2020 to 2023 to survive the COVID19 crisis and remain competitive to survive in the market.

The theory used was Porter's competitiveness and innovation was indicated by the Oslo Manual. Based on this, an analysis of twelve case studies was carried out where the actions carried out by MSMEs were investigated by conducting interviews with owners, customers, and observation guides.

The results were that both MSMEs in the trade and services sector used differentiation and cost strategies. He highlights that despite being MSMEs, the cost strategy was used in all cases. Additionally, it was observed that the innovations were mainly in processes and marketing.

Keywords: MSMEs, Covid-19, competitive strategies, innovation, Mexico.

1. INTRODUCTION

Micro, small and medium-sized enterprises (MSMEs) have great relevance within the country's economy. Since they are responsible for being the generators of employment and sustenance for the population. These have a high impact on GDP, as it is estimated that they contribute 42% to it.

Consequently, the development and maintenance of MSMEs is of great importance to reduce poverty and the economic development of the country [1].

In Mexico, MSMEs are mostly family businesses, however, they are often in the informal sector because they lack the organization and planning to manage the business well. Likewise, the most common problems they face are the lack of liquidity and consequently they do not have good financing.

However, MSMEs report a series of competitive obstacles such as the limits they have within the market, their financing, lack of technology and innovation, among other circumstances. This position leads to productivity gaps that establish great challenges to diversify the country's economy.

This study seeks in general terms to know the competitive and innovative strategies implemented by MSMEs to survive during the Covid-19 crisis. In this way, the objective that guided the research was to establish what competitive and innovative strategies were implemented by some of the MSMEs of the Tlalpan and La Magdalena Contreras mayor's office during March 2020 to March 2023 to survive the COVID19 crisis and remain competitive and survive.

2. MATERIALS AND METHODS

In 2020, the impact of the Covid-19 pandemic began to be seen, [1] released the average life expectancy of businesses from 2019 to 2021, where it was identified:

The monthly death rate is 1.45% while the birth rate is 0.81%, which means that, for every

10,000 establishments existing at any given time, in the span of a month 145 die and 81 are born [1]. As can be seen in Figure 1.

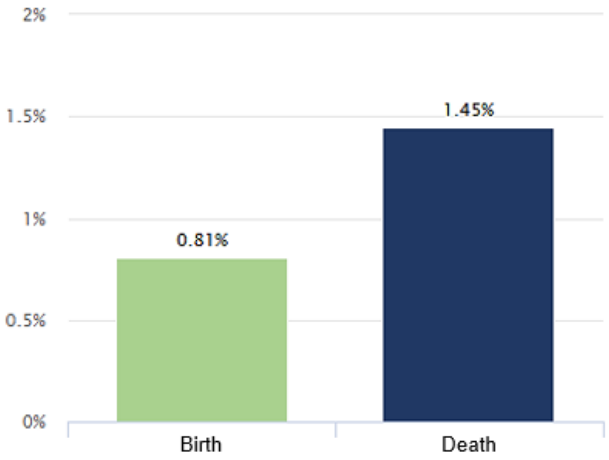

Figure 1. Monthly Business Birth and Death Rate 2019-2021 [1].

Porter [2] indicates that competitive strategies are essential for companies to survive and thrive in an increasingly competitive market. Among the strategies are cost, differentiation and approach. Porter suggests that for MSMEs, strategies should be differentiated because they must be attractive to the customer in the midst of similar competitors, in contrast to the cost strategy where the company, due to its size, can make use of economies of scale. This strategy is best suited for large companies. [2].

When it comes to innovation, according to the Oslo Manual [3], there are four types of innovation: product, processes, marketing, and organization. According to these innovations in MSMEs in the commercial sector, innovation would be expected mainly in processes and marketing, for MSMEs in the services sector in processes and marketing. (OECD/Eurostat, 2005).

2.1. Subsection

The research is based on the design of a case study and considers twelve representative cases of the population of MSMEs in the commerce and services sector located in the municipalities of Tlalpan and La Magdalena Contreras.

As it is a case study, the triangulation of the information is sought to give reliability to the results, for this there are three sources of information: Owners of MSMEs, customers of MSMEs and direct observation of the facts.

For the case studies, the categories of analysis were "competitive strategies" and "innovation".

The collection of information was developed in 4 phases:

1) Information collection and qualitative analysis: It consisted of collecting direct qualitative information through interviews with the direct owners of MSMEs.

2) Information collection and quantitative analysis: It consisted of collecting direct quantitative information through interviews with the direct customers of MSMEs in relation to the categories of analysis.

3) An observation guide was made in which the researcher paid attention to details and carefully observed what happened in the object of study of the research to collect pertinent data.

4) Finally, the data collected by the three instruments were analyzed, then a comparison was made between the businesses of the two municipalities, and it was identified if there was a relationship of similar competitive and innovative strategies that allow answering Porter's theory and innovation.

3. RESULTS AND DISCUSSION

The results indicate that MSMEs used competitive differentiation strategies as Porter points out in both the trade and service sectors, but also made use of cost strategies in both sectors while maintaining fixed prices. It should be noted that Porter's theory in the case of cost strategy was applied despite the size of MSMEs.

Likewise, the results indicate that in MSMEs in the commerce sector, innovation was that of

processes with new forms of collection and innovation in products introducing products suitable for the needs according to Covid -19, innovations in marketing were the least.

As for MSMEs in the service sector, innovation was process with the introduction of home delivery service and marketing innovation with 2-for-1 promotions, which confirms what is indicated in the Oslo Manual. It is worth mentioning that these innovations presented in MSMEs are as a whole innovation activities that result in innovation within companies.

4. CONCLUSIONS

Covid-19 was a pandemic of great changes that came to reform the lives of everyone, as people, since it was a world-class pandemic, there were changes in all aspects of daily life, it affected society in many ways.

This thesis emphasizes that Mexico has been economically destabilized, considering that MSMEs contribute 42% of the Gross Domestic Product (GDP) and generate 78% of national employment. In addition, with everything that happened with the pandemic, many businesses did die.

Therefore, the development of this work allows us to answer the question: what were the competitive strategies implemented by MSMEs in the commerce and service sector in the municipalities of Tlalpan and La Magdalena Contreras to survive the Covid-19 crisis in the period March 2020 to March 2023?

Among the competitive strategies used by MSMEs were differentiation and cost strategies. In the commercial sector, various differentiation strategies are presented, such as night service, extended hours, etc., but cost strategies using affordable prices while taking care of customers' pockets stand out. For the service sector, the differentiation strategies were mainly home delivery and in the cost strategies they maintained their fixed prices.

The strategies were innovative for MSMEs because they resulted from an innovative activity that occurred due to the crisis. They were mainly processing innovation in activities that were not carried out prior to the crisis such as the introduction of home delivery service, new forms of collection, secondly, there is product innovation with the introduction of products required by customers and as a result of the pandemic. Finally, there was an innovation in marketing with the use of promotions, discounts and the use of social networks for promotion.

Acknowledgements

I thank the 12 MSMEs and their clients who gave me their support to be able to carry out this research.

Conflicts of interest

The authors declare that they have no conflict of interest.

REFERENCES

[1] INEGI, (2021). [Online]. Available: https://www.inegi.org.mx/temas/dn/#Informacion_general.

[2] S. Suñol, "Aspectos Teoricos de la Competitividad," *Ciencia y sociedad,* (2006) pp. 179-198.

[3] OECD/Eurostat, «Oslo Manual: Guidelines for Collecting and Interpreting Innovation Data,» (OECD Publishg, Paris, 2005) https://doi.org/10.1787/9789264013100-en.

61-III-PO ACCESSIBILITY IN TOURIST SITES FOR THE CARE OF VISITORS WITH CHRONIC-DEGENERATIVE DISEASES IN THE MUNICIPALITY OF CULIACAN, SINALOA

L. A. Tomás Fernández[1]*, M. M. Maldonado Ávalos[2], L. A. Gaytán[3]

[1]Instituto Politécnico Nacional, Escuela Superior de Turismo, Av. Miguel Bernard 39, C.P. 07630, Ciudad de México, México.

*Correspondence: leslieamericatf@outlook.com

Abstract: This study focuses on the importance of accessible tourism in Culiacán, Sinaloa, and its positive impact on people with chronic diseases. The municipality, with its geographic and cultural wealth, faces public health challenges such as diabetes and hypertension. These people in tourism not only promote equal rights but can also boost economic development and improve the reputation of the destination.

Part of the documentary research carried out so far has revealed that the importance of accessible tourism is contemplated in the Sinaloa State Development Plan 2022-2027 (PED) and that inclusive tourism is part of public policies aimed at the Sustainable Development Goals (SDGs), specifically SDG 11, which seeks to make cities and human settlements inclusive, safe, resilient and sustainable. Inclusive tourism, as a key component of accessibility, plays a crucial role in this goal by ensuring that tourism experiences are accessible to everyone, regardless of physical or health limitations.

The qualitative research will be developed in several stages that are still ongoing. First, a documentary search will be carried out to identify the current barriers in the existing tourist infrastructure. Subsequently, strategies will be proposed to improve said infrastructure and create adapted services. Data will be collected, and the results will be analyzed and interpreted.

The objective of this research is to facilitate universal access to tourist experiences and promote a more inclusive and sustainable society.

Keywords: tourism, accessibility, chronic-degenerative, public policies, SDGs.

1. INTRODUCTION

Accessible tourism has become essential to create an inclusive society, in which all people, regardless of their abilities or health limitations, can enjoy barrier-free tourist experiences. In the state of Sinaloa, the commitment to accessible tourism is part of the public policies outlined in the State Development Plan 2022-2027, whose specific objective (Strategy 2.1.1) is to promote inclusive tourism in the state's tourist destinations [8]. In this context, Culiacán, the state capital, faces accessibility challenges that directly impact a significant portion of its population. According to the National Institute of Statistics and Geography (INEGI), there are 147,958 people with disabilities in Sinaloa, representing 4.7% of the total population, of which 63,781 are older adults, a sector especially vulnerable to chronic-degenerative diseases [5]. These diseases, such as diabetes, hypertension, and heart disease, affect mobility and reduce the possibilities of participation in recreational and tourist activities, impacting the quality of life of those affected and hindering their social inclusion.

In addition, life expectancy in Sinaloa is 75.1 years, close to the national average of 75.2 years [4], which reinforces the need to adapt tourism services to ensure that older people and people with chronic health conditions have access to these spaces safely and comfortably. Incorporating the context of chronic-degenerative diseases is crucial, since these conditions not only limit mobility, but also represent unique challenges for

accessibility in tourism services. Addressing this reality allows for the design of adequate infrastructures and services, offering an inclusive experience and promoting the right of all people to participate in the social and cultural life of their community.

The main objective of this research is to identify and evaluate the barriers in Culiacán's tourism infrastructure that affect accessibility for people with chronic-degenerative diseases. In addition, it seeks to propose universal design strategies and accessibility policies that allow these visitors to enjoy tourist resources safely and comfortably, promoting inclusive tourism that contributes to the economic and social development of the municipality.

This study contributes to the field of inclusive tourism, addressing a gap in the literature on tourist accessibility in specific contexts of chronic diseases and in Mexican cities such as Culiacán. On a practical level, it provides recommendations that align the municipality's tourism development with the policies established in the Sinaloa State Development Plan 2022-2027 and the SDGs. It also promotes an accessible tourism model that can be replicated in other cities with similar characteristics.

2. MATERIALS AND METHODS

This research is cross-sectional with a qualitative approach, using the ethnographic method to gather information.

With the information obtained from documentary research and that recovered from secondary sources of information (government sites and web pages), the research continued with the preparation of a diagnosis, which allows to identify mainly the accessibility that the tourist sites in the municipality have, considering the current regulations and the technical aspects that they require. From the analysis of this information, information will be obtained in a documentary manner by experts in the treatment of chronic diseases (specialist doctors, psychologists and psychiatrists) that will allow to identify the basic requirements so that this sector can have enjoyment and pleasure within the recreational, leisure and tourist activities, these being a driver part of their treatment in the management and control of stress. In this way, the necessary bases will be supported to generate an adequate analysis on a significant part of the real problem, since later we will seek to obtain information from the other substantial part where it will be identified through interviews with visitors with chronic conditions on what aspects would help improve their experience within the tourism value chain, these aspects could derive beyond the limitations in the physical infrastructure, but rather the social, discriminatory or emotional aspect that they could perceive.

Table 1. Data collection.

Source	Instrument	Result
Tourist Attractions	Inventory of attractions and accessibility verification sheets	Offer and degree of accessibility.
Attraction managers	Semi-structured interviews	Interest in compliance with current regulations.
Medical specialists	Semi-structured interviews	Contribution of tourism activity to the treatment of patients.
Psychologists and psychiatrists	Semi-structured interviews	Stress management and control in participation in tourism activities.
Sectur Sinaloa	Semi-structured interviews	Compliance with public policies.
Visitors with chronic conditions	Semi-structured interviews	Most significant barriers.

Source: Own elaboration.

3. RESULTS AND DISCUSSION

The evaluation carried out in the main tourist attractions of Culiacán allowed us to identify the current state of accessibility and the efforts underway in terms of inclusion. The most relevant findings are presented below:

1. Number of Tourist Attractions Evaluated: 15 representative sites of the tourist offer of Culiacán were evaluated. These sites include museums, public squares, recreational spaces and places of cultural interest.

2. Current Level of Accessibility: None of the 15 tourist attractions evaluated complies 100% with the accessibility parameters established by national and international standards. However, most of the sites have partial initiatives, such as access ramps and signage, although with significant areas of improvement in terms of design and quality of accessibility elements.

3. Classification of Inclusion and Accessibility Initiatives: At each site, the presence of at least one initiative in terms of inclusion was observed, but significant variability was identified in the quality and functionality of these measures.

4. Need for Quantification and Classification of Accessibility Quality: A lack of quality metrics to assess the effectiveness of implemented accessibility initiatives was identified. This makes it difficult to identify priority areas for improvement and to plan meaningful interventions. For example, some existing ramps do not meet slope standards, which affects their usability for people with motor disabilities.

5. Areas for Improvement Detected: Although there is progress in accessibility initiatives, a more structured and in-depth approach is required to achieve full accessibility. Below are some of the key areas for improvement observed:

- ✓ Improve signage for people with visual impairments.
- ✓ Increase accessibility in sanitary services and rest areas.
- ✓ Implement accessible maps and Braille signage at points of interest.

The results of this study indicate that, although Culiacán has taken some steps towards inclusion and accessibility, progress remains limited and fragmented. The absence of a site that fully complies with accessibility standards highlights the urgent need to integrate a more comprehensive approach aligned with international regulations.

These findings are consistent with previous studies on tourist destinations in Mexico and Latin America, which have identified low compliance with full accessibility in destinations, despite having partial initiatives [1]. The situation in Culiacán is like that of other cities that, although they have accessibility regulations, face challenges in their implementation due to limited resources and lack of awareness in the tourism sector.

An unexpected finding was the variability in the quality of accessible ramps and areas within the same tourist attraction. This suggests that, although initiatives exist, supervision and maintenance of the infrastructure is limited, possibly due to the lack of monitoring protocols or funding.

The implementation of quality criteria and a continuous evaluation system could significantly improve access to tourist sites in Culiacán. In addition, accessibility training for tourism staff and collaboration with the private sector would be crucial steps to strengthen accessibility in the municipality's tourism sector.

This study has some limitations. By focusing on a specific group - people with chronic-degenerative diseases - the analysis of accessibility has been limited to their specific needs. However, the inclusion of this group has revealed a greater need to adapt accessibility to meet a wide range of requirements. This suggests that inclusive accessibility should also consider the needs of other vulnerable

groups or those with different limitations, increasing the complexity of the criteria to be evaluated and the resources needed to achieve universal accessibility. In addition, the sample size, limited to 15 tourist attractions in Culiacán, restricts the generalization of the results at the state level.

4. CONCLUSIONS

This study has highlighted the importance of improving the tourist infrastructure in Culiacán to make it accessible and safe for people with chronic degenerative diseases. However, it is based on the premise that no tourist site can be 100% accessible, since there will always be aspects that cannot be fully covered, even with the highest standards of accessibility and universal design. The findings show that the main tourist attractions in Culiacán implement inclusion and accessibility initiatives, although there is still a need to quantify and classify these efforts to create a quality experience that is equitable for all.

This research highlights the importance of integrating accessibility on an ongoing basis, supporting the right to social inclusion and contributing to the health and well-being of people with chronic conditions. By pointing out the impossibility of achieving full accessibility, this study promotes the idea of accessibility as a process of constant improvement. In doing so, it is aligned with public policies, such as those of the Sinaloa State Development Plan 2022-2027, and with the Sustainable Development Goals (SDG), especially SDG 11, which promotes inclusive and sustainable cities and spaces.

Tourist accessibility directly contributes to the emotional and physical well-being of people with chronic diseases, who benefit from the stress reduction and rehabilitation opportunities offered by recreational spaces. These benefits have significant implications, since promoting accessible tourism reduces pressure on health services while supporting social and economic inclusion. The premise that there will always be more to improve drives the need for continuous audits and updates to Culiacán's tourist infrastructure.

It is recommended to establish clear standards for accessibility in the municipality's tourist attractions and apply periodic audits to ensure that these measures evolve and adapt. By promoting a culture of constant improvement in accessibility, tourism operators are encouraged to invest in inclusive infrastructure, aligning with the State Development Plan and the SDGs. Furthermore, future studies could explore the applicability of this model in other municipalities and for other vulnerable groups, thus expanding the positive impact of accessible tourism.

This study reaffirms the importance of accessible and inclusive tourism as a fundamental right. Accessibility in tourism not only fosters equality and well-being for visitors, but also becomes an opportunity for sustainable economic and social development in Culiacán and beyond.

Conflict of Interest

The authors declare that they have no conflict of interest.

REFERENCES

[1] Alén E, Losada N, de Carlos P. Accessibility tourism in Latin America: An analysis of the current situation. Journal of Tourism and Development. 2017;27:21-36

[2] Gobierno del Estado de Sinaloa. Plan Estatal de Desarrollo de Sinaloa 2022-2027. Culiacán: Gobierno del Estado de Sinaloa; 2022

[3] Gobierno Municipal de Culiacán. Reglamento de construcciones para el municipio de Culiacán. Culiacán: Gobierno Municipal de Culiacán; 2020

[4] Instituto Nacional de Estadística y Geografía (INEGI). Censo de Población y Vivienda 2020: Esperanza de vida en Sinaloa. [INEGI]. Sinaloa: INEGI; 2020 [citado 2024 oct 26]. Disponible en: https://www.inegi.org.mx

[5] Instituto Nacional de Estadística y Geografía (INEGI). Informe Anual sobre la Situación de Pobreza y Rezago Social en Sinaloa. [Internet]. Aguascalientes: INEGI; 2024 [citado 2024 oct 26]. Disponible en: https://www.inegi.org.mx

[6] Organización de las Naciones Unidas (ONU). Objetivos de Desarrollo Sostenible [ODS]. [Internet]. 2015 [citado 2024 oct 26]. Disponible en: https://sdgs.un.org/goals

[7] Organización Internacional de Normalización (ISO). UNE-ISO 21902: Turismo accesible para todos. Requisitos y recomendaciones. Ginebra: ISO; 2021

[8] Plan Estatal de Desarrollo 2022-2027 (PDE). Estrategia 2.1.1: Fomentar el impulso del turismo accesible en los destinos turísticos del estado de Sinaloa. Culiacán: Gobierno del Estado de Sinaloa; 2022

90-III-PP MANAGEMENT STRATEGIES FOR IMPROVING FINANCIAL EDUCATION IN FEMALE HIGH SCHOOL STUDENTS

M. Hernández González[1], J. M. Ramos Quiroz[1], F. J. Chávez Maciel[1]*

[1]Instituto Politécnico Nacional, Escuela Superior de Comercio y Administración, Unidad Santo Tomás, Manuel Carpio 471, C.P. 11340, Ciudad de México, México.

*Correspondence: mahego19@gmail.com

Abstract: Currently, the skills developed by female students during their school career are increasingly relevant, both for their personal and professional lives, so the integration of financial education within their academic career represents an urgent need, and the role of the school principal is crucial for their insertion in the academic environment. This paper analyzes previous studies related to the subject, in addition to the information generated through the application of questionnaires and interviews to a sample of students, teachers and school principals. Methodologically, worked under a mixed approach using mainly qualitative techniques and instruments complemented with quantitative data.

Among the main results, it was found that most of the female students manage money at an early age, besides being heads of household and even being part of the main family income. They show interest in being financially educated within the school environment. In the case of the results generated by teachers and directors, both recognize their role in the promotion of financial education, however, there are several obstacles that prevent its insertion, such as the lack of links between private and public organizations for its dissemination within schools, apathy to learn and teach it by students and teachers, added to the delegation of functions that correspond to the directive management to promote it.

Among the practical implications that this study suggests are: planning from the Continuous Improvement Plan (CIP) of managers, for the linkage with institutions that are dedicated to the promotion of financial education with a gender perspective, in addition to promoting the insertion of at least two activities related to financial education during the school year, implementation of existing teaching materials on financial education aimed at women, in the long term it is considered relevant to design a financial education program aimed exclusively at female students.

Keywords: management, strategies, financial education, female students, high school.

1. INTRODUCTION

Financial education is considered one of the engines of a country's social and economic development because it gives its citizens the ability to make better decisions in this area of their lives [1].

Financial education focused on women has gained relevance in school activities at a global, regional and national level, despite this, in high school institutions in Mexico its presence is null or minimal, being this an element that could prevent students from obtaining skills that improve their quality of life and reduce stereotypes and gender gaps existing in their environment.

This is due to several factors, but the lack of participation of school authorities, specifically at the management level, is what hinders their insertion in schools.

Under these two contexts, both the existence of a deficit in the teaching of financial education at the high school level, which represents the last stage of formal education for a large part of the female student

population, and considering that school authorities are key players in promoting these educational activities, the problem that sustains this research derives from the great relevance that financial education with a gender approach has acquired in the educational sphere. However, in high school institutions in Mexico, its implementation is nonexistent, which limits the development of financial skills in female students, which could improve their quality of life and reduce existing gender gaps.

Therefore, the objective of this research is to propose viable management strategies for the promotion of financial education applicable to female students in two general high school zones in the State of Mexico. In order to achieve this, four specific questions were posed with their respective objectives, which include the economic and financial context of the students, the existing contents that can be applicable to the students, what are the main obstacles that prevent management from promoting financial education, and what are the elements that will allow the design of strategies that promote this type of content.

Regarding the importance of this work, in terms of theoretical value, it will allow to generate knowledge in an area in which not enough information has been found in the literature, allowing to fill a gap that consists in identifying and addressing problems such as the gender gaps that still exist in financial education in the educational environment, specifically in female students. In terms of management, it will make it possible to plan and connect specialized activities on the subject, in coordination with the different internal and external agents of the school.

In terms of social relevance, these strategies aim to contribute to reduce the gender gap, provide female students with skills to improve their financial future and show the importance of the managers of educational institutions in the development of female students.

2. MATERIALS AND METHODS

For the purposes of this research, two high schools were selected as the object of study, both established in the eastern part of the State of Mexico and of public support. In each school, three populations were considered, made up of students, teachers, and administrators, as shown in Table 1.

Table 1. Research samples.

Samples	High school 1	High school 2
Students	140	109
Teachers	8	6
Managers	3	1

This research is considered under the mixed approach, since it generates a more complete understanding regarding the objectives and enrichments on educational phenomena, in this work we mainly used qualitative techniques and instruments such as semi-structured and flexible interviews, complemented with quantitative data collection techniques and instruments such as structured questionnaires, both with the purpose of broadening and deepening the information and opinions of the research subjects.

It is considered an exploratory, descriptive, and cross-sectional study, since the study will only be carried out during a given period. In order to achieve the research objectives, the documentary analysis or research method was used in the first instance, which consisted of detecting, consulting and obtaining various primary and secondary sources of information. Subsequently, field work was carried out to complement and support the information obtained from the documentary research through questionnaires and interviews whose validity and reliability was guaranteed through a pilot test of the instruments, which were validated through the review of two experts in the field of management and financial education, to be subsequently applied to 20 female students, two teachers who had held

management positions at some point in their professional careers, and an active manager in office.

The analysis of the information from the surveys was carried out through the creation of content analysis categories according to each of the main responses; for the interviews, content analysis techniques were applied through the reading of the interviews to obtain relevant information for the research.

The next step was to implement the method of generation and evaluation of strategies, since it constitutes an important phase, as it is an effective resource in the creation and proposal of strategies that promote educational and social development projects, in addition to considering it as the basis for the proposal of this work.

3. RESULTS

3.1 Analysis of results female students

Seventy-five percent of the respondents were between 15 and 17 years of age, while 24% were between 18 and 21 years of age.

249 female students surveyed, 45% of them responded that they do have economic dependents, in some cases being mother, father, siblings and/or children, as stated by CONDUSEF one out of every three households in Mexico are headed by a female between 15 and 19 years of age.

Regarding the economic income of female students, Figure 1 shows that it is divided into two groups: those who work and receive the Benito Juárez Universal Scholarship for their studies (39%) and those who do not work but also receive school support (61%), receiving this money has made them part of the support of their households and given them obligations for which many of them are not qualified because of the stage they are in. Due to situations such as the one mentioned in the previous paragraph, [2] emphasizes that it is important for women to have financial knowledge, as this will provide them with a better use of their resources, not only economically but also socially and at work.

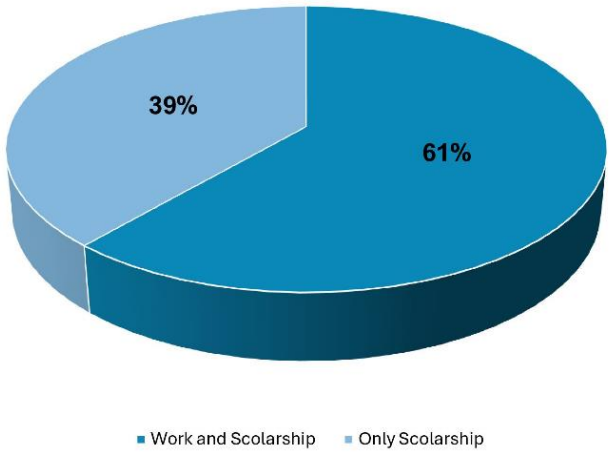

Figure 1. The economic income of female students.

In terms of their autonomy and financial administration, 68% mentioned that they are completely responsible for the administration of their resources, while 29% do it together with another person, 4% of them assure that it is another person who oversees administering their resources. Although the results of the sample showed positive data on the autonomy of resources, part of this sample shows that there is still what [3] calls a lack of economic autonomy in women, where despite generational and role changes, there are still families in which women's decision making requires authorization from one or more members of their close circle, encouraging the control of a third party in their finances and widening the gap in financial autonomy between men and women.

3.1.1 Analysis of results female students about financial education

Regarding financial knowledge, 51% answered yes, while 49% answered in the negative, Figure 2. When asked if they know what financial education or personal finance education is, 51% of the sample answered yes, while 49% answered negatively.

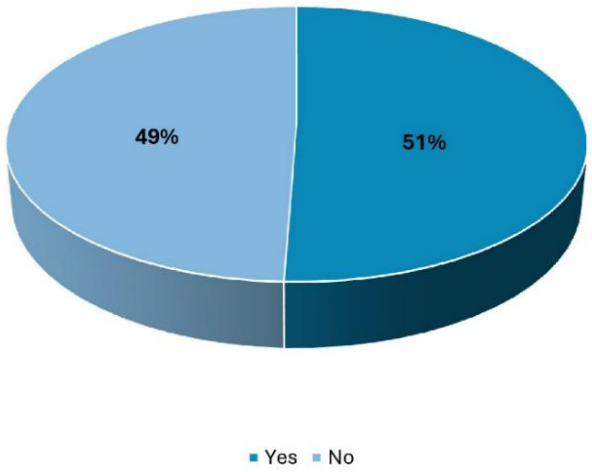

Figure 2. Willingness to learn financial education.

The motives for learning financial education, as shown in Figure 3, are mainly to improve their money management and quality of life, financial independence and avoid debt, while fewer female students consider this as an opportunity to learn new knowledge and increase their capital.

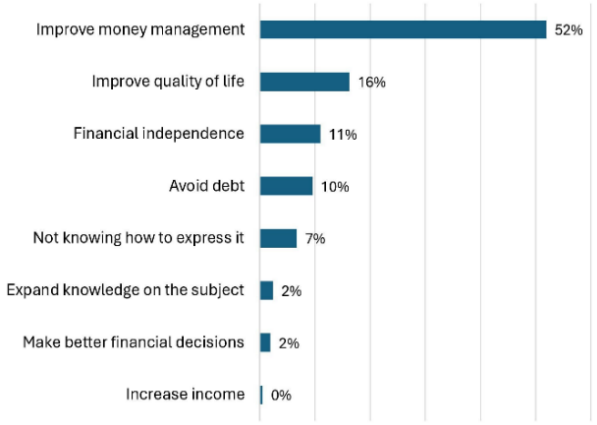

Figure 3. Reasons to learn financial education.

The results are positive, teaching financial education with a gender perspective allows women to develop financial skills that will ultimately pay off in positive abilities to access, compare and choose the best financial services, both for themselves and their families, and in the creation of entrepreneurship.

3.2 Perception of teaching financial education to female students

100% of the teachers surveyed agree that it is necessary and very important to teach this content to female students during their school career. Teachers were asked if they have ever promoted any financial education program or topics in their classes, 29% of them answered yes, while 71% answered negatively.

As a result of the above, they were also asked if they would be interested in promoting financial education topics, in this case the answers were 79% positive and 21% negative.

3.3 Perception of management financial education to female students

Regarding the question of whether the management team considers it is important to educate female students about financial topics, all four affirmed that it is important.

Regarding the opinions on whether self-managed financial education is valid, in addition to that which could be provided at some point in the school, the directors consider it relevant, mainly because little or no financial education is taught in the schools, due to the fact that, for more than 15 years, the study plans and programs no longer contemplate specific financial content within the curriculum.

Although they support the fact that students should learn about these topics outside the classroom, they consider that they should do from credible sources, to avoid biases that could lead them to make wrong decisions, due to the amount of false information that circulates in the context in which they are immersed.

3.3.1 Management to promote financial education programs in your institution

When asked about who they consider should be the educational authority in responsible for managing and providing financial education to female students, they suggest that at the state level it should be the General Direction,

and at the zone level, school supervision should propose related activities.

In their respective schools, they recognize that this is a work they should promote, but that due to their busy schedules they have delegated these activities to other school figures such as guidance counselors and teachers, since they have autonomy in their classes with respect to the activities, they are the ones who would be more involved in developing activities of this type.

The other two directors, in their management role, must manage and provide support in matters of protocol and signatures on permissions, official documents, certificates and others.

With respect to the directors who had not managed programs or activities related to financial education, they stated that they are interested in doing so, but they do not consider that they have the school's economic resources to access them if they are paid, and they do not know if they have the teaching staff trained to carry out these actions or if they are interested in promoting and generating contacts to access these activities.

4. DISCUSSION

Through a combination of a review of the existing literature related to the topic, together with the analysis of the results obtained in the research, some relevant aspects are discussed below.

It is important to highlight the need to teach financial education with a gender perspective to female students in this context, since they can be considered a group at risk of vulnerability, both because of the level of obligations acquired at their young age, as well as because of the access to financial resources delegated to them by the fact of receiving a scholarship, This should represent an opportunity for them to learn how to manage these resources in the best possible way and to provide them with the skills to make better decisions derived from the range of products available in the market, which financial inclusion has placed within their reach and which, as shown in the results, [4] mentions that a financial education program that intends to address the gender perspective should go beyond changing the colors for those that are considered exclusive to women, or make the contents simpler and have specific characteristics that generate competencies that help women solve problems.

In the case of teachers, 100% of the sample answered yes and justified their answers from aspects that benefit female students, recognizing their vulnerability due to their sex and context. As mentioned by [5], financial education programs tend to have successful and positive results when they comply with certain characteristics, among which are: being focused (aimed at a specific group), specifying a specific topic or content, and when it is understood that this will contribute to the wellbeing of a vulnerable group.

The reasons mentioned are diverse, but the substantial majority are concentrated on lack of content within their study plans, lack of incentives, lack of time and not knowing how to include it in their planning because they do not know the topic. Although at first it can be considered that the above can be taken as pretexts or apathy, [6] can consider it as part of the challenges faced by teachers at the level, since changing or addressing unknown topics as well as using new methods and techniques is something that can cause frustration in them, since the above can have an impact on students learning and developing competencies that can help them to have a full and valuable life.

The teachers also suggested the most appropriate activities for the students, remembering that due to the time they spend with them during classes, they are the expert and appropriate figures, after the students themselves, to provide better ways to bring this knowledge to them.

Regarding the contributions made by the directors, it is worth mentioning that these were made using the interview method, which

gave us the opportunity to observe in greater depth the experiences, perceptions and contributions that the directors in charge of the educational institutions have regarding the subject of this research.

Certainly, the task of linkage and management is already a well-known activity, but the topic of financial education with a gender perspective is not, and although it could be considered a topic that has already been discussed at global and regional educational levels, it certainly still has many areas of opportunity to work on in Mexico's high schools.

5. CONCLUSIONS

In general, it is concluded that students, teachers, and directors recognize, to a greater or lesser extent, the importance of financial education.

Regarding the economic context, this is based on several factors, marked by economic inequality, whose members in most of their homes depend both on the income from informal employment and on the receiver of educational scholarships granted by the government. In terms of the financial knowledge they have about financial education, most of them understand the term and recognize that it can be important knowledge for their daily and future life. About the existence of financial education contents that can be useful in teaching this specific group, after analyzing the answers where they specify the topics that most interest them, added to the topics that teachers also consider essential, it is concluded that the ones that present adequate contents for the audience by age and gender are the following: Cuentas Contigo by Junior Achievement, Finanzas para Jovenes by FOVISSTE, Zentra tus finanzas and Taller de Finanzas personales by Inspiring girls and Black Rock México.

Regarding the obstacles that limit management, the following were found lack of resources, lack of knowledge of the importance and impact of this knowledge on female students, little or no training of teachers on financial issues, lack of time to implement more activities than those scheduled, and apathy of teachers and students.

With respect to the elements that would allow the design of management strategies, it was concluded that an in-depth diagnosis of needs and the context in which female students develop is necessary, evaluating their levels of knowledge on the subject, their financial practices, and the main socioeconomic barriers they face. Adaptation of the contents of the study programs in an integral manner, urging those that can be transversalized and that are specifically designed for female students.

Conflict of Interest

The authors declare that they have no conflict of interest.

REFERENCES

[1] Sundarasen, S., Usha R., Malathi K., and Kamilah K. "Women's Financial Literacy: A Bibliometric Study on Current Research and Future Directions." Heliyon 9, no. 12 (2023): e21379.https://doi.org/10.1016/j.heliyon.2023.e21379

[2] Bannier, E., & Milena S. "Gender- and Education-Related Effects of Financial Literacy and Confidence on Financial Wealth." Journal of Economic Psychology 67 (2018): 66-86. https://doi.org/10.1016/j.joep.2018.05.005

[3] Choudhary, H. & Jain, H. Addressing Financial Exclusion through Financial Literacy training programs: a Systematic Literature Review. Empirical Res Voc Ed Train 15, 8 (2023). https://doi.org/10.1186/s40461-023-00147-9

[4] Castañeda, K., Ramírez-Montoya, M.S., y Morita, A. Educación financiera con perspectiva de género: revisión sistemática de literatura. IE Revista de Investigación Educativa de la REDIECH, 14, e1826. (2023).

https://doi.org/10.33010/ie_rie_rediech.v14i0.1826

[5] Kaiser, T., Lusardi, A., Menkhoff, L. & Urban, C. J. Financial education affects financial knowledge and downstream behaviors. National Bureau of Economic Research. Working Paper, 27057. (2020). http://www.nber.org/papers/w270571050

[6] De Beckker, K., Compen, B., De Bock, D., & Schelfhout, W. The capabilities of secondary school teachers to provide financial education. Citizenship, Social and Economic Education, 18(2), 66-81. (2019). https://doi.org/10.1177/2047173419850152

109-III-PO MANAGEMENT PRACTICES FOR THE ACCREDITATION OF ENGINEERING PROGRAMS IN MEXICO

L. Lobato Azuceno[1]*, R. A. Gómez Ortiz[1]*, L. Rocha Lona[1]*

[1]Instituto Politécnico Nacional, Escuela Superior de Comercio y Administración, Unidad Santo Tomás, Manuel Carpio 471, C.P. 11340, Ciudad de México, México.

*Correspondence: llobato@ipn.mx, ragomez@ipn.mx, lrocha@ipn.mx

Abstract: Higher education in Mexico is confronted with significant challenges pertaining to its quality and the assurance that its graduates possess the requisite competencies and skills to enter the labor market, both nationally and internationally. The accreditation of engineering academic programs serves as a mechanism to substantiate the quality of education provided in higher education institutions, with the objective of enhancing competitiveness, facilitating internationalization, and promoting international collaboration within the academic community.

The aim of this paper is to present the findings of a doctoral thesis which contextualises the problematization of management policies on the accreditation of educational programmes.

The methodology is of an analytical reflexive type, derived from a review of the literature on international accreditation of engineering programs. The analysis yielded the following main problems: the high costs of the accreditation process, the difficulty of incorporating CACEI criteria into the development of academic programs, the level of participation of the different actors in higher education institutions (HEIs) in the accreditation process, and the role of accrediting bodies as a decisive figure in the accreditation process.
In conclusion, the policies for the accreditation of higher education programs underwent significant changes in 2018, affecting both HEIs and accrediting agencies, as well as government agencies responsible for higher evaluation and accreditation. The aforementioned changes may exacerbate the issues identified in this study; however, understanding their underlying causes may facilitate their resolution.

Keywords: Accreditation, Higher Education, Engineering, Quality

1. INTRODUCTION

The need for competitive engineering professionals in the global context has prompted Higher Education Institutions (HEIs) to adopt strategies aimed at enhancing the competitiveness of their engineering students and demonstrating that their educational programmes align with international quality standards. This approach enables professionals to develop their skills in a context characterised by constant change.

The accreditation of engineering education programmes is one of the demands made by international organisations, such as the Organisation for Economic Co-operation and Development (OECD), the World Bank, the Inter-American Development Bank and others, to the different member countries of these organisations. This is with the purpose of favouring internationalization and international cooperation.

The accreditation of engineering programmes that meet international criteria offers a number of benefits, including the ability to project internationally, facilitate academic and research mobility, and identify areas for improvement in line with the evaluation criteria.

In Mexico, the accreditation of engineering programmes is voluntary. However, the current General Law of Higher Education,

published in 2021, promotes the evaluation of engineering programmes.

Engineering in Mexico

Mexico has public and private institutions that teach engineering, from technical, undergraduate and postgraduate levels; these institutions are offering quality programmes, which result in engineers who are highly qualified to provide solutions to the country's problems, favouring the economy and offering technological innovation in different fields.

The Mexican Ministry of Economy (SE) in its report Mexican talent for growth and relocation, in 2023, reports that: 'there are 335 careers and higher education programmes related to information technologies, engineering, manufacturing and construction [1]. It also records that 37.5% of the 451,000 undergraduate, graduate and postgraduate students studied science, technology, engineering and mathematics (STEM) each year. This places Mexico among the seven OECD countries with the highest proportion of STEM graduates [1].

The [1], records that:

'The supply of engineering in Mexico is mainly focused on the fields of electronics, industrial, mechanical, construction and chemical processes. In 2021, a little more than 83 thousand engineers graduated in these areas (69.5 % of the total engineering supply).

37.9% of STEM graduates come from State Public Universities (UPES), being the National Polytechnic Institute the institution that has a graduation rate of 9000 undergraduates. With this number of engineering graduates, Mexico is positioned as one of the countries in Latin America that has qualified and specialised human capital to enter the national and international labour market; and while it has the talent, it is necessary to demonstrate it through the accreditation of study programmes.

The National Polytechnic Institute, a federal public HEI, offers 41 engineering education programmes, thus training engineers who will benefit the development of the country in different areas. Among the engineering programmes offered are data management, artificial intelligence and biotechnology, which contribute to the UN's sustainable development objectives and therefore to the country's development.

Background to Accreditation in Mexico

The evaluation of Higher Education is a process that has been carried out in Mexico since 1950, when the National Association of Universities and Higher Education Institutions (ANUIES) was constituted, 'the purpose of which was to study the problems of higher education and the adoption of policies and recommendations. '[2]. In 1978, the National System of Permanent Planning of Higher Education (SINAPPES) was created, which in turn set up bodies to coordinate its objective of improving and evaluating higher education; in 1989, the National Commission for the Evaluation of Higher Education (CONAEVA) was established, which would serve as a link between the federal government and the institutions, mainly promoting self-evaluation in higher education institutions.

The creation of the different bodies mentioned above was aimed at improving higher education, as well as enabling the Mexican education system to face the demands of the global context. Their activities laid the foundations for the creation of accreditation bodies for higher education programmes in Mexico.

In 1994, the accreditation or certification of higher education programmes was not something that was contemplated in Mexico's educational policies, which is why the construction of the system began.

While there were Inter-institutional Committees for the Evaluation of Higher Education (CIEES) that had been formed in 1991, and had the task of carrying out inter-institutional evaluations, without going as far as accreditation. In June 1995, in Washington, D.C., the document of recommendations on the 'Mutual Recognition of Registration and Licensing of Engineers for the Jurisdictions of Canada, the United States and Mexico for the

Facilitation of their Mobility under NAFTA' was signed.[3] In this document signed by the three countries, Mexico was asked to create an accrediting body for engineering study programmes.

The first accreditation body to be created was the Consejo de Acreditación para la Enseñanza de la Ingeniería, A. C. (CACEI), in 1994, which was integrated on the basis of the experience of the CIEES. At that time it was necessary to guarantee the quality of the educational programmes, and to be able to participate in the mobility of professionals with North American countries, which led some HEIs to request accreditation by foreign organisations [4]. The fact that CACEI was the first Mexican accrediting body was due to the fact that engineers were one of the professionals with the greatest demand for exchange between the three countries, which is why the criteria for engineering programmes to be evaluated in order to obtain accreditation were established quickly. In 2002, the North American free trade agreement countries produced a document entitled 'Memorandum of Understanding: Western Hemisphere Initiative'. It was signed by the Accreditation Board for Engineering and Technology (ABET, USA), CACEI, and two Canadian bodies: the Council for Engineering Accreditation (CEAB) and the Canadian Council of the Engineering Profession (CCPE). This document provides for the recognition of accreditation of engineering education by accrediting bodies in all three countries. [4]

The above described here sets the beginning of the accreditation of engineering programmes in Mexico, a process that has continued to develop until today, and becomes even more evident from the enactment of the General Law of Higher Education in 2021, which is more specific in the field of Higher Education, and also incorporates the System of Evaluation and Accreditation of Higher Education (SEAES), with the aim of seeking continuous improvement of engineering programmes allowing in turn the projection of professionals at national and international level , maintaining the quality of education as an objective.

Problem Statement The engineering programmes taught in Higher Education Institutions do not meet the accreditation criteria of the accrediting bodies, which has led to a decrease in the number of accredited engineering programmes in Mexico.

Research Objectives To identify the management practices and the problematisation of the accreditation of engineering programmes in Mexican Higher Education Institutions that hinder compliance with accreditation criteria.

2. MATERIALS AND METHODS

A reflective analytical review of the literature on public policies on accreditation and management in HEIs was carried out, considering the topics of accreditation, higher education, barriers, quality and engineering, with the aim of providing frontier knowledge on the accreditation of engineering programmes.

3. RESULTS AND DISCUSSION

Since the late 1980s, the quality of Higher Education (HE) has been an agenda item for the Mexican state, hand in hand with the evolution of public policies focused on education. According to the literature review, the following problems in the accreditation process were found:

- HEIs have been forced to incorporate both academic and administrative organization the guidelines of the accreditation bodies, and in this way satisfy evaluation criteria, thus limiting the HEIs in their decision-making power to modify their plans and programmes, and in their projection towards society.[5] With this, the HEIs may tend to work only towards the fulfilment of the accreditation criteria and leave aside the contextualisation of the academic programmes they offer, and base the quality of higher education on the fulfilment of the evaluation criteria for accreditation.

[6], points out as a problem, that the accreditation agencies face difficulties to encourage self-evaluation practices because the accreditation criteria are very detailed and standardized; since the evaluation criteria do not consider the context and culture of each educational institution where the programs to be accredited are taught [7]; therefore, having such standardized criteria limits the flexibility of the programs and contexts, leaving institutions out of compliance with them. The lack of linkage between accrediting agencies and HEIs generates information gaps that do not allow both parties to know their expectations about the information requested in the accreditation process; thus, HEIs generate information that is often not useful and does not reflect the work of the programs that are in the accreditation process; however, since this information is requested through not very explicit indicators, the error is usually frequent. Although the accrediting agencies and the HEIs have an approach during the accreditation period, once this process concludes, communication is not encouraged with the purpose of feedback, between both actors, which limits the process of continuous improvement that can be implemented in the HEIs.

- Accreditation bodies, although endorsed by COPAES, operate independently and must finance their activities through the cost of the accreditation process; these costs are one of the parameters that HEIs must consider when thinking about undergoing an accreditation process. In the case of public HEIs that are subject to a federal budget, some of them may not be able to cover such costs since the educational policy does not consider accreditation as mandatory, and some of the private HEIs may not have the resources to cover such costs; This leads to the segregation of HEIs between those that can afford to pay for accreditation and those that cannot, with the result that the demonstration of quality in the academic program will not be the result of the evaluation of the academic program, but of the budget assigned to it, opening an abyss that separates those HEIs that can pay to demonstrate their quality from those that cannot.

  The cost aspect becomes relevant with the enactment of the General Education Law (2021), which implemented the National Policy for the Evaluation and Accreditation of Higher Education (PNEAES), since with the objective of improving the quality of Higher Education, it seeks to integrate the evaluation and accreditation of HEIs and their academic programs through the Higher Education Evaluation and Accreditation System (SEAES). With this implementation, HEIs must designate a budget for this activity in order to comply with the established policy and/or find sources of funding to cover these costs.
- HEIs have a community made up of directors, administrators, teachers and students; who participate in the accreditation process from different areas of incidence [6], [8] mention: “Problems of accreditation around the degree of participation of the members of the educational community of HEIs”. Depending on the role of those involved in the accreditation process will be the importance and the conception they have about this process; since the impact on the academic program is appreciated in different ways according to the area in which they work. In the case of teachers, they are the ones who have the material with which the scope of the educational objectives of each educational program is demonstrated; however, many times it is required to process the information to be presented to the accrediting body, a task that is carried out hand in hand with the administrative staff; and it is at this point where communication is key to the process and requires the participation of both communities; if this communication is not assertive, it can lead to misunderstandings or non-accreditation. Thus, communication is of vital importance to work towards a common good.
- There is no reported relationship between the results of the evaluation process carried out during accreditation and the strategic planning process in HEIs that

have accredited their educational programs. This raises questions about the contribution of accreditation to the institution. HEIs have been trying for a long time to integrate the results of the evaluation carried out for accreditation into their planning; however, since these institutions must comply with educational policies, many times they cannot integrate the results of the evaluation into their planning due to incompatibility with the new policies or social reality.

- Accreditation Bodies (ABs) have become central players in the regulation of quality in higher education and, these have their own interests and strategies with a view to continue prevailing [6]. As mentioned by [8] “Problems of accreditation around credibility in external agencies.” Although accrediting agencies answer to the Higher Education Accreditation Council (COPAES), they have their own policies and procedures, in which COPAES or governmental entities cannot intervene. Among the procedures questioned is the evaluation by academic peers who are academics, of analogous programs in other institutions; however, many times their partiality in the judgments issued is questioned, since these may take as a reference their own experience in their institution of origin or the model of the same; generating with this inconformity in the HEIs. [9].
- With the information presented above, the problem of not complying with the accreditation criteria of the accrediting agencies, faced by engineering programs can be observed in (Table 1), where the number of programs accredited by CACEI, in the period 2018 to 2022, are presented.[10]

Table 1. Programs of engineering accredited by CACEI during 2018 – 2022.

year	Evaluated programs	Accredited programs (public)	Accredited programs (public)	Evaluated programs (private)	Accredited programs (private)
2018	96	89	71	18	**18**
2019	166	153	121	34	**32**
2020	139	130	109	22	**21**
2021	190	167	142	26	**25**
2022	**213**	**139**	**108**	**37**	**31**

(Table 1) shows how in the case of public programs (PP), the percentage of evaluated versus accredited programs decreased, since in 2018, 78 PP were evaluated and 71 were accredited, resulting in 91% of accredited programs; however, by 2022, 176 were evaluated and only 108 were accredited, meaning 61.36% of accredited programs. In the case of 'private educational programs in 2018, 100% of the 18 evaluated programs were accredited and in 2022 out of 37 evaluated programs 31 were accredited, resulting in 83.78% of accredited programs.

The accreditation carried out by CACEI is an international accreditation; however, the decrease of programs accredited by this international organization could give the impression that it does not comply with the policies of evaluation and higher accreditation in Mexico, established as of the year 2021, which request educational programs to be evaluated and/or accredited (LGES). In view of this situation, many HEIs have opted to be evaluated by organizations that do not provide international accreditation or only reach the point of being evaluated without going through the accreditation process.

4. CONCLUSIONS

Before applying for the accreditation process, HEIs should check if they have the financial resources to cover the costs of the accreditation process. accreditation process, they should check if they have the economic resources to cover the costs of the accreditation process, since if they have the economic resources assigned to this process it will be feasible, otherwise they should seek financing, and if they do not have the economic resources, they should simply not apply for accreditation.

- Academic programs should consider gradually integrating accreditation criteria into their program redesign, into their teaching-learning procedures, and also into their administrative procedures, in order to give continuity to the process of continuous improvement that is sought from the moment academic programs are accredited.
- HEIs have the task of integrating the results of the evaluation carried out during the accreditation process to their improvement plans and link this with the current

educational policies, this will not only generate continuous improvement, but will also allow them to optimize their work.

- Accreditation agencies, although endorsed by a Council, they must adapt to the new policies that affect the accreditation processes and seek a closer relationship with the HEIs in order to work for quality education.

With the knowledge of the obstacles that have arisen in the process of accreditation of academic programs, HEIs will be able to design strategies that will allow them to comply with the new evaluation and accreditation policies (established in 2021), keeping in mind that the objective is quality education.

Conflicts of Interest

The authors declare no conflict of interest.

REFERENCES

[1] SE. Talento mexicano para el crecimiento y la relocalizacion. Secretaría de Economía, Secretaría de Economía, 2023.

[2] ANUIES. (2018). Vision y accion 2030, la propuesta de la ANUIES para renovar la educación superior en México. Ciudad de México: ANUIES. Recuperado el 26 de marzo de 2023, de https://visionyaccion2030.anuies.mx/Vision_accion2030.pdf

[3] Rodríguez, R. (2013). El TLCAN y las profesiones. Un Estado de la cuestión. Revista de la Educación Superior, XLII(168). Obtenido de https://www.ses.unam.mx/integrantes/uploadfile/rrodriguez/RRG2013_ElTLCANYLasProfesiones.pdf

[4] IPN. (2004). Materiales para la reforma: la acreditación de programas educativos en México y en el IPN (Vol. 13). México , D.F.: Dirección de publicaciones IPN.

[5] Krüger, K., Parellada, M., Samoilovich, D., & Sursok, A. (Julio-Septiembre de 2019). Implementando las reformas de la gobernanza: Las reglas de juego en los sistemas universitarios europeos. Revista de Educación(385), 11-37. https://doi.org/10.4438/1988-592X-RE-2019-385-415

[6] IESALC, U. (3 de junio de 2020). riaces.org. Obtenido de http://riaces.org/la-garantia-de-calidad-y-los-criterios-de-acreditacion-en-la-educacion-superior-perspectivas-internacionales/

[7] Llarena, R. (Enero-MArzo de 1994). La evaluación de la educación superior en México. Revista de la Educación Superior , 23(89). Recuperado el 26 de marzo de 2023, de http://publicaciones.anuies.mx/revista/89

[8] Martínez, J., Tobón, S., & Aaron, R. (Enero de 2017). Problemáticas relacionadas con la acreditación de la calidad de la educación superior en América Latina. Innovacion Educativa, 17, 79-95. Obtenido de https://www.scielo.org.mx/pdf/ie/v17n73/1665-2673-ie-17-73-00079.pdf

[9] Marquina, Monica. «Académicos como pares evaluadores en el sistema argentino de evaluación de.» Revista de la Educación Superior (ANUIES) XXXVII, nº 4 (2008): 7-21.

[10] CACEI. (2023). cacei.org.mx. Recuperado el Marzo de 2023, de http://cacei.org.mx/nvfs/nvfs01/nvfs0101.php

118-III-PP INTEGRATION OF RENEWABLE ENERGY FOR A SUSTAINABLE SMART CITY. THE CASE OF: ICELAND, NORWAY, AND DENMARK

M. Santiago Villeda[1]*, M. del R. Soto Flores [1]

[1]Instituto Politécnico Nacional, Escuela Superior de Comercio y Administración, Unidad Santo Tomas, Manuel Carpio 471, C.P. 11340 CDMX, México.

*Correspondence: msantiagov1000@alumno.ipn.mx; msotof@ipn.mx

Abstract: The objective of the work is to explore the integration of renewable energies to promote its progress towards a Sustainable Smart City; To this end, an in-depth analysis of the specialized literature on Sustainable Smart Cities and renewable energies was carried out with respect to the first three countries in the IESE Cities in Motion (ICIM) ranking (2022) in the environmental dimension, that is, the research is documentary type.

The results of the study suggest that the countries studied have renewable energy as a strategy to improve the environment; Due to these, they reduce greenhouse gas emissions and waste, improve the quality of life of the inhabitants, among other aspects that contribute to sustainable development.

Therefore, the conclusions of the work suggest that renewable energies are a tool to contribute to the environment of a country, and in this way improve the aspects that contribute to a sustainable smart city.

Keywords: Sustainable smart cities, renewable energy, environment.

1. INTRODUCTION

The 2030 agenda raised Goal 11 “Make cities more inclusive, safe, resilient and sustainable” because urban concentrations represent around 70% of global carbon emissions and more than 60% of resource use [1].

For what, for its advancement, the concept of sustainable smart cities is proposed for the use of new technologies in areas such as logistics, digital service platforms, social innovation, transportation and energy production, with the aim of improving inclusion, environmental quality, social well and the intelligent development for citizens [2].

Likewise, at a global level, the IESE Cities in Motion (ICIM) institution (2022) with based on nine dimensions, evaluates ninety-two countries. In the environmental dimension, the leading countries were Iceland, Norway, and Denmark, due to their low indices of pollution, the use of renewable energies, its environmental indicators and its hydraulic sources) [3].

Therefore, the objective of this research is to explore the integration of renewable energies in leading countries in the environmental dimension because these are an example to improve the path towards a Sustainable Smart City. The results suggest that these countries use renewable energies such as geothermal, hydroelectric, and wind energy to reduce the emission of greenhouse gases, in addition to increasing the quality of life of their citizens.

2. METHODS

The research methodology is documentary, so the following steps were conducted: selection, review, understanding, analysis, and synthesis. In accordance with what was established by Levy & Ellis (2006), this process guarantees a structured and effective review. The references that were reviewed include articles from scientific journals and books with managerial impact on the topic [4].

Likewise, the objective of the research was to document the integration of renewable energies in three representative countries:

Iceland, Norway, and Denmark, with the aim of analysing how the use of renewable sources in the energy sector contributes towards a Sustainable Smart City. Likewise, three countries were chosen for the design within the IESE Cities in Motion Smart Cities Ranking, so their competitiveness in production, population supply, and applications they use were described.

3. SUSTAINABLE SMART CITIES

The United Nations Organization (2015) define the concept of Sustainable Smart Cities., in the report "Habitat III Program", as the combination of efforts to promote economic growth, increase the quality of life of citizens and take care of the environment [5].

Likewise, smart cities integrate six characteristics which imply innovation and sustainability as the axis for achieving the objectives, in addition to technologies as a tool for improving current and future citizen services and demands *[1]***.**, these features are:

1. Generate integration.
2. Optimize resource allocation.
3. Use performance indicators to measure, compare and improve public policies.
4. Attention to citizens to increase the degree of satisfaction of the inhabitants.
5. Optimize processes to increase government efficiency.
6. Greater participation of civil society in the administration.

Furthermore, to measure these cities, the IESE Cities in Motion (2022) proposes nine dimensions which are: Human capital, social cohesion, economy, environment, governance, mobility and transportation, urban planning, international projection, and technology *[3]***.**

3.1 Sustainable Smart Cities Worldwide

At a global level, the IESE Cities in Motion (ICIM) institution (2022), based on 9 dimensions and 114 indicators, evaluates 92 countries, 183 cities and 85 capitals, to determine the ranking of smart cities, of which during the 2022 highlights the cities of London, New York, Paris, Tokyo, among others, which are displayed in (Table 1) [3].

Table 1. Ranking of Smart *Cities according to* ICEMI (2022) *[3]*.

Ranking	**City**
1	London - United Kingdom
2	New York - United States
3	París – France
4	Tokio - Japan
5	Berlin. Germany
6	Washington - United States
7	Singapore-Singapore
8	Amsterdam - Netherlands
9	Oslo- Norway
10	Copenhagen-Denmark

Likewise, the ICEMI institution (2022) conducts an evaluation for each of the nine dimensions, already mentioned above, (Table 2) shows the environmental dimension *[3]*.

Table 2. Top ten of the Environment dimension *according to* ICEMI (2022) *[3]*.

Environmental
1. Reykjavik – Iceland
2. Oslo - Norway
3. Copenhagen - Denmark
4. Gothenburg - Sweden
5. Wellington - New Zealand
6. Stockholm - Sweden
7. Helsinki - Finland

8. Canberra - Australia
9. Tallinn - Estonia
10. Edinburgh - United Kingdom

4. RENEWABLE ENERGY

Renewable energies are defined as those that are inexhaustible on a human scale, are continually renewed and are obtained from natural sources which are friendly to the environment *[5]*.

Renewable energy sources can generate environmentally friendly electricity, fuel, and thermal energy, meaning their emissions and waste are below established regulatory levels *[6]*. These energy sources are a product of the flow that the Earth continually receives, and which has its origin in the Sun, although in certain cases there is a certain contribution from the terrestrial and lunar gravitational fields *[7]*.

Among the renewable energy sources that are most frequently used are wind (wind energy), the sun (solar energy), the internal heat of the earth (geothermal energy), organic matter (bioenergy), water (hydroelectric), and tides, waves and salinity (marine energy) *[7]* These energy sources are described below.

- Wind energy

Wind energy works through the wind which is a consequence of solar radiation. It has been calculated that approximately 2% of the solar energy that reaches the Earth is converted into wind and that 35% of this is dissipated in the lower zone of the atmosphere [*7]*.

- Marine energies

The oceans function as energy capture and accumulator systems, so tides, thermal gradients, waves, ocean winds, bioconversion, sea currents and saline gradients are used to produce energy *[7]*.

- Solar energy

Solar energy is that, produced through the sun's rays, can generate the following types of uses photovoltaic, thermal solar, concentrated solar (CSP) (indirect) *[8]*.

- Hydroelectric energy

Hydroelectric energy can be defined as energy that is obtained by taking advantage of the potential of a body of water located in the riverbed or with water retained in high-altitude reservoirs or swamps *[9]*.

- Geothermal energy

Geothermal energy is one of the least known renewable energy sources and is stored under the Earth's surface in the form of heat and linked to volcanoes, hot springs, fumaroles and geysers. Geothermal energy resources vary in temperature from 25°C to 350°C, so they have the following [*10-11]*:

High enthalpy geothermal energy (greater than 200°C): They are used for the generation of energy with conventional technology.

Medium enthalpy geothermal energy (150 to 200°C): Its main applications are thermal, and it is also used for the generation of electricity with binary plants.

- Low enthalpy geothermal energy (less than 150°C): Its use can be for thermal uses.

- Bioenergy

Bioenergy is the only renewable source that involves isolation. It is produced from residual biomass, which is defined as the set of organic and biodegradable material waste obtained from waste from agricultural, transformation and urban activities. Bioenergy must be separated into two different energy sources which are *[7-12]*:

- Solid biomass
- Urban waste

5. RESULTS AND DISCUSSION

Results: The results of the research are a comparison of three representative countries in the environmental dimension of the IESE,

which are Iceland, Norway, and Denmark. Therefore, each of these is described below:

- Iceland

This city leads the number one position in the environmental dimension due to its low pollution rates and the use of renewable energy. Furthermore, according to the UN (2020), 100% of the electricity in this country is generated by renewable sources, the main ones being hydroelectric and geothermal energy *[13-14]***.**

During 2011, hydroelectric energy represented 75% of total electricity and geothermal energy 25%, in addition to this, this country has 7 Geothermal Fields of private origin.

Furthermore, Koebrich, Samuel, Bowen, Thomas, & Sharpe, Austen (2018), say that this country began using thermal energy through geothermal energy centuries ago with applications for personal hygiene and bathing, later during the century In the 20th century, geothermal centralized city heating systems were implemented on a commercial scale, as well as spas for skin care, tourist balneology, and food heating *[15]***.**

Likewise, it has recently introduced policies aimed at mobility, sustainability and the environment. Among the most notable initiatives are the implementation of a public transportation system that uses real-time data to optimize routes, improve service efficiency and reduce waiting times, as well as the installation of sensors, LED technology and smart meters. for the efficient management of energy and water, and the promotion of citizen participation through digital platforms and mobile applications. Also, the city has a respectable number of energy chargers for electric vehicles [16].

- Denmark

This city stands out for occupying the number four place in the ranking of smart cities in 2022, likewise, in the dimension of social cohesion it is number four and in the dimension of the environment it is number three [3].

In addition to this, it is considered the safest city in the world, due to its social cohesion, with a low crime rate and a narrow wealth gap. In addition, its inhabitants mostly travel by public transport, bicycle or on foot, and have as a goal to achieve lower carbon emissions by 2025 [13].

Furthermore, in 2019 solar photovoltaics and wind energy generated the equivalent of 50% of Denmark's electricity consumption. And in 2021, most of its energy came from wind turbines with an installed capacity of 6,235MW [17].

Likewise, the Government of Denmark created projects such as energy islands, carbon capture, green energy transition, green heating based on biome and heat pumps, and an ecological tax reform [18].

- Norway

During 2021, according to REN21, Norway was the number two leader in total final energy consumption of renewable energies. In addition to this, at the end of 2019 (%) it conducted the first commercial floating offshore wind project of 88 MW together with some other European countries [19].

Furthermore, 100% of its electricity is produced by renewable sources and represents 3% of global hydroelectric capacity worldwide. Likewise, it invested 380 million dollars to support mixed hydrogen projects, as well as other renewable projects. It also creates renewable energy policies and phasing out fossil fuels [19].

It has also introduced changes to its residential solar rebate system for installations to allow for further market expansion.

Added to this, (Table 3) shows how these countries integrate different renewable energies, which contributes to their top positions in the environmental dimension of the sustainable smart cities ranking.

Table 3. Integration of renewable energy in Iceland, Denmark and Norway

	Iceland	**Norway**	**Denmark**
Wind energy			✓
Marine energies		✓	
Solar energy		✓	✓
Geothermal energy	✓		
Bioenergy			✓
Hydroelectric energy	✓	✓	

Based on the analysis of the countries of Iceland, Denmark and Norway, it is found that these countries use renewable energies to be Sustainable Smart Cities, because the use of these technologies allows them to have new energy markets and in turn increase the standard of living of its inhabitants.

In addition to this, these countries are a model for sustainability because most of them have national action plans that include reducing their greenhouse gas emissions, as well as investing in sustainable energy sources. Likewise, as mentioned by the UN (2020), they are countries that take advantage of their geographical conditions to have energy self-sufficiency [14].

Therefore, their sustainable policies are an example for other countries because, as State of Green (2021) *[18]* mentions, they establish ambitious and reliable long-term objectives to achieve an ecological transition, through public incentives, competition, and pilot projects [18].

6. CONCLUSIONS

The findings of the study suggest that Iceland, Denmark, and Norway are ranked in the environmental dimension because most of their electricity is based on renewable energy, they also use sustainable heating, for example, through biomass, and they encourage the use of public transportation, which is efficient, uses cutting-edge technologies, and renewable sources.

In addition to this, these countries made this transition through public investments, tax reforms, and incentives for the use of these renewable energies, so that the inhabitants would also implement them in their homes.

It should be noted that these countries conducted their energy transition using renewable sources due to their high consumption of imported fossil fuels, so, based on their geographical conditions, they used energy alternatives such as geothermal, wind, and hydroelectric energy.

Therefore, they are an example for other countries, which can use their strategies to encourage the production of renewable sources to contribute on the path to a sustainable smart city.

Conflict of interest

The authors declare that they have no conflict of interest.

REFERENCES

[1] Cabello, S. (2022). The development path of smart cities, An assessment of Bogotá, Buenos Aires, Mexico City, and São Paulo. Retrieved from Project Documents (LC/TS.2022/86), Santiago, Economic Commission for Latin America, and the Caribbean (ECLAC)

[2] ITU. (13/10/2024). International Telecommunication Union. Retrieved from Smart Sustainable Cities: https://www.itu.int/web/pp-

18/en/backgrounder/smart-sustainable-cities

[3] ICEMI. (2022). IESE Cities in Motion Index. Navarra, Spain: IESE Business School University of Navarra

[4] Levy, Y., & Ellis, T. J. (2006). A Systems Approach to Conduct an Effective Literature Review in Support of Information Systems Research. International Journal of an Emerging Transdiscipline, 9, 181-212. https://doi.org/10.28945/479

[5] ITC. (2008). Instituto Technologic Canarias. Retrieved from Energía renewables: https://www.itccanarias.org/web/es/areas/energias-renovables

[6] INNEL. (12 2020). What are clean energy? Retrieved from SENER: https://dgel.energia.gob.mx/inel/CleanEnergies.html

[7] Jarabo, F. F., & Pérez, D. C. (1988). Energies Renewables. Spain: Publications Technical S.A

[8] IDAE. (2011). National Action Plan for Renewable Energy (PANER) 2011-2020. Retrieved October 2019, from the Institute for Energy Diversification and Saving: https://energia.gob.es/desarrollo/EnergiaRenovable/Documents/20100630_PANER_Espanaversion_final.pdf

[9] IDAE. (November 2019). Hydroelectric Energy. Obtained from the Institute for Energy Diversification and Saving.: https://www.idae.es/tecnologias/energias-renovables/uso-electrico/energia-hidroelectrica#:~:targetText=La%20energ%C3%ADa%20hidroel%C3%A9ctrica%20es%20aquella,punto%20m%C3%A1s%20bajo%20del%20aprovechamiento

[10] IDAE. (06 2008). Geothermal Handbook. Retrieved 2019, from https://www.idae.es/publicaciones/manual-de-geotermia-represión

[11] CEGA. (2016). Geothermal Centre of Excellence in the Andes. Retrieved September 2019, from http://www.cega-uchile.cl/informacion-sobre-geotermia/#videos

[12] Cerda, T. E. (2008). Bioenergy in the European Union. Eukonomiaz, 26.

[13] ICEMI. (2020). IESE Cities in Motion Index. Navarra, Spain: IESE Business School University of Navarra

[14] UN. (2020, 15). Iceland's sustainable energy story. Retrieved from Iceland's sustainable energy story: A model for world, https://www.un.org/chronicle/article/iceland-sustainable-energy-story-a-model-for-the-world?

[15] Koebrich, Samuel, Bowen, Thomas, & Sharpe, Austen. (2018). *Renewable Energy Data Book*. Recuperate the 04 de 2021, de Department of Energy (DOE), Office of Energy Efficiency & Renewable Energy (EERE): https://www.nrel.gov/docs/fy20osti/75284.pdf

[16] Galgiardo, F. (01/04/2023). What makes Reykjavik a true smart city. Retrieved from https://federicogagliardo.com/2023/04/01/que-hace-de-reykjavik-una-verdadera-smart-city/

[17] Hivepower. (17 Jan 2022). Renewable Energy in Denmark: What You Should Know. Retrieved from Hivepower: https://www.hivepower.tech/es//blog/energ%C3%ADa-renovable-en-dinamarca-lo-que-debe-saber

[18] State of Green. (2021). from Black to Green: A Danish Story of Sustainable Energy Growth. Retrieved From Black to Green: A Danish Story of Sustainable Energy Growth

[19] REN21. (2019). *Renewables 2018 Global Status Report*. Paris: REN21 Secretariat)

157-III-PO DESIGN OF A VIRTUAL REALITY ENVIRONMENT AS DIGITAL TOURISM MARKETING TOOL IN PAHUATLÁN

M. de la C. Sánchez Llabona[1]*, V. R. Oliva Aguilar[1]; R. J. Garnica Peña[2]

[1]Instituto Politécnico Nacional, Escuela Superior de Turismo, Sección de Estudios de Posgrado e Investigación, Maestría en Administración e Innovación del Turismo, Av Miguel Bernard 39, C.P. 07630 CDMX, México.
[2] Universidad Nacional Autónoma de México, Instituto de Geografía, Circuito de la Investigación Científica S/N, 04510 CDMX, México.

*Correspondence: msanchezll2300@alumno.ipn.mx

Abstract: In the digital age, tourism marketing has undergone a remarkable transformation thanks to the integration of advanced technologies such as Virtual Reality (VR). This study aims to design a VR environment for Pahuatlán, a Magical Town in Puebla, Mexico, with the purpose of optimizing its tourism promotion, in line with the dynamics of marketing-mix. The research, which began in 2023, is structured in four phases, preceded by a preliminary stage focused on the analysis of the state-of-the-art. This paper focuses on the progress of the first two phases.

The first phase consisted of a pre-inventory of resources, attractions and tourist products in the area, complemented by an analysis of trends in Google Trends and the classification of Valls (2006), which allowed to identify the central elements, complementary and peripheral to the destination. This approach contributed to defining the territory's morphological structure and developing a preliminary design for the digital tool.

In the second phase, a diagnosis of tourist supply and demand was made. In the demand analysis, customer and buyer profiles were developed, while in the supply study key actors were mapped, resources and attractions were inventoried, the marketing policies were evaluated, and a comparative analysis of the municipality's websites was carried out. All this information consolidated the database for the development of the tool.

To date, the first phase has been completed in full and significant results have been achieved on the second phase, with phases three and four scheduled for completion by the end of 2024 and 2025, respectively. The third phase will involve developing a 360-degree virtual tour, integrating the information collected, and the fourth phase will assess the feasibility of this tool within the promotional strategy. The main result will be a 360-degree tour as a digital marketing tool, complemented by an implementation strategy to maximize the impact of technological innovations in tourism promotion in Pahuatlán.

Keywords: Virtual Reality, Digital Marketing, Tourism

1. INTRODUCTION

The Magic Villages program in Mexico has evolved into a well-recognized tourist Brand of great representativeness at national and international level, standing out over other government initiatives [1]. This strategy has contributed to the positioning of numerous communities, including Pahuatlán, through the implementation of tourism development policies that seek to preserve the cultural and natural identity of these places. However, despite Mexico's willingness to implement technological advances in tourism, the benefits of these policies have not yet been spread

evenly. There is resistance to change in some communities that see digitization as a potential threat to their traditional values [2].

The tourism standardization promoted by the Magic Villages program creates a uniform identity, facilitating national and international recognition of the destination at national and international level. However, this uniformity can lead to a loss of local identity by prioritizing the overall brand image over each community's unique characteristics, reducing its cultural wealth to commercial attractiveness [3]. Moreover, as [4] point out, the management of these destinations is in many cases lacking guidelines that promote a balance between tourism development and community welfare. This results in over-exploitation of resources without comprehensive conservation plans.

The situation in Pahuatlán reflects this problem: the limitations in marketing and adoption of digital tools restrict their presence in new communication and distribution channels, which affects their competitiveness in today's tourism market. In this context, virtual reality (VR) emerges as an innovative alternative within digital tourism marketing, allowing an effective and meaningful connection between supply and demand through an immersive experience that respects the authenticity of the destination [5, 6]. In fact, the use of digital platforms and tools such as VR represents a fundamental change in the way tourism destinations are marketed, given the growing trend of travelers to plan and document themselves online [7].

This research focuses on the design of a VR environment for Pahuatlán, Magic Village of Puebla, Mexico, with the objective of improving its tourism promotion by highlighting its cultural values, natural resources and traditional products. In this way, it is intended to create a promotion model that goes beyond standardization, providing the destination with a digital marketing strategy that attracts visitors through authentic and meaningful experiences, strengthening the emotional connection of the visitor with the place and contributing to the sustainable development of the community.

2. METHODOLOGY

The research was conducted under a mixed and descriptive approach in four phases, preceded by a preliminary stage. At this stage, a state-of-the-art analysis was carried out through a descriptive, cross-sectional and retrospective study of academic publications on the use of virtual reality (VR) as a digital marketing tool in Magic Villages. To do this, repositories such as SciELO Mexico, TesisUNAM and Web of Science were consulted, using keywords in English and Spanish. This analysis identified the existing scientific literature and built the conceptual framework for research, providing a solid basis for the next phases.

During Phase one, a pre-inventory of Pahuatlán's resources and tourist attractions was conducted through a familiarization visit, using an observation guide and documentary analysis. Following the methodology of MINCETUR [8], tourist resources were categorized and ranked in order to create a detailed structure of the elements of the destination. Phase two is divided into two stages: the demand study, in which information obtained through surveys, non-participatory observation and interviews with tourist providers will be triangulated to develop customer and buyer people profiles; and the study of supply, which will include an inventory of tourism resources based on CICATUR and OAS methodologies, as well as interviews with key actors.

In Phase three, the 3DVista software will be used to develop a 360-degree virtual tour. This process included the interface design, content integration, testing and creation of the final version in formats compatible with various platforms. Phase four consisted of the assessment of the feasibility of the tool from a technical, social, economic and environmental perspective. For this evaluation, the application was made available to service providers and the Pahuatlán Tourism Authority, and a discussion group with key actors who had interacted with

the application was developed. Finally, a survey was applied to a group of visitors to measure the impact of the tool from the perspective of the end user, providing valuable information on the knowledge and perception of the tourist offer in Pahuatlán.

3. RESULTS AND DISCUSSION

The research has made significant progress in two key elements: the theoretical foundation and the initial assessment of Pahuatlán as a tourist destination. The theoretical foundation established a solid framework that integrates the principles of digital marketing and the use of virtual reality (VR) technologies in tourism. The review of studies identified how VR can enrich the user experience and increase the intention to visit tourist destinations, confirming its value as an innovative tool to capture visitor interest. This conceptual basis highlights that VR, beyond being a visualization technology, is a means of interaction that can emotionally connect users with the destination and at the same time reduce pressure on physical tourism resources.

The initial evaluation of Pahuatlán as a tourist destination included the preparation of a pre-inventory of 169 elements categorized into resources, attractions, products and infrastructure. This analysis showed that, although Pahuatlán has a multifaceted tourist offer, there are notable disparities between the amount and type of resources available. Of the items inventoried, 42 correspond to natural and cultural resources, while 34 are tourist attractions and 86 products.

The cultural and natural wealth of the destination, reflected in a high proportion of resources, highlights its potential to diversify and enrich supply, and suggests opportunities to design more integrated tourism experiences that take advantage of these resources and enhance the competitiveness of the destination. However, the limited number of specialized products in relation to natural and cultural resources raises the need for improving the variety and quality of supply.

The analysis of the ranking of elements revealed that the category of cultural attractions predominates in the higher hierarchy, with 24 elements, 15 of which are cultural events that could attract tourists interested in the authenticity and cultural richness of the destination. This finding underlines the importance of cultural events in Pahuatlán as a differentiating component that can be key to developing tourism products focused on local culture. In contrast, accommodation and catering categories are mainly concentrated at the bottom of the hierarchy, suggesting a limited range of services that could be improved in terms of infrastructure and quality to meet visitor expectations.

Regarding the level of tourism vocation, the analysis reaffirms that Pahuatlán has a unique identity focused on cultural, gastronomic and nature tourism. This profile, based on the authenticity of its traditions and landscapes, offers a high potential to consolidate the municipality as a sustainable and attractive destination. However, challenges such as the limited promotion and visibility of handicrafts, especially embroidery by Nahua communities, highlight the need for inclusive marketing strategies that allow diversification of supply and support less-favoured communities. These promotion strategies would not only diversify tourism in Pahuatlán, but also strengthen local economic development and broaden the destination's reach in an increasingly competitive tourist market. In this sense, the analysis of online search trends provides a valuable insight to adapt marketing campaigns to visitors' preferences and optimize the promotion of the cultural and craft offer of the municipality.

4. CONCLUSIONS

Progress in developing a virtual reality (VR) environment for Pahuatlán shows promise, marking a significant step towards innovative tourism marketing. The implementation of a prototype VR not only responds to the trends of digitalization, but also suggests a sustainable alternative that can transform the promotion and communication of emerging destinations

such as Pahuatlán, adding value to its attractiveness and strengthening its position in the tourist market. However, to maximize the impact of this technology, it will be crucial to establish training and support strategies for local service providers, Who need to adapt and take advantage of the opportunities this tool can offer in terms of visitor experience.

Preliminary results of the research suggest that visitors' interest in experiencing virtual environments is high, reinforcing the need for greater investment in technology and human capital training. The creation of a VR environment would not only improve the tourist experience, but also serve as a regulator of the tourism carrying capacity in Pahuatlán, allowing some visitors to opt for a virtual experience when the availability of resources at the physical destination is limited. Thus, the VR environment contributes to protecting natural and cultural resources by reducing direct pressure on them and promoting sustainable management plans.

Acknowledgements

The support provided for the development of research is appreciated by the key actors in Pahuatlán, specifically the Tourism Direction, as well as the IPN for its support during each visit to the territory.

Conflicts of Interest

The authors declare no conflict of interest.

REFERENCES

[1] García González, E., López Guevara, V. M. Propuesta de una agenda para la investigación del turismo sustentable en los pueblos mágicos de Puebla. Regiones y Desarrollo Sustentable, 18(34), (2018), pp. 9-26

[2] Landa Díaz, H. O. Restricción financiera y crecimiento económico en México. Investigación económica, 78(309), (2019), pp. 27-57.

[3] Levi, L. L. Las territorialidades del turismo: el caso de los Pueblos Mágicos en México. Ateliê Geográfico, 12(1), (2018) pp. 6-24

[4] Shaadi Rodríguez, R.M.; Pulido Fernández, J.I. Rodríguez Herrera, I.M. La consolidación turística en los territorios que conforman el Programa Pueblos Mágicos (México). Un análisis de sus estrategias competitivas. Investigaciones Turísticas, (15), (2018), pp. 1-33 http://dx.doi.org/10.14198/INTURI2018.15.01

[5] Carrasco, T. Marketing digital como una estrategia para el turismo. Explorador digital, 2(4), (2018), pp. 20-33.

[6] Mariani, M., Bresciani, S., Dagnino, G.B. The competitive productivity (CP) of tourism destinations: an integrative conceptual framework and a reflection on big data and analytics. International Journal of Contemporary Hospitality Management, 33(9), (2021), pp. 2970- 3002.

[7] Cooper, M.A., Camprubí, R., Koc, E., Buckley, R. Digital destination matching: practices, priorities and predictions. Sustainability, 13(19), (2021).

[8] Ministerio de Comercio Exterior y Turismo (MINCETUR) MANUAL PARA LA ELABORACIÓN Y ACTUALIZACIÓN DEL INVENTARIO DE RECURSOS TURÍSTICOS. (1.st edición). Impresiones & Publicidad Viserza S.A.C. (2018)

325-III-PP IN SEARCH OF A VIABLE WATER MANAGEMENT SYSTEM MODEL IN BOUTIQUE HOTELS IN TULUM

C. Pérez[1]*, R. Tejeida[2]*, S. Romero[3]*

[1]Instituto Politécnico Nacional, Escuela Superior de Turismo, Sección de Estudios de Posgrado e Investigación, Grupo de Investigación en Sistémica y Turismo, Av Miguel Bernard 39, C.P. 07630 CDMX, México.
[2]Instituto Politécnico Nacional, Escuela Superior de Ingeniería Mecánica y Eléctrica unidad Zacatenco, Unidad Profesional Adolfo López Mateos, Edificio 1 Planta baja, C.P. 07738 CDMX, México.
[3]Universidad Autónoma del Estado de Hidalgo, Grupo de Investigación en Sistémica y Turismo, Hidalgo, México.

*Correspondence: cperezp2300@alumno.ipn.mx, rtejeidap@ipn.mx, sromerojuarez78@gmail.com

Abstract: This research focuses on water management in boutique hotels in Tulum, a tourist destination currently experiencing significant growth, which has also brought with it environmental challenges such as water scarcity.

The objective is to examine water management in boutique hotel establishments in Tulum, based on a systemic analysis of the interrelationships between the actors of the hotel system and their environment. The study is based on the General Systems Theory (GST) and the Systemic Paradigm, using the Soft Systems Methodology (SSM) and the Viable System Model (VSM) of Organizational Cybernetics.

Through this systemic approach, we seek to improve efficiency in the use of water resources, promote the preservation of natural resources, support the well-being of local communities, increase competitiveness, and reduce the environmental impact of the hotel sector in Tulum.

Keywords: tourism, boutique hotels, water management, Systemic Paradigm

1. INTRODUCTION

The rise of the global tourism industry has placed significant pressure on hotel sustainability. Managing water, energy, and solid waste has become one of the greatest challenges for tourist establishments [1]. These negative impacts are evident in local communities, the environment, and natural resources. As a result, sector-specific actions are required to help mitigate solid waste generation and optimize water management. This will necessitate changes in the internal operations of hospitality businesses and a costly transformation of municipal services.

Sustainable water management and water scarcity are critical challenges in tourist destinations like Tulum, a municipality currently experiencing unprecedented tourism growth that has shown a notable transformation, evolving from a modest coastal town into an international tourist destination [2]. This rapid growth, especially in the hotel sector, has driven the expansion of the tourism industry [3]. Therefore, this study focuses on boutique hotels in Tulum, proposing a systemic model to improve water efficiency and sustainability.

Boutique hotels are considered in this study due to their unique position as alternatives to traditional hotels. They are closely associated

with personalized service, offering a limited number of rooms and prioritizing high levels of customer interaction in their services [4]. Additionally, the study explores the link between the theory and application of sustainable behavior in hotels, and its link with economic, environmental, and social dimensions [5].

2. MATERIALS AND METHODS

This research adopts a systemic approach, utilizing the Soft Systems Methodology (SSM) and the Viable System Model (VSM) to develop an integrated water management model for boutique hotels in Tulum. The study begins with a literature review to establish the background and application of the Systemic Paradigm. The methodology is then detailed, including descriptions of the Soft Systems Methodology (SSM) and the Viable System Model (VSM). Finally, the preliminary results from the initial stages of SSM are presented, followed by the study's conclusions, which highlight key contributions and suggest guidelines for future research.

The General Systems Theory, developed by Ludwig von Bertalanffy, is a theoretical framework that describes the principles and concepts common to all systems, regardless of their nature [6], therefore, this theory is useful for understanding and managing complex systems such as water systems. By applying the principles of General Systems Theory to water management in boutique hotels, the interdependence of all elements of the water system is understood. The application of feedback mechanisms facilitates the constant adaptation of hotel practices, ensuring their operation within the limits of the local ecosystem and promoting their stability.

On the other hand, Organizational Cybernetics has emerged as a valuable approach for the management of resources, including water, in complex contexts such as the boutique hotels in Tulum.

Organizational Cybernetics is made up of five essential elements: 1. Viability, 2. Variety, 3. Ashby's Law, 4. Conant-Ashby theorem and 5. Viable System Model (VSM).

The latter is a Cyber tool that can be used to structure water management in boutique hotels. According to [7], the MSV allows organizations to maintain their viability through adaptation and continuous learning.

In Tulum, this can translate into engaging the community in water conservation initiatives, such as education and awareness programs on the responsible use of resources and creating alliances with other companies and non-governmental organizations to share best practices and resources in water management.

Systems Thinking is crucial for dealing with dynamic entities or heterogeneous systems, where traditional mathematical laws cannot be applied without denaturing them. Based on Jackson's Context-Problem matrix (2003) and the Systems Methodology System, Table 1 and Table 2, the category of system, participants, appropriate thinking and context to study are chosen.

Table 1. Context-problem matrix.

Participants	**Unitary**	**Pluralistic**	**Coercive**
System			
Simple	Hard Systems Thinking	Soft Systems	Emancipatory Systems
Complex	Systems Dynamics	Pluralistic Complex	Postmodern Systems
	Complexity Theory		
	Organizational Cybernetics		

Source: [7]

Table 2. System of System Methodology.

Participants	Unitary	Pluralistic	Coercive
System			
Simple	Simple Unitary	Simple Pluralistic	Simple Coercive
Complex	Complex Unitary	Complex Pluralistic	Complex Coercive

Source: [8]

[9] proposes these two matrices to categorize problems into simple and complex systems and describes the relationships between participants. Simple systems have few individuals and interactions, are relatively closed and static. Complex systems have numerous elements and interactions, are dynamic, and evolve with their environment. The relationships between the participants can be; Unitary: Those involved share objectives, interests, and values, facilitating joint decision-making. Pluralistic: Participants have different interests and objectives, but they reach agreements to achieve them. Coercive: There is little common interest, with conflicts resolved through force and domination.

In this research, the object of study adjusts to a complex and pluralistic system. There are numerous elements and complex interrelationships, with participants who, although they have different objectives, share a common objective. In addition, the unitary relationship is considered, where interests, beliefs, and values are compatible, allowing inclusive decision-making.

Organizational Cybernetics and MSS are suitable approaches to address complex and plural problems. Cybernetics organizes and controls autonomous and self-regulated systems, while MSS, based on phenomenology and hermeneutics, is useful for studying and interpreting unstructured or soft problems [10].

Since tourism is studied as a transdisciplinary and dynamic system, Systems Science provides valuable tools for theoretical and practical approaches to tourism [11]. This research uses the Soft Systems Methodology which consists of 7 stages, as shown in Figure 1: 1) investigation of the unstructured situation; 2) structuring of the situation; 3) identification of relevant systems; 4) construction of conceptual models; 5) comparison of models; 6) definition of feasible and desirable changes; and 7) implementation of changes.

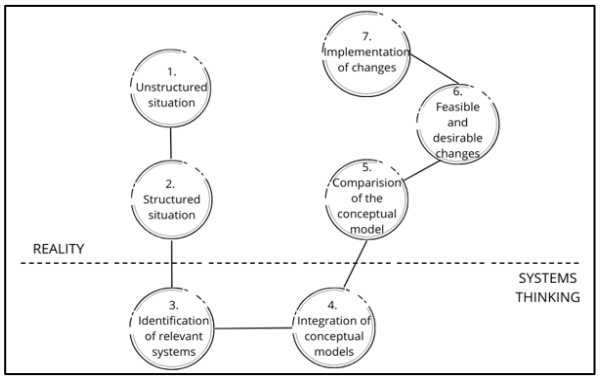

Figure 1. Soft Systems Methodology.

Source, Own elaboration, based on [12]

The Soft Systems Methodology (SSM) aims to study systems with high social content based on the interpretation of the dynamics of the interrelationships of actors and entities [13], where problems are covered. unstructured, although it can also be applied in structured systems [14].

3. RESULTS AND DISCUSSION

Stage 1. Unstructured situation: This stage is essential to understand the context and challenges associated with the use and management of this water resource. At this stage, a preliminary investigation was carried out to understand the context and problems associated with water management in boutique hotels in Tulum. Here data was collected on water sources, consumption, management practices, local policies, and the perception of the different actors involved.

Figure 2 shows the elements that comprise the system, as well as its environment and macroenvironment. The key systems refer to boutique hotels in Tulum and water management, from here we start to identify

actors and elements directly linked to the activities carried out by the systems, which is why water sources, water consumption, and practices are considered. of water management in Tulum boutique hotels and the participation of guests and inhabitants. The environment is made up of all the elements that have a direct relationship with the system and that hinder viability therefore, the system must cope. Here we can find policies and regulations related to water management at the local level by local, state, and municipal government organizations, as well as civil associations. Finally, the macroenvironment is made up of specific elements that have an indirect impact on the system, so they can limit or allow the ideal development of its activities, but they are elements that compete, which are technological, social trends, legal environment, political factors, and ecological factors.

Source: Own elaboration

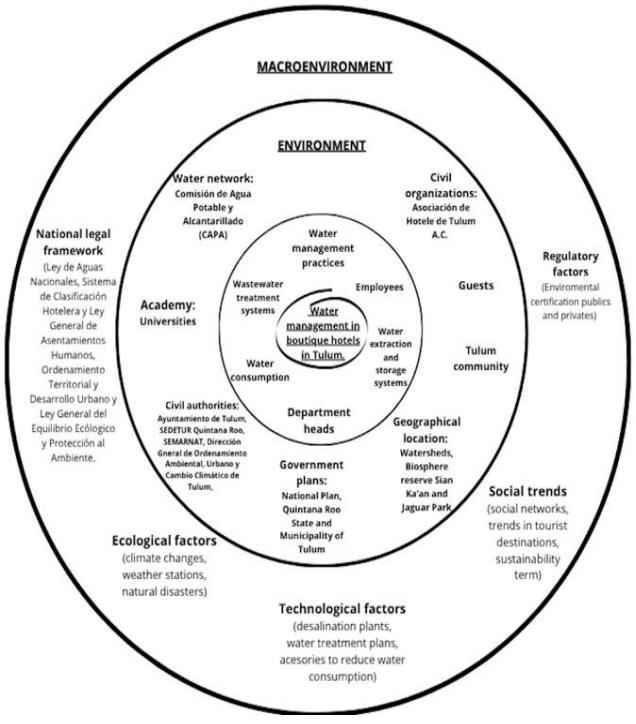

Figure 2. Vision of the System and its environment.

Stage 2. Structured situation: Stage 2 of the SSM focuses on organizing the information collected to identify the main elements and relationships in the water management system in boutique hotels. It is integrated into the generation of a rich vision of the system and its connection with the environment. To enrich and understand Figure 2, the actors replaced by icons are represented below as shown in Figure 3.

Source: own elaboration.

Figure 3. Iconographic representation of the actors that influence the system.

Figure 4 shows the rich vision scheme and its environment, here the elements and interrelationships are appreciated and the degrees of conflict between each of them are established through a traffic light by colors represented in red, yellow, and green, it manifests the highest degree of conflict, the second an intermediate degree and the last does not show any conflict.

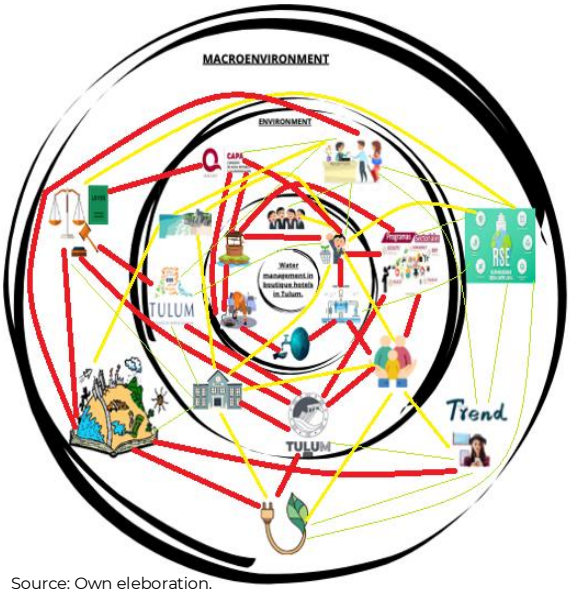

Source: Own eleboration.

Figure 4. Rich vision and its environment.

In the graphic representation of the previous figure, we observe that the relationships of the inner circle present greater conflict due to the

lack of organization on the part of the managers/owners of the hotels to the services offered to the guests and as a consequence they also affect the community. On the other hand, within the environment, the main conflicts identified correspond to ineffective governance and governability by local, state, and national authorities, thus affecting water management in the municipality. Finally, in the macroenvironment, the need to enforce laws and regulations is identified, which shows that there is no optimal application.

When grouping the three levels, the disconnection between government, companies, civil society and the environment can be seen, in addition to the ineffective compliance with laws and regulations by the hotel sector, as well as the inefficient water management infrastructure, which are obsolete and insufficient. to meet current needs.

Stage 3. Identification of relevant systems: This stage seeks to identify the key components of the water management system in the boutique hotels of Tulum. To do this, we will use the CATWOE mnemonic, which helps define the limits and characteristics of each subsystem that interacts with the others forming a complex network. The elements that make up the root definition are presented to prove that it is valid and corresponds to the situation of the unstructured and expressed problem.

C – Clients: The main beneficiaries and affected by water management are the guests who benefit from quality services and sustainable practices, the local community that depends on water resources, and the regulatory authorities that ensure the conservation of resources. water resources and compliance with environmental regulations.

A – Actors: Includes hotel managers, hotel staff, local authorities, and water service providers. Managers are responsible for designing and implementing efficient water use policies; hotel staff execute these policies in their daily tasks. Local authorities set the regulations and standards that frame water use, while water service providers ensure the proper supply and treatment of wastewater. The interaction between these actors is crucial for efficient water management.

T – Transformation: The process of water transformation in the hotel context involves a cycle that ranges from the collection of the resource to its final disposal. This process involves activities such as purification, distribution, use in facilities, and wastewater treatment. The objective is to reduce water consumption and waste and maximize reuse, all without compromising the quality of guest service.

W – Worldview: The worldview considers the importance of sustainability and social responsibility in water management. It seeks to conserve the environment and protect natural resources, ensuring that hotel operations do not compromise the availability of water for future generations.

O – Owner: The owners of the system are the hotel owners and the regulatory authorities. They have the authority to implement and modify water management policies, as well as to invest in infrastructure and technologies that promote the efficient use of water.

E – Environment: These include water scarcity at certain times of the year, the quality of available water, wastewater discharge regulations, and local community expectations regarding environmental protection.

Based on CATWOE, the root definitions for relevant systems in water management in boutique hotels in Tulum focus on ensuring efficient and sustainable use of water, respecting environmental regulations, and meeting the needs of guests and the local community. Collaboration between actors and adaptation to environmental restrictions are essential to achieve effective and sustainable water management.

The preliminary results of this study are based on the first four stages of the Soft Systems Methodology (SSM):

1° In the unstructured situation stage, the main sources of water for the boutique hotels in Tulum were identified, including underground aquifers and the public network.

2° The structured situation revealed a complex network of interactions between various actors, including hotel managers, collaborators, guests, and local authorities. and the community. Critical external factors were identified such as climate, tourism, and the economic, legal, social, and technological environments.

3° In the identification of relevant systems, the importance of the transformation of water resources and the worldview focused on sustainability is highlighted.

Preliminary findings suggest that water management in Tulum boutique hotels is a highly complex and interconnected system. The richly structured view Figure 4, reveals the intricate web of relationships between water sources, uses, involved actors, and external factors. A key finding is the importance of collaboration between different actors. Hotel managers, employees, guests, local authorities, and the community play crucial roles in efficient water management. The interaction between these groups is essential to implement sustainable practices and adapt to environmental challenges.

4. CONCLUSIONS

This study provides a solid basis for understanding and improving water management in boutique hotels in Tulum. The systemic approach adopted based on the early stages of SSM has allowed visualizing a complex and interconnected system among various factors and actors. The structured analysis identified the main sources of water for the hotels, including groundwater aquifers and the public network; it also showed an intricate web of interactions between various actors and the need for close collaboration, from hotel managers to local authorities and the community, which is fundamental to achieve truly sustainable water management in Tulum, and the findings emphasize the crucial need for collaboration between all the actors involved.

Although the results are preliminary, this study lays the foundation for future research and practical actions in sustainable water management in the Tulum hotel sector. The implementation of the remaining stages of the SSM, along with the planned interviews with hotel managers and the creation of a systemic model through the VSM will provide additional information that will allow to fulfill the purpose of comparing ideal conditions with the current reality and propose improvements.

Conflict of Interest

The authors declare that they have no conflict of interest.

REFERENCES

[1] Hewa-Heenipellage A, Fernando M, Gibbons B. Upper echelon characteristics and environmental sustainability practices: Evidence from upper echelons in the hotel industry. Journal of Cleaner Production. Vol. 379, pp. 134618. 2022. Disponible en https://doi.org/10.1016/J.JCLEPRO.2022.134618

[2] SEDETUS. PDU CENTRO DE POBLACION TULUM 2006-2030. GOB, México. 2008. Disponible en https://qroo.gob.mx/sedetus/bitacoraterritorial/pdu-centro-de-poblacion-tulum-2006-2030

[3] Arroyo-Arcos L, López-López A, Segrado-Pavón R, Estructura hotelera como modificadora del espacio litoral en Tulum México. Teoría y Praxis. pp. 116-137. 2015 disponible en http://www.redalyc.org/articulo.oa?id=456144904007

[4] Loureiro S.M.C, Rita P, Sarmento E.M. What is the core essence of small city boutique hotels? International Journal of Culture, Tourism and Hospitality Research. Vol. 14 N° 1, pp. 44-67. 2019.

Disponible en https://doi.org/10.1108/IJCTHR-01-2019-0007

[5] Barr S, Shaw G, Coles T. Times for (Un)sustainability? Challenges and opportunities for developing behaviour change policy. A case study of consumers at home and away. Global Environmental Change. Vol. 21 N° 4, pp. 1234-1244. 2011. Disponible en https://doi.org/10.1016/j.gloenvcha.2011.07.011

[6] Bertalanffy L. Teoría General de los Sistemas. Fundamentos, desarrollo, aplicaciones. Fondo de Cultura Económica. 1989.

[7] Vahidi A. Evolution of Management Cybernetics and Viable System Model. Systemic Practice and Action Research. Vol. 32 N° 8, pp. 297-314. 2019. Disponible en https://doi.org/10.1007/s11213-019-9478-y

[8,9] Jackson M.C. Systems Thinking: Creative Holism for Managers. Chichester. England: John Wiley y Sons. 2003

[10,12] Checkland P. La Metodología de Sistemas Suaves en Acción / Soft Systems Methodology in Action. México: Editorial Limusa. 2002

[11] Briones A, Tejeida R, Morales O. Toward the Evolution of the Tourism´s Conceptual System. 53rd Annual Conference of the International Society for the Systems Sciences, Making Liveable, Sustainable Systems Unremarkable. Vol. 48 N° 1, pp. 72–79. 2009 Disponible en https://doi.org/10.1590/s0036-36342006000100011

[13] Checkland P. Systems Thinking, Systems Practice. U.K. Wiley. 1981

[14] Ramírez A, Cardoso P, Tejeida R. A Methodological Proposal for the Complementarity of the SSM and the VSM for the Analysis of Viability in Organizations. Systemic Practice and Action Research. Vol. 34, pp. 331-357. Disponible en https://doi.org/10.1007/s11213-020-09536-7

371-III-PP TOWARDS A DECISION SUPPORT SYSTEM FOR HUMAN RESOURCES MANAGEMENT IN 4-STAR HOTEL SMEs IN MEXICO CITY

C. García*, R. Tejeida[1], J. Juárez[1], J. Núñez[2]

[1]Instituto Politécnico Nacional, Escuela Superior de Turismo, Sección de Estudios de Posgrado e Investigación, Av Miguel Bernard 39, C.P. 07630 CDMX, México.
[2]Universidad Panamericana CG, FCEE, Álvaro del Portillo No. 49, Ciudad Granja CP 45010, Zapopan, Jalisco.

*Correspondence: cgarciag2300@alumno.ipn.mx

Abstract: Nowadays, it is increasingly important to manage human resources (HR) properly, which leads to an increase in the competitiveness and survival of tourism companies in the face of the dynamic and changing scenario they are witnessing. Technologies and digitalization occupy a strategic place in business processes and management, especially in the decision-making process, allowing managers access to a vast amount of internal and external data, as well as efficient and quality analysis. The objective of this manuscript is to analyze the current situation of 4-star hotel SMEs in Mexico City in the face of the incorporation of a Decision Support System (DSS) in their HR management processes, using the systemic method and the first two stages of the Soft Systems Methodology. The purpose of the above is to identify the actors and elements involved in the incorporation of the DSS, which will serve as a theoretical basis for the future design of the conceptual model of the aforementioned system. The DSS will make it possible to improve the management of human resources currently carried out by hotel SMEs and may influence the decision made to be fairer, more transparent, based on valid arguments and with a favorable impact on leadership styles and working conditions.

Keywords: Human Resources Management in Tourism, Decision Support System, Systemic Approach.

1. INTRODUCTION

The proper management of human resources in tourism companies is increasingly important to ensure their survival [1]. Despite the above, companies in the world have not focused on these processes with due seriousness and, in the case of Mexico, many programs and certifications have been implemented by the government to support the improvement of business processes, but have not prevented certain problems related to human resources, affecting the competitiveness of the destination [2].

In the hotel SMEs sector in Mexico, there is currently a medium level of labor precariousness, as a result of problems related to hiring, payment of wages and compensation, irregular schedules, intense working hours, among others. In addition, there are deficiencies in the recruitment and selection systems, the organization of tasks and functions, the scheduling of training and personal development, and the underuse of technologies [3-6].

There is a close relationship between the management of the human factor and the quality of tourism services, guiding the company on the path to competitiveness and the satisfaction of customer expectations. Due to this, and taking into account the identified problem, the need to bring about a change in the way in which 4-star hotel SMEs in Mexico City manage their human resources is conceived, in order to achieve complementary

objectives, both personal, business and final consumer.

Therefore, this manuscript aims to create the theoretical basis for the implementation in this kind of companies of a technological innovation that encourages an effective management of their human resources. In this regard, the objective of this manuscript is to analyze the interrelationships between the actor and elements involved in the inclusion of a DSS in the HR management of 4-star hotel SMEs in Mexico City.

This analysis is carried out by means of the systemic method and the soft systems methodology, give its holistic and integrative vision, which allows understanding both the internal and external interrelationships of the phenomenon under study [7]. It is valid to highlight the usefulness of this research for the future design of a DSS, which guarantees greater efficiency and effectiveness in personnel management processes, providing greater scope and data analysis capacity, for accurate, fast and quality decision making.

2. MATERIALS AND METHODS

As mentioned above, this research uses the systemic method and the soft systems methodology to support the analysis of the incorporation of a DSS in the human resources management of 4-star hotel SMEs in Mexico City. The systemic research paradigm was selected, taking into account first of all that human resource management is a system in which its elements must maintain a constant balance and area characterized by cooperation, interdependence and complementarity [8].

Although there are several research paradigms, such as logical positivism, interpretative and critical, these are considered insufficient for the analysis intended in tis manuscript. Therefore, the systemic paradigm was selected because it guarantees an integral, totalizing and holistic vision of the phenomena, and it uses induction, deduction, and abduction. In addition, there is a complementarity between the idealist and materialist processes of dialectics, and real and conceptual systems are defined and interpreted, discerning the interrelationships between their components and position they occupy within the system [7].

Considering that human resources management is a complex system, where a wide variety of actor are involved, constituting a complex intellectual, emotional and psychological system [9], the Total Systems Intervention Methodology [10] was used to identify the characteristics of the system under study through the context-problem matrix and also to frame it in the corresponding category using the System of Systems Methodology matrix. The above is shown in (Table 1), where it can be seen that the system in question is complex-pluralistic, since HR management involves all the subjects within an organization, in addition to elements and actor outside the tourism companies.

Table 1. System of systems methodology.

Participants relationships				
		Unitary	Pluralistic	Coercive
System complexity	Simple	Simple-Unitary	Simple-Pluralistic	Simple-Coercive
	Complex	Complex-Unitary	Complex-Pluralistic	Complex-Coercive
Participants relationships				
		Unitary	Pluralistic	Coercive
System complexity	Simple	Hard systems thinking	Soft systems approach	Emancipatory systems thinking
	Complex	Dynamic systems, organizational cybernetics, complexity theory		Postmodern systems thinking

Note. Prepared by the authors, based on Tejeida et al. [8].

With respect to the above, this makes it possible to identify the "Soft Systems" category and the Soft Systems Methodology [11] as suitable for approaching this kind of system.

The Soft Systems Methodology is a flexible methodology, which has its foundations in phenomenology and hermeneutics and whose stages go between the real world and that of systems thinking. In addition, it employs the concept "Weltanschauung", which contemplates the worldview of each individual regarding the phenomenon [7].

This methodology has 7 stages, as can be seen in Figure 1, which do not need to be implemented in their entirety or following a logical order, and starts with the analysis of the system situation, both unstructured and expressed, going on to the identification of the root definitions of the relevant systems and the construction of their conceptual models, to subsequently compare it with reality an identify feasible and desirable changes [7].

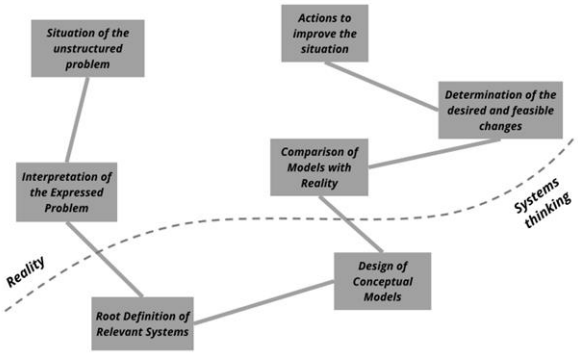

Note. Prepared by the authors, based on Checkland y Scholes (1994), cited by Tejeida et al. [8].

Figure 1. Soft Systems Methodology.

This is a methodology of great utility for the understanding of systems with a high social content [12], with the capacity to face complex and pluralistic situations, so it has a significant contribution, from its first two stages, to the integral study of the phenomenon that constitutes the incorporation of a DSS to the HR management of 4-star hotel SMEs in Mexico City, allowing the identification of the actors and elements involved, and the interrelationships between them.

The data was collected through a literature and bibliographic review of the current situation of HR management in hotel SMEs in Mexico City, as well as their environment and macro-environment. The above was synthesized for its analysis by means of the rich vision of the system and its environment, as established in 2nd stage of the methodology, being able to visualize the conflicting relationships within the system.

3. RESULTS AND DISCUSSION

As part of the analysis of the current situation of the system under study, the following shows the deployment of stages 1 and 2 of the soft system methodology, where in stage 1 the unstructured analysis of the problem is carried out, without making visible the relationships between the actors and elements, which happens in stage 2 with the generation of the rich vision of the system.

In stage 1, the system under analysis is defined, and the actors and elements linked to it are identified, specifically those that intervene directly or indirectly in the implementation of a DSS in the human resources management processes in 4-star hotel SMEs in Mexico City. This can be seen in figure 2, shown below.

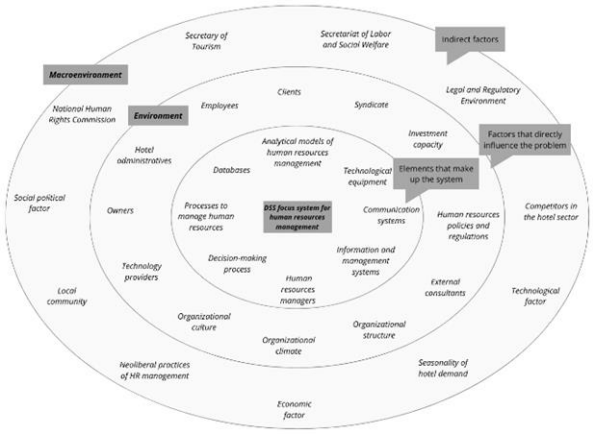

Figure 2. Vision of the system and its environment.

In relation to the system in focus, this is the HR management that would be carried out by the

hotel SMEs in Mexico City, in case of incorporating a Decision Support System within their processes. The inner circle of Figure 2 shows the elements that make up the system under study and that represent the basis structure of a DSS, where elements such as software, hardware, HR management processes, decision-making process, among others, appear. The intermediate circle corresponds to the environment, which shows actor and elements that do not belong to the system, but have a direct impact on it, affecting its viability.

The macro-environment, located in the outer circle, contains those elements that have a weak influence on the system's activities, but which constitute limiting and permissive elements of its behavior.

Next, stage 2 of the methodology is developed, which consists of the analysis of the situation of the expressed problem or the elaboration of the rich vision of the system and its environment. In this stage, the interrelationships between the actor and elements detailed previously are identified and schematized. First, (Table 2) is prepared with the iconographic representation of the elements identified in step 1, to facilitate the schematization of the relationships.

Table 2. Iconographic representation of the actors influencing the system.

Communication system	Information and management system	HR managers	Decision-making process	HR management processes
Databases	Analytic models	Technological equipment	Clients	Staff
Managers	Proprietaries	Technology suppliers	Organizational culture	Organizational climate
Organizational structure	External consultants	HR policies and regulations	Syndicate	Investment capacity
Sectur	Legal and Regulatory environment	Demand seasonality	Ministry of labor and social welfare	Economic factor
Technological factor	Community	Political-social factor	National Human Right Commission	Competition of hotel sector
Neoliberal practices in HR management				

Among the above elements, there are a set of interrelationships that can be both healthy and in conflict, as shown in Figure 3. Among the main conflicts identified are the absence of the main components necessary for the functioning of the DSS, the weak autonomy of HR managers in decision making, the underuse of macro-environmental variables for decision making, the insufficient linkage between governmental organizations to control compliance with laws and regulations, the existence of databases with low capacity, the scarce use of ERP systems in HR management.

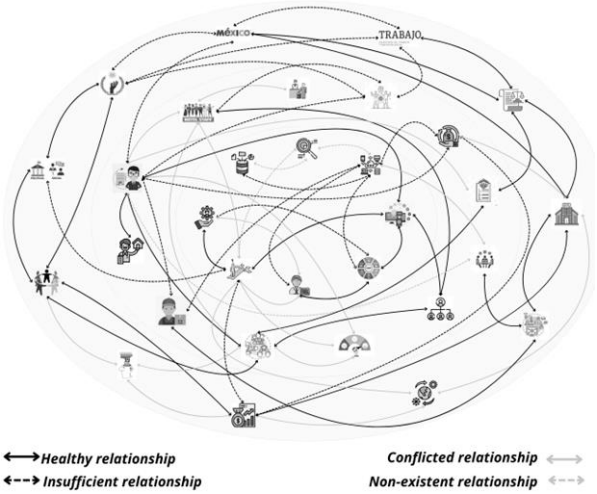

Figure 3. Rich vision of the system and its environment.

There is also a lack of compliance with internal HR management regulations and their reflection in working conditions and the work environment, insufficient relationship with technology and consulting suppliers, poor affiliation to syndicates and, therefore, lack of representation, and the weak financial capacity of many hotels to acquire technology.

When comparing the results obtained in this research with previous research related to the subject, it can be seen that none of the studies taken as background studies pursues the objective outlined in this manuscript, nor do they focus on the population under study. Some of these studies only focus on the incorporation of the DSS in some HR management processes, or in industrial processes, or in activities such as communication within tourism, among others. However, none of those researches, use the systemic paradigm to analyze this topic, with the exception of Núñez et al. [12] that uses the soft systems methodology to analyze a model human capital management in hotel SMEs in the City of Oaxaca.

For future research, it is suggested to proceed with the rest of the stages of the soft system methodology, in order to design the conceptual model of the proposed DSS and thus, through comparison with reality, identify those elements that need to be transformed within the hotel SMEs for its proper functioning.

4. CONCLUSIONS

This research aims to conduct an analysis of the interrelationships between the actors and elements involved in the incorporation of a DSS in the HR management of 4-star hotel SMEs in Mexico City. It is important for this type of company to develop adequate human resources management in order to have a positive impact on its survival and competitiveness in the market. Poor management of this resource can affect the quality of hotel service and customer satisfaction.

The identification and analysis of these relationships will contribute to the future design of a decision support system that will allow SMEs to face the problems they currently face, where managers can feel supported by a tool with ample data analysis capacity, for quality, accurate, fair and well-founded decision making. A DSS will not only improve operational efficiency, but can also contribute to greater staff satisfaction and retention.

The systemic paradigm and the soft system methodology are very useful for the elaboration of this analysis, since it has an integral and holistic approach, capable of deepening the understanding of systems of huge complexity, such as human activity systems.

By incorporating an innovation, like a decision support system, in HR management processes, the occurrence of some conflict relationships that need to be addressed to positively impact the satisfaction and achievement of the objectives of each actor involved is appreciated.

It is recommended that future research focus on the conceptual design and creation of the proposed DSS, as well as its practical implementation and the evaluation of its actual impact on huma resources management. In addition, it would be beneficial to explore the integration of emerging technologies, such as artificial intelligence and machine learning, to further enhance the effectiveness of these systems.

Acknowledgements

Acknowledgments: This research is supported by the Instituto Politécnico Nacional through projects SIP 20242464 and SIP 2024241727 by the Secretaría de Investigación y Posgrado and the Consejo Nacional de Humanidades, Ciencias y Tecnologías de México.

Conflicts of Interest

The authors declare no conflict of interest.

REFERENCES

[1] Calp MH, Agarwal S. An AHP-based Decision Support System for Personnel Selection for Manager Position in Businesses. ACSIS [Internet]. 2021 [cited 2024 November 1]; 28: 1-7. Retrieved from https://doi.org/ 10.15439/2021KM98

[2] Acosta C, Guzmán A. The development of human resource in the tourism sector of

Mexico. Journal of Tourism and Heritage Research [Internet]. 2020 [cited 2024 November 1]; 3(3): 339-359. Retrieved from http://www.jthr.es/index.php/journal/article/view/215

[3] Sosa J, Roy A, Bautista A. Micro, small and medium enterprises and social networks in tourism industry in Manzanillo, Colima, Mexico. International journal of business & management [Internet]. 2021 [cited 2024 November 1]; 9(1): 78-92. Retrieved from https://doi.org/10.20472/BM.2021.9.1.005

[4] Méndez MDC, Vargas EE, Román YG. Precariedad laboral en el sector hotelero. Caso de estudio: Chapultepec-Polanco de la Ciudad de México. Revista Científica Compendium [Internet]. 2021 [cited 2024 November 1]; 24(46) Retrieved from https://revistas.uclave.org/index.php/Compendium/article/view/3860

[5] Saavedra-García ML, Demuner-Flores MR, Choy-Zevallos EE. Use of SME marketing practices in Mexico City and their relationship to competitiveness. Retos [Internet]. 2020 [cited 2024 November 1]; 10(20): 283-305. Retrieved from https://doi.org/10.17163/ret.n20.2020.06

[6] Caldera DC, Arredendo MG, Zárate LE. Rotación de personal en la industria hotelera en el estado de Guanajuato, México. Revista Ibero Americana de Estratégia [Internet]. 2019 [cited 2024 Nobember 1]; 18(4): 615-629. Retrieved from https://www.redalyc.org/articulo.oa?id=331267304006

[7] Tejeida R, Cruz E, Briones A. Sistémica y turismo. 1ª ed. Universidad Autónoma del Estado de Hidalgo: Miguel Ángel Porrúa. 2016

[8] Cai C, Chen C. Optimization of human resource file information decision support system based on cloud computing. Complexity [Internet]. 2021 [cited 2024 November 1]; 2021: 1-12. Retrieved from https://doi.org/10.1155/2021/8919625

[9] Mitsel A, Shilnikov A, Senchenko P, Sidorov A. Enterprise Compensation System Statistical Modeling for Decision Support System Development. Mathematics [Internet]. 2021 [cited 2024 November 1]; 9(23): 3126. Retrieved from https://doi.org/10.3390/math9233126

[10] Jackson MC. Systems Thinking: Creative Holism for Managers. Chichester, England: John Wiley y Sons; 2003

[11] Checkland P. Systems Thinking, Systems Practice. Chichester, United Kingdom: Wiley; 2001

[12] Núñez JE, Sánchez JY, Tejeida R, Coria AL. Perspectiva sistémica en los procesos de capital humano en pymes orientadas al servicio de hospedaje. Nova scientia [Internet]. 2018 [cited 2024 November 1]; 10(20): 481-509. Retrieved from https://doi.org/10.21640/ns.v10i20.1150

HORIZONTES
de Investigación y Desarrollo

IV

Interdisciplinary

39-IV-PO EXTRACTION AND CHARACTERIZATION OF NANOCELLULOSE FROM AGROINDUSTRIAL WASTE TO OBTAIN HYDROGELS

R. Hernández Leal[1], S. B. Brachetti Sibaja[1], A. M. Torres Huerta[2*], M. A. Domínguez Crespo[2**], Á. I. Licona Aguilar[3]

[1]TecNM- IT de Cd. Madero, DEPI, Av. 1° de Mayo esq. Sor Juana Inés de la Cruz s/n Col. Los Mangos, C.P. 89440, Cd. Madero, Tamps., México.
[2]Instituto Politécnico Nacional, Unidad Profesional Interdisciplinaria de Ingeniería campus Hidalgo, Sección de Estudios de Posgrado e Investigación, C.P. 42162, San Agustín Tlaxiaca, Hgo., México.
[3]Instituto Politécnico Nacional, Unidad Profesional Interdisciplinaria de Ingeniería campus Palenque, C.P. 29960, Palenque, Chis., México.

*Correspondence: *atorresh@ipn.mx, **mdominguezc@ipn.mx

Abstract: In this work, the extraction and characterization of cellulose and nanocellulose from sugarcane bagasse, banana pseudostem and *Aloe vera* bagasse, was carried out. The extraction of nanocellulose is performed by acid hydrolysis at 65 wt% H_2SO_4 with a reaction time of 15 minutes at 25 °C. The obtained nanocellulose was characterized by Fourier transform infrared spectroscopy (FTIR), X-ray diffraction (XRD), dynamic light scattering (DLS) and scanning electron microscopy (SEM); the extraction yields were greater than 45%. Subsequently, nanocellulose and chitosan hydrogels were synthesized, with weight ratios of 1:1, 1:1.5 and 1:2, citric acid as crosslinking agent, which were characterized by FTIR, SEM and their percentage of water absorption was also determined, obtaining percentages higher than 200%.

Keywords: Nanocellulose, hydrogels, agroindustrial wastes.

1. INTRODUCTION

Today, the need to create greater environmental awareness has contributed to the search for green materials; the excess of agro-industrial waste generated in the various processes of raw materials, generates an adverse environmental impact on soil, water and air, due to its inefficient disposal. Their availability, chemical and biological characteristics, make them an attractive source for various types of industries, textile, pharmaceutical, biomedical and others; these remnants are mainly composed of lignin, cellulose and hemicellulose, so they are also known as lignocellulosic residues. The lignin, cellulose and hemicellulose percentages depend on the source of extraction and processing [1]. They are currently responsible for the great interest of being used through innovative technologies, as potential raw material for the creation of new sustainable materials. Nanocellulose is cellulose on a nanometric scale, it has attractive characteristics: low density, mechanical properties, non-toxicity [2], biocompatibility [3], which makes it a raw material for a variety of specialized industries.

Recent studies show diverse residues as a source of cellulose extraction, among which it can find bagasse, seeds, agave

fibers, corn cobs, palm stalks, coconut fibers, rice straw [4] etc. These have been studied for various applications: biomedical implants, agriculture [5], food coatings, wastewater treatment [4], hydrogels [6], etc., due to their physical, chemical and biological characteristics.

In this research, the extraction, comparison and characterization of nanocellulose from three agroindustrial wastes generated in Mexico, sugarcane bagasse (SCB), a lignocellulosic agroindustrial by-product obtained during the extraction process of sugarcane juice to obtain sugar, was carried out. Fibers represent approximately 30% of the total weight in sugarcane processing; these fibers are composed of approximately 30 to 50% cellulose, 20 to 25% hemicellulose and 20 to 25% lignin. Due to their abundant availability, several methodologies using sugarcane bagasse as raw material have been reported; banana pseudostem (BPS), in banana harvest, only the fruit is used, leaving a large part of the plant unused, mainly the pseudostem, rachis, leaves and peel of the fruit, which can contain from 63.6 to 68.8% cellulose, making it attractive as a natural source for conversion to nanocellulose; Aloe vera bagasse (AVB), residue generated during the extraction process of Aloe vera gel, the bark or bagasse represents 20 to 30% of the weight of the entire plant and this structure is green or blue-green in color.

2. MATERIALS AND METHODS

2.1. Characterization techniques

FTIR analysis was performed to identify functional groups of the materials, using a spectrometer Perkin, Elmer Spectrum 100, in the range from 4000 to 500 cm^{-1}. The crystalline structures, with an X-ray diffractometer (XRD), Cu Kα radiation (λ = 0.15405 nm) in 2θ range of 6 to 40 ° with a scanning speed of 1 min^{-1}; the hydrodynamic nanocellulose particle diameter was analyzed using a Litesizer 500 equipment Dynamic Light Scattering, Particle Analyzer, Anton Paar. The morphological features were observed using a scanning electron microscope, JEOL JSM-6O10LA, applying an accelerating voltage of 20 kV with BSE, and different magnifications.

2.2. Waste treatment

The sugarcane bagasse is washed to remove any dirt it may contain during the grinding process and then dried at 90 °C for 48 hours. After drying the different residues, in a FOSS Cyclotec CT 293 mill, they are crushed to obtain biomasses with particle sizes smaller than 500 µm. The banana pseudostem (*Musa paradisiaca*) is washed and cut into small squares, crushed in a conventional blender and dried at 105 °C for 24 hours. The *Aloe vera* plant is washed, a horizontal cut is made in the lower part of the leaf, it is left to rest for 10 hours to eliminate the aloin, the gel is extracted; the residual *Aloe vera* bagasse is crushed in a conventional blender, washed as many times as necessary to eliminate the residual gel and then dried at 90 °C for a period of 24 hours.

2.3. Cellulose and nanocellulose extraction

During this procedure a solid-liquid Soxhlet extraction equipment is used to eliminate unwanted compounds; for this purpose, ethanol/toluene is used with a ratio of 1: 1 at 110 °C for 8 hours; then, the fibers are washed to remove residual compounds and dried at 60 °C; subsequently, during the delignification process, 3 g of previously treated fiber are

weighed, poured into a solution of 100 mL of sodium chlorite at 2.0 wt% (Sigma Aldrich, 80% purity) and 1 mL of glacial acetic acid (Sigma Aldrich, 99.8% purity), at a temperature of 60 °C, with a reaction time of 2 hours with constant agitation; during this procedure, the change of coloration to white is observed, these fibers are washed and dried, later a solution of NaOH at 10 wt% is added, with constant agitation during a period of 3 hours. Finally, it is filtered, washed until neutral pH and dried at 60 °C; then, to 1. 5 g of cellulose previously extracted, 100 mL of H_2SO_4 solution (JT Baker, 98.3% purity), is added with constant agitation for a period of time of 15 minutes, at a temperature of 25 °C, the hydrolyzed nanocellulose, is centrifuged at 5000 rpm, for 20 min in two cycles. The supernatant is removed and poured into a dialysis membrane, to ensure the removal of residual particles of acid hydrolysis, during this process the pH is controlled to be stable and close to 7.

2.4. Synthesis of hydrogels

The chitosan (Sigma Aldrich, medium molecular weight) is dissolved in 2 wt% glacial acetic acid, stirred for 24 h; the nanocellulose is dissolved in a crosslinking solution of 0.5 molar citric acid in a 2:1 ratio, then when the chitosan time is reached, the citric acid solution with nanocellulose is added, stirred for 24 hours, poured into the molds and dried at 45 °C.

3. RESULTS AND DISCUSSION

The production of nanocellulose is characterized by FTIR to know its chemical structure, XRD to study its crystallographic structure and DLS to determine the size of the nanocellulose particles, the hydrogels are characterized by FTIR, and the swelling percentage is determined.

3.1. Yield of nanocellulose

The percent yield of nanocellulose from the different residues for its application in hydrogels is determined, obtaining a higher yield in BPS 56.05 ± 2.97, followed by AVB 48.39 ± 2.59 and then SCB 45.70 ± 1.94, which can be affected by the type of residue.

3.2. Fourier transform infrared spectroscopy (FTIR)

Through this analysis, the functional groups of the nanocellulose obtained from agroindustrial waste were identified, as shown in Figure 1. The nanocellulose obtained from AVB shows 3 absorption bands with higher intensity in the interval from 3700 to 2976 cm^{-1} attributed to the vibration of stretching OH groups of water and cellulose molecules [7], in the signals of 2917 cm^{-1} CH_2 groups corresponding to asymmetric stretching, this signal is also observed in BPS and SCB; the signal of 2841 cm^{-1} is attributed to symmetric type stretching of the CH groups characteristic of the fibers; at 1730 cm^{-1} is attributed to the C-O and C=O groups of the acetyl and uronic ester groups of lignin and hemicellulose belonging to pectin, hemicellulose or to the esters and carboxyl bonds of lignin [8], which is observed with greater intensity in AVB; the 1627 cm^{-1} band corresponds to the symmetrical stretching vibration of the aromatic C=C or aromatic ring present in lignin and is observed with low intensity in the three types of nanocellulose [9]; the signal present in 1465 cm^{-1} corresponds to the asymmetric bending of CH_2 present in the amorphous zone of cellulose I and CH_3 of hemicellulose. The signals in the absorption bands of 1310 cm^{-1} with slight displacements at 1314 cm^{-1} are observed in the three samples, with greater intensity in BPS and are due to the vibrations of CH_2

of cellulose, the signals at 1258 and 1245 cm^{-1} belong to the C-O vibration in guaiacol ring belonging to the lignin present in AVB and SCB, the absorption bands at around 1160 and 1108 cm^{-1} present asymmetric C-O-C stretching vibrations in the association of the bands of the absorption molecules of cellulose and hemicellulose[10, 11]; the bands of higher intensity in the spectra of the 3 samples present signals in intervals from 1033 to 1020 cm^{-1} which are attributed to C-O vibrations in ester group in methoxyl and β(1→4) bonds in guaiacol units corresponding to lignin , the signal present at 949 cm^{-1} of the AVB fiber is an OH deformation out of the plane of carboxylic acids, the signals of the 3 biomasses obtained from in the 900-897 cm^{-1} intervals corresponds to C-O-C vibration and stretching in cellulose [8]. The absorption band at 826 cm^{-1} is an out-of-plane CH bending of guaiacol units in lignin, the 782 cm^{-1} signal presents C-C stretching vibration of the pyranose ring belonging to the lignin signal in the BPS spectrum; the 670 cm^{-1} signal C-O-H stretching is observed in BPS and SCB.

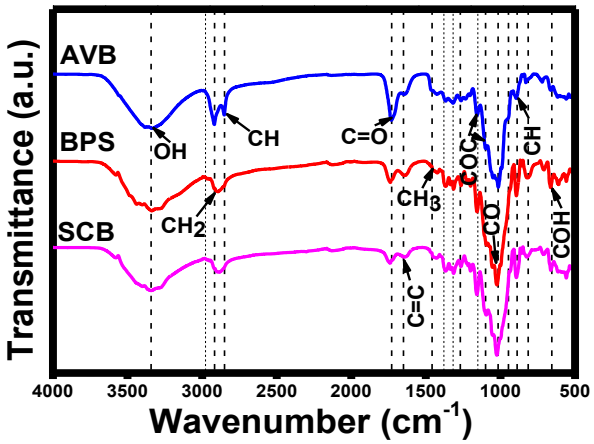

Figure 1. FTIR spectra of nanocellulose obtained from different biomasses, *Aloe vera* bagasse (AVB), banana pseudostem (BPS) and sugarcane bagasse (SCB).

3.3. X-ray diffraction (XRD)

By means of XRD analysis, the crystalline planes of the nanocellulose were analyzed, which were identified with the crystallographic charts PDF#00-56-1719, 00561718 and 00-56171717, for cellulose I alpha, beta and cellulose II, respectively.

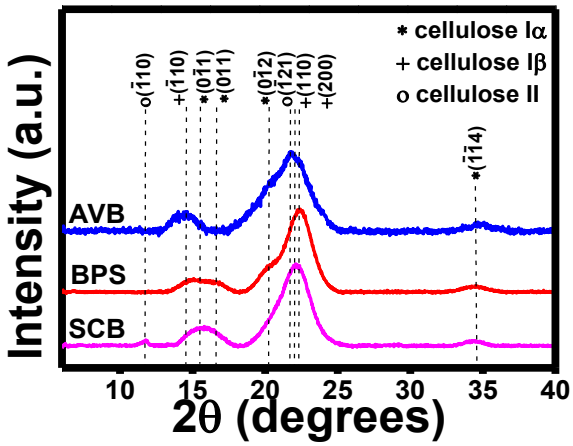

Figure 2. Diffractogram of agro-industrial waste nanocellulose.

Figure 2 shows that cellulose Iα is found in angle 2θ at 15.46° and 16.58° with the (01̄1) and (011) plane, respectively; in BPS and SCB; the angle of 20.19° and 34.54° correspond to (01̄2), (1̄14) planes in AVB, BPS and SCB; cellulose Iβ at 14.47°, 21.96° and 22.31° are the (1̄10), (110) and (200) planes observed in the three types of nanocellulose. Furthermore, cellulose II at angle 2θ of 11.71 is (1̄10) plane is only observed in SCB and 21.71° of (1̄21) plane in the three samples

3.4. Dynamic light scattering (DLS)

After the dialysis process to remove H_2SO_4 from the nanocellulose, 100 µL of a sample is taken and diluted in 10 mL of water; subsequently, three more dilutions are performed using 1 µL of each dilution and with the help of an ultrasonic bath the final dilution is dispersed for a time of 60 min for further analysis. This dilution is the

means to evaluate the behavior of the nanocellulose by Brownian motion.

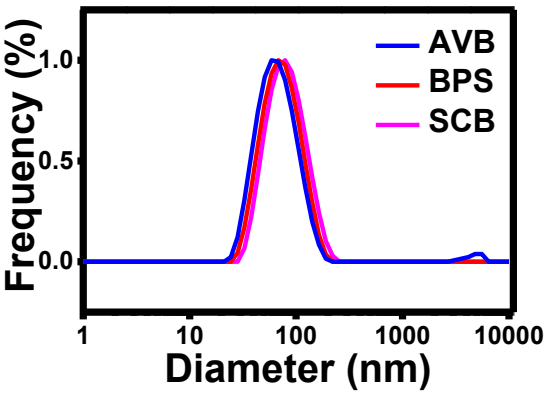

Figure 3. Nanocellulose dispersion, a) *Aloe vera* bagasse, b) banana pseudostem, c) sugarcane bagasse.

In Figure 3 it can be observed that, by the procedure used to obtain nanocellulose from the 3 agroindustrial wastes, it is possible to find nanometric sizes; however, it is also observed that there are particle sizes greater than 100 nm, this can be attributed to the fact that the cellulose was not dispersed correctly and that it tends to agglomerate, since in recent publications it has been reported that the nanocellulose agglomerates during the time that elapses for its measurement and the value obtained is usually not the most accurate; in addition, this technique measures the hydrodynamic radius of spherical particles and nanocellulose is in the form of a needle, so it is necessary to perform other analyses to complement the sizes obtained during this technique.

3.5. Scanning Electron Microscopy (SEM)

The nanocellulose obtained from the biomasses presented a diversity of sizes in the different samples; when dried, nanocellulose tends to agglomerate forming larger particles [12], as shown in Figure 4. where particles in the form of flakes and larger fibers formed by the agglomeration of nanofibers and cellulose nanoparticles can be seen; in addition, small fractures that possibly arose during the drying process can also be observed.

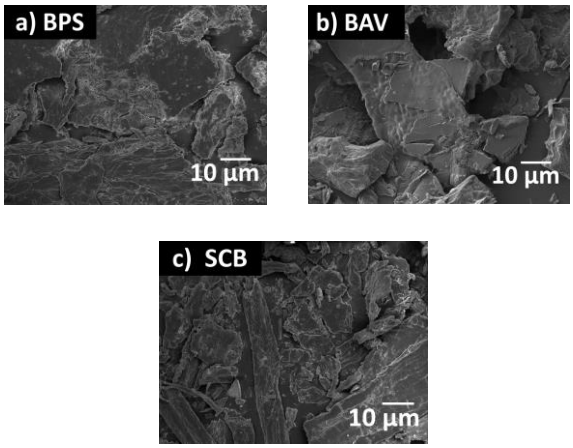

Figure 4. Micrographs of nanocellulose obtained from a) banana pseudostem, b) *Aloe vera* bagasse and c) sugarcane bagasse.

3.6. Hydrogels

The hydrogels obtained from the synthesis of nanocellulose (AVB, BPS and SCB), chitosan and citric acid were studied by FTIR, Figure 5. The signals between 3700-3100 cm^{-1} are observed the OH functional groups in the esterification reaction of citric acid with cellulose and chitosan [13], the absorption bands observed at 2916 and 2844 cm^{-1} correspond to the symmetric and asymmetric stretching of cellulose and chitosan, the band at 1737 cm^{-1} is an absorption signal derived from the stretching of the C=O functional groups ; likewise, a strong absorption band is observed between 1687-1640 cm^{-1} attributed to the stretching vibration of the C=O groups of the amide in chitosan [14], in the 1418-1400 cm^{-1} signal corresponds to the asymmetric CH_2 group present in the amorphous zone of cellulose I, the 1377 cm^{-1} signal bending vibrations of the CO and CH_3 groups

corresponding to the amorphous zone of cellulose, 1167 cm^{-1} asymmetric and symmetric C-O-C stretching in cellulose, 1135-1083 cm^{-1} stretching of the C-O-C glycosidic bond of chitosan, the signals between 900-897 cm^{-1} vibration and stretching of C-O-C and CH in β-glycosidic bonds in cellulose, the 780 cm^{-1} signal presents C-C stretching of the pyranose ring belonging to lignin.

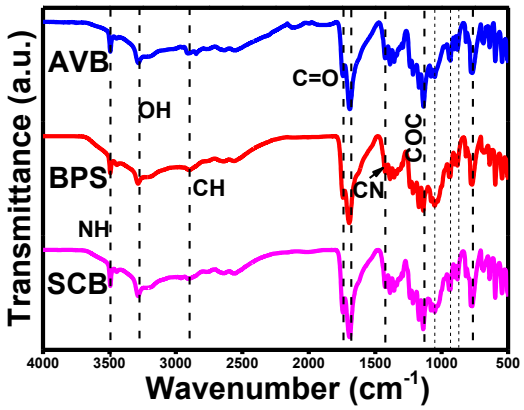

Figure 5. FTIR spectra of hydrogels obtained from the nanocellulose of the different residues.

3.7. Determination of the swelling behavior

The swelling property of the hydrogels was evaluated by immersing the dried samples in deionized water at room temperature for 24 h until equilibrium swelling was reached. Excess surface moisture of the swollen hydrogels was carefully blotted dry with absorbent paper before immediate weighing. The percentage swelling rate of all hydrogels was determined using equation (1).

$$Swelling\ ratio\ (\%) = \frac{Hi-Hs}{Hs}\ X\ 100 \qquad \text{Eq. (1)}$$

Where: Hs, Initial weight of hydrogel and Hi, Swollen hydrogel weight.

Figure 6 shows that the SCB nanocellulose hydrogel presented the highest percentage of absorption with 205.62%, followed by AVB with 204.88% and BPS with 188.97%.

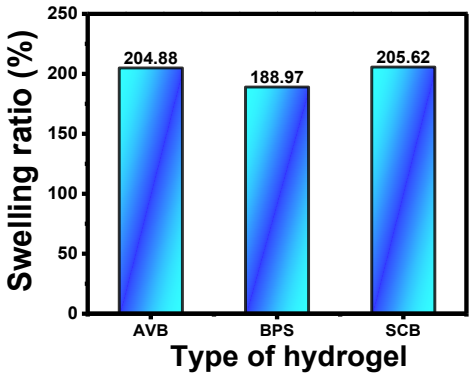

Figure 6. % swelling of the nanocellulose hydrogels obtained from the different wastes.

CONCLUSIONS

The results obtained in the FTIR spectra confirm the presence of functional groups characteristic of the residues; acid hydrolysis proves the elimination and significant changes of absorption bands of functional groups corresponding to hemicellulose and lignin. The presence of cellulose I alpha, cellulose I beta and cellulose II polymorphs was also verified by X-ray diffraction; nanometric sizes of cellulose are observed by DLS and an agglomerated morphology in the form of flakes by SEM; the analysis of hydrogels by FTIR shows interaction of the functional groups of chitosan and cellulose by means of the crosslinking agent citric acid, the swelling percentages of hydrogels show their potential use in various industries.

Agro-industrial waste biomasses such as *Aloe vera* bagasse, banana pseudostem and sugarcane bagasse are non-conventional sources of cellulose. The nanocellulose yield is affected by the nature and processing of the waste. Those obtained in this research work are suitable

for use as raw material for its extraction, which contribute to improving the environmental impact and to the generation of new materials such as hydrogels for various applications.

Acknowledgements

Rocío Hernández Leal is very grateful to CONAHCYT for her fellowship. The authors are thankful for the financial support provided by Instituto Politécnico Nacional through the SIP projects: 2025–0250, 2025–4746, 2025–0637, 2024–1065, the Energy Network project, COFAA, and SNII–SECIHTI.

Conflicts of Interest

The authors declare no conflict of interest.

REFERENCES

[1] R. Abolore, S. Jaiswal, A. Jaiswal, Carbohydr. Polym. Technol. Appl., 7, 100396 (2023).

[2] R. M. Cherian, R. T. Varghese, T. Antony, A. Malhotra, H. Kargarzadeh, S. R. Chauhan, A. Chauhan, C. J. Chirayil, S. Thomas, Int. J. Biol. Macromol., 253, 126571 (2023).

[3] J. Chen, Y. Ren, W. Liu, T. Wang, F. Chen, Z. Ling, Q. Yong, Int. J. Biol. Macromol., 193, 1324 (2021).

[4] M. Kaur, J. Pal, Carbohydr. Polym. Technol. Appl., 6, 100350 (2023).

[5] D. Skrzypczak, G. Izydorczyk, R. Taf, K. Moustakas, K. Chojnacka, Ind. Crops Prod., 205, 117500 (2023).

[6] R. Saberi Riseh, M. Vatankhah, M. Hassanisaadi, J. F. Kennedy, Carbohydr. Polym., 321, 121313 (2023).

[7] M. Raza, J. Mustafa, A. H. Al-Marzouqi, B. Abu-Jdayil, Int. J. Thermofluids, 21, 100548 (2024).

[8] G. D. Anukwah, V. P. Y. Gadzekpo, Heliyon, 10, e37701 (2024).

[9] D. S. Himmelsbach, S. Khalili, D. E. Akin, J. Sci. Food Agric., 82, 685 (2002).

[10] H. Yu, S. Y. H. Abdalkarim, H. Zhang, C. Wang, K. C. Tam, ACS Sustain. Chem. Eng., 7, 4912 (2019).

[11] N. Atykyan, V. Revin, V. Shutova, AMB Expr., 10, 84 (2020).

[12] M. Basak, E. Gandy, L. A. Lucia, L. Pal, Cell Rep. Phys. Sci., 4, 101689 (2023).

[13] J. Fehrmann, B. Belleville, B. Ozarska, M. Ismayati, W. Dwianto, Ind. Crops Prod., 210, 118070 (2024).

[14] J. Lan, J. Chen, R. Zhu, C. Lin, X. Ma, S. Cao, Int. J. Biol. Macromol., 231, 123587 (2023

145-IV-PO CHARACTERIZATION OF COOPERATIVISM FROM THE CREATIVE ECONOMY APPROACH

G. C. Lescas-Montes[1], J. Y. López-Cruz[1]*, G. Lugo-Espinosa[1]

[1]Instituto Politécnico Nacional, Centro Interdisciplinario de Investigación para el Desarrollo Integral Regional, Unidad Oaxaca, Hornos No. 1003, Colonia Noche Buena, Santa Cruz Xoxocotlán, Oaxaca, C.P. 71233.

*Correspondence: jylopez@ipn.mx

Abstract: Teotitlán del Valle, Oaxaca, is a Zapotec community known for its traditions and the production of wool textile crafts. However, the commercialization of crafts in the community faces challenges that affect the preservation of traditional knowledge. Here, a local artisan cooperative uses traditional dyeing and weaving techniques while promoting sustainability to cope with this tension and ensure the well-being of its members. This situation raises the need to analyze how cooperativism influences the social well-being of artisans by achieving balance amid this tension.

In this sense, the creative economy approach allows us to understand how creativity, culture, and sustainability are integrated into economic activities. From this perspective, the cooperative practices of artisans are explored, as well as their relationship with cultural preservation and alignment with the principles of equity, social justice, and sustainable development.

To this end, this research focuses on characterizing cooperativism from the creative economy perspective, as a first step to understanding the role of cooperativism in this framework. The document is part of a thesis, still in progress, on a case study of this cooperative in Teotitlán del Valle.

To this end, qualitative research with an exploratory and descriptive design was chosen, where a theoretical review, participant observation and semi-structured interviews were carried out. The preliminary results indicate that the practices and relationships of the partners are determined by the sociocultural context, which influences social well-being. Also, three dimensions of cooperativism were distinguished from the creative economy approach, as well as characteristics of each of them to better understand this approach.

These findings reinforce the relevance of cooperativism as a model of sustainable local development, showing how the community can be a way to achieve social well-being.

Keywords: Artisans, Cooperativism, creative economy, handicrafts.

1. INTRODUCTION

Teotitlán del Valle is a Zapotec community in Oaxaca, known for the cultural heritage of the community's traditional wool rugs and crafts. In this municipality, in 2003, around twenty artisans joined a cooperative where the need to unite efforts and resources to work collectively in the production of textiles for sale led to the creation of this cooperative the following year.

The main problem that the now ten partners continue to face is unfair competition, since the commercialization of textiles has expanded to other artisans who do not adhere to sustainability in this trade. This has generated social tensions between achieving constant production that satisfies the demand for crafts, and the care of the environment and natural resources.

Derived from this problem, the question arose: what are the characteristics of cooperativism that influence the generation of social and environmental well-being in this context? As a tentative hypothesis, it was proposed that from the collaborative approach, benefits arise that contribute to promoting social well-being and sustainability. In this sense, from the perspective of the creative economy, it is evident that creativity, culture and innovation can act as engines of development [1], as long as they integrate society into caring for the environment through sustainable practices in economic activities [2].

It is worth emphasizing that cultural manifestations alone would not have significance, but rather, it is in social everyday life where people relive the meaning of their practices. Thus, it is society and its actions that give meaning and significance to all manifestations of culture. An example of this is how artisans continue to weave Zapotec symbols and iconography present in archaeological remains of the region, as well as elements of nature and its environment that reflect their worldview.

Research is ongoing because, based on the analysis of the influence of cooperativism on social welfare, strategies can be proposed to strengthen the organization, providing members with greater tools to promote social cohesion and sustainability in the medium and long term. Specifically, this document aims to characterize cooperativism from the perspective of the creative economy, as a first step to comprehensively understanding cooperativism as a driver of change, considering the particularities of the sociocultural context.

2. MATERIALS AND METHODS

To understand the experiences and meanings that artisans have about their craft and well-being, as well as the relevance of the sociocultural context, qualitative research with an exploratory and descriptive design was chosen. Thus, through a case study, still in progress, the aim is to achieve a deep immersion in the reality of artisans and their links with the community [3]. The methodological process was structured in four stages: problem statement; data collection; analysis; and conclusions.

For data collection, a bibliographic review was first carried out to conceive a theoretical framework that addressed a vision of cooperativism from the creative economy. This theoretical basis provided a first set of categories that guided the collection of data in the field. At the same time, participant observation and semi-structured interviews were carried out with artisans to learn about their opinions and experiences at cooperative, as well as relevant aspects at the individual and community level. This process was a key factor in interpreting and giving meaning to the results, as it allowed for a contextualized analysis of the processes and motivations that are manifested in the activities carried out by the cooperative.

A sample of typical cases was used, which, as defined by Hernández-Sampieri et al. [4], consists of carrying out a detailed and well-founded study that explores the practices, beliefs and symbolism within a specific social group.

The selection of the analysis units was determined by the selection criteria that included: active members, seniority of more than eight years in the cooperative, native language speakers and natives of Teotitlán del Valle. Thus, emphasis was placed on a well-structured non-probabilistic sampling that would allow the collection of reliable and relevant data. In this way, through interviews with six of ten members, five of them founders, valuable information was obtained to understand the social phenomenon.

For the analysis of the information, the coding was done manually, without the use of software. From the interviews and observation, codes were assigned to the relevant data that were found, such as intangible value, social cohesion, innovation, environmental awareness, and development opportunities. These codes were organized into open

categories that in turn allowed the data to be grouped into emerging dimensions.

From this open coding, the data obtained in the field from the key actors was compared with the categories previously identified in the literature. The information was organized through a theoretical content analysis, to conduct the triangulation of methods and data that grant the validity of the qualitative research [4]. By integrating the theory with the data obtained from the artisans, a more complete and precise interpretation of the reality of the cooperative in Teotitlán del Valle was achieved.

3. RESULTS AND DISCUSSION

Teotitlán del Valle, whose name means "place of gods" in Nahuatl [5] is a Zapotec community with a cultural heritage that is evident in its language, gastronomy, crafts, festivities and community traditions. For centuries, its inhabitants have made wool garments dyed with plants, although since the 1980s, this activity has acquired greater relevance, consolidating the rise of local artisans. However, the Zapotec identity of Teotitlán remains alive through the transmission of traditional knowledge, the perpetuation of practices and rites of its ancestors, and the inclusion of the family in these activities, reflecting the commitment of its inhabitants to their roots and the desire to preserve their heritage.

The contextualization of Teotitlán del Valle constitutes a fundamental element to understanding the sociocultural context of this community, considering, for example, the significant number of artisan workshops it has. Here, cooperativism emerges as an alternative that transcends neoliberal economic models, integrating with the creative economy to promote social well-being, culture and respect for nature, in an equitable manner [6].

This integration also redefines the relationship between cooperativism and well-being, by interweaving collaboration, sustainability, culture, and equity to create an environment conducive to development. As Gogoi mentions [7], cooperatives based on local practices and with a cultural background can help rethink the economy, focusing on the ethics of care, interdependence, solidarity and collectivity. Thus, a concrete and feasible alternative to hegemonic ideas about development is presented.

To characterize cooperativism from the perspective of the creative economy, three dimensions were identified as an approximation to better understand the nature of these cooperatives: cultural-social; development-opportunities; and sustainability.

Thus, in the cultural-social dimension, three fundamental characteristics can be distinguished that reflect how cooperatives enrich and preserve cultural identity, while strengthening community solidarity:

- Intangible value, visible through aspects such as shared identity and the sense of belonging that members share towards the cooperative and the community; as well as satisfaction with the benefits obtained, both material (employment, workspace, inputs) and immaterial (learning and recognition).
- Social cohesion, which is manifested in the capacity of cooperatives to foster collaboration and solidarity in their relationships, as well as resilience to face crises and adapt to changes, in accordance with a shared historical worldview.
- Cultural diversity, which is observed in how cooperatives recognize and value cultural identity, preserving local traditions and knowledge, placing them as a differentiating element for development [8].

In this dimension, elements are distinguished that help create stronger and more resilient cooperatives, while valuing and protecting their cultural and social identity.

On the other hand, the development-opportunities dimension includes

characteristics related to economic growth and the creation of opportunities that are feasible for a greater number of people.

- Relationship with other economic sectors, which is observed in the interaction of cooperatives with other industries, which facilitate collaboration through joint festivities and events, generating in turn, economies of scale.
- Innovation, in which the development of competencies based on ethnographic and cultural elements is distinguished, which respects community identity. Likewise, the inclusion of new practices and technologies to improve efficiency and sustainability in their activities [9].
- Inclusion, in which cooperatives generate employment, access to resources and training for people of different ages, skills and knowledge. This allows integrating a diversity of voices and perspectives that contribute to improving the well-being of a greater number of people [10].

These characteristics highlight the role of cooperatives in economic development, inclusion, and the creation of equitable opportunities for more people.

Finally, the Sustainability dimension, which integrates the characteristics related to environmental commitment and the reproduction of local knowledge by these cooperatives.

- Use of sustainable materials and techniques, which is seen in the practices and processes that cooperatives adopt to minimize their environmental impact and conservation of the territory, as an inherent need of the space where they live.
- Environmental awareness, recognizing that, beyond carrying out an activity that provides them with economic sustenance, they must also find a balance between the preservation of traditions, historical knowledge and community identity, which guarantees that this can continue to be feasible for future generations [11].

This framework was a preamble to have a broader panorama that allows us to understand that the practices and actions that are implemented in cooperative societies immersed in a significant sociocultural context will be strongly determined by said context.

In this sense, as Rojas-Herrera and Méndez-Rojas [12] summarize in their research on the experience in the case of the Tosepan Titataniske Cooperative Union, for the partners to achieve success, and above all the "Yeknemelis", that is, the "good life", one of the main elements was the union they have made between the indigenous culture and the principles of cooperativism [12].

In turn, Fernández et al. [13] reiterate the link between the sociocultural context and the cooperatives, identifying them as "local development agents", since they emerge from local spaces and from inhabitants of these communities. However, they object that, for the cooperatives to fulfill this role, it is essential that they actively involve themselves in the transformation of their communities, taking advantage of the strengths of the environment to promote progress and social well-being.

Thus, in the cooperative society under study, significant cultural elements were identified both in its members and in the community, to analyze and understand the processes that they developed during the twenty years that they have been in operation, and which led them to their current consolidation.

Thus, the elements identified include the preservation of Zapotec traditions, such as the use of ancestral techniques in the production and dyeing of textiles, as well as a deep respect for their environment. This cultural preservation is not only reflected in the crafts, but also in daily life and their relationships.

For example, the cooperative initially began to work with the extraction of plants in natural

spaces in the community to dye their products, as their ancestors had historically done. However, due to the concern about not degrading the environment that surrounds them, over time, they integrated sustainable practices in a collective garden where they began with the production of the organic inputs necessary to continue with the natural dyeing techniques. In this way, these values and meanings play a key role in the structure and dynamics of the organization.

The analysis of these characteristics and of the processes developed shows that the cooperative has managed to consolidate itself thanks to its capacity to articulate cultural values, cooperative principles, and sustainability. In this regard, Olmedo-Barchello [14] mentions that the creative economy is manifested in areas related to crafts and cultural tourism, favoring vulnerable communities. However, she distinguishes it is worth noting that beyond the economic impact they generate, they perpetuate social and cultural values, acting as tools to reduce inequality through a social awareness that contributes to people's identity by reinforcing their cultural practices.

Specifically, the cooperative in Teotitlán del Valle, by integrating these characteristics, has facilitated the creation of a resilient organizational model, with a high degree of cohesion, capable of facing the challenges of the market and, at the same time, preserving its cultural identity and historical legacy.

However, it must be recognized that one cannot have an idealizing vision of cooperativism, the creative economy or their combination, since even though the members share a previous community identity, the human condition and the current hegemonic system significantly influence the processes and challenges that arise in their operation and test the resilience of the group.

Also, although it is assumed that certain characteristics of the creative economy are present in these cooperatives, in practice they do not always manifest themselves. This is due to two factors: first, cooperatives are not often identified as part of the creative economy, as they arise from specific needs and common objectives in a particular context. Second, the creative economy is a relatively new approach and lacks sufficient dissemination by (national) authorities, which leads to a lack of awareness among cooperatives about its scope and how to include it in their organization.

4. CONCLUSIONS

In conclusion, cooperativism is characterized by intrinsic values of support, integration, respect, solidarity, and collective financing that support their collaborative work, which positively influences the well-being of the members.

Based on this, they develop an exchange of experiences, transmission of knowledge, resolution of marketing problems, better organization to reduce costs and integrate sustainable practices with the environment.

Working with traditional wool textiles under the cooperative model has allowed members to strengthen ties of social cohesion and promote the safeguarding of their intangible cultural heritage, which reflects the worldview of their Zapotec community.

The cooperative has solid foundations that encourage the inclusion of people in vulnerable conditions who are dedicated to the production of artisanal textiles within the community of Teotitlán del Valle, promoting equity and local development.

In addition, they are committed to sustainability and preservation through responsible practices implemented in their production, such as the work they do in their collective garden to obtain organic products that they use as natural dyes.

In this case study, cooperativism has been a great support for the production and continuity of artisanal work, family livelihood, and the preservation of the historical and cultural heritage of Teotitlán del Valle.

Among the challenges to be faced are the search for and opening of cultural spaces in more central areas of the state of Oaxaca to promote the sale of their textiles; the positioning of crafts dyed with natural products that they make, against mass productions and imitations; the transmission of knowledge to new generations; and the recognition of their authorship as designers of Zapotec textile art.

Acknowledgements

This study was developed within the framework of the SIP project 20242329. Special thanks are extended to the textile artisans of the Centro de Arte Textil Zapoteco Bii Daüü cooperative society, who have generously shared their time, experiences, knowledge, and concerns for this research that seeks to give them greater recognition. Also, thanks to CIIDIR Oaxaca; to CONAHCYT for its MCCARN postgraduate scholarship; and to the National Polytechnic Institute through project SIP 20242329.

Conflicts of Interest

The authors declare no conflict of interest.

REFERENCES

[1] F. Buitrago, I. Duque. La economía naranja; 1nd edn. (Bogotá, Puntoaparte Bookversiting, 2013) p. 244.

[2] L. Deheinzelin. Revista Mexicana de Bachillerato a Distancia. (2011) https://doi.org/10.22201/cuaed.20074751e.2011.5.47417

[3] R. Hernández-Sampieri, C.P. Méndoza-Torres, Metodología de la investigación: las rutas cuantitativa, cualitativa y mixta. 2da edn. (Ciudad de México: McGrawHill Interamericana Editores; 2023) p.752

[4] R. Hernández-Sampieri, C. Fernández-Collado, P. Baptista-Lucio. Metodología de la investigación: las rutas cuantitativa, cualitativa y mixta, 6ta ed. (México: McGrawHill; 2014). p.634

[5] Biidaüü. Centro de Arte Textil Zapoteco Biidaüü. (Newlight Technologies, Inc. 2024) http://www.biidauu.com.mx/spanish/03.html. Accessed 10 October 2024.

[6] C. L. Gomes. La economía creativa y las industrias culturales y creativas: ¿una alternativa postcapitalista?. (Universitat de Barcelona, 2018) https://www.ub.edu/geocrit/Sociedad-postcapitalista/ChristianneGomes.pdf Accessed 13 April 2024

[7] R. Gogoi, J. Sage. (2023) https://doi.org/10.1177/09722661231158508

[8] A. Pereira de Castro-Pacheco, E.G., Benini, M. A. Pasquotto-Mariani, (2017). Estudios y perspectivas en turismo, 26(3), p.678-697. https://www.scielo.org.ar/scielo.php?script=sci_arttext&pid=S1851-17322017000300010&lng=es&tlng=es Accessed 21 october 2024

[9] B.V. Cruz-Barrionuevo, L.R. Charro-Chasipanta, V.P. Velásquez-Albarracín, A.P. Villalta-Baquero. Dominio de las ciencias(2020) http://dx.doi.org/10.23857/dc.v6i5.1578

[10] C. Martínez-Olivera, C.A. Ken-Rodríguez, A.E. Miguel-Velasco. Economía creativa. (2020) https://doi.org/10.46840/ec.2021.16.06

[11] L.I. Rodríguez-Oliva, Economía creativa, cultura como bien público y desarrollo sostenible: intersecciones en las políticas culturales (Ministerio de cultura, República de Panamá, UNESCO, 2023), https://micultura.gob.pa/wp-content/uploads/2023/04/Edicion-2023-Economia-creativa-LIRO-Baja-resolucion.pdf. Accessed 22 October 2024

[12] M.E. Rojas-Herrera, D.A. Méndez-Rojas. Textual. (2020) https://dx.doi.org/10.5154/r.textual.2020.76.02

[13] G. Fernández, M. Narváez, A. Senior, (2010). Revista Venezolana de Gerencia, 15(49), p.87–102. http://ve.scielo.org/scielo.php?script=sci_arttext&pid=S1315-99842010000100006&lng=es&nrm=iso&tlng=es. Accessed 21 october 2024

[14] S. Olmedo-Barchello, Población y Desarrollo. (2017) https://dx.doi.org/10.18004/pdfce/2076-054x/2017.023(45).061-073

203-IV-PO INSECTS AS AN ALTERNATIVE TO HUMAN AND ANIMAL NUTRITION

T. Aquino-Aguilar[1*], J. A. Morales-López[1], Y. D. Ortiz-Hernández[2], T. Aquino-Bolaños[2], K. Cruz García[1], T. Aquino López[1]

[1]Secretaría de Ciencias, Humanidades, Tecnología e Innovación (SECIHTI), Instituto Politécnico Nacional, CIIDIR Unidad Oaxaca, Santa Cruz Xoxocotlán 71230, Oaxaca, México. [2]Instituto Politécnico Nacional, Centro Interdisciplinario de Investigación para el Desarrollo Integral Regional, Unidad Oaxaca. Hornos 1003, 71230 Santa Cruz Xoxocotlán, Oaxaca.

*Correspondence: taquinoa2000@alumno.ipn.mx

Abstract: The search for foods that provide nutritional benefits, and a smaller environmental footprint has become a necessity due to population growth, climate change, overexploitation of natural resources and loss of biodiversity. However, the use of insects in human and animal feed could be an alternative, so the aim of this study was to gather information on the use of insects in human and animal feed, for this, a search was conducted for scientific articles related to the implementation of insects in human and animal diets was carried out, and the insects used, proportion, mode of administration, as well as advantages and disadvantages of their consumption were identified.

It was found that the use of insects is an alternative food that can be implemented in the diet of humans and animals due to the benefits of their consumption, as they have a high content of protein (38-65%), lipids, vitamins and minerals, which can vary depending on the species, development cycle, form of consumption and level of inclusion. Additionally, it is considered a sustainable and environmentally friendly alternative, because less water and soil are used for its production compared to agriculture and livestock farming, and it also reduces the emission of greenhouse gases, which are one of the main problems in the livestock sector. However, it is necessary to continue to evaluate the biological parameters in humans and animals to determine the most important benefits and detriments that can be caused by its consumption.

Keywords: diet, food, animal feed, sustainable

1. INTRODUCTION

The number of inhabitants is expected to be at least 10 billion by 2050, and food demand is expected to increase by approximately 50% [1], generating problems of food and fodder insecurity, loss of biodiversity, environmental degradation, disproportionate disposal of food and resources, as well as unsustainable food production practices [2], so it is necessary to find alternative foods that are sustainable and efficient for human and animal consumption.

Insects possess characteristics that make them a promising alternative to address food security issues [3]. 1) Nutritional characteristics: protein, mineral, vitamin and carbohydrate content; 2) Environmental: lower soil and water use requirements and a reduction in greenhouse gas and ammonia emissions compared to livestock; 3) Economic: lower capital and technology investment for insect collection and cultivation [4]. However, it is necessary to evaluate the impact of insects on human and animal food.

There are approximately 2300 species of edible insects in the world, which are consumed in different stages of development (egg, larva, pupa and adult) [5]. In Mexico, insects are part of the traditional gastronomy of pre-Hispanic cultures such as the Aztec, Zapotec and Mixtec. However, currently their consumption continues to be part of their legacy, since in

some states of the republic such as Guerrero, Oaxaca and Chiapas some insects are consumed, as is the case of "chapulines" (*Sphenarium* sp), "chicatanas" (*Atta mexicana* sp) and "chicharras" (*Diceroprocta* sp), insects with high nutritional content, and in some places of Mexico they are considered pests of some crops [6,7]

For this reason, the objective of this work is to collect information about insect consumption, forms of intake, methods of procurement, levels of inclusion and the advantages and disadvantages of their possible implementation in human and animal diets.

The importance of this work lies in raising awareness about the use of insects as a food and feed alternative, as well as showing how insects can contribute to global food security.

2. MATERIALS AND METHODS

The methodology used was qualitative. Information was collected from primary sources using techniques such as direct observation, as well as scientific articles published in various journals and books published in the last decade on the use of insects in human and animal food.

3. RESULTS AND DISCUSSION

3.1 Insects as a food alternative

The implementation of insects as part of food for humans and animals is an idea that should be considered, because it has been reported in several scientific studies that insects have a high protein content, as well as a wide diversity of amino acids, lipids (polyunsaturated fatty acids), carbohydrates, vitamins and minerals [8]. However, their nutritional composition may vary according to species, sex, developmental stage, diet and geographical origin [9,10].

The use of insects as food and feed is a promising option for a more sustainable food system due to the characteristics of their cultivation. Table 1 shows some of the insects that have been cultivated to obtain oils and flours that serve as ingredients in animal diets [11] and in common edible products to increase their acceptance and consumption [12].

Table 1. Insects reared for food and fodder purposes [3].

Scientific name	Common name
Tenebrio molitor	Mealworm yellow
Alphitobius diaperinus	Lesser mealworm
Zophoba morio	King worm
Acheta domesticus	domestic cricket
Gryllodes sigallatus	Tropical house Cricket
Gryllus bicmaculatus	Two spotted cricket
Locusta migratoria	Migratory locust
Galleria mellonella	Wax moth
Bombyx mori	silkworms
Hermetia illucens	Black soldier fly
Musca domestica	Domestic fly
Rhynchophorus ferrugineus	Red palm weevil
Rhynchophorus phoenicis	African palm weevil
Pachnoda marginata	African flower beetle
Apis mellifera	Bee
Lucilia sericata	Green fly

3.2 Insects for human consumption

Insects have been food for humans since prehistoric times and today their consumption is part of the traditions of many regions of the world [3]. More than 3,000 ethnic groups distributed in Asian, African and Latin American countries are consumers of insects in different presentations (raw, boiled, roasted or fried) as part of their diet [12]. The exact

number of insects consumed in the world is not known, however, it is estimated that there are approximately 2300 species of edible insects [13], distributed in 37.67% in the African continent, 36.45% in America, 17.75% in Asia, 6.19% in Australia and only 1.94% in Europe.

The most consumed insects worldwide are beetles (Coleoptera) and caterpillars (Lepidoptera), followed by other insects such as grasshoppers (Orthoptera), crickets, locusts, ants, wasps, bees (Hyminoptera), termites (Isoptera) and flies (Diptera) [9].

In Mexico, the most consumed insects are: ”chapulín” (*Shephenarium* sp), “chicatana” (*A. mexicana*), “escamoles” (*Liometopum apiculatum*), “gusano blanco de maguey” (*Aegiale hesperiaris*), “jumiles” (*Ascra cordifera*), “gusano rojo de maguey” (*Comadia redtembacheri*), “cuetlas” (*Arsenura armida*) [14,15], however, there are approximately 500 species of edible insects in Mexico Téllez-Morales et al. [16], which are part of the diet in various regions of Mexico, mainly in the center and south of the country (especially in the states of Hidalgo, State of Mexico, Chiapas, Guerrero, Oaxaca, Puebla and Yucatán) [17]. As for their preparation and forms of consumption, it was found that before being ingested, insects go through a process of collection, processing, storage and sale, where they can be found dried, fried, roasted, live and boiled [14]. Figure 1 shows three different edible insects (chapulines, chicatanas and red maguey worms) that are sold in downtown Oaxaca City, Mexico.

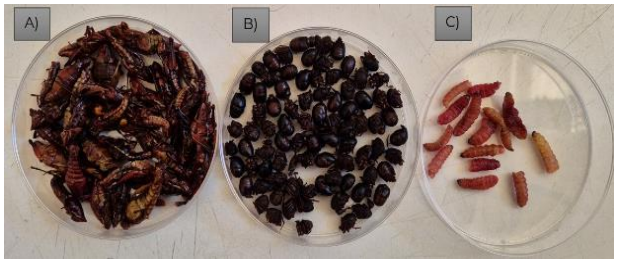

Figure 1. Sale of edible insects in the market of Oaxaca City, Mexico: A) Chapulín, B) Chicatana, C) gusano rojo de maguey.

In the last decade, research has been carried out to determine the nutritional composition of insects, and it was found that on average insects contain 23.72 ± 16.08 g/100 g of fat, 48.25 g/100 g of protein and in terms of carbohydrate content, a variation between 0.1 g/100 g (*Gryllodes sigillatus)* and 81.2 g/100 g (*M. melliger*) was found [10]. Ordóñez-Araque and Egas-Montenegro [18] they also mention that insects are a source of minerals (Cu, Fe, Mg, Mn, P and Se and Zn), however, the content of each mineral varies according to the species, diet and developmental stage of the insect, an example is the larvae of *T. molitor* that had higher mineral content than adults [1]. Insects can provide more energy than foods derived from livestock and vegetables, providing 217-777 Kcal/100 g, while livestock and vegetables provide an energy content of 165-705 and 308-352 Kcal/100 g, respectively [3].

3.3 Is the consumption of insects beneficial or harmful to health?

The consumption of insects has benefits for human health, including energy intake [10], reduction of the risk of degenerative diseases and iron deficiency anemia due to their iron and zinc content [19], nutritional contribution as they help to reduce malnutrition since insects contain high amounts of proteins and fatty acids, and lipids are essential in cell metabolism and function as transport for fat-soluble vitamins [20]. Insects possess chitin, a carbohydrate that functions as a prebiotic, shows anti-inflammatory capacity, stimulates the immune response and serves to prevent diabetes and control obesity [21]. It possesses compounds with antioxidant and antihypertensive activity, such compounds capable of inhibiting angiotensin-converting enzyme, which helps in the treatment of arterial hypertension [22].

However, the ingestion of insects can also cause some health problems since some species present antinutrients such as: oxalate, which causes a poor absorption of calcium and magnesium, and forms complexes with proteins that impair metabolism; phytates reduce the bioavailability of some minerals, mainly affecting zinc, since this molecule binds to proteins and minerals [23]. Similarly, they can be carriers or transmitters of

microorganisms associated infections in the intestinal tract, which can act as opportunistic pathogens in humans (*Listeria* spp., *Bacillus* spp., *Staphylococcus* spp., and *Clostridium* spp.) [24]. Likewise, the presence of heavy metals (As, Cd, Pb and Hg) has been described in some edible insects of the order Coleoptera, Lepidoptera and Orthoptera although they were below the limit recommended by the European commission (Commission Regulation 1881/2006) [25].

3.4 Insects as animal feed

The use of insects in animal feed is becoming an increasingly attractive alternative because they provide animals with high quality proteins in a sustainable way, considering that most insects can satisfy the nutritional needs of animal diets, specifically in the amino acid and protein content [26]. In addition, their ability to be reared on a large scale stands out, as well as their short life cycles, which helps to obtain harvests in short periods of time.

Regarding their production, insects require lower volumes of feed, soil and water compared to the production of farm animals, which contributes to generate a lower environmental impact [3]. Therefore, the inclusion of insect meals in animal diets is an interesting option.

However, the implementation of vegetable meals in diets generates a deficit of essential amino acids (AA) such as lysine, methionine and leucine, making necessary the implementation of other flours such as fishmeal, which have a negative impact on aquaculture ecosystems. Insect meal can substitute these meals, since they include the AA limited in vegetable proteins and contain a higher number of proteins ranging from 20 to 80%. For this reason, the insects most used in animal feed are *H. illucens, T. molitor, A. domesticus* and *M. domestica*.

3.4.1 Poultry

The collection and use of pest (agricultural) insects in poultry feed can reduce the consumption of pesticides harmful to humans that are used on agricultural crops as a control method, as well as reduce the use of corn and soybean meals, which hinders the production of conventional feeds due to the scarcity of these products [27]. There are places such as India, Guinea, Burkina Faso and Togo where live termites are fed to poultry (chickens, ostriches), and other places (South Korea, Russia, Cameroon and Nigeria) use fresh and dried larvae of M. domestica [28]. Some studies have shown that maggot meal can replace fish meal in broiler production, improving meat quality and increasing live weight rate by 10-15 % [29], Secci et al [30] reported that the use of *H. illucens* in broilers with a 5 % dry matter portion improved growth rate, feed efficiency, meat and immune status. In addition, arginine and methionine present in *A. domesticus* meal improve feed conversion ratio in poultry, and positive results have been observed when 15% *Acridia cinere*, *Anabrux simplex* and *G. testaceus* meal is included in broiler diets.

3.4.2 Livestock

In the world, 33% of the world's cropland is used for livestock feed production, so it is crucial to find more efficient ways to feed livestock. Insects are an alternative to supplement current feed sources, mainly based on fish meal and soybean meal [18]. Moula et al. [31] reported that protein digestibility in ruminants was 90.49 % when fed fresh termites and 85.67 % when fed brown locusts. Jayanegara et al [32] mention that Holstein Friesian cattle fed *H. illucens* larvae produce less gas due to higher fiber content. It has also been observed that when pigs consume 4-8% *H. illucens* prepupae as a supplement, their homeostasis increases [33], and piglets fed diets supplemented with *H. illucens* meal show no significant differences in blood, intestinal and histological profile compared to conventional feeding [34].

3.4.3 Aquaculture

Currently aquaculture feeds are mainly made from cereals, oilseeds and components of marine origin, however, the demand for feed by terrestrial animal production poses a challenge to the profitability of aquaculture

feeds, so the use of insect meals in aquaculture is a viable alternative, since naturally many aquatic species feed on insects, currently the insect species that are considered suitable for the production of feed combined with other ingredients are: *H. illucens, M. domestica, Anaphe panda, Acrididae, Kalotermes flavicollis, T. molitor* [35].

Hasan [36] concludes in his book that fish meal used in diets for omnivorous fish (*Bagre* sp. and *Cyprinus* sp.) can be partially substituted by insect meal as they provide sufficient protein for growth; however, he stresses that profitable large-scale insect farming practices need to be developed to meet the demand for psiculture. Linh et al. [37] mention that the benefits of *H. illucens* meal have been effectively studied in several fish species (*Salmo salar*, *Cyprinus carpio, Oreochromis niloticus, Oncorhynchus mykiss*, among others), however, the optimal amount of substitution must be considered, as incorrect substitution can cause negative effects on physiological processes, growth and fillet quality. Another study using *H. illucens* meal for shrimp farming revealed no taste differences between shrimp fed traditional feeds. *T. molitor* meal has been evaluated in diets for different fish species and it is mainly recommended to include 25-30 % *T. molitor* in diets [38]. Improved growth of *Pagrus major* was observed when 65 % defatted *T. molitor* meal was included and *O. mykiss* showed better performance with different inclusion levels. Table 2 shows the optimum inclusion levels of some insect meals for each different fish species.

Table 2. Insects used as an ingredient in experimental fish feed diets [39].

Insect	Inclusion (%)	Fishe
T. molitor	5-25 15-30	*Oncorhynchus mykiss* *Oreochromis niloticus*
H. illucens	33-100 18.5-37 10-30	*Salmo salar* *Acipenser baerii* *O. mykiss*
A. domesticus	15	*Argyrosomus regius*
L. migratoria	20	*Dicentrarchus labrax*

It should be noted that, according to the information found, insects are an alternative for human and animal feed due to their nutritional properties, which provide benefits to human and animal health. However, it is important to continue studying the effects of including insects and to emphasize the negative effects and how they could be avoided. It is also important to investigate and propose methods for the mass production of insects and for the breeding of new insect species.

4. CONCLUSIONS

Insects are a viable alternative for human and animal feed due to their nutritional properties.

The consumption of insects provides nutrients and has benefits to human health, by providing energy, reducing the risk of suffering from degenerative diseases, as well as favoring the growth of animals, when included in their diet. However, the levels of inclusion must be considered, since it can cause damage to health, due to the presence of antinutrients in some insects.

The importance of this work lies in making insects known as a sustainable alternative in the human diet and promoting their application as a source of protein in animal production.

On the other hand, further research is needed into all aspects necessary to create standards and regulations for the consumption and marketing of insects as food and feed.

Acknowledgements

To the Instituto Politécnico Nacional CIIDIR Oaxaca for the financial resources and space provided for this research. To the Consejo Nacional de Humanidades Ciencia y Tecnologías (CONAHCYT) for the support given to the first author to carry out postgraduate studies in Conservation and Use of Natural Resources at CIIDIR Oaxaca and to the Sistema Nacional de Investigadoras e Investigadores SNII-CONAHCYT for the support given to the professors of the Instituto Politécnico Nacional.

Conflicts of Interest

The authors declare no conflict of interest.

REFERENCES

[1] M. Lu, C. Zhu, M. Zhao, H. Zhang, F. Zhang, Y. Du, Food Science and Human Wellness. (2024) http://doi.org/10.26599/FSHW.2022.9250005

[2] R.P.F Guiné. S.G. Florenca, E. Bartkiene, M. Tarcea, C. Chuck-Hernández, I. Djekic, S.M. Matek, N.M. Boustani, M. Korzeniowska, Journal of Culinary Science y Technology. (2024) https://doi.org/10.1080/15428052.2024.2354216

[3] C. Hancz, S. Sultana, S. Nagy, J. Biró, Animals. (2024) https://doi.org/10.3390/ani14071009

[4] S. Govorushko, Trends in Food Science & Technology. (2019) https://doi.org/10.1016/j.tifs.2019.07.032

[5] B. D. Choi, N.A. Wong, J.H. Auh, *Journal for Food Science of Animal Resources*. (2017). https://doi.org/10.5851/kosfa.2017.37.6.955

[6] S.C. Tejada, A.A. García, P.B.C. Torres, L.J.F. Olguín. Southwestern Entomologist (2017) https://doi.org/10.3958/059.042.0123

[7] J.A. Sánchez-García, H.M. Guzmán-Vásquez, R. Jarquín-López, Bol. Sociedad Mexicana de entomología. 6, 2 (2020)

[8] J.P. Williams, J.R. Williams, A. Kirabo, D. Chester, M. Peterson, Insects as sustainable Food Ingredients, 1era edn. (Production, Processing and Food Applications, 2016), pp 61-84

[9] J. Rodríguez-Miranda, J.P. Alcantar, J. M. Juárez, European Food Research and Technology. (2019) https://doi.org/10.1007/s00217-019-03383-0

[10] J. Weru, P. chege, J. Kinyuru, Int. J. Trop. Insect Sci. 2015, 2037 (2021)

[11] A. Van-Huis, L. Gasco, Food Production. (2023) DOI: 10.1126/ciencia.adc9165

[12] S.O. Cruz-López, Y.M. Álvarez-Cisneros, J. Domínguez-Soberanes, C. N. Sánchez, Foods. (2022) https://doi.org/10.3390/foods11050704

[13] P. Nolan, A.E. Mahmound, R.R. Kavle, A. Carne, A. El-Din, A. Bekhit, D. Agyei, Processing Technologies and Food Protein Digestion. (2023) https://doi.org/10.1016/B978-0-323-95052-7.00020-0

[14] J.C. Hernández-Ramírez, G.B. Avendaño-Rodriguez, T. Enríquez-Concepción, M. Jarquín-Olivera, Rev Esp Nutr Comunitaria. (2020) DOI: 10.14642/RENC.2020.26.1.5313

[15] S. Cortázar-Moya, B. Mejía-Garibay, A. López-Malo, J.I. Morales-Camacho, Food Research International. (2023) https://doi.org/10.1016/j.foodres.2023.113445

[16] J.A. Téllez-Morales, B. Hernández-Santos, R.O. Navarro-Cortez, J. Rodríguez-Miranda, Applied Food Research. (2022) https://doi.org/10.1016/j.afres.2022.100149

[17] J. Youssef, C. Spence, International Journal of Gastronomy and Food

Science. (2021) https://doi.org/10.1016/j.ijgfs.2021.100371

[18] R. Ordóñez-Araque, E. Egas-Montenegro, Food. (2021) 10.1016/j.ijgfs.2021.100304

[19] J.M. Muriuki, A.J. Mentzer, E.L. Webb, A. Morovat, W. Kimita, F.M. Ndungu, A.W. Macharia, BMC Med. (2020) https://doi.org/10.1186/s12916-020-1502-7

[20] M.M. Pinheiro, T. Wilson, Springer International Publishing 241, 247 (2017)

[21] A. Lopez-Santamarina, A.D.C Mondragon, A. Lamas, J.M. Miranda, C.M. Franco, A. Cepeda, Foods. (2020) https://doi.org/10.3390/foods9060782

[22] A. Van-Huis, B. Rumpold, C. Maya, N. Roos. Rev. Nutr. (2020) https://doi.org/10.1146/annurev-nutr-041520-010856

[23] R. Kohler, L. Kariuki, C. Lambert, H.K. Biesalski, Journal of Asia-Pacif Entomology. (2019) https://doi.org/10.1016/j.aspen.2019.02.002

[24] C. Garofalo, A. Osimani, V. Milanovic, M. Taccari, F. Cardinali, L. Aquilanti, P. Riolo, S. Ruschioni, N. Isidoro, F. Clementi, Food Microbiology. (2017) https://doi.org/10.1016/j.fm.2016.09.012

[25] G. Poma, M. Cuykx, E. Amato, C. Calaprice, J.F. Focant, A. Covaci, Food and Chemical Toxicology. (2017) DOI: 10.1016/j.fct.2016.12.006

[26] H.P.S. Makkar, Animal. (2018) doi:10.1017/S175173111700324X

[27] A. Van-huis, Entomological Research. (2022) DOI: 10.1111/1748-5967.12582

[28] FAO, Insectos para alimentación y piensos (FAO. ORG 2020), https://www.fao.org/edible-insects/en/ Accessed 29 novembre 2024

[29] M.F. Al-Qazzaz, D.B. Ismail, Animal Nutrition and Feed Technology. (2016) DOI: 10.5958/0974-181X.2016.00038.X

[30] G. Secci, G. Moniello, L. Gasco, F. Bovera, G. Parisi, Food Res Int. (2018) doi: 10.1016/j.foodres.2018.06.045.

[31] N. Moula, J. Detilleux, Animals. (2019) https://doi.org/10.3390/ani9050201

[32] A. Jayanegara, B. Novandri, N. Yantina, M. Ridla, Veterinary World. (2017) 10.14202/vetworld.2017.1439-1446

[33] M. Yu, Z. Li, W. Chen, T. Rong, G. Wang, X. Ma, Journal of Animal Science and Biotechnology. (2019) 10.1186/s40104-019-0358-1

[34] I. Biasato, M. Renna, F. Gai, S. Dabbou, M. Meneguz, G. Perona, M.T. Capucchio, Journal of Animal Science and Biotechnology. (2019) 10.1186/s40104-019-0325-x

[35] L. Gasco, F. Gai, G. Maricchiolo, L. Genovese, S. Ragonese, T. Bottari, G. Caruso, L. Gasco, F. Gai, G. Maricchiolo, SpringerBriefs in Molecular Science. (2018) https://doi.org/10.1007/978-3-319-77941-6_1

[36] I. Hasan, S. Rimoldi, J. Sarogila G. Terova, Animals. (2023) https://doi.org/10.3390/ani13101633

[37] N.V. Linh, S. Wannavijit, K. Tayyamath, N. Dinh-Hung, T. Nititanarapee, M.A.A Sumon, O. Srinual, P. Permpoonpattana, H. Van-Doan, C.L. Brown, Fishes. (2024) https://doi.org/10.3390/fishes9020053

[38] A.D. Diwan, S.N. Harke, A.N. Panche, J. Anim. Physiol. Anim. Nutr. (2022) https://doi.org/10.1111/jpn.13619

[39] W. Vale-Hagan, S. Singhal, I. Grigoletto, C. Tataro-Fila, K. Theodoridou, A. Koidis, Food and Humanity. (2023) https://doi.org/10.1016/j.foohum.2023.09.011

250-IV-PO SYNTHESIS AND CHARACTERIZATION OF SiO_2 MESOPOROUS NANOPARTICLES AS NANOCARRIERS OF IRON

R. I. Rojas-Jimenez[1]*, A. Muñoz-Diosdado[1], M. Rubio Osorinio[2]

[1]Instituto Politécnico Nacional, Unidad Profesional Interdisciplinaria de Biotecnología, CDMX, México.
[2]Instituto Nacional de Neurología y Neurocirugía, CDMX, México.

*Correspondence: rrojasj1500@alumno.ipn.mx

Abstract: Parkinson's disease is characterized, at histological level, by a type of iron-mediated cellular death process called ferroptosis. Iron plays a central role in dopamine synthesis, acting as a cofactor for the enzyme tyrosine hydroxylase, which converts tyrosine into L-dopa, the precursor of dopamine. The lack of this neurotransmitter leads to the signs and symptoms of Parkinson's disease. Replicating iron accumulation would be an initial step toward developing a model to thoroughly investigate the biochemical processes involved in ferroptosis. Therefore, mesoporous SiO_2 nanoparticles are proposed to gradually and controllably increase iron concentration

Keywords: Parkinson's disease, ferroptosis, SiO_2 nanoparticles, mesoporous, iron.

1. INTRODUCTION

Parkinson's disease (PD) is a neurological disorder described for the first time by James Parkinson in 1817, it affects senior patients (older than 60 years) [1] The rise on the incidence of PD is due to the increment of life expectancy and industrialization [2].

The main characteristic of Parkinson's disease (PD) is dopamine deficiency *[1]* Further studies in the anatomy, physiology, and biochemistry of the basal ganglia have revealed that the substantia nigra pars compacta (SNpc) is the primary midbrain structure affected in PD [3]. The loss of dopaminergic neurons in the SNpc leads to disruptions in the nigrostriatal pathway, altering movement control and initiation, resulting in the well-known motor symptoms of PD: resting tremor, bradykinesia, rigidity, and Parkinsonian gait *[1]*. Additionally, typical treatment with dopamine precursors such as levodopa has no effect on disease progression [4]. Familial cases of Parkinson's disease (PD) represent a minority, estimated to account for 5-10% of cases [5].

At the histological level, PD exhibits the presence of Lewy bodies (LBs), cytosolic deposits primarily composed of α-synuclein (α-syn) [6], a 140-amino-acid presynaptic protein expressed in the midbrain that provides stability to neuronal membranes and transport functions [7]. It is known that α-syn misfolds and aggregates in multiple system atrophy (MSA), Lewy body disease (LBD), and unspecified PD [8]. LBs are primarily composed of misfolded protein aggregates, such as oligomers and fibrils, mainly of α-syn [5].

Although the primary cause of Parkinson's disease (PD) remains unknown, iron accumulation has been observed in the basal ganglia [9], which may trigger dopaminergic neuron death through a process called ferroptosis [10]. This includes the generation of reactive oxygen species via the Fenton reaction, mitochondrial dysfunction, and the misfolding of α-synuclein, considered a damage-associated molecular pattern (DAMP) capable of eliciting an immune response by activating microglial cells [11]. Although there are in vitro and in vivo models of PD, they rely on neurotoxins that induce dopaminergic neuron death prior to detecting whether an acute inflammatory process exists [12].

2. MATERIALS AND METHODS

2.1. Nanomaterials synthesis

Mesoporous SiO_2 nanomaterials were synthesized with the modified sol-gel Stöber method [13], where the hydrolysis of tetraethyl orthosilicate (TEOS) in a basic environment at a stable temperature of 70°C. The pores are created by electrostatic interactions between a positively charged surfactant, such as cetyltrimethylammonium bromide (CTAB), and the negatively charged silica under alkaline conditions (pH>7). This also promotes silica condensation, nucleation, and nanoparticle growth. Finally, the surfactant was removed by calcination at 550°C [14].

2.1. Nanomaterial characterization

2.2.1 Scanning and Transmission Microscopies

The SiO_2 NPs were diluted in isopropanol with a ratio of 1 ppm and deposited onto aluminum foil to facilitate the application of a thin gold layer via sputtering with a vacuum of $9.5x10^{-5}$ Torr, enhancing conductivity. Subsequently, the NPs were examined using a JEOL JSM-7800F SEM with a 0.70 kV acceleration to prevent sample charging.

In order to perform TEM analysis, SiO_2 NPs were once again diluted in isopropanol and dispersed in an ultrasonic sonicator at 50 kHz. A drop of the solution was then placed on a TEM grid and allowed to dry. Samples (with and without iron) were observed using a JEOL JEM-2100 transmission electron microscope at an acceleration of 200 kV to confirm pore presence.

2.2.2 Nitrogen sorption. Brunauer- Emmmett-Teller (BET) and Barret-Joyner-Halenda (BJH) methods

The iron-free dried sample was placed in a Quantachrome NOVA 4200e surface area and pore size analyzer. The sample was degassed at 200°C for 48 hours to remove any water molecules present on the nanoparticles. Finally, BET and Barrett-Joyner-Halenda (BJH) analyses were performed to determine pore shape and size.

3. RESULTS AND DISCUSSION

In Figure 1, SEM of the SiO_2 NPs depicts a rough spherical material, histograms in the bottom left corners displaying the size distribution, average size is 95±5 nm. TEM images in Figures 2 and 3 depict a spherical morphology and the presence of pores is confirmed. The main difference between the SiO_2 (Figure 2) and the ones loaded with iron (Figure 3) lies in the lack of visibility of the pores in the second group, the one with iron. This may be an indicator of the interaction between iron and the silanol groups (Si-OH) in the SiO_2 NPs surface and the internalization into the mesopores.

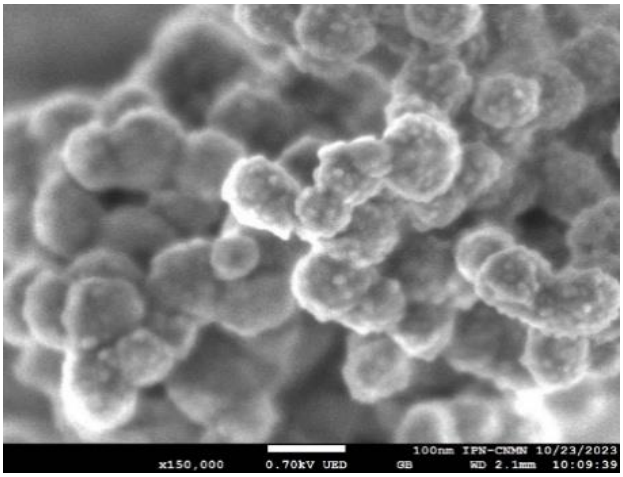

Figure 1. Scanning electron microscopy of SiO_2 NPs without iron x150,000 magnification at 0.70 kV acceleration.

An elemental analysis by energy-dispersive spectroscopy (EDS) was performed in the scanning electron microscopy (SEM), taking advantage of the agglomeration of the NPs, facilitating the interaction between the SEM's electron beam and the surface, ejecting electrons from the sample, creating holes which are filled by an electron in the outer shell emitting a characteristic X-ray in the process, this is specific to each element and is shown in Figure 4.

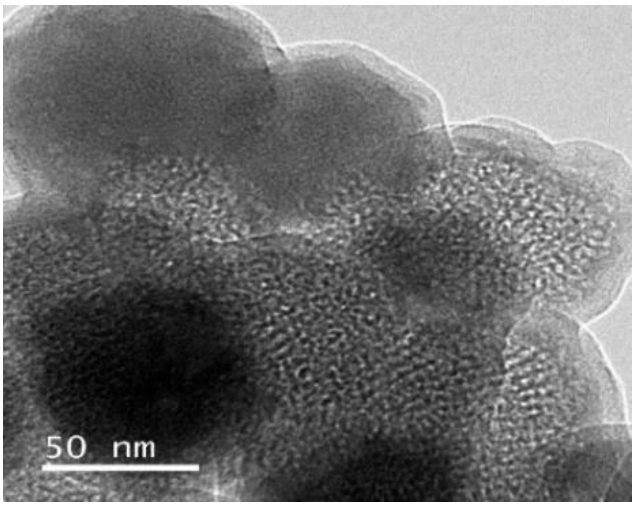

Figure 2. SiO_2 NPs without iron. Mesopores (2 nm approximately) can be observed.

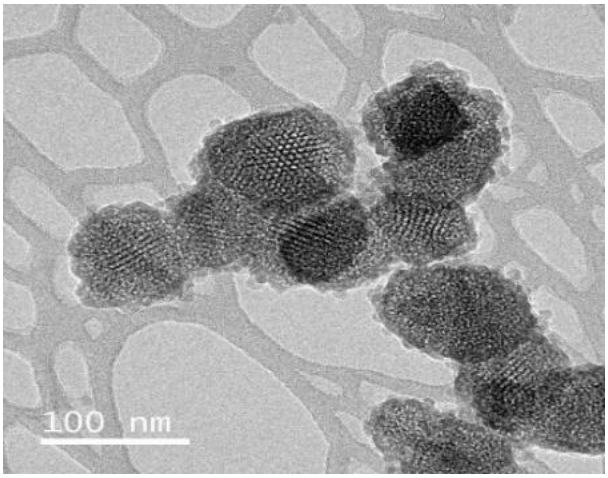

Figure 3. SiO_2 NPs loaded with iron. Although there are mesopores visible, some of them appear to be occluded, indicator of the presence of iron.

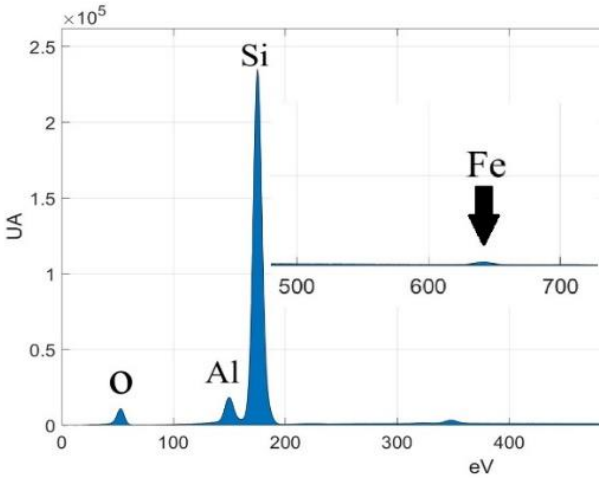

Figure 4. SEM EDS graph of elements present in SiO_2 MSNPs, mainly composed by Si and O, with presence of iron in the surface (insert).

The main elements in the sample are silica (Si) and oxygen (O) as expected, with the presence of aluminum (Al) which acted as substrate for the sample, and a small peal in iron (insert of Figure 4), this due to its release prior to the SEM analysis.

On the other hand, Figure 5 depicts the nitrogen adsorption-desorption hysteresis curve type IV, which according to the UPAC corresponds to a mesoporous material (pore radius between 2 and 50 nm), performed in the SiO_2 nanomaterials. Through BJH and BET methods it was determined: superficial area 47.182 m^2/g, pore radius 2.6793 nm and pore volume 0.127 cc/g.

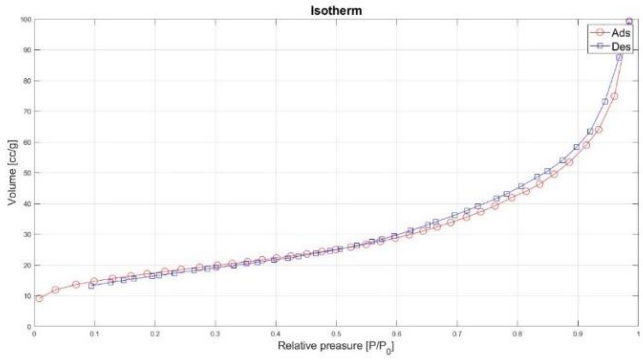

Figure 5. Hysteresis curve type IV for SiO_2 mesoporous (2-50 nm pore radius) Nanoparticles.

The iron adsorption kinetics, conducted over 45 minutes with phenanthroline, an iron chelator, in a spectrophotometer at 510 nm, showed a decreasing exponential trend (Figure 6), suggesting that the organometallic compound was incorporated into the SiO_2 structure. When calculating the logarithm of the data obtained, a linear behavior was observed with a linear correlation coefficient of 0.9833 (Figure 7).

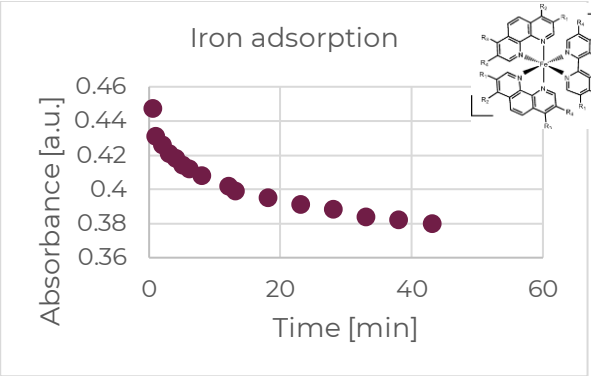

Figure 6. Decremental iron adsorption curve. Insert: phenanthroline molecule.

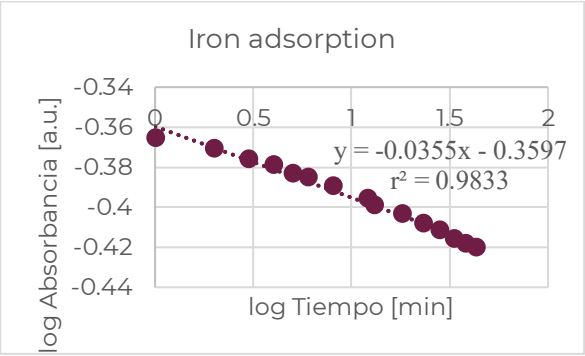

Figure 7. Iron adsorption logarithm, linearity implies iron adsorption has an exponential behavior.

4. CONCLUSIONS

Mesoporous SiO_2 nanoparticles were synthesized using the Stöber method, achieving a spherical morphology with an average size of 95 nm and the presence of surface pores, as confirmed by TEM. Using BET and BJH methods, the surface area was determined to be 47.182 m^2/g, the pore volume 0.127 cc/g, and the pore radius 2.6793 nm. Additionally, the capacity of SiO_2 nanoparticles to incorporate iron into their structure was evaluated using phenanthroline to chelate the iron and observe the change in absorbance at 510 nm. The detailed synthesis and characterization of these mesoporous nanoparticles are essential for their future application in biomedical studies. The ability of the nanoparticles to incorporate iron and their stability under biological conditions are key aspects that will enable their use in advanced therapies and diagnostics."

Acknowledgements

The experimental support of CNMN-IPN in conducting the presented work is acknowledged.

Conflicts of Interest

The authors declare no conflict of interest.

REFERENCES

[1] L. V. Kalia and A. E. Lang, “Parkinson’s disease,” The Lancet, vol. 386, no. 9996, pp. 896–912, 2015, https://doi.org/10.1016/S0140-6736(14)61393-3

[2] E. R. Dorsey, T. Sherer, M. S. Okun, and B. R. Bloemd, “The emerging evidence of the Parkinson pandemic,” J Parkinsons Dis, vol. 8, no. s1, pp. S3–S8, 2018, https://doi.org/10.3233/JPD-181474

[3] C. G. Goetz, “The history of Parkinson’s disease: Early clinical descriptions and neurological therapies,” Cold Spring Harb Perspect Med, vol. 1, no. 1, pp. 1–16, 2011. https://doi.org/10.1101/cshperspect.a008862

[4] S. J. Guiney, P. A. Adlard, A. I. Bush, D. I. Finkelstein, and S. Ayton, “Ferroptosis and cell death mechanisms in Parkinson’s disease,” Mar. 01, 2017, Elsevier Ltd. https://doi.org/10.1016/j.neuint.2017.01.004

[5] P. Riederer et al., "α-Synuclein in Parkinson's disease: causal or bystander?," Jul. 01, 2019, Springer-Verlag Wien. https://doi.org/10.1007/s00702-019-02025-9

A. Kouli, K. M. Torsney, and W.-L. Kuan, "Parkinson's Disease: Etiology, Neuropathology, and Pathogenesis," in Parkinson's Disease: Pathogenesis and Clinical Aspects, Codon Publications, 2018. https://doi.org/10.15586/codonpublications.parkinsonsdisease.2018

[6] K. Y. Yamashita, S. Bhoopatiraju, B. D. Silverglate, and G. T. Grossberg, "Biomarkers in Parkinson's disease: A state of the art review," Dec. 01, 2023, Elsevier B.V. https://doi.org/10.1016/j.bionps.2023.100074

[7] P. Riederer, T. Nagatsu, M. B. H. Youdim, M. Wulf, J. M. Dijkstra, and J. Sian-Huelsmann, "Lewy bodies, iron, inflammation and neuromelanin: pathological aspects underlying Parkinson's disease," May 01, 2023, Springer. https://doi.org/10.1007/s00702-023-02630-9

[8] [L. Zecca et al., "The role of iron and molecules in the neuronal vulnerability of locus coeruleus and substantia nigra during aging," Proc Natl Acad Sci U S A, vol. 101, no. 26, pp. 9843–9848, 2004. https://doi.org/10.1073/pnas.0403495101

[9] S. J. Dixon et al., "Ferroptosis: An iron-dependent form of nonapoptotic cell death," Cell, vol. 149, no. 5, pp. 1060–1072, May 2012. https://doi.org/10.1016/j.cell.2012.03.042

[10] J. K. Sterling et al., "Interleukin-6 triggers toxic neuronal iron sequestration in response to pathological α-synuclein," Cell Rep, vol. 38, no. 7, Feb. 2022. https://doi.org/10.1016/j.celrep.2022.110358

[11] Y. M. Flores-Martinez et al., "Acute neuroinflammatory response in the substantia nigra pars compacta of rats after a local injection of lipopolysaccharide," J Immunol Res, vol. 2018, 2018. https://doi.org/10.1155/2018/1838921

[12] E. Ortiz-Islas, A. Sosa-Arróniz, M. E. Manríquez-Ramírez, C. E. Rodríguez-Pérez, F. Tzompantzi, and J. M. Padilla, "Mesoporous silica nanoparticles functionalized with folic acid for targeted release Cis-Pt to glioblastoma cells," Reviews on Advanced Materials Science, vol. 60, no. 1, pp. 25–37, Jan. 2021. https://doi.org/10.1515/rams-2021-0009

[13] S. H. Wu and H. P. Lin, "Synthesis of mesoporous silica nanoparticles," Chem Soc Rev, vol. 42, no. 9, pp. 3862–3875, Apr. 2013 https://doi.org/10.1039/c3cs35405a

281-IV-PO BAKERY WITH COFFEE PULP AS A CIRCULAR ECONOMY STRATEGY IN OAXACA

M. A. Terán- Ramírez[1], J. Y. López-Cruz[1]*, G. Lugo Espinosa[1]

[1]Instituto Politécnico Nacional, Centro Interdisciplinario de Investigación para el Desarrollo Integral Regional, Unidad Oaxaca. Calle Hornos 1003, Col. Nochebuena, 07320, Santa Cruz Xoxocotlán, Oaxaca, México.

*Correspondence: jylopez@ipn.mx

Abstract: San Juan Juquila Vijanos is a community located in the Sierra Norte of Oaxaca, dedicated to the production of coffee with on average of 367.5 tons of cherries of which 154.35 tons of pulp are discarded, that have a relevant content of nutrients and minerals. So, the aim is analyzing the use and acceptability of coffee pulp in bakery. In this work a qualitative method was applied, through documentary review, participatory observation, semi-structured interviews, tests in bakery substituting wheat flour for coffee pulp flour, complemented with sensory test. As a result, it was observed that agricultural practices are free of toxic products, so the pulp can be used in food. The coffee pulp could replace 30% of wheat flour with good acceptance in terms of sensory attributes, flavor, color, smell, and texture. In addition, interest in using coffee pulp increased, which until now is thrown away on farmland to return nutrients to the soil. In conclusion, the pulp is suitable for use in bakeries, which would reduce waste, and thus create alternatives that promote economic development, with a good contribution of nutrients, which improve the quality of life of coffee producers.

Keywords: local producers, Organic coffee, waste, sustainable practices.

1. INTRODUCTION

Food production systems currently face enormous challenges due to food losses and waste, which is why there is a need for alternatives that promote the sustainability of production systems [1], improve the efficiency of post-harvest activities through the reuse or recycling of waste, promote the circular economy, and the use of renewable energy [2].

One of these systems with high demand and that generate a large amount of waste is coffee production, since only 10% of the coffee cherry is used [3], the rest is waste, of which the pulp stands out for being the largest volume, constituting between 39% [4] and 50% of the fresh weight [5], which is generally discarded, becoming an environmental problem and an economic loss. On the other hand, coffee pulp has 36.07% fiber, 10.63% protein, 5.78% fat and 45.67% [6] reducing sugars that make it useful in the medicinal [7], cosmetic and food industries [8], however, it is still undervalued as in San Juan Juquila Vijanos, therefore, the objective is to analyze the use and acceptability of coffee pulp in bakery that allows it to be incorporated into a new productive cycle through the circular economy approach [9]. Which will help the family economy to improve the quality of life of the population, in addition to reducing the environmental impacts produced by discarding the pulp [10].

2. MATERIALS AND METHODS

The applied methodology was mixed. The qualitative part was to characterize the coffee production process to propose an innovation to produce flour as a circular economy process.

The quantitative part was an experimental test in bakery using a homemade recipe, replacing wheat flour with coffee pulp flour with two treatments (30% = T1 and 60% = T2), and a

control (0% =T1) and was complemented with 9-level hedonic scale tests with 100 untrained panelists.

3. RESULTS AND DISCUSSION

The good agricultural practices conducted by inhabitants of the community in the production of coffee, and the organic crops free of chemical fertilizers, pesticides and herbicides indicate that the coffee pulp can be used for food.

The flour production process consists of collecting the coffee pulp in the pulping phase, then drying, milled, and sifting, which is a process like coffee production, which can be carried out alternately.

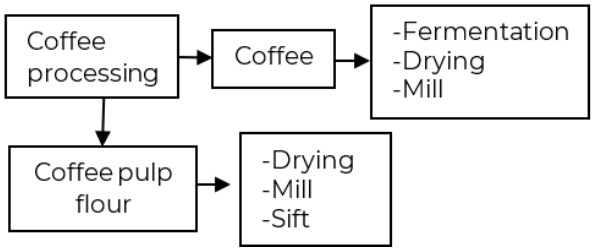

Figure 1. Coffee and coffee pulp flour production process.

Figure 2 shows the level of acceptability in the sensory evaluation of the treatments across 4 attributes: flavor, smell, color, and texture. No significant differences were observed between treatment 0 and T1; however, T3 did show significant differences, having lower acceptability mainly in flavor and texture.

Although some authors have used a larger amount of coffee pulp in their products, this depends on the recipe, as in the case of brownies, which are characterized by their firm and more compact consistency, to which 50% can be incorporated while preserving its characteristics [11].

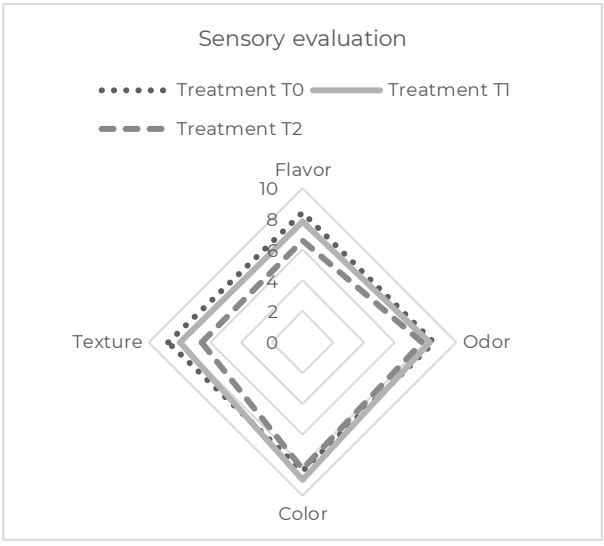

Figure 2. Mean scores (n=100) of 1-9 scale of 1 to 9 for overall acceptance of breads with coffee pulp T0 control (0% coffee pulp flour) T1 (30% coffee pulp flour) and T2 (60% coffee pulp).

In cookies, different concentrations of coffee pulp from 6% to 10% [12] from 3% to 12% [13] to 25% coffee pulp flour [14].

Adding more than 30% coffee pulp flour results in a drier consistency and coarser texture, which decreases its acceptability [15,16]. "To improve the consistency and texture of the cake, it is possible to add guar gum to the recipe, which is commonly used in gluten-free breads [16].

According to the interviews, 80% of the participants use the coffee pulp just as unprocessed fertilizer, 10% use it to make compost, and the remaining participants simply discard it. As for its use as food, only 5% of the participants have consumed coffee pulp infusion.

Regarding whether they would consume coffee pulp cake again and whether they would buy it, 95% of the participants responded affirmatively.

It is important to highlight that these results are advancements of the doctoral research work, and further studies are still being conducted to figure out the nutritional value of bread with coffee pulp.

4. CONCLUSIONS

The use of coffee pulp as an ingredient in bakery and pastry represents an alternative that promotes the circular economy by using waste material, thereby reducing emissions of liquids and gases that affect the environment. Sensory analysis allows us to infer that coffee flour can be used in foods with good acceptance, and it can add value to the coffee production chain, which can help the community improve their economy.

Acknowledgements

This study was developed within the framework of the SIP project 20242329. The authors gratefully acknowledges the participants in the sensory evaluation and the support received through the academic scholarship provided by SECIHTI.

Conflicts of Interest

The authors declare no conflict of interest.

REFERENCES

[1] FAO. Sustainable Food and Agriculture. (FAO 2024) http://www.fao.org/sustainability/es/ Accessed 8 December 2024

[2] FAO. Transformar la alimentación y la agricultura para alcanzar los ODS. (FAO,2018) p. 35

[3] C. Dauber, M. Romero, C. Chaparro, C. Ureta, C. Ferrari, R. Lans, L. Frugoni, M. Echeverry, B. Sánchez, A. Trostchansky, M. Miraballes, A. Gámbaro, I. Vieitez. Applied Food Res. (2024) https://doi.org/10.1016/j.afres.2023.100373

[4] R. Campos, R. Arruda, L. Fernandes, S. Rocha, J. Coimbra. Future foods. (2024). https://doi.org/10.1016/j.fufo.2021.100058

[5] E. Dos Santos, L. de Macedo, J. Ataide. Sci. reports (2024) https://doi.org/10.1038/s41598-024-54797-0

[6] N. Fierro-Cabrales, A. Contreras-Oliva, O. González-Ríos, E. Rosas-Mendoza, V. Morales-Ramos. Agroproductividad. 11, 4 (2018)

[7] C. Andrade, R. Perestrelo, J. Camara. Molecules (2022). https://doi.org/10.3390/molecules27217504

[8] B. Biernacka, D. Dziki, U.Gawlik-Dziki, R. Różyło. J. LWT (2021). https://doi.org/10.1016/j.lwt.2020.110516

[9] N. Bocken, I. De Pauw, C. Bakker y B.Van Der Grinten. J. of indus. and Pro. Eng. (2016) https://doi.org/10.1080/21681015.2016.1172124

[10] M. Albaladejo, P. Mirazo, La economía circular: un cambio de paradigma para soluciones globales, (UNIDO, 2021), https://www.unido.org/stories/la-economa-circular-un-cambio-de-paradigma-para-soluciones-globales. Accessed 12 December 2024

[11] J. Barrera, O. Álvarez, M. Hernández. Evaluación de la cascarilla de café como sustituto a las grasas utilizadas en la elaboración de Brownies. (UNIANDES 2015). https://repositorio.uniandes.edu.co/server/api/core/bitstreams/b2941b1b-1807-4282-9114-9e036a58ddd6/content. Accessed 12 December 2024

[12] E. Martínez-Morales, R. Jaramillo-Gamboa. Informador técnico (2023). http://doi.org/10.23850/22565035.5192

[13] N. Desai, B. Mallik, S. Sakhare, P. Murthy. LWT. (2020) https://doi.org/10.1016/j.lwt.2020.109924

[14] F. Ponce. Efecto de la sustitución parcial de la harina de trigo por harina de pulpa de café (coffea arabica) en el color, textura y contenido de minerales en galletas dulces. (UNDAC, 2018). http://repositorio.undac.edu.pe/bitstream/undac/1407/1/Mg.%20Fortunato%20Candelario%20PONCE%20ROSAS.pdf. Accessed 10 Dec. 2024

[15] A. Guglielmetti, B. Fernandez-Gomez, G. Zeppa, M. Castillo. Pol. J. Food Nutr. Sci (2024). https://doi.org/10.31883/pjfns-2019-0012

[16] C. Rivas-Vela, S. Amaya-Llano, E. Castaño-Tostado. J. food sci. and Technol. (2023) https://doi.org/10.1007/s13197-023-05797-

321-IV-PP ULTRASOUND ASSISTED SYNTHESIS OF ZnO-GO CORE-SHELL WITH ENHANCED OPTICAL PROPERTIES OF NITROGEN AND SULFUR FUNCTIONALIZED

A.J. López Ramírez[1], A.I. Díaz Cano[1], A. García Murillo[2], U. Garduño Terán[1]

[1]Instituto Politécnico Nacional, Unidad Profesional Interdisciplinaria en Ingeniería y Tecnologías Avanzadas, Avenida Instituto Politécnico Nacional No. 2580, Col. Barrio La Laguna Ticomán, C.P. 07340 CDMX, México.
[2]Instituto Politécnico Nacional, Centro de Investigación Innovación Tecnológica, Cerrada Cecati S/N, Col. Santa Catarina, C.P. 02250 CDMX, México.

*Correspondence: aidiaz@ipn.mx

Abstract: This study presents a novel sonochemical method for synthesizing ZnO-GO core-shell (CS) nanostructures using an ultrasonic bath and different stabilizers: ethylene glycol, dimethyl sulfoxide (DMSO) and sodium dodecyl sulfate (SDS). To introduce nitrogen and sulfur heteroatoms, the core-shells were functionalized via ultrasound with nitrogen and sulfur. This method enables the formation of ZnO cores coated with GO layers containing functional groups.

Characterizations performed through Fourier Transform Infrared Spectroscopy (FT-IR) analysis verified surface modifications and Transmission Electron Microscopy (TEM) confirmed the successful formation of 6 nm homogeneous core-shell structures and their functionalization with N and S.

This work makes a significant contribution to understanding control of nanohybrid structure formation and redesigning the synthesis.

Keywords: ZnO QDs, GO, Core-Shell

1. INTRODUCTION

Graphene is defined as a network honeycomb lattice one-atom thick layer of sp^2 hybridized carbon atoms arranged in a two-dimensional 2D crystal one possesses great mechanical and optical properties. It was stacked to construct 3D graphite, rolled 1D nanotube and wrapped to form 0D[1], [2].

There is great interest in the study of graphene materials due to its surprising as its electrical conductivity, thermal conductivity, optical transmittance in the visible-infrared region, surface area and mechanical strength; graphene has great potential applications in many fields such as electronic devices, sensors, supercapacitors, solar cells and hydrogen storage.

The core-shell structure consisted of assembling two different materials with a core at the center and covering by a shell on the surface with materials thus different intrinsic properties, such as high electrical conductivity or high electrochemical activity[3]. The CS have many advantages as multiple combinations by materials and properties intrinsic as morphologies. The CS nanostructures have broad applications in the electrochemical field, including electrocatalysis and energy storage[4].

The dispersion and chemical functionalization of CS also prevents the agglomeration of surfaces of graphene to helps to maintain the properties. The “functionalization” means to the strategies the manipulation over the surface of layer of graphene, including chemical oxidation, physical stabilization with absorbed species and decoration in polymer matrices. Significantly affecting chemical reactions taking place at the interfaces, resulting in high electrochemical performance[5], [6].

The poor solubility of GO limited the applications in either organics and inorganics solvents; the surface of GO can be easily to improve the solubility has oxygen-containing groups such as carboxyl, carbonyl, hydroxyl/epoxy, organic and inorganic materials. The planar structure of the graphene lattice may be distorted at high N and S doping levels. [7], [8].

Various studies have explored the production of ZnO-GO core-shell (CS) structures through methods such as mechanochemical, hydrothermal, and tip-based ultrasound techniques. However, this study focuses on investigating the properties of GO/ZnO CS structures functionalized with S and N, synthesized via a sonochemical technique in an ultrasonic bath. This method is simple, cost-effective, and innovative. In this article, the formation mechanism of the CS structures will be discussed, along with the novel properties of this nanostructure.

2. MATERIALS AND METHODS

2.1 Synthesis of GO

GO was synthesized through a modified version of the Hummers method. (MHM); 1 g of graphite powder was mixed with 0.5 g of $NaNO_3$ and 50 ml of H_2SO_4. After that, the mixture was stirred vigorously for 1 h. After, the solution was cooled in an ice bath with stirring, and at the same time, $KMnO_4$ (3 g) was slowly added and stirred for 30 minutes. Once this stage was concluded, 10 ml HNO_3 was slowly added dropwise and the stirring continued for 1 h. Then, it was purified by filtration using a 5 µm filter and washing with deionized water to obtain a dark-colored tablet. This was placed in a glass and left to dry in an oven at 80 °C for 24 h to remove excess moisture.

2.2 Synthesis of ZnO QDs

ZnO QDs were synthesized following the method developed by Spanhel and Anderson. First, 5 mmol of zinc acetate dihydrate ($Zn(CH_3COO)_2{\cdot}2H_2O$) was dissolved in 50 mL of boiling ethanol and then rapidly cooled in an ice bath. Separately, 7 mmol of $LiOH{\cdot}H_2O$ was dissolved in 50 mL of ethanol using an ultrasonic bath of 40 KHz, followed by cooling to 0 °C. This $LiOH{\cdot}H_2O$ solution was then added dropwise, under constant stirring, to the $Zn(CH_3COO)_2{\cdot}2H_2O$ solution until the entire $LiOH{\cdot}H_2O$ solution in ethanol had been incorporated.

2.3 Synthesis of ZnO-GO Core-Shell

The ZnO-GO core-shell nanocomposite is synthesized using ultrasonic bath of 40 KHz. GO was dispersed in DMSO at a concentration of 2.9 mmol and sonicated for 1 hour. Then, 10 mL of ZnO QDs were added to the GO solution and further sonicated for 20 minutes. Afterward, 30 mL of EG and 1 mL of SDS were introduced into the mixture, followed by an additional 2 hours of sonication.

2.4 Functionalization of the CS

The CS synthesized above are functionalized with Octadecylamide (ODA), in the case of nitrogen, in different concentrations from 0.050 g. 0.1 g, 0.2 g and 0.3 g (ODA 0.5, ODA 1, ODA 2 and ODA 3 respectively) in 5 ml in isopropyl alcohol, each sample is sonicated in 5 ml of CS solution. This is how the same procedure is carried out with sodium dodecyl sulfate (SDS), in the case of sulfur, in different concentrations from 0.050 g. 0.1 g, 0.2 g, 0.3 g and 0.4 g (SDS 0.5, SDS 1, SDS 2, SDS 3 and SDS 4 respectively).

2.5 Method

Infrared FTIR analyses were carried out using a Perkin-Elmer Frontier FTIR spectrometer in a spectral range from 4000 to 800 cm−1. Micrographs were obtained by a High-Resolution Transmission Electron Microscope (HRTM) Jeol JEM 2100.

3. RESULTS AND DISCUSSION

3.1 FT-IR

In the Figure 1 the spectra show the presence of N-H amines can be observed at 890 cm^{-1} and 3300 cm^{-1}[9], corresponding to a bending vibrational mode. Peaks between 700 and 1300 cm^{-1} indicate the stretching mode of aromatic rings for the ODA samples. The intensity of the

peaks at 990 cm^{-1} decreases due to the presence of epoxide groups (C-O-C). Carbonyl-type groups (C=C) also appear at a tensile vibration link of 1400 cm^{-1}[10]. The peak at 1620 cm^{-1}, associated with can be attributed to olefinic group stretching vibrations[11], shows an increase in intensity in comparison to the CS, and with increasing ODA concentration, it indicates that GO is being functionalized with ODA. Peaks at 2800 and 2900 cm^{-1} observed in the CS-ODA spectra indicate the presence of aromatic and aliphatic groups on the GO shell [12].

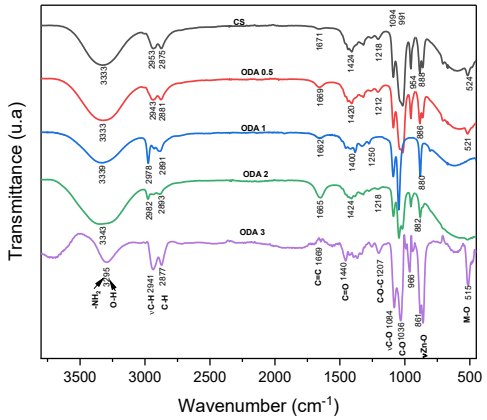

Figure 1. FT-IR spectra of CS functionalized with nitrogen in different concentrations from 0.050 g. 0.1 g, 0.2 g and 0.3 g ODA.

In the Figure 2 the peak associated with Zn-O is observed at 490 cm^{-1}[13]. In the range of 1050 to 1400 cm^{-1}, there is evidence of sulfoxides and sulfides in a tensile vibrational mode, characteristic of the interaction between the core-shell (CS) and SDS. This interaction results in an increase in intensities, indicating an accumulation of sulfides at the edges and surface of the GO CS. The intensity of the peak at 950 cm^{-1} decreases with the presence of epoxy groups (C-O-C). The hydroxyl group (C-OH) shows a peak at 1300 cm^{-1} which is due to the sulphate groups of SDS located on GO, with a slight increase in intensity due to the rise in functional group. The carbonyl group (C=C), characteristic of the basal plane of GO, appears at 1400 cm^{-1}, peaks at around 2800 cm^{-1} are associated with C-H stretching[14]

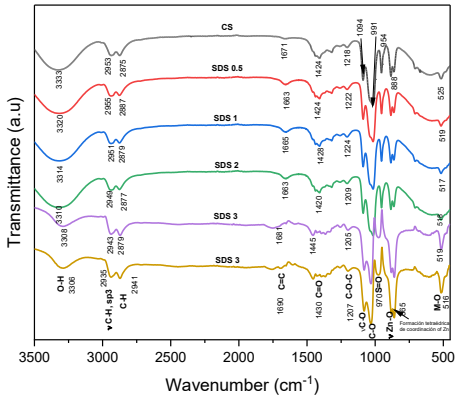

Figure 2. FT-IR spectra of CS functionalized with sulfur in different concentrations from 0.050 g. 0.1 g, 0.2 g and 0.4 g SDS.

3.2 TEM

Confirmation of the successful functionalization of GO-ZnO CS structures was obtained through TEM imaging, where the following features were observed:

ZnO cores are small, dark, dispersed particles with spherical or elongated shapes. GO layers are lighter, translucent coatings surrounding each ZnO core Figure 3 and also, homogeneous distribution in functionalized CS is successful, the GO layer forms a uniform coating around the ZnO core, without areas of excessively thin or thick coverage Figure 4.

Figure 3. TEM image of CS-ODA.

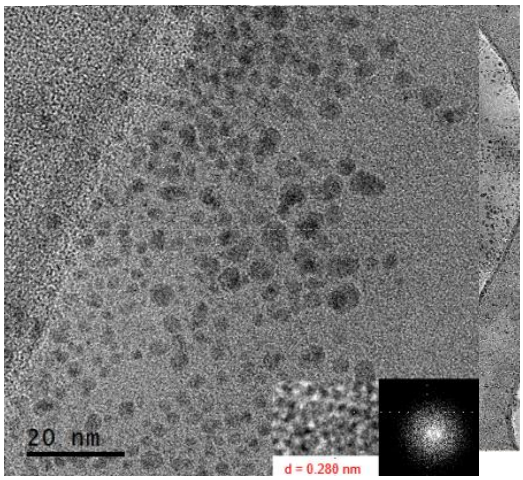

Figure 4. TEM image of CS-SDS.

4. CONCLUSIONS

The functionalized CS with amine and sulfur groups exhibit the presence of surface functional groups, confirmed by FT-IR through characteristic signals such as N-H and S-O. These modifications result in significant changes in bands corresponding to carboxyl, carbonyl, sulfide and amine groups. TEM analysis demonstrates a homogeneous distribution of the CS, confirming their uniformity and effective dispersion.

Acknowledgements

The authors gratefully acknowledge the financial support of this work by the Instituto Politécnico Nacional through SIP-IPN projects 20242751 and 20241489. A.J. López Ramírez acknowledges the CONAHCYT Ph D scholarship. The authors thank CNMN-IPN for its experimental support.

Conflicts of Interest

The authors declare no conflict of interest.

REFERENCES

[1] Ciesielski, A. & Samorì, P. Graphene via sonication assisted liquid-phase exfoliation. Chemical Society Reviews vol. 43 381–398 Preprint at https://doi.org/10.1039/c3cs60217f (2014).

[2] Speranza, G. The Role of Functionalization in the Applications of Carbon Materials: An Overview. C (Basel) 5, 84 (2019).

[3] Shankar, P. et al. ZnO@graphene oxide core@shell nanoparticles prepared via one-pot approach based on laser ablation in water. Appl Surf Sci 531, (2020).

[4] Nandanapalli, K. R., Mudusu, D. & Lee, S. Functionalization of graphene layers and advancements in device applications. Carbon vol. 152 954–985 Preprint at https://doi.org/10.1016/j.carbon.2019.06.081 (2019).

[5] Kuila, T. et al. Chemical functionalization of graphene and its applications. Progress in Materials Science vol. 57 1061–1105 Preprint at https://doi.org/10.1016/j.pmatsci.2012.03.002 (2012).

[6] Douda, J. et al. Optical properties of amine-functionalized graphene oxide. Applied Nanoscience (Switzerland) 9, 567–578 (2019).

[7] Kumar, R. et al. Heteroatom doped graphene engineering for energy storage and conversion. Materials Today vol. 39 47–65 Preprint at https://doi.org/10.1016/j.mattod.2020.04.010 (2020).

[8] Ardyani, T. et al. Surfactants with aromatic headgroups for optimizing properties of graphene/natural rubber latex composites (NRL): Surfactants with aromatic amine polar heads. J Colloid Interface Sci 545, 184–194 (2019).

[9] Alharbi, F. N., Abaker, Z. M. & Makawi, S. Z. A. Phytochemical Substances—Mediated Synthesis of Zinc Oxide Nanoparticles (ZnO NPS). Inorganics (Basel) 11, (2023).

[10] Dumée, L. F. et al. Tuning the grade of graphene: Gamma ray irradiation of free-standing graphene oxide films in gaseous phase. Appl Surf Sci 322, 126–135 (2014).

[11] Ţucureanu, V., Matei, A. & Avram, A. M. FTIR Spectroscopy for Carbon Family Study. Critical Reviews in Analytical Chemistry vol. 46 502–520 Preprint at https://doi.org/10.1080/10408347.2016.1157013 (2016).

[12] Doustkhah, E. & Rostamnia, S. Covalently bonded sulfonic acid magnetic graphene oxide: Fe3O4@GO-Pr-SO3H as a powerful hybrid catalyst for synthesis of indazolophthalazinetriones. J Colloid Interface Sci 478, 280–287 (2016).

[13] Motelica, L. et al. Antibacterial Activity of Zinc Oxide Nanoparticles Loaded with Essential Oils. Pharmaceutics 15, (2023).

[14] Salihi, E. Ç., Wang, J., Coleman, D. J. L. & Šiller, L. Enhanced removal of nickel(II) ions from aqueous solutions by SDS-functionalized graphene oxide. Separation Science and Technology (Philadelphia) 51, 1317–1327 (2016).

AUTHOR INDEX

Author	ID	Pages
A. Adauto-Arriola	212-I-PO	50, 54
A. B. Guzmán Urbieta	160-II-PP	117, 121
A. Cruz	115-II-PP	112, 116
A. Ezeta-Mejía	49-I–PO 253-I-PO	7, 12, 61, 66
A. Flores-Miranda	84-II-PP	107, 111
A. García Murillo	321-IV-PP	247, 252
A. Hernández Zavala	172-II-PP	139, 144
Á. I. Licona Aguilar	39-IV-PO	217, 223
A. M. Torres Huerta	39-IV-PO	217, 223
A. Manzo-Robledo	49-I–PO 253-I-PO	7, 12, 61, 66
A. Méndez-Tenorio	59-II-PP	102, 106
A. Muñoz-Diosdado	250-IV-PO	238, 242
A. Reséndiz-Mora	7-II-PO	95, 101
A. Reyes-Ramírez	115-II-PP	112, 116
A. Reyes-Salas	212-I-PO	50, 54
A. Rojas-Bernabé	59-II-PP	102, 106
A. V. Pérez Domínguez	44-III-PO	172, 174
A. Zacarías	201-I-PO	44, 49
A. Zacarías	312-I-PO	73, 78
A. Zacarías Santiago	217-I-PO	55, 60
A.I. Díaz Cano	321-IV-PP	247, 252
A.J. López Ramírez	321-IV-PP	247, 252
A.Trejo León	4-I-PO	2, 6
B. Gamboa Loya	134-I-PO	32, 38
B. I. Rodríguez Romero	171-II-PO	135, 138
C. Aylin Salinas Olivo	21-III-PP	166, 171
C. D. Téllez-Uribe	94-I-PO 95-I-PO	13, 19, 20, 26
C. García	371-III-PP	210, 215
C. Jiménez	201-I-PO	44, 49
C. Jiménez	312-I-PO	73, 78
C. M. Jácome Gordillo	166-II-PP	128, 134
C. Monreal	139-I-PO	39, 43
C. Monreal Jiménez	134-I-PO	32, 38
C. Pérez	325-III-PP	203, 209
C. Wong-Baeza	7-II-PO	95, 101
C. X. Tirado-López	49-I–PO 253-I-PO	7, 12, 61, 66
D. de Lange	139-I-PO	39, 43
D. I. Rivas López	366-I-PO	79, 86
D. M. González Fong	366-I-PO	79, 86
D. Mimic	395-I-PO	87, 93
D. V. Gomez-Navarro	301-I-PP	67, 72
De-León Cruz Vargas	84-II-PP	107, 111
E. A. Davila del Rio	302-II-PP	151, 154
E. D. Rodríguez Rojas	166-II-PP	128, 134
E. E. Barrera	201-I-PO	44, 49
E. E. Barrera	312-I-PO	73, 78
E. E. Barrera García	217-I-PO	55, 60
E. F. Galicia Haro	44-III-PO	172, 174
E. Galarce-Sosa	7-II-PO	95, 101
E. J. Córdova Alarcón	172-II-PP	139, 144
E. M. Arce-Estrada	253-I-PO	61, 66
E. R. García Davalos	301-I-PP	67, 72
E. Rundquist-Sánchez	7-II-PO	95, 101
E. S. Aguilar Barrera	302-II-PP	151, 154
E. S. Cruz Ruiz	162-II-PP	122, 127
F. J. Chávez Maciel	90-III-PP	180, 186
F. Martínez Zúñiga	4-I-PO	2, 6
F. Oviedo	139-I-PO	39, 43
F. Pérez	139-I-PO	39, 43
G Gutierrez-Urueta	312-I-PO	73, 78
G. Barrera-Aveleida	7-II-PO	95, 101
G. C. Lescas-Montes	145-IV–PO	224, 230
G. Gutiérrez Urueta	134-I-PO 139-I-PO 201-I-PO	32, 38, 39, 43, 44, 49
G. Ibáñez-Cervantes	59-II-PP	102, 106
G. Lugo Espinosa	145-IV–PO 281-IV-PO	224, 230, 243, 245

G. Romage	201-I-PO 217-I-PO 312-I-PO	44, 49, 55, 60, 73, 78
G. S. Abarca-Jiménez	212-I-PO	50, 54
H. Méndez	134-I-PO	32, 38
I. Araujo-Vargas	94-I-PO 95-I-PO	13, 19, 20, 26
I. Baeza-Ramírez	7-II-PO	95, 101
I. C. Ortega Moreno	44-III-PO	172, 174
I. F. Contreras-Hernández	84-II-PP	107, 111
J. A. Alcocer Zuñiga	172-II-PP	139, 144
J. A. Guevara Salazar	160-II-PP 162-II-PP 166-II-PP 259-II-PP	117, 121, 122, 127, 128, 134, 145, 150
J. A. Morales-López	203-IV-PO	231, 237
J. C. López-Vázquez	402-II-PO	155, 158
J. Castillo Cuauhtémoc	217-I-PO	55, 60
J. Cruz-Castro	212-I-PO	50, 54
J. F. Villegas-Alcaraz	94-I-PO	13, 19
J. G. Sánchez	201-I-PO 312-I-PO	44, 49, 73, 78
J. G. Trujillo Ferrara	160-II-PP 162-II-PP 166-II-PP 259-II-PP	117, 121, 122, 127, 128, 134, 145, 150
J. Juárez	371-III-PP	210, 215
J. L. Reyes Rodríguez	114-I-PO	27, 31
J. Luna-Herrera	402-II-PO	155, 158
J. M. Ramos Quiroz	90-III-PP	180, 186
J. M. Sandoval Pineda	114-I-PO	27, 31
J. Madrigal Acevedo	302-II-PP	151, 154
J. Mares-Carreño	212-I-PO	50, 54
J. Mendieta-Wejebe	115-II-PP	112, 116
J. Michael Cruz	201-I-PO 312-I-PO	44, 49, 73, 78
J. Núñez	371-III-PP	210, 215
J. Patiño Ortiz	17-III-PP	160, 165
J. R. Moran Diaz	160-II-PP 162-II-PP 166-II-PP	117, 121, 122, 127, 128, 134
J. R. Sosa Pedroza	4-I-PO	2, 6
J. Rojas-Rica	139-I-PO	39, 43
J. Y. López-Cruz	145-IV–PO 281-IV-PO	224, 230, 243, 245
K. Cruz García	203-IV-PO	231, 237
K. Delgadillo-Gutiérrez	402-II-PO	155, 158
L. A. Tomás Fernández	61-III-PO	175, 179
L. Abascal Gaytán	61-III-PO	175, 179
L. Lobato Azuceno	109-III-PO	187, 192
L. R. García-Cortes	84-II-PP	107, 111
L. Rocha Lona	109-III-PO	187, 192
M. A. Beltrán Zúñiga	366-I-PO	79, 86
M. A. Castro Reyes	302-II-PP	151, 154
M. A. Domínguez Crespo	39-IV-PO	217, 223
M. Á. López-Luis	59-II-PP	102, 106
M. Á. Martínez García	21-III-PP	166, 171
M. Á. Soto-Mendoza	49-I–PO 253-I-PO	7, 12, 61, 66
M. A. Vazquez-Avila	59-II-PP	102, 106
M. Atalí Terán-Ramírez	281-IV-PO	243, 245
M. de la C. Sánchez Llabona	157-III-PO	199, 202
M. del R. Soto Flores	118-III-PP	193, 198
M. E. Ocharan-Hernández	84-II-PP	107, 111
M. F. Camacho Merino	259-II-PP	145, 150
M. G. Arellano Mendoza	162-II-PP	122, 127
M. Hernández González	90-III-PP	180, 186
M. L. Hernández Pichardo	114-I-PO	27, 31
M. M. Maldonado Ávalos	61-III-PO	175, 179
M. Romero	134-I-PO	32, 38
M. Rubio Osorinio	250-IV-PO	238, 242
M. Santiago Villeda	118-III-PP	193, 198
M. Toledo Velazquez	395-I-PO	87, 93
M. Valdes-Guevara	115-II-PP	112, 116

N. Mondragón-Escamilla	94-I-PO 95-I-PO	13, 19, 20, 26
N. Reyes-Vallejo	115-II-PP	112, 116
O. Guarneros	134-I-PO	32, 38
O. Hernández Alonso	395-I-PO	87, 93
P. López Sánchez	172-II-PP	139, 144
R. A. Gómez Ortiz	109-III-PO	187, 192
R. G. González Huerta	114-I-PO	27, 31
R. G. Sánchez-Alvarado	49-I–PO 253-I-PO	7, 12, 61, 66
R. Hernández Leal	39-IV-PO	217, 223
R. Isaac Rojas-Jimenez	250-IV-PO	238, 242
R. J. Garnica Peña	157-III-PO	199, 202
R. Jäckel	134-I-PO 139-I-PO	32, 38
R. K. Salgado-Cristobal	94-I-PO 95-I-PO	13, 19, 20, 26
R. M. Ordóñez Razo	171-II-PO	135, 138
R. Montoya González	114-I-PO	27, 31
R. Ramos-Monteagudo	7-II-PO	95, 101
R. Romero-Nava	84-II-PP	107, 111
R. Tejeida	325-III-PP 371-III-PP	203, 209, 210, 215
S. B. Brachetti Sibaja	39-IV-PO	217, 223
S. Pérez-Rodríguez	95-I-PO	20, 26
S. Romero	325-III-PP	203, 209
T. Aquino López	203-IV-PO	231, 237
T. Aquino-Aguilar	203-IV-PO	231, 237
T. Aquino-Bolaños	203-IV-PO	231, 237
U. Garduño Terán	321-IV-PP	247, 252
V. de la C. Díaz Valdes	17-III-PP	160, 165
V. García Rodríguez	217-I-PO	55, 60
V. R. Oliva Aguilar	157-III-PO	199, 202
V. Sánchez Monroy	171-II-PO	135, 138
Y. D. Ortiz-Hernández	203-IV-PO	231, 237
Y. López-Grijalba	212-I-PO	50, 54

Issue No. 1, 2025.
ISSN in Process

Horizontes de Investigación y Desarrollo, Year 2025, Issue No. 1, is a special edition of the Interpolytechnic Congress on Research and Graduate Studies (ICRGS-2024). This publication is edited by the Instituto Politécnico Nacional (IPN) through the Dirección de Posgrado of the Secretaría de Investigación y Posgrado (SIP). Secretaría Académica Building, 2nd Floor, Av. Luis Enrique Erro s/n, Unidad Profesional Adolfo López Mateos, Zacatenco, Gustavo A. Madero, C.P. 07738, Mexico City. Phone: +52 (55) 5729 6000, ext. 50563. Email: jhorizontes@ipn.mx.

IPN-SIP 2025